

Investigation and characterisation of diamide insecticide resistance conferred by target-site mutations in the Ryanodine Receptor of lepidopteran pests

*Thesis submitted in accordance with the requirements of Cardiff
University for the degree of Doctor in Philosophy (Medicine)*

Ewan Patrick Blockey Richardson

December 2019



Word Count: 45,848

Pages: 195

Summary

Lepidopteran crop pests such as *Tuta absoluta*, *Chilo suppressalis*, *Spodoptera frugiperda* and *Plutella xylostella* are becoming increasingly problematic, as populations colonise new regions of the globe. The diamide insecticides are a relatively new class that is especially effective, and important, for controlling lepidopteran pests. However, over the past 10 years, resistance to diamides has emerged amongst various lepidopteran species, and is a major threat to crop protection in some cases. Resistance is thought to be caused by alterations to the Ryanodine Receptor, which is the target-site of Diamide insecticides, and previous studies have identified a variety of alterations, in field-populations of multiple lepidopteran species, which may be implicated in diamide resistance.

This thesis aims to characterise RyR alterations in terms of their impact on the control-efficacy of diamide insecticides. A previously cloned RyR sequence from the moth, *Plutella xylostella*, was altered to reflect resistance-alterations present in the field. Alteration of positions 4946 and 4790 was found to reduce activation by diamides when expressed in cell lines. These same altered moth RyR sequences were inserted into *Drosophila*, by way of *in-vivo* confirmation. Flies expressing the resistant RyR genotypes survived diamide challenge more readily than those expressing the wild-type genotype of moth RyR. However, the resistant genotypes also climbed and crawled more slowly, suggesting a potential drawback of resistance.

The alterations to residues 4946 and 4790 suggested a location of diamide interaction within the voltage-sensor-like domain of the RyR. In order to further define the interaction site, further alterations were made within the same region. Preliminary investigations indicated that these alterations strongly reduce diamide efficacy, when in combination, but exhibit somewhat minor reductions of efficacy as individual changes. It was concluded that the diamide interaction lies proximal to the Voltage-Sensor-like-Domain of the RyR.

Table of Contents

<i>Table of Figures</i>	<i>i</i>
<i>Acknowledgements</i>	<i>vi</i>
<i>Abbreviations</i>	<i>vii</i>

Chapter 1: Introduction

<i>1.1 Modern Agriculture: Feeding a growing population</i>	
<i>1.1.1 A strain on the planet</i>	<i>1</i>
<i>1.2 Insect control in the era of ‘Sustainable Intensification’</i>	<i>2</i>
<i>1.2.1 Non-synthetic modes of insect control</i>	<i>3</i>
<i>1.2.2 Insecticidal Spray: There’s no better way</i>	<i>6</i>
<i>1.2.3 Strain on the Insecticide industry</i>	<i>6</i>
<i>1.3 Diamide insecticides</i>	<i>8</i>
<i>1.3.1 A New Hope</i>	<i>9</i>
<i>1.3.2 Flubendiamide: An exceptionally selective insecticide</i>	<i>9</i>
<i>1.3.3 Chlorantraniliprole and Cyantraniliprole: A wider range of control</i>	<i>10</i>
<i>1.3.4 New diamide actives under development</i>	<i>12</i>
<i>1.4 The rise of resistance to diamide insecticides</i>	<i>14</i>
<i>1.4.1 Spodoptera frugiperda and other Noctuidae</i>	<i>14</i>
<i>1.4.2 Tuta absoluta</i>	<i>17</i>
<i>1.4.3 Diamide Resistance in other Lepidopteran Species</i>	<i>21</i>

1.4.4 <i>Plutella xylostella</i>	23
1.4.5 <i>The Root of Resistance: Alterations to the Diamide target</i> ..	24
1.5 <i>Diamide Mode of Action</i>	25
1.5.1 <i>The Ryanodine Receptor</i>	26
1.5.2 <i>Calcium Homeostasis</i>	27
1.5.3 <i>RyR2</i>	27
1.5.4 <i>Excitation Contraction Coupling</i>	28
1.5.5 <i>Modulation of RyRs</i>	29
1.6 <i>RyR Sequence, Structure and Function</i>	33
Box 1.3: <i>Highlights of imaging studies</i>	34
1.6.1 <i>General Structural overview</i>	35
1.6.2 <i>Opening Mechanism: An Overview</i>	36
1.6.3 <i>Opening Mechanism: Detailed investigations</i>	37
1.6.4 <i>Calcium and Caffeine: In search of a binding site</i>	39
1.6.5 <i>RyR amino acid alterations in disease states: clues to function</i>	41

Chapter 2: Methods

2.1 <i>General Methods</i>	46
2.1.1 <i>Genomic DNA extraction</i>	46
2.1.2 <i>RNA extraction</i>	46
2.1.3 <i>cDNA synthesis</i>	47

2.2 Polymerase chain reaction (PCR)	47
2.2.1 Primer Design.....	47
2.2.2 Standard PCR	47
2.2.3 High-fidelity PCR	48
2.2.4 Site-directed Mutagenesis by PCR	48
2.2.5 PCR product purification	49
2.2.6 Agarose gel electrophoresis	49
2.2.7 Extraction of PCR products from agarose gels.....	49
2.3 Molecular Cloning and Transformation	50
2.3.1 Plasmid assembly by endonuclease digestion and ligation ..	50
2.3.2 Concentration by Ethanol Precipitation.....	50
2.3.3 Bacterial transformation.....	51
2.3.4 Transformation Validation and plasmid Propagation	51
2.3.5 Plasmid purification.....	52
2.4 Final Product Validation and Sequencing	53
2.4.1 Restriction Fragment Length Validation.....	53
2.4.2 Sequencing.....	53
2.5 Generating RyR mutant genotypes (with RFCLM as example) - specific cloning strategy for RyR mutagenesis and assembly	53
2.5.1 Mutagenesis on individual PxRyR fragments	56
2.5.2 fragment assembly into the plasmid and plasmid propagation.....	56

2.5.3 <i>pcDNA3.1(-) / pIZ/V5-His modified plasmid creation, for fragment assembly</i>	58
2.5.4 <i>Plasmid Assembly Validation</i>	58
2.5.5 <i>Transfer of Recombinant RyR constructs between vectors</i> ..	59

Chapter 3: Validation of the perfusion Calcium Imaging system for quantifying diamide response in Sf9 cells

3.1 <i>Chapter Summary</i>	64
3.2 <i>The need for a novel method for rapid in-vitro investigation of insecticide resistance mechanisms</i>	64
3.3 <i>Chapter Specific Methods</i>	67
3.3.1 <i>Overview of the experimental system</i>	67
3.3.2 <i>Insect cell husbandry</i>	68
3.4 <i>Characterising PxRyR-expressing Sf9 cells response to caffeine and diamides using the Ratiometric Imaging Perfusion Rig</i>	69
3.4.1 <i>Identification of the caffeine ‘type-response’ and cellular selection</i>	69
3.4.2 <i>Protocol optimisation to maximize the cat A response in PxRyR transfected cells</i>	73
3.4.3 <i>Calcium Imaging</i>	80
3.4.4 <i>Characterisation of the recombinant WT-PxRyR Caffeine-response in Sf9 cells</i>	82
3.4.5 <i>Characterisation of the recombinant WT-PxRyR diamide-response in Sf9 cells</i>	87
3.4.5.1 <i>Agonist Diluents and Background Fluorescence</i>	88

3.4.5.2 Absolute $[Ca^{2+}]$ was not measured	89
3.5 Absolute Ca^{2+} Imaging: An alternative method of diamide response quantification	94
3.5.1 Drawbacks of the Absolute Imaging system	97
3.6 Conclusions	99

Chapter 4: Target-Site Resistance to Diamide Insecticides

4.1 Chapter Summary	100
4.2 Introduction	100
4.2.1 Target Site Resistance	100
4.2.2 I4790M– A novel cause of resistance in diverse lepidopteran pests	102
4.3 Methods	106
4.3.1 Concentration-response assays	106
4.3.2 In-silico analysis methods.....	106
4.4 Results	109
4.4.1 Generation of novel PxRyR constructs.....	109
4.4.2 Functional Expression of modified PxRyR constructs.....	110
4.4.3 Quantifying the impact of field-derived mutations on PxRyR stimulation by diamides	118
4.5 Discussion	124
4.6 Conclusion and future work	124

Chapter 5: *In-vivo* investigations of Diamide resistance

5.1 Chapter Summary	128
5.1.1 An in-vivo model of diamide resistance.....	128
5.2 Chapter Introduction	128
5.2.1 Resistance, but at what cost.....	128
5.3 Methods	130
5.3.1 <i>D. melanogaster</i> rearing	130
5.3.2 The germline transformation strategy, and generation of the injection line	130
5.3.3 Generation of UAS-PxRyR genome modified <i>Drosophila</i> lines	132
5.3.4 Screening of UAS-PxRyR flies.....	134
5.3.5 Driving Expression of UAS-PxRyR.....	135
5.3.6 Confirming Knock-in and Driving of PxRyR.....	138
5.3.7 Experimental Methods on PxRyR-containing Fly Models ..	138
5.4 Results	143
5.4.1 Insecticide Bioassays	
5.4.2 Fitness costs of PxRyR alteration	147
5.5 Discussion	150
5.5.1 What is the value of ‘pestified’ drosophila	150
5.5.2 Are these lines good models of fitness costs associated with TSR?	152
5.5.3 A future model of resistance spread?.....	153

5.5 Conclusion	153
----------------	-----

Chapter 6: Chimeric investigations into the diamide binding site on the lepidopteran RyR

6.1 Chapter Summary	154
6.2 Introduction	155
6.2.1 Diamides are highly selective against mammalian RyR	155
6.2.2 What is the cause of the discrepancy in binding and activation	
6.2.3 The diamide binding region	
6.3 Results	162
6.3.1 RFCLM: A chimeric RyR channel combining moth with mammal	
6.3.2 Unpicking the RFCLM modification	167
6.4 Discussion	176
6.4.1 Why is there a disparity between the effects of residue changes in isolation, and their effect in combination?	176
6.4.2 What is the mechanism of the observed resistance effects conferred by Y4701F?	177
6.5 Conclusion	177

Ch7: General Thesis conclusion

7.1 An early warning system to combat diamide resistance in the field **Error! Bookmark not defined.**

7.2 *This thesis has defined the position and extent of the diamide binding pocket*

Error! Bookmark not defined.

7.2.1 4946 **Error! Bookmark not defined.**

7.2.2 4701 **Error! Bookmark not defined.**

7.2.3 4700 **Error! Bookmark not defined.**

7.2.4 4790 **Error! Bookmark not defined.**

7.2.5 *Conclusions regarding the diamide binding site* **Error! Bookmark not defined.**

7.3 *Future Steps toward greater resolution of the binding pocket*

Error! Bookmark not defined.

Appendix and Supplementary Materials

S1 Recipes 191

S1.1 Molecular Biology recipes..... 191

S1.2 Fly Transformation recipes..... 192

S2 Supplementary Materials 192

Reference List

Table of Figures

<i>Fig 1.1</i>	<i>Top five synthetic insecticides, ranked by Annual Gross Profit</i>	4
<i>Fig 1.2</i>	<i>Challenges in insecticide development</i>	4
<i>Box 1.1</i>	<i>Insect Armageddon</i>	7
<i>Box 1.2</i>	<i>Early Development of Diamides</i>	10
<i>Fig 1.3</i>	<i>Diamide Structures</i>	12
<i>Fig 1.4</i>	<i>Transnational spread of diamide-resistant <i>S. frugiperda</i></i>	18
<i>Fig 1.5</i>	<i>Transnational spread of diamide-resistant <i>T. absoluta</i></i>	18
<i>Fig 1.6</i>	<i>Transnational spread of diamide-resistant <i>P. xylostella</i></i>	18
<i>Fig 1.7</i>	<i>RyR2 channel opening and regulation</i>	30
<i>Box 1.3</i>	<i>Highlights of Ryr imaging studies</i>	33
<i>Fig 1.8</i>	<i>Diagram of structurally important RyR domains</i>	41
<i>Table 2.1</i>	<i>List of RyR constructs generated during this PhD</i>	54
<i>Table 2.2</i>	<i>Mutagenesis Oligos</i>	55
<i>Fig 2.1</i>	<i>PxRyR construct assembly</i>	57
<i>Table 2.3</i>	<i>Ligation ratios for RFCLM-PxRyR</i>	57
<i>Table 2.4</i>	<i>Mutagenesis Oligos</i>	58
<i>Fig 2.2</i>	<i>PxRyR assembly validation by digest</i>	60
<i>Fig 2.3</i>	<i>PxRyR assembly validation by sequencing</i>	61
<i>Fig 2.4</i>	<i>Method for rapid mutation swapping between RyR constructs</i>	62

<i>Fig 3.1</i>	<i>Perfusion chamber setup diagram, RIPS</i>	<i>67</i>
<i>Fig 3.2</i>	<i>Compton perfusion chamber diagram, AIS</i>	<i>68</i>
<i>Fig 3.3</i>	<i>Validation and processing of caffeine responses</i>	<i>71</i>
<i>Fig 3.4</i>	<i>Cell culture optimisation</i>	<i>75</i>
<i>Fig 3.5</i>	<i>Transfection optimisation</i>	<i>78</i>
<i>Fig 3.6</i>	<i>Variation in caffeine response amplitude</i>	<i>83</i>
<i>Fig 3.7</i>	<i>Characterising other caffeine response properties</i>	<i>85</i>
<i>Box 3.1</i>	<i>Calculating Proportional Normalised Response to diamide insecticides</i>	<i>90</i>
<i>Fig 3.8</i>	<i>Characterising diamide response variation</i>	<i>92</i>
<i>Fig 3.9</i>	<i>Concentration-response curves for WT-PxRyR vs diamides, RIPS</i>	<i>94</i>
<i>Fig 3.10</i>	<i>Concentration-response curves for WT-PxRyR vs diamides, AIS</i>	<i>96</i>
<i>Box 3.2</i>	<i>Pipeline for cell identification and fluometric analysis, following Absolute Ca²⁺ imaging</i>	<i>97</i>
<i>Fig 4.1</i>	<i>Transmembrane protein topology of PxRyR</i>	<i>102</i>
<i>Table 4.1</i>	<i>Summary of major global diamide resistance occurrences</i>	<i>104</i>
<i>Table 4.2</i>	<i>Comparison of CLR resistance in 3 species</i>	<i>109</i>
<i>Table 4.3</i>	<i>CLR and FLB spray dosage information</i>	<i>110</i>
<i>Fig 4.2</i>	<i>Sequence comparison of altered PxRyR constructs</i>	<i>111</i>
<i>Fig 4.3</i>	<i>Preliminary diamide dosing of mutant PxRyR-expressing cells</i>	<i>112</i>

Fig 4.4	<i>Response of WT and GE to increasing caffeine concentration</i>	114
Fig 4.5	<i>Response comparison of PxRyR constructs to caffeine</i>	115
Fig 4.6	<i>PxRyR homology model indicating hypothetical caffeine binding site</i>	117
Fig 4.7	<i>Correlation of caffeine responses vs diamide responses</i>	118
Fig 4.8	<i>Concentration-Response of G4946E to CLR and FLB</i>	121
Fig 4.9	<i>Concentration-Response of G4946V to CLR and FLB</i>	121
Fig 4.10	<i>Amino acid alignment indicating segregation at the I4790 locus</i>	123
Fig 4.11	<i>Concentration-response of I4790M to CLR and FLB</i>	124
Fig 4.12	<i>Boxplot comparison of all PxRyR mutant responses to CLR and FLB</i>	124
Fig 4.13	<i>Potential future resistance-causing mutations on the RyR</i>	128
Fig 5.1	<i>Crossing pattern for FC31 injection line</i>	133
Fig 5.2	<i>Needle pulling and injection parameters</i>	135
Table 5.1	<i>Optimal injection conditions</i>	135
Fig 5.3	<i>Crossing pattern to generate PxRyR-integrated flies</i>	137
Fig 5.4	<i>Crossing pattern to drive PxRyR expression</i>	139
Fig 5.5	<i>Proof of null-RyR lethality</i>	140
Fig 5.6	<i>Drosophila lines generated in this thesis</i>	141

Fig 5.7	<i>The fly climber apparatus</i>	144
Fig 5.8	<i>Concentration-response of WT and IM drosophila lines vs CLR and FLB</i>	146
Fig 5.9	<i>Concentration-response of GE drosophila line vs CLR and FLB</i>	148
Fig 5.10	<i>Diamide resistant drosophila lines do not differ in fecundity or fertility</i>	150
Fig 5.11	<i>Drosophila lines differ in larval crawling speed</i>	152
Fig 5.12	<i>Drosophila lines differ in adult climbing speed</i>	153
Fig 6.1	<i>Lack of CLR efficacy on non lepidopteran RyR channels</i>	158
Fig 6.2	<i>The 'diamide resistance region' in lepidopteran RyR</i>	163
Fig 6.3	<i>The five aa residue changes studied in this chapter</i>	164
Table 6.1	<i>PxRyR alterations and their identity in other species</i>	165
Fig 6.4	<i>Response of RFCLM-PxRyR to increasing dosage of caffeine</i>	166
Fig 6.5	<i>Concentration response RFCLM-PxRyR vs CLR and FLB</i>	168
Fig 6.6	<i>Caffeine vs Diamide response correlation</i>	170
Fig 6.7	<i>RF-PxRyR and RFCLM response to CLR exposure</i>	173
Fig 6.8	<i>Comparison of responses to 10mM caffeine</i>	174
Fig 6.9	<i>Comparison of responses to CLR dosage</i>	175
Table 6.2	<i>Comparison of responses to CLR dosage</i>	176
Fig 6.10	<i>WT-PxRyR and YF-PxRyR response to FLB</i>	177

<i>Fig 7.1</i>	<i>Positional summary of all amino acid residues studied in this thesis</i>	<i>186</i>
<i>Fig S1</i>	<i>Vector maps</i>	<i>193</i>
<i>Table S1</i>	<i>PxRyR sequencing primers</i>	<i>194</i>
<i>Table S2</i>	<i>hRyR2 sequencing primers</i>	<i>195</i>

Acknowledgements

Thanks be to Bartek Troczka for teaching me everything there was to know about ryanodine receptors, despite my chronic idiocy. And to Rafael Homem, for continually drumming the principals of scientific rigour into my skull. It is scarcely possible to be more patient or persistent than these two, and it is not an exaggeration to say that the successful completion of this thesis is owed almost entirely to their combined efforts.

Also, to Emyr Davies, my supervisor, for the huge time and effort and help given to me in writing this thesis, especially during the final months. To Martin Williamson for some light relief and to Lin Field for her unwavering support, and to all at IMB, past and present, for helping to drag me through to the other side.

To Christopher George for his cutting wit, honest words and dedication.

To Ralf Nauen for his kindness, his drive and his infectious excitement for the work that we do, and also to Ulli E-K for his patient assistance. Thanks especially to Annette Jacobs, without whose kindness and stimulating conversation, I would surely have gone insane in the cold, dark electrophysiology lab.

To all those at Rothamsted, who make it such a weird and wonderful place. To shopping trolleys, to blue vomit, to the-floor-is-liquid-nitrogen, to footballers and scythers and singers and climbers.

To the Superfriends™, for providing a collection of alternative realities, in which everything is even more terrifying, but at least PhDs don't matter.

Lastly to Chiara. For her love, interest, support, distraction and inspiration. But above all for telling me that I am good at what I do and making me believe it (against all available evidence).

Funding for this PhD was generously provided by BBRSC and Bayer CropScience.

Abbreviations

AA	Amino Acid
AI	Active ingredient
ANOVA	Analysis of Variance
bp	Base pair(s)
C	Celsius
CABI	Centre for Agriculture and Bioscience International
cDNA	complementary deoxyribonucleic acid
CDS	Coding sequence
CF	Cellfectin™
Ch	Chapter
CICR	Calcium Induced Calcium Release
CLR	Chlorantraniliprole
cm	Centimetre
CTD	C-Terminal Domain
CYA	Cyantraniliprole
DBM	Diamond-Back Moth
DNA	deoxyribonucleic acid
dNTPs	deoxyribonucleoside triphosphates
EC	Effective Concentration
EC50	Effective Concentration (50% Mortality)
ECC	Excitation Contraction Coupling
EPA	Environmental Protection Agency
FAO	Food and Agricultural Organisation
FLB	Flubendiamide
FOV	Field of View
g	Gram
gDNA	genomic deoxyribonucleic acid
h	Hour
IP3R	inositol triphosphate receptors
IPM	Integrated Pest Management
IRAC	Insecticide Resistance Action Committee
<i>kdr</i>	Knockdown resistance
L	Litre
LC	Lethal concentration
LD	Lethal dose
LSD	Least Significant Difference
mg	Milligram
min	Minute
mL	millilitre
mM	Millimolar
MOA	Mode of Action
mT	megaTonnes
N.S.	Non-Significant

ng	Nanogram
NGO	Non-Governmental Organisation
nt	Nucleotide
P450s	Cytochrome P450-dependent monooxygenase(s)
PCR	Polymerase chain reaction
PNR	Proportional Normalised Response
P_o	Channel-Open-Probability
ppb	parts per billion
ppm	parts per million
qRT-PCR	Quantitative reverse transcription polymerase chain reaction
RD	Recommended Dose
RNA	ribonucleic acid
RNAi	Ribonucleic Acid interference
RR	Resistance ratio
RyR	Ryanodine Receptor
s	Second
SE	Standard error
T-CLR	Cyclaniliprole
TET	Tetraniliprole
TM	Trans-Membrane Domain
T_m	Melting temperature
TM	Transmembrane domain
TSR	Target Site Resistance
USD	United States Dollars
μg	Microgram
μL	microliter

Chapter I: Introduction

1.1 Modern Agriculture: Feeding a growing population

Between the tropical lines of Cancer and Capricorn, a very rapid population expansion and demographic alteration is occurring. Models predict that 6 billion people will occupy this narrow region of the globe by 2050 (FAO 2009, 2017). In order to feed this population, global cereal production will need to increase by at least 0.9% each year, even if other factors remain stable (Alexandratos and Bruinsma 2012). However, crop production is likely to become more difficult as global temperatures rise, with 20 - 40% declines in yield expected in tropical regions (Battisti and Naylor 2009; Lobell et al. 2008). Negative predictions made a decade ago, regarding food availability, are now beginning to play out in reality (Zhao et al. 2017).

Yield reductions and food shortages lead to global price increases which in turn prevents market access for populations within Low Income Economies, leading to food crises and famine (Fader et al. 2016; Steinbach et al. 2015). Food crisis is strongly associated with local malcontent and rioting, which in turn ferments geopolitical instability, such that food insecurity eventually traps entire countries and regions into unending cycles of conflict (Brinkman 2011; Tsakok 2011). Food security and agricultural redundancy are critical in rescuing economies from this trap. As a growing population and a changing environment threaten caloric availability, efforts to increase agricultural efficiency have never been more important.

1.1.1 A strain on the planet

It is now clear that global heating is to some degree attributable to the agri-food industry. Almost one third of anthropogenic greenhouse gas emissions are a result of agricultural production (Bajzelj et al. 2013), with a large proportion stemming from livestock production (Herrero et al. 2016). Contribution to global warming is far from the only measure by which agriculture has impacted the planet. Topsoil depletion due to over-farming is of major concern and is starting to impact productivity and yield. Biodiversity loss due to land-usage for agriculture is also to a certain extent responsible for global reductions in key beneficial species, including

pollinators (Alexander, 2017). It is now widely recognised that agricultural methods, developed during the green revolution, are unsustainable and have resulted in ecological damage and contributed to climate change.

A key conclusion of the 2015 Paris United Nations Climate Change Conference was that Bio-Energy/Carbon-Capture-Storage (BECCS) should play an integral role in reversing anthropogenic climate change. 400-800 million additional hectares of trees should be planted in order to maintain a global temperature within 1.5°C of pre-industrial levels (IEA, 2016). By comparison, 600 million hectares is the area of additional farm land required in order to feed 10 billion humans in 2050 (Searchinger et al. 2018), based on current yields. Thus, the requirement to prevent human starvation currently directly contradicts the requirement to prevent global heating.

Therein lies a fundamental conflict, to which there is no obvious solution. Humanity will require a 'second green revolution' (Pingali, 2012) in order to match resource demands. Simultaneously, restoration of natural resources will require a focus on 'reuse, recycling, and long term design', or what has come to be known as 'circularity' [Tim Benton pers. Comm] (EMF 2019). In the current era of 'sustainable intensification', global agriculture is under pressure from all sides.

1.2 Insect control in the era of 'Sustainable Intensification'

Advances in pest control was a key element of the 20th century's 'green revolution', helping to achieve a 300% increase in crop yield with only a concomitant 30% increase in farmed land. However, despite our best efforts to date, pest insects, pathogens and weeds still reduce crop yields by around one third (Oerke, 2006). If all crop protection practises were to cease, it is estimated that we would lose upwards of 70% of crops prior to harvest (Popp et al. 2013). Insects, in particular, contribute to a large proportion of this damage. An estimated 45 million tonnes (Mt) of wheat, 50Mt of maize and 75Mt of potential rice yield is consumed each year – amounting to up to 20% of global grain yields lost in total (Deutsch et al. 2018). Furthermore, insect metabolic rates currently restrict insects in most areas of the globe but on average, crop destruction by insect pests will increase by 10-25% per degree rise in global temperature, as higher metabolic rates allow higher reproductive rates (Deutch et al, 2018). Finally, rising temperatures, coupled with ever-increasing international trade, can be expected to increase invasiveness of

crop pests, especially in the Northern Hemisphere (Biondi et al. 2018). Therefore, the need for insect control is greater now than ever.

1.2.1 Non-synthetic modes of insect control

Modern pest control falls into four broad categories: cultural and mechanical control; biological control; genetic control; and synthetic chemical control.

Cultural and mechanical control refers broadly to the steps that can be taken to create unfavourable conditions for pest insect infestations, such as manual removal of pests (All, 1999). These generally require some knowledge of insect biology and behaviour on the part of the farmer, compared to other approaches documented below. Biological control entails the use of natural insect enemies, be they an insect predator or a pathogen (Bale et al. 2008). For example, the *cry* toxins produced by *Bacillus thuringiensis*, which is a pathogen of insects, show potent insecticidal activity and have become one of the more successful biocontrol agents to date (Schnepf et al. 1998; Phipps, 2002). Genetic control at its most fundamental includes the deliberate encouragement of host-plant resistance through genetic crossing. More recent developments include a host of emerging tools, the unifying concept of which is mass-modification of insect genetic material to bring about population reduction or replacement. Gene-Drive is one such tool, in which a homing endonuclease (e.g. Cas9) copies itself, and any linked 'cargo' genes, into the opposing homologous chromosome in order to drive the gene from heterozygosity to homozygosity (Haghighat-Khah et al. 2015). This is a major upgrade to the decades-old Sterile Insect Technique, in which release of chemically sterilized insects causes population disruption (Black et al. 2011). Recent employment of gene drive in Brazil has seen populations of Zika-carrying *Aedes aegypti* being replaced by Zika-refractive mosquitoes (Buchman et al. 2019), thereby reducing cases of the Zika disease in humans. The second major development in genetic control is RNA interference (RNAi) – the dsDNA-mediated knock-down of targeted genes via hijacking of anti-viral pathways in the insect (Zhang et al. 2017). One goal is to create crops capable of defending themselves against insect herbivores by activation of such pathways to inhibit insect metabolism (Gordon and Waterhouse 2007).

A combination of cultural control, biocontrol and genetic control have the potential to revolutionise the ecological sustainability of crop defence, by reducing

destruction of non-pest insect populations, reducing reliance upon petrochemical cracking, and reduced environmental run-off of synthetic chemistry. Ironically, a major impediment to the adoption of genetic technologies is the lobbying of Non-Governmental Organisations claiming to oppose global environmental problems (France-Pressse 2016).

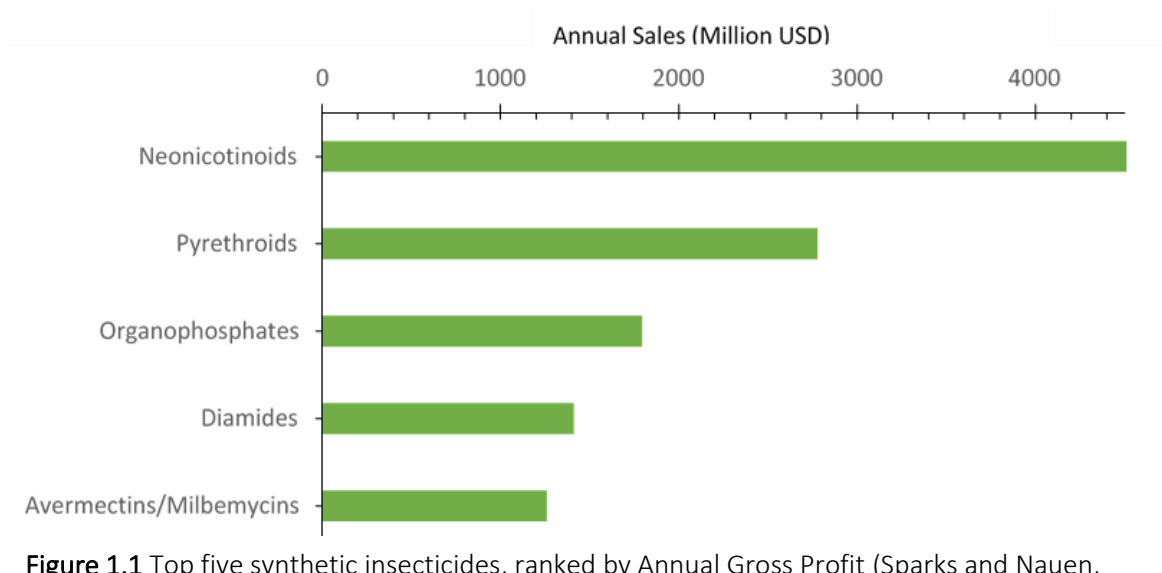


Figure 1.1 Top five synthetic insecticides, ranked by Annual Gross Profit (Sparks and Nauen, 2015)

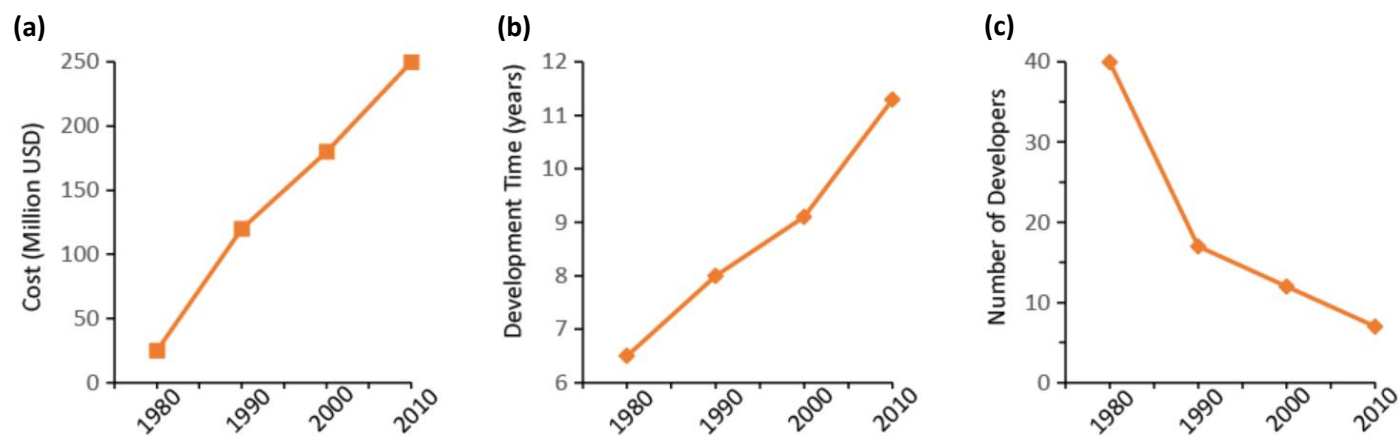


Figure 1.2 Challenges in insecticide development. Cost (a) and time (b) to bring a successful compound to market is increasing, whilst the number of individual organisations involved decreases (c). Analysis based on data reported in (Sparks and Lorschbach 2016).

1.2.2 Insecticidal Spray: There's no better way

Synthetic insecticides remain by far the most widely used control measure for insect pests. It was estimated that in 2007 the global insecticide market was worth \$8.2 Billion (Bn) USD and in 2017 that value had almost doubled to \$14.51Bn USD. By 2022, at the current growth rate, it will reach \$19.27Bn USD (AGI2527 2017). Thus, despite promising developments in alternative control methods, the insecticide market is growing faster than ever. Delayed uptake of insecticide alternatives by policy-makers, and the general public, is partially responsible for such ongoing growth, but their ability to act predictably, quickly, and effectively makes synthetic chemical pesticides a valuable asset, especially in developing countries (Sparks 2013). As GDP rises across the African and Asian sub-continent, agricultural intensification, with a heavy reliance on synthetic insecticides, is set to increase, to help fill the emerging food gap.

Mainstream modern insecticides target one of five biochemical systems: chitin synthesis; mitochondrial respiration; the voltage-gated sodium channel (Na_v); the nicotinic acetylcholine receptor (nAChR); and the γ -aminobutyric acid (GABA) receptor. Thus, the vast majority of insecticides are nerve and muscle agents (<80% by market value – calculations based on (Sparks and Nauen 2015)). Of these, the neonicotinoids, pyrethroids and organophosphates are the most widely used (Fig 1.1).

1.2.3 Strain on the Insecticide industry

It is estimated that around 600 insect and mite species are resistant to at least one class of currently used commercial compound (Bass and Field 2011), constituting something of an epidemic of resistance across almost all insecticide classes (e.g. (Bass, 2015). Therefore, insect control in the current era will focus, by necessity, on chemicals with new Modes of Action (MoAs) which are not subject to cross-resistance. There is compelling evidence that the insecticide industry is already struggling to keep up with the rise of resistance (Sparks and Lorsbach 2016). Decade on decade, the cost of bringing a compound to market increases, standing now above \$250 million USD on average (Fig 1.2a). Profit-margins may fall, as such rises threaten to out-strip the aforementioned increase in sales. Furthermore, the ability of the industry to react quickly to insect control crises is limited, with development time now averaging 10 years (Fig 1.2b). One limiting factor may be the global consolidation of insecticide developers, such that currently a small number of agri-

chemical industries are taking on the vast majority of the development work (Fig 1.2c). Such a state of affairs does not encourage the 'pivot' attitude that is required, if a greater diversity of cost-effective MoAs is to be developed (Wu et al. 2019).

Already fighting a losing battle against field-resistance, industrial agriculture today suffers from a second major issue - insecticides are in the midst of a public-relations crisis. Concern about the ecological impacts of large scale insecticide use is rising amongst the general public and policy-makers (e.g. (Pretty et al. 2018), largely due to potential damage to beneficial insects. As various global eco-systems show signs of instability, insecticides (and occasionally other chemical pesticides) are being blamed, often with minimal evidence (See Box 1.1). Pressure from non-governmental organisations (NGOs) opposing insecticide usage has been brought to bear on the pesticide industry and governments, for example, such lobbying has already resulted in certain members of the neonicotinoid insecticide class (imidacloprid being the most prominent example) being banned across Europe (EU Official, 2019).

Thus, there is an urgent need for the development of new and safer insecticidal chemistries, with improved specificity and toxicological profiles, in order to meet public expectations and reduce off-target mortality. MoA diversity ideally ensures that resistance build-up never occurs (Sparks and Nauen, 2015). In the meantime, Integrated Pest Management (IPM) is accepted as the ideal model of insect control that should be promoted going forward. The spread of resistance can potentially be (locally) contained by the current trend for expansion in the deployment of advanced monitoring techniques, thereby supplying timely information to growers. To this end, resistance mechanisms must be understood, and insecticide modes of action classified.

The insecticide industry has historically been a key driver, but also a key beneficiary of the green revolution in agriculture. Today, both the industry, and agriculture itself, stand at a crossroads. If they are to survive in this confrontational climate, all parties must embrace collaboration, novel approaches to crop defence, and most importantly a commitment to sustainability in all matters.

Box 1.1: Insect ‘Armageddon’ – Fact vs Fiction and what this means for modern agriculture

A slew of recent papers report insect-decline on a ‘catastrophic’ scale (Janzen and Hallwachs 2019). These include reported declines in insect biomass of 75% (Hallman and al 2017), 80% (Loboda et al. 2017), or over 95% (Sanchez-Bayo and Wyckhuys 2019), and a claim that total global insect eradication could occur within a century (Lister and Garcia 2018). It must be acknowledged that massive insect-decline probably is occurring: taken together, studies consistently report a reduction in insect-biomass at least as significant as that seen across vertebrate taxa, if not orders of magnitude more severe. Such reductions in insect populations are a threat to modern agriculture, and humanity as a whole. However, it must also be acknowledged that there are major and compromising flaws in some of the reports of insect decline.

For example, the latest meta-analysis of published data, guarantees a negative view by using the search terms ‘[insect*] AND [decline*]’(Lister and Garcia 2018). For this, and many other reasons, estimations of population decline therein are simply unusable. Of other recent studies, three ((Janzen and Hallwachs 2019), (Hallman and al 2017), (Loboda et al. 2017) suffer from one or more sampling biases that hamper entomological studies in general:

- Non replicable ‘opportunistic’ sampling is sometimes susceptible to such heavy sampling bias as to be almost unusable (e.g. (van Strien et al. 2019).
- Infrequent and inconsistent sampling prevents interpretation of natural fluctuations in populations, this makes drawing conclusions from long-term studies of insects challenging (Fox et al. 2018).

See (Thomas et al. 2019) and Shortall et al (in-press) for a more complete review. Scant few data sets have been collected in a controlled manner (e.g. purpose-built sampling traps ensuring consistent methodology) with reasonable sampling rates (at-least yearly, over a 10-year period). Those that have, tend to report reductions in community biomass, often partially balanced by increases in common-species biomass. For example, Shortall et al. 2009 reported declines in flying insect biomass at (just) one of four sample sites over a 30-year period (Shortall and Harrington 2009). Fox et al. 2014 reported that, whilst 260 British moth species declined, 160 increased significantly. However, many excellent studies continue to report heavy declines (e.g. (Loboda et al. 2017).

It is clear that insect biomass is declining alarmingly in some regions, but it is not so clear what the underlying causes of such decline actually are. Logically, application of anti-insect chemistry is likely to play a role (Ewald et al. 2015), however all evidence points to reduction and simplification of habitat due to monocultural agriculture as being a far greater risk factor for decline (Lichtenberg et al. 2017).

Insect decline is fundamentally a symptom of a system designed to promote the existence of humans. The impossible task at hand is to prevent insect decline without compromising human food and new high value (energy / nutraceutical) crop production, which may require expropriating additional natural habitat thus exacerbating insect decline.

Against the backdrop of escalating resistance episodes, as described above, a welcome addition to the insecticidal arsenal duly arrived. Diamides are a relatively new class of synthetic compounds, which act on the nerve-muscle boundary, causing contraction and paralysis of insect muscle cells. Control is highly potent and specific against lepidopteran and other insect pests. Members of the class vary in their spectrum of control, but the majority of these insecticides display extremely clean toxicological profiles.

The following two sections will cover the commercial development of the first three diamide insecticides, currently on the market, as well as those due for future release. Mode of Action will be discussed in the context of the protein target of this insecticide, including its biology and regulation. The chapter will conclude with the challenges facing the diamide class, including field-evolved resistance and the drive toward toxicological perfection.

1.3.1 A New Hope

Diamides have been a stunning commercial success. Having an entirely novel MoA, they quickly became the preferred means of dealing with pests that had developed resistance to other modes of action (Cordova et al. 2006). The first product to be marketed was flubendiamide (FLB) (in 2007), which was co-developed by Nihon Nohyaku Co., Ltd and Bayer CropScience (Ebbinghaus-Kintscher et al. 2007). This was followed a year later by chlorantraniliprole (CLR), and later cyantraniliprole (CYA), developed by DuPont (Lahm et al. 2007) (See Box 1.2). Annually, diamide sales are currently worth upwards of \$1.4Bn USD, making them the fourth most valuable insecticide class (Fig 1.1).

1.3.2 Flubendiamide: An exceptionally selective insecticide

After its release in 2007, FLB achieved rapid commercial success, largely due to its high potency against generally hard-to-kill insects (Lahm et al. 2009). Lepidopteran species, which are primarily targeted by FLB, are known to develop resistance to insecticides at an alarming rate, discussed further in Section 1.4, below. For example, the diamondback moth (DBM, *Plutella xylostella*), a prominent pest of Brassicaceae, has gained notoriety for its resistance against almost all available insecticidal treatments (IRAC 2019). However, initial bioassays on *P. xylostella* larvae resistant to pyrethroids, organo-phosphates, carbamates and benzoylphenylurea showed that there was no cross resistance to FLB, giving a level

of control equal to the susceptible reference strain (Toshinishi 2005). The effective concentration for disabling half of this *P. xylostella* population (EC₅₀) was stunningly low, at just 0.004ppm.

The potency of this compound against damaging crop pests gives immense value (Hamaguchi et al. 2012), but it is the selectivity that makes it exceptional. Bioassays against common insects showed that at concentrations deadly to Lepidoptera, other insects were entirely unharmed: – EC₅₀ values for various beetles and hemipterans were on average >5000-fold higher than those for lepidopterans (Hall 2007). This is matched by very low mammalian toxicity, with an acute LD₅₀ in rats of >2000 mg/kg (Toshinishi 2005).

The high specificity of FLB towards insects was also confirmed by assays on mammalian cell lines (Ebbinghaus-Kintscher et al. 2006; Ebbinghaus-Kintscher et al. 2007). Ecotoxicological studies found no acute toxicity towards rats and birds (2,000 mg/kg) and no acute toxicity towards freshwater fish when tested at the limit of aqueous solubility (29.8 ppb) (Hall 2007).

In an ideal world, insecticides should control their target pest without impacting the existence of others – they should be ‘deadly to the pest and harmless to the rest’. This compound is a gold standard in this context and would make an excellent model for development of novel chemistry. Only with an arsenal of insecticides as potent and as specific as FLB can humans hope to protect their food supply without harming their ecological environment.

1.3.3 Chlorantraniliprole and Cyantraniliprole: A wider range of control
CLR, the second diamide to be commercially released, is an anthranilamide. Thus, it differs from the phthalic FLB by reversal of the central amide bond. It also differs in the range of insecticidal activity offered, giving good control not only of Lepidoptera but also Coleoptera (beetles), Diptera (flies) and Isoptera (termites) species (Lahm et al. 2009). Despite the broader range of insect control, the excellent mammalian toxicological profile is maintained. In cell lines, human RyR2 is activated with 2000-fold decreased potency in comparison to insect channels, with an LD₅₀ value of acute oral toxicity of >5000mg/kg of body weight for vertebrates (Lahm et al. 2009).

Box 1.2: Early development of diamides

1993 – Nihon Nohyaku Co.,Ltd begin investigating the insecticidal properties of protoporphyrinogen-IX-oxidase inhibitors. Some members of this newly developed herbicide class showed insecticidal activity (Jeanguenat 2013).

1998 – This investigation culminated in the discovery of phthalamides as highly active anti-lepidopteran compounds (Toshinishi 2005).

2006 – FLB, the most successful of the phthalamides, was brought to market after a joint development between Nihon Nohyaku and Bayer CropScience (Ebbinghaus-Kintscher et al. 2007).

2007 – Calcium release imaging on Sf9 cells expressing *Drosophila melanogaster* calcium ion channel, the Ryanodine Receptor, revealed this to be the diamide target (Ebbinghaus-Kintscher et al. 2007).

2008 – CLR is developed and brought to market by DuPont. Reversal of the central amide (NH₂O) bond puts CLR into a new diamide class; the first of the anthranilamides. Simplification of the heptafluoro (C₂F₇) group on FLB into a lone chloride (Cl), as well as insertion of a chloropyridine (C₆Cl) in place of the large methyl *o*-substituent group (C₅SO₂), allows this compound to achieve strong activity against a range of insect pests (Selby 2016).

2012 – Cyantraniliprole (DuPont) first commercial application (Birkett 2012). Replacing the chloride group with a nitrile (CN) group at C4 of the anthranilimide ring gives improved systemic properties, such as lower logP and higher water solubility which aid in plant uptake and translocation.

2017 – Cyclaniliprole (ISK bioscience) is approved in US, Canada, Japan and Korea ‘for the control or suppression of various insect pests on a range of fruit, vegetable and tree nut crops’ (ISKBC 2017).

2019 – Tetraniliprole (Bayer CropScience) is approved in Korea for use as a broad spectrum foliar, drip, drench or seed treatment (Ralf Nauen pers. Comm).

Finally, CYA was the third diamide to be released. In comparison with CLR, a substitution of the chloride group for a cyanide group confers a further broadening of effectiveness. Solubility is also improved, allowing the compound to move through the plant xylem, such that it can be applied as a systemic insecticide (Selby et al. 2013). This allows it to target chewing and sucking

pests such as Coleoptera and Hemiptera – achieving up to 10-fold improvement in activity against the latter (Foster et al. 2012). However, activity against most lepidopteran species is reduced in comparison to CLR, whilst coleopteran activity is generally equal (Selby et al. 2017).

1.3.4 New diamide actives under development

With the expressed aim of improving upon existing molecules, the search for environmentally benign diamides, with high activity and low toxicity, continues (Zhao et al. 2012). Iterative substitution of almost every available active site on the molecule has taken place, with attempted additions of sulfoxamines (Gnamm et al. 2012), various ethers (Zhao et al. 2012), pyrazoles (Wang et al. 2013a), thiadiazoles, naphthalenes and more. From this effort, some excellent molecules present themselves, with studies claiming to improve upon activity of first and second generation anthranilimides by more than 5-fold (Zhao et al. 2012). Of these, at least two have been taken forward for commercialisation, tetraniliprole (Bayer CropScience) and cyclaniliprole (ISK bioscience). It remains to be seen which of the other candidates are sufficiently effective to compete with those diamides already in the market.

Much can be learnt from comparison of the commercialisation candidates presented here. Some studies have attempted to find patterns or periodicities in activity. For example, during CLR modification, increasing electronegativity (Br→Cl→F) was associated with increased biological activity on both the upper chloride and the lower bromide group (Liu et al. 2018). A similar pattern is seen in the development of tetraniliprole (Ralf Nauen 2019, unpublished), in which reductions in group size, as well as increases in electronegativity, tend to correlate with higher potency. Such a pattern has been supported by several studies regarding other insecticides (Jeschke 2010).

Cyclaniliprole (ISK Biosciences) was the first of a new era of diamides to reach market, applied for the first time in South Korea in 2017. Based on the structure of CLR, this compound possesses a cyclopropane group attached to one of the amides, as well as an additional bromide group (Fig 1.3). These additions are both designed to increase the electronegativity of the structure, with bond-strain in the cyclopropane increasing electron density in that region. According to the developers, it is for 'control of various insect pests on a range of fruit, vegetable and tree nut crops' (ISKBC 2017). Aqueous solubility is lower than that of CLR, possibly due to its larger size, which limits this compound to foliar application. Baseline effective concentration against lepidopteran species is very similar to that of the other diamides – an LC50 of 0.03ppm was found in one independent study

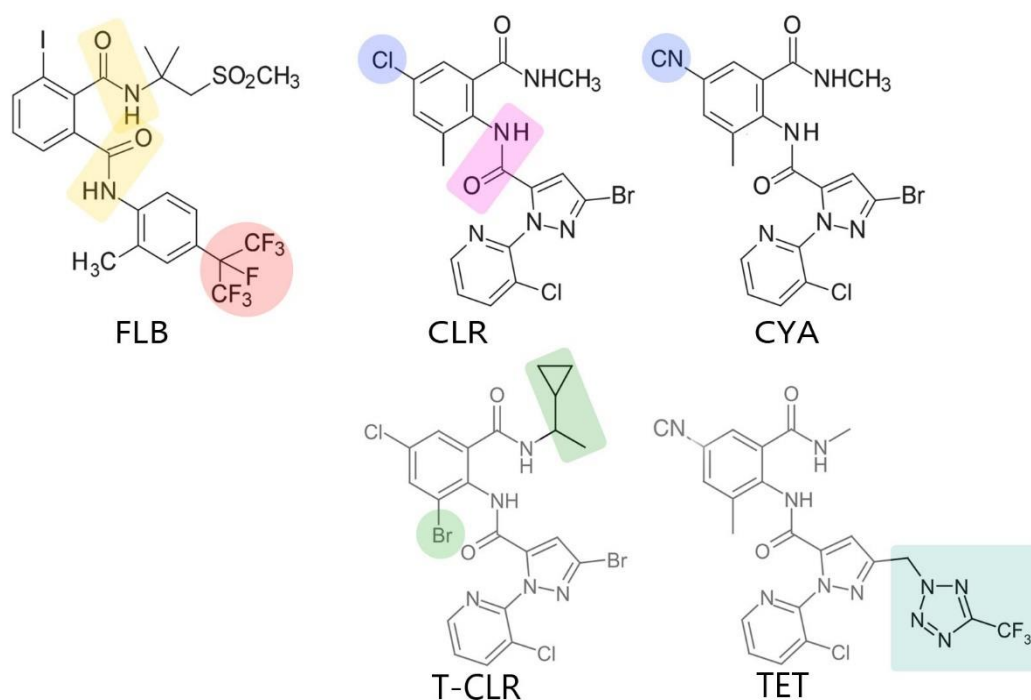


Figure 1.3. Diamides derive their name from the double amide groups, located on positions 1 and 2 (yellow) of the central benzenoid ring. Flubendiamide (FLB) is phthalic and its name is derived from the terminal hepta-floryl group (red). Chlorantraniliprole (CLR) is anthranilic, differing from FLB by a reversal of the central amide bond (pink). Cyantraniliprole (CYA) possesses an almost identical structure to CLR but differs in the replacement of a chlorine group with a cyanide group (blue). Cyclaniliprole (T-CLR) possesses an almost identical structure to CLR apart from the substitution of a methyl group for a bromide group (green) and the addition of a cyclopropane group (green). Tetraniliprole (TET), is the newest diamide release, and differs from CYA by the substitution of the bromide group with a large trifluoromethyl-tetrazole group.

(Cho and et al 2018). Finally, tetraniliprole (Bayer CropScience) is the latest addition to the diamide arsenal, due for release in 2019. This is designed as a broad-spectrum, multi-use compound for foliar applications or in drench or drip applications and as a seed treatment. Derived from CYA, the molecule maintains its cyanide group, and with it, some of the characteristic systemicity of that compound. Uniquely, tetraniliprole possesses a trifluoro-methyl azole ring not seen in any other commercial pesticide (Ralf Nauen 2019, unpublished). Both of these novel compounds have excellent safety ratings against vertebrates, for example >2000mg/kg toxicity on birds, as has become the hallmark of diamides in general (EPA 2019). On the other hand, studies on beneficial insect toxicity are yet to be undertaken.

New entries to the diamide market must address at least one of the two major issues in IPM today: 1. toxicity to beneficial insects and 2. evolution of insecticide resistance. Thus, new releases should aim either for high specificity, following the example of FLB, or they should aim to break resistance. Increased lepidopteran activity is no longer a useful goal for novel diamides.

1.4 The rise of resistance to diamide insecticides

Despite the excellent characteristics of diamide insecticides, resistance to their action evolved just 18 months after their market debut (Trocza et al. 2012). The first control failures occurred in the Philippines in a population of DBM (*P. xylostella*) and was quickly followed by further episodes in nearby locations. A decade on from those first reports of diamide resistance in *Plutella* (Trocza et al. 2012), resistance has evolved independently in at least nine lepidopteran species (see below). Subsequent expansion of some of these species out of their native range has been a major factor in the spread of diamide resistance, with several species making the transition from regional to global pest status. An overview of the current global state of diamide control efficacy is the focus of this section.

1.4.1 *Spodoptera frugiperda* and other Noctuidae

The fall armyworm, *Spodoptera frugiperda*, is a highly destructive pest of maize, frequently responsible for causing 40-70% yield loss (Wyckhuys and O'Neil 2006). The caterpillars can additionally feed on at-least 186 other plant species (Montezano et al. 2018), making this a broad-ranging and highly adaptable insect. Native to Central and South America, year-round populations extend southward to Brazil and Argentina, whilst migratory populations make their way annually from the Caribbean up the Eastern coast of the USA, as far north as Canada (Westbrook et al. 2016). However, the pest has recently spread outside of this range in a dramatic expansion that exemplifies the worrisome ease of movement of invasive species in the modern world (Fig 1.4).

In Brazil, where insecticides are applied frequently to control lepidopteran pests, *S. frugiperda* is resistant to most synthetic chemistries. Diamide insecticides therefore have become an important element of integrated pest management (IPM) (Bolzan et al. 2019). Recently however, resistance to CLR was rapidly selected for in a field strain collected in Correntina, Bahia state, suggesting the presence of resistance alleles in the field (Boaventura et al. 2019). At the same time, 4000km North,

farmers in Puerto Rico were reporting reduced diamide control efficacy, with RRs of 160-fold against CLR and 500-fold against FLB being documented. Maize yields in these regions are comparably higher with respect to other South American nations (FAO 2019), which is most likely a reflection of the more intense insecticide application regimes in Brazil. Both *S. frugiperda* populations had previously developed Bt resistance, as reported in 2014, suggesting that the management practises and ecology of these populations is potentially conducive to resistance development (Boaventura et al. 2019). As of 2016, actual control failure likelihood remained low, with the LD80 still far below Recommended Dose (RD) for CLR, suggesting that resistance spread could be delayed if the correct IRM strategies were implemented.

As diamide resistance was emerging over its native range, *S. frugiperda* populations were about to spread and have a major impact elsewhere. The moth was detected in Ghana and Togo (West Africa) in early 2016 (Nagoshi et al. 2017), heralding the start of an overseas invasion and expansion of unprecedented speed and scale, which would end with populations distributed across all the major maize producing regions of the globe. Barcoding analysis shows that the invaders are derived from the Florida genepool, a migratory population whose range covers the USA, and extends south down to Puerto Rico (Nagoshi et al. 2017). Suspected to have been carried in the luggage-hold aboard a commercial aircraft, the moths quickly spread, sweeping across most of sub-Saharan Africa within just 16 months (Stokstad, 2017). Sub-Saharan Africa was an ideal environment for moth expansion, with an average temperature well within its development range of 25-33°C and medium to low rainfall for much of the year (Early et al. 2018). The moth's capacity to migrate thousands of kilometres on high-altitude winds allowed it to rapidly colonise the large tracts of open plains, which provided excellent rearing grounds (Westbrook et al. 2016). After 2 years, it would inhabit 44 countries in Africa with permanent year-round populations (CABI 2019). The spread across Africa had been accurately predicted by a computational model, based on biotic, abiotic and human factors (Early et al. 2018). The same model warned that India would be the next target of invasion, and prescribed monitoring procedures to prevent a repetition of the airline-assisted route.

In May 2018, *S. frugiperda* was detected in Karnataka, India (Sharanabasappa and et al 2018). From there, it spreads east into Myanmar and Thailand and, in January

2019, finally reached China. By April 2019 it had reached the edge of China's Corn-Belt, which runs North-East from Hunan ((NATESC) 2019), with predictions of a very rapid North-Easterly expansion (Li and et al. 2019; Ma et al. 2019). As of July, the pest had already spread to 20 provinces, with high infestation levels in the sweet-corn producing southern regions (Ralf Nauen pers. comm). It was also recorded, for the first time, in Kagoshima prefecture, Japan. Communications indicate that diamide, pyrethroid and emamectin benzoate sprays all currently remain effective in China and are being recommended in the emergency control guidelines issued by the Ministry of Agriculture and Rural Affairs (MARA) (Ralf Nauen pers. comm). The National Agro-technical Extension and Service Centre (NATESC) has additionally established geographically specific control strategies including weekly forecasts and monitoring, biocontrol and potential chemical seed treatment.

Pinpointing the global spread's origin to the *S. frugiperda* Florida population raised the possibility that the African invaders may have been resistant to diamides (Nagoshi et al. 2017). Very few studies have reported on insecticide control efficacy since the spread. One study in Ethiopia reported close to base-line susceptibility toward diamides and several other insecticide classes (Sisay et al. 2019). If true, this is extremely fortunate, and is probably accounted for by an extreme genetic bottleneck in the founders of the Afro-Asian population, in which insufficient genetic diversity was present for resistance to emerge (Day et al. 2017). Organophosphates and pyrethroids are the primary method of lepidopteran control across the continent, which may help to slow the development of diamide resistance (Day et al. 2017). Two factors may increase the probability of resistance emergence now that the species has reached South-East Asia. First, diamide application in this area is traditionally high, whilst IPM practices have in the past been poor (Trocza et al. 2016). Second, this region harbours beet armyworm, *Spodoptera exigua* a relative of *S. frugiperda*, and the track record of resistance development for this other noctuid pest provides a worrying indication of what may be in store (Che et al. 2013).

The beet armyworm is a generalist pest, capable of targeting cereals, legumes (beans, peas), solanacea (potatoes, tomatoes), cotton, tobacco and cannabis crops. Originating in East Asia, and reaching the Americas in the late 19th century, *S. exigua* is now a worldwide pest (Capinera 1999). As with other lepidopterans, this pest has evolved resistance to most approved products currently on the market (Che et al.

2013). It took just a few years for borderline control failures involving diamide insecticides to emerge in East Asia, with farmers in Jiangsu, China reporting a 44-fold CLR resistance in 2010 (Lai et al. 2011; Che et al. 2013). By 2018 resistance had increased to 150-fold and spread to Shandong (Zuo and al. 2019). Now, *S. frugiperda* is predicted to be heading toward the same area. Further east, in South Korea, extremely potent, 2500-fold CLR resistance has arisen in beet armyworm. In 2014, *S. exigua* resistance to diamides in South Korea had been noted as minimal, therefore this case represents a prime example of the rate at which Lepidoptera, and noctuids in particular, are capable of adapting to diamide exposure (Cho and et al 2018). Finally, it is notable that, of the Noctuidae, *Spodoptera litura* has yet to develop meaningful diamide resistance. Reports from Southern China of CLR resistance in 2012 did not develop into a lasting crisis, with resistance in some regions returning to near-baseline by 2015 (Su et al. 2012)(Sang et al. 2016).

1.4.2 *Tuta absoluta*

The tomato pinworm, *Tuta absoluta*, targets tomato crops through leaf mining and fruit infestation, although it can prosper on other solanaceous species such as potato and nightshade. Yield losses on tomatoes have reached 100% where control has been inadequate (Desneux et al. 2010). In tomato plants, colonisation occurs early, meaning damage prevention requires a fast-acting means of control (Silva et al. 2011). However, as against other moth species, a heavy reliance on diamide insecticides has accelerated resistance development, especially as other MOAs had already lost efficacy and therefore were not available for rotation (Guedes et al. 2019); (Silva et al. 2011). In a survey carried out in 2011, diamides provided excellent levels of control against Brazilian populations, with FLB LD50 at less than 0.1mg/L - 0.25mg/L (Campos et al. 2015). By 2014, high levels of resistance was present across the country, reaching >100,000-fold in Pesqueira and America Dourada (Silva et al. 2016).

As with other South American-derived pests, the optimal developmental temperature in *T. absoluta* is high; around 30°C (Mohamadi et al. 2017). Capable of producing up to 10 generations per year in tropical climates and under greenhouse conditions, this pest is adapted to invade. Furthermore, unlike *Spodoptera*, *Tuta* is capable of surviving short periods of near-freezing temperatures, potentially opening its range to a more northerly expansion (Biondi et al. 2018).

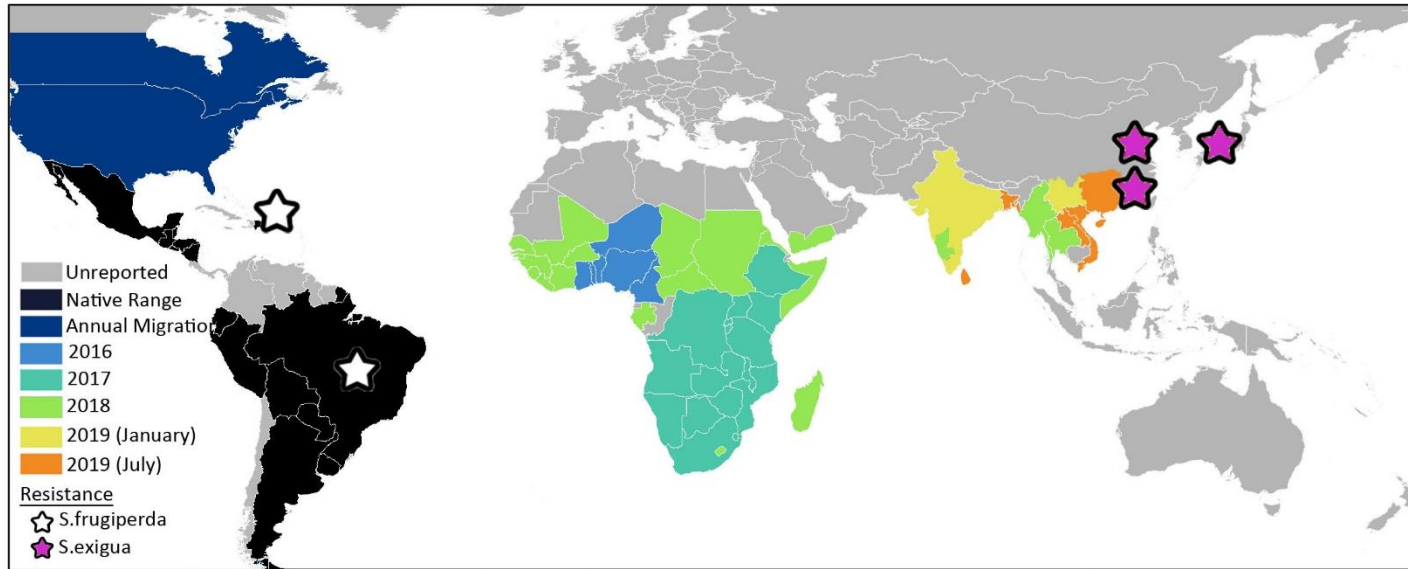


Figure 1.4

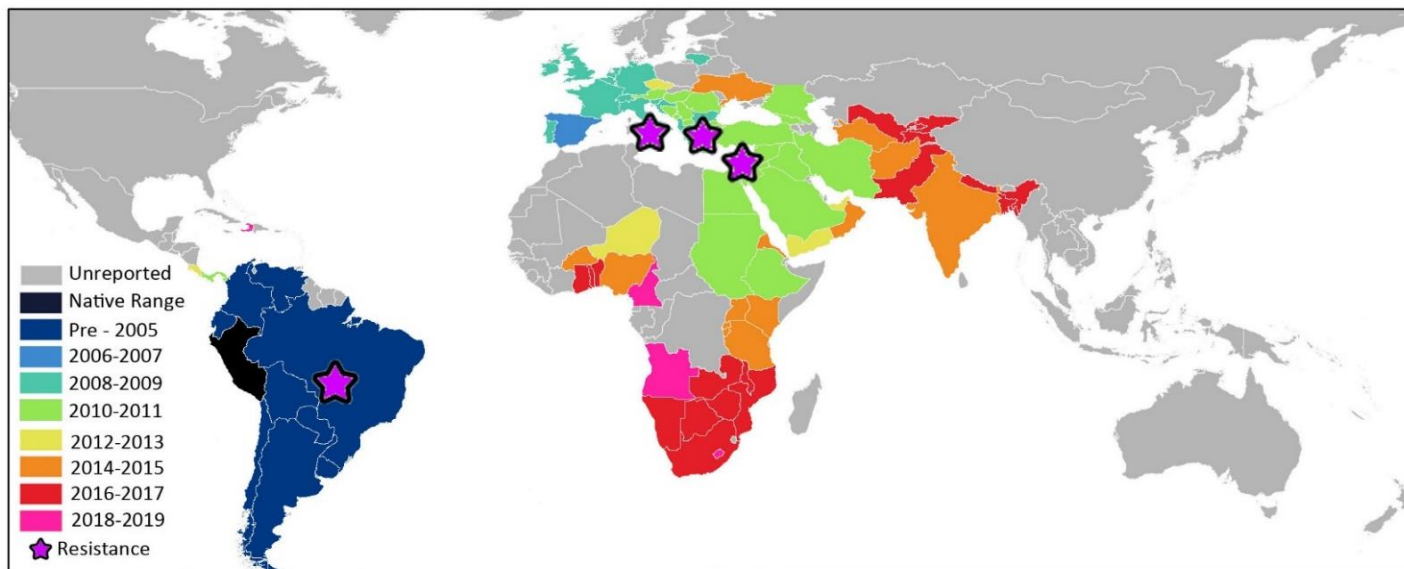


Figure 1.5

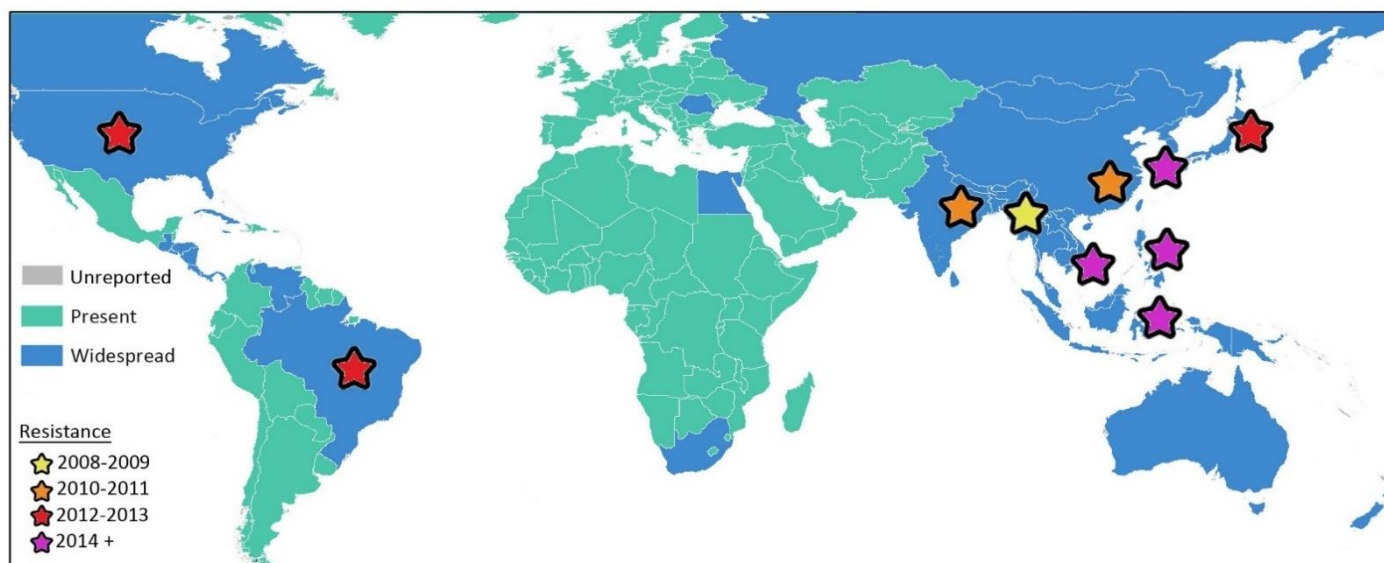


Figure 1.6

Figure 1.4 Transnational spread of *Spodoptera frugiperda*, with diamide resistance episodes of *S. frugiperda* and *S. exigua* labelled. Diamide resistance confirmed in Brazil and Costa Rica for *S. frugiperda*; in Shandong, Jiangsu (China) and South Korea for *S. exigua*. Layout from (Biondi et al. 2018); Data from references in text and CABI invasive pest monitoring.

Figure 1.5 Transnational spread of *Tuta absoluta*, with diamide resistance episodes labelled. Diamide resistance confirmed in Brazil, Italy, Greece and Israel. Layout from (Biondi et al. 2018); Distribution data from references in text and CABI invasive pest monitoring; Resistance data from (Roditakis and . 2018) and other references in text.

Figure 1.6 Global distribution of *Plutella xylostella* with diamide resistance episodes labelled. Diamide resistance confirmed in Philippines, Thailand, India, China, Brazil, USA, Japan, Korea, Indonesia, Vietnam. Layout from (Biondi et al. 2018); Distribution data from references in text and CABI invasive pest monitoring; Resistance data from (Troccka et al. 2012) and other references in text.

In 2006, *T. absoluta* was detected in Spain, having spread from a Chilean population (Biondi et al. 2018). Subsequent expansion down the coastal regions of Southern Europe was rapid. Collectively, Italy, Spain, Portugal and Greece produce some 15MegaTonnes (mT) of tomatoes (2017 data), providing ample feed-stock for the new invader (FAO 2019). Migration further northward was aided by greenhouse occupation. The Netherlands produces 0.9mT of tomatoes almost entirely under controlled environments, occupation of which seems to have allowed *T. absoluta* populations to expand year-round in otherwise inhospitable northern latitudes (Van Damme et al. 2015). The rapid and immediate threat to European tomato production, and lack of alternative management strategies, prompted a heavy reliance on diamide applications (Desneux et al. 2010). The Chilean population that invaded Europe was already known to be resistant to pyrethroids and organophosphates (Silva et al. 2011). Unsurprisingly, diamide resistance development in Brazil was soon mirrored by resistance in Europe. As of 2013, highly resistant tomato leaf miner populations had been identified in greenhouses in southern Italy (Roditakis et al. 2015). A year later, CLR resistance was widespread across Italy, causing severe control failures in Sicily and the South (RR 1402-fold and 706-fold, respectively). *T. absoluta* in Greece remained susceptible until 2015, when a Cretan population quickly developed >3200-fold resistance (Roditakis and . 2018).

By this point, other populations of *T. absoluta* had spread across Europe and on to Africa and Asia. In 2008, the coastal route had taken them to Morocco, and east to Turkey by 2009. From there, it was predicted that they would spread to Sub-Saharan Africa and across the rest of Asia (Desneux et al. 2010). This forewarning did not prevent their onward expansion, however, and the pest reached South Africa (Sylla et al. 2017) and India (Han et al. 2018) in 2016. The resistance status of the African and East Asian populations is not clear, as they presumably disengaged from gene-flow with the European population before the latter developed resistance. Very severe control failures registered in Israel in 2015, with 22,573-fold resistance against CLR, may be an independent episode distinct from that of the somewhat milder European resistance (Roditakis and . 2018).

In the space of 10 years, a little known tomato-pest, which was present in just 3% of global regions dedicated to tomato production, became a menace to 60% of worldwide tomato production (Fig 1.5) (Biondi et al. 2018). Forecasts now look

anxiously toward future invasions. Mexico produces 2mT of tomatoes per year, mostly under controlled environments, making it an ideal *Tuta* target (Nations 2019). However, tomato is not extensively grown in south-central America, which currently provides a 4000km barrier between Mexico and California and moth populations in Columbia, Ecuador and Peru, meaning that any jump would have to happen via commercial transport or trade. The risk is that, if this does occur, invasion of the extensive Californian tomato vines from Mexico will be almost immediate, as 95% of Mexican tomatoes are exported directly to the USA. Lastly, *T. absoluta* will very likely invade China. Producing almost a third of the world's tomatoes in 2017, and with sub-tropical climates in southern regions, China would be an excellent habitat for this pest. India has already been invaded, and overland vegetable trade between India and China is extensive, suggesting that it is only a matter of time before *T. absoluta* arrives in China. However, the Chinese government have taken extensive measures to prevent such a circumstance, monitoring for the pest at 41,000 stations countrywide, as well as the strategic deployment of more targeted surveillance strategies by the Chinese Department of Biological invasions (DBI) (Xian et al. 2017).

1.4.3 Diamide Resistance in other Lepidopteran Species

Resistance in *Spodoptera* and *Tuta* species poses a phenomenal risk to the associated crops in global agricultural systems. However, far from being exclusive to those species, damaging levels of diamide resistance have also been detected in *Adoxophyes honmai* (tea tortrix), *Chilo suppressalis* (rice stem borer), *Helicoverpa armigera* (Old world bollworm) and *Plutella xylostella* as will be covered below (Uchiyama and Ozawa 2014; IRAC 2014). Indications of low levels of resistance have also been reported for *Cnaphalocrocis medinalis* (rice leafroller) (Zhang et al. 2014), *Choristoneura rosaceana* (oblique banded leaf roller) (Sial and Brunner 2012) and *Chrysodeixis includens* (soybean looper) (Owen et al. 2013), but will not be covered further here as they do not as yet compromise diamide field efficacy.

A. honmai, the tea tortrix, is a leaf boring pest of high-value crops such as tea, coffee, tobacco, citrus and cacao (CABI 2019). Whilst control via the parasitic wasp *Macrocentrus homonae* is highly effective in Sri Lanka and India, insecticide application is required outside of this range. Diamide efficacy on *A. honmai* was tracked over a period of six years following this insecticides introduction in Japan, with enlightening results (Uchiyama and Ozawa 2014). Applying FLB at the RD of

48ppm gave 96% mortality in 2007, with mortality rates declining only gradually over the following year. Between 2009-2010 mortality dropped suddenly to just 52%. Application of insecticide at sub-80% mortality dosage (LD80) is associated with a dramatically increased probability of resistance emergence, which probably explains this pattern of gradual, followed by sudden, resistance (Silva et al. 2011). In this case, resistance severity continued to increase in the following years, reaching ratios of 105-fold (CLR) and 77-fold (FLB).

C. suppressalis is a devastating pest of rice, boring into the plant stem to cause 'dead heart', whereby the stem borer larvae kill the growing points of young shoots and surrounding leaves. Yield losses have been known to reach 100% (BAYER 2019) as the upper parts of the plant die off, leaves fall and the head becomes shredded. Believed to have originated in East Asia, *C. suppressalis* spread across the Pacific islands, down to Australia, and also west across the Silk Road and into southern Europe. It has thus colonised 84% of the world's rice (by yield, (Nations 2019)), with West Africa and South America the only major rice producing regions left untouched. In an attempt to halt the damage, insecticides have been frequently applied, which has selected for resistance against organophosphates, fiproles and cartap (Yao and et al; 2017). The first wave of diamides were registered in China in 2008, with baseline susceptibilities of 0.1mg/l (FLB) and 1.5mg/L (CLR) (Wu et al. 2014; Gao et al. 2013). Resistance in *C. suppressalis* was first detected in Hubei in 2013 (Committee 2014). Gradual declines in field efficacy followed in eastern China (spanning Hunan, Zheijiang and Shandong) in 2014, when RR's of 77.6 (CLR) and 42.6 (FLB) were recorded. Resistance values remained largely constant through 2015 (Lu et al. 2017), increasing to RR of 250 (CLR) by the end of 2016 in Jiangxi (Sun et al. 2018). Resistance in *Chilo* has remained moderate and constant over the past half-decade, with resistant moths remaining (at last check) at least partially susceptible (Sun et al. 2018). By comparison, most other episodes of resistance detailed in this section quickly escalated into complete control failure.

H. armigera, the Old World bollworm, is a broad range pest that causes especially severe damage to tomato, soybean, corn and cotton crops (Cunningham and Zalucki 2014). A potent combination of physiological characteristics, including high fecundity (700 eggs/female), migrational range (1000km/generation), facultative diapause capability and drought tolerance, give this pest high invasive capacity across a wide latitude (thoroughly reviewed in (Tembrock et al. 2019)). Ranging

globally from Oceania, Asia, Europe and Africa, the Old-World bollworm recently expanded its range dramatically by colonising the New World (CABI 2019). Detected in Bahia, Brazil, in 2013 (Tay et al. 2013), *H. armigera* is now present in Paraguay, Uruguay, Argentina, Bolivia and its presence suspected in Peru, Surinam and the Dominican Republic (Gilligan et al. 2015). The risk of spread into North America is high, having already reached Puerto Rico, and multiple border incursions already detected in Florida (Kriticos et al. 2015). *H. armigera* is known to be resistant to a wide range of synthetic insecticides (McCaffery 1998). Furthermore, hybridisation with *Helicoverpa zea*, a North American close-cousin of *H. armigera*, is expected to boost gene-pool size and thereby increase the adaptive capacity of both species to insecticide spray (Anderson et al. 2019). In response to this threat, multiple teams have established baseline susceptibility measurements against the anthranilamides, CLR (Liu et al. 2017) and CYA (Bird 2016), however bioassays are yet to report any indication of diamide resistance. The Ryanodine Receptor (RyR) gene has already been cloned for this species (Wang et al. 2013b) offering the potential for proactive resistance detection measures based on RyR sequencing. Frequent monitoring of diamide susceptibility, especially in Brazilian populations is recommended, both due to the history of lepidopteran diamide resistance development in this region, and due to the extensive tomato crop, which is a primary food source for *H. armigera* (Pratissoli et al. 2015).

1.4.4 *Plutella xylostella*

One pest so far omitted from this discussion is *Plutella xylostella*, and it is pest without which no bona fide discussion of insecticide resistance can take place. *P. xylostella* is a billion-dollar worldwide pest of cruciferous vegetables. Attempts to control the larvae, and to prevent their notoriously damaging tunnelling activity, equates to a gross annual expenditure of up to \$2.3bn US. Despite these measures, *Plutella* succeeds in causing US \$2.7bn of annual yield losses due to spoilage and crop damage (Zalucki et al. 2012). With historical resistance to almost all synthetic insecticides, this is arguably the most resistant insect species on the planet (Whalon M et al. 2016; Sparks and Nauen 2015). Assumed to have originated in the brassica homelands of Europe or Southern Africa, *P. xylostella* now makes its presence felt worldwide (Kfir 1998).

It was towards this species in particular that diamide insecticides were initially targeted. Breaking the insecticide resistance epidemic was an urgent necessity in

China, where 46% of the world's brassica crops are produced (FAO 2019). An added bonus was the extremely high activity of FLB against *P. xylostella* (Ebbinghaus-Kintscher et al. 2007) (Troczka et al. 2016). FLB was first launched in the Philippines in 2006 and subsequently in Thailand in May 2007. However, by December 2008 resistance would develop and control efficacy would be dramatically reduced in both countries. Whilst early cases of resistance merely bordered on control failure (e.g. FLB 66.3-fold), resistance ratios quickly rose from 407-fold in Sai Noi, to 4817-fold in Tha Muang, up to 26,602-fold in Pathum Thani (Troczka et al. 2016).

Episodes of resistance did not for long remain isolated to the Philippines and Thailand. In 2011, reports of resistance came from India and China (Troczka et al. 2016), followed by a rapid spread west across Asia. By 2013, resistance had reached Japan, but it also emerged, possibly independently, across the Atlantic in Brazil and the USA (IRAC 33). By 2014, it had spread to Vietnam, Indonesia, Philippines and Korea (Fig 1.6) (Steinbach et al. 2015; Kang et al. 2017; Cho and et al 2018).

1.4.5 The Root of Resistance: Alterations to the Diamide target

The extent of modern global pest monitoring means that new pest invasions can be tracked with sufficient accuracy to detect, in some cases, the first entry into a country, as with *T. absoluta* in Sicilian greenhouses (Roditakis et al. 2015). More impressive still were the accurate and precise predictions made of future spread for both *T. absoluta* (Desneux et al. 2010) and *S. frugiperda* (Early et al. 2018). One goal of IRAC is to see such population tracking successes mirrored in the context of insecticide resistance (Sparks and Nauen 2015). Efforts to track and predict resistance spread are augmented by identifying and characterising the cause of the resistance episode. Possible mechanisms include cuticular changes affecting insecticide penetration; behavioural adaptations for avoidance; metabolic upregulation to speed up detoxification and removal; and target-site alterations to reduce insecticide efficacy (IRAC 2019).

Metabolic resistance to diamide insecticides has been thoroughly reviewed in (Nauen and Steinbach 2016). In general, studies have shown that upregulation of metabolic pathways does not equate to meaningful diamide resistance ratios, on its own. However, some notable cases of metabolic resistance exist, including that of a 43-fold CLR resistant Chinese strain of *C. suppressalis*, in which diamide

susceptibility was restored almost entirely by P450 monooxygenase suppression (He et al. 2014).

By far the most impactful cause of diamide control failure is molecular alteration of the insecticide target site by changes in the amino acid sequence coding for the protein, where those changes evolve to increase in frequency within the population concerned. This phenomenon is known as Target-Site Resistance (TSR) and it is the central recurring topic of this thesis. The first incidences of diamide resistance were discovered to result from an alteration to the diamide target site (Trocza et al. 2012), and the same alteration has latterly been found to have evolved in other populations around the globe (Steinbach et al. 2015). In the decade since the first evolution of resistance to diamides, a variety of further target-site alterations have arisen. Chapters 4, 5 and 6 of this thesis will focus on investigating these alterations, and each will be preceded by a thorough review of the particular alteration under discussion. Prior to such investigations, it is necessary to establish a detailed understanding of the protein target of these insecticides. The target of the diamides is a 2.2-megadalton ion channel, crucial to the function of animal muscle cells, and its name is the Ryanodine Receptor.

1.5 Diamide Mode of Action

The Ryanodine Receptor (RyR), a large calcium release channel, mediates the conversion of nerve impulses into muscular contraction (Ebbinghaus-Kintscher et al. 2006). Binding of diamides to this channel locks it into an open configuration, causing uncontrolled calcium release, leading rapidly to feeding cessation, muscle paralysis and death. All diamides target the RyR at a region located within the transmembrane domain, close to the channel pore. Although the precise site of interaction remains unclear, a series of residues between amino acids 4700 and 4955 have been associated with altered binding properties (see Ch6 for more information). The importance of this site was confirmed by experiments on various chimeras made between *Bombyx mori* and rabbit RyR. These experiments also revealed an N-terminal region (amino acids 183-290) important for channel sensitivity to FLB, hinting that this region likely connects to the C-terminal region via the central core of the structure (Kato et al. 2009). Binding at this site occurs irreversibly (in contrast to most ligands which unbind in a concentration-dependent manner), fixing the structure into an open configuration. The diamide may form a physical obstruction, possibly preventing rotation of the channel core, prior to

closing. There is thought to be a slight difference in the manner in which the two groups of diamides occupy the site, as shown by radioligand studies (Isaacs et al. 2012) (Ralf Nauen 2019, unpublished). This binding site difference can result in meaningful disparities in field efficacy between the compounds (e.g.(Cho et al 2018)). The binding site is not connected to that of ryanodine, the pharmacological probe that gives the receptor its name (Williams and Tanna 2004). This plant alkaloid, whose insecticidal properties are well known, does not inhibit or prevent diamide binding in any way. Investigations into diamide binding have primarily been achieved by radioligand binding assays, in combination with mutagenesis of suspected key sites (Casida 2018). The latter type of study has been aided by the evolution and selection of RyR mutations which have been shown to inhibit binding to the insect RyR (Trocza et al. 2016). Chapters 3, 4, 5 and 6 will return to the theme of diamide action upon the RyR following a detailed account of the channel's physiology, below.

1.5.1 The Ryanodine Receptor

Long before its significance as the target of a globally important class of insecticides was realised, the RyR has been the subject of thorough medical investigation for several decades. This large ion channel is a central player in calcium homeostasis in humans, which is not only critical to muscle function but also gene regulation and a variety of developmental processes (Mikoshiha 2011). Mutations in the RyR in humans can lead to an array of severe conditions including Malignant Hyperthermia (MH) (Zvaritch et al. 2009); Central Core Disease (CCD) (Loy et al. 2010); and Catecholaminergic Polymorphic Ventricular Tachycardia (CPVT) (George et al 2007), each of which is reviewed further in section 1.6.5.

This section will summarize the properties of the RyR, and key information on the mammalian receptor that facilitated the study of the insect channel. A recent leap forward in the state of knowledge on insect RyRs, due to their role in diamide efficacy and resistance, has paved the way for their study in the same way as the mammalian protein. For example, high resolution cryo-imaging structures of mammalian RyRs can be used as scaffolds for homology models of insect RyRs. Broad similarities between insect and mammalian tertiary structures, at all but the most divergent regions or most detailed investigations, largely circumvent the requirement for an insect 3D structure, especially in the light of recent homology modelling efforts (see Ch6+Ch7). Cloning efforts for various insect RyRs allows

discussion of variability amongst the order, and discussion of genetic regulation, in a manner arguably more advanced than that seen in the mammalian literature (Trocza et al. 2018).

Four decades of medical knowledge on mammalian RyR manifestly lays the foundations for any discussion of insect RyR, such that the two will be discussed side by side during this introduction. The terms RyR1, RyR2 and insect RyR will be used throughout, where RyR1 refers to the mammalian skeletal isoform; RyR2 refers to the mammalian cardiac isoform; and insect RyR refers to that from any insect species.

1.5.2 Calcium Homeostasis

Normal cell function is maintained by the homeostatic balance of Ca^{2+} at low cytosolic concentrations ($\sim 100\text{nM}$), via a variety of pumps and active transporters which counter the leak that occurs both from the extracellular space and from internal stores (Taylor et al. 2009; Berridge et al. 2003). The endo/sarcoplasmic reticulum (ER/SR) in muscle cells is the site of calcium storage from which calcium release is mediated by the RyR, along with the inositol triphosphate receptors (IP_3Rs). Just half the size of their neighbour, IP_3Rs follow a different regulatory pathway to the RyR and are important in cell development (Furuichi et al. 1989). In the context of muscle contraction, IP_3Rs play a secondary role.

Studies on *Drosophila melanogaster* have shown that the Ca^{2+} regulatory process described in this section is broadly conserved, albeit lacking some proteins of lower importance (Chorna and Hasan 2012). Functional differences between mammals and insects will be discussed.

1.5.3 RyR2

Mammals, on which much of this discussion focuses, have three RyR isoforms, with RyR1 expressed primarily in skeletal muscle, RyR2 in cardiac muscle and cerebral tissue, and RyR3 (not discussed here) at low levels in a variety of cells (McPherson and Campbell 1993; Fill and Copello 2002). All isoforms are also expressed in non-muscle tissues such as liver and nerves, with variation in transcriptional splicing allowing tissue-specific expression patterns and function (Zalk et al. 2007).

Non-mammalian vertebrates have only two isoforms, α -RyR and β -RyR, both of which are expressed in muscle cells, with functions broadly comparable to RyR1

and RyR3, respectively (Murayama and Kurebayashi 2011; Ottini et al. 1996). Insects have just one isoform, although variation in transcriptional splicing potentially allows moderation of protein function across time and space, in a manner similar to that seen in the mammalian isoforms. It is known, for example, that *P. xylostella* has 21 different splice forms, with expression of 7 of these being crucial during S1 development (Trocza et al. 2018).

The insect RyR shares highest homology with the human RyR2 isoform, and as such the following discussion will focus on this isoform.

1.5.4 Excitation Contraction Coupling

Mammalian muscle contraction occurs through a highly regimented and repeatable process called Excitation-Contraction-Coupling (ECC), in which nervous stimulation of a muscle fibril results in calcium release into the cytosol of that fibril, mediating contraction of the cell via sliding myo-filaments (Bers 2002).

As a nervous impulse arrives and permeates the sarcolemma (the muscle fibril sheath), this causes Na⁺ channel activation and acetylcholine release. Invaginations of the sheath, called T-tubules, then transmit the acetylcholine to the muscle cells, where it activates activating Ca_v1.1 channels (also called L-type Ca²⁺ channels or DiHydroPyridine Receptors) (Santulli et al. 2017). Ca_v1.1 opening allows a small amount of Ca²⁺ influx from the extracellular space, however this is insufficient to elicit coordinated contraction. Up to 90% of the required Ca²⁺ flows from the SR, primarily via the RyR, following a process known as Ca²⁺-Induced-Ca²⁺-Release (CICR) (Fabiato 1977). In this fashion, free-Ca²⁺ in the cytosol is increased by an order of magnitude in a fraction of a second (Bers 2002). In mammals, RyRs in muscle cells form regular arrays, in which the channels are allosterically coupled, such that near simultaneous opening can occur (Porta 2012) – it is not known whether insect RyR form similar arrays. Ca²⁺ binds to the troponin complex (a complex of three regulatory proteins that is integral to muscle contraction in skeletal and cardiac muscle, but not smooth muscle), causing a conformational change that exposes binding sites for myosin on the muscle actin filaments. Myosin binding leads to the formation of an actin-myosin bridge that allows muscle contraction to begin. Simultaneously, the evacuation of Ca²⁺ from the cytosol takes place. Depletion of SR calcium stores causes RyR closure (Zima et al. 2008), whilst

the NCX ($\text{Na}^+/\text{Ca}^{2+}$ exchanger) and SERCA (Sarco/Endoplasmic Reticulum Ca^{2+} ATPase) pump Ca^{2+} back to the extra-cellular space, and the SR, respectively.

On a macro-physiological level, ECC in insects appears to be identical to the above (Takekura and Franzini-Armstrong 2002). By contrast, microscopic observations of the king scallop, *Pecten maximus* (Bivalvia) found no evidence of T-tubules, with the SR instead situated close enough to the cell periphery to make contact with the outer membrane, with archetypal ‘foot-like structures’ of the RyR observed bridging that gap (Abe et al. 1997). However, it appears that insects do possess T-tubules and the neuronal-muscle boundary bears physiological similarity to that of insects (Takekura and Franzini-Armstrong 2002). Indeed, recent investigations suggest that insects possess all the main components of vertebrate striated muscle (Collet and Belzunces 2007) (Collet 2009). Like mammals, insects have striated and non-striated muscle, with the striated (or fibrillar) form required for flight (Domingo et al 1998; Royuela et al. 2000). The function of non-striated muscle has so far received minimal investigation.

1.5.5 Modulation of RyRs

The entire process of muscle contraction is mediated by changes in Ca^{2+} concentrations, where the RyR is the primary Ca^{2+} regulator. However, it does not act alone in this role, but is supported by a host of components that together make up the RyR-macromolecular complex, as described below. Studies on single channels have shown that Ca^{2+} concentration ($[\text{Ca}^{2+}]$) also mediates changes to the RyR itself, with channel-gating probability (or channel-open probability, P_o) dependent upon free- Ca^{2+} (Mukherjee et al. 2012). In discussion of P_o and channel regulation, the term ‘gating’ refers to the structural transition between the closed (non-conducting) and open (conducting) state of the channel pore itself, a phenomenon that occurs stochastically, but is influenced by the propensity of the channel to open, governed by localised factors (e.g. Ca^{2+} , ATP, Mg^{2+} , redox, pH) (see Figure 1.7). Specifically, ‘activation’ refers to the increase in P_o of a channel, which occurs as a result of the large-scale conformational change brought about by ligand binding.

1.5.6.1 Free Ca^{2+} ions

The RyR has the capacity to detect $[\text{free-}\text{Ca}^{2+}]$ on both sides of the SR membrane and P_o reflects that balance (Fig. 1.7). When cytosolic $[\text{free-}\text{Ca}^{2+}]$ is below 100nM,

P_o is zero. Opening of the L-type calcium channel releases ions into the cytosol, as described previously, increasing $[free-Ca^{2+}]$ dramatically. At $10\mu M$, the channel reaches its maximum P_o . As cytosolic concentrations reach up to $100\mu M$, and luminal concentrations reach a minimum, P_o drops sharply, indicating the end of CICR and the resumption of normal calcium homeostasis. P_o thus forms a bell-shaped curve (Bezprozvanny et al. 1993), which indicates the presence of a moderate/high affinity activating site and a relatively low affinity ($100\mu M$) inhibition site on the cytosolic side (Santulli et al. 2017), and possibly an additional inhibition site on the luminal side (Song et al. 2011). The relationship between P_o and $[free-Ca^{2+}]$ is known to differ between RyR isoforms and is certainly likely to differ between mammals and insects (Hwang et al. 2012). Electrophysiological measurements on *D. melanogaster* RyRs show a much larger conductance of Ca^{2+} ions, for example, despite similar overall kinetics (Sattelle et al. 2008).

1.5.6.2 The Macromolecular Complex

RyRs have been referred to as ‘allosteric giants’ (Van Petagem 2014) in reference to their size, but also for the extensive regulatory web surrounding them, including the macromolecular complex. The list of regulatory components includes calmodulin (CAM), two FK506-binding proteins, (FKBP12 (Calstabin 1) and FKBP12.6 (Calstabin 2)) and the soluble resistance-related Ca^{2+} binding protein (Sorcin), Protein Kinase A (PKA), protein phosphatases 1 (PP1) and 2A (PP2A), phosphodiesterase 4D3 and calmodulin-dependent protein kinase II (CaMKII). Combined, these components help prevent stochastic channel gating, or ‘subconductance’, to give the receptor a binary output. The roles of each component will be described briefly below, and their combined action is illustrated in Fig 1.7 A major caveat to this discussion is that the composition of the RyR-macromolecular complex in insect muscle cells is not known. Furthermore, insect Sf9 cells (Ch3, 4 and 6) are unlikely to have many of the accessory co-proteins discussed here and may have other co-proteins that are not included here.

1.5.6.3 Calstabins and Calmodulin: Stabilising Ca^{2+} flow

Calstabins and calmodulin are modulators located on the cytosolic side of the RyR complex, working together to accelerate the transition between high and low P_o . CaM is a 16.7 kDa Ca^{2+} binding protein, and the best-studied ligand of RyR2. With

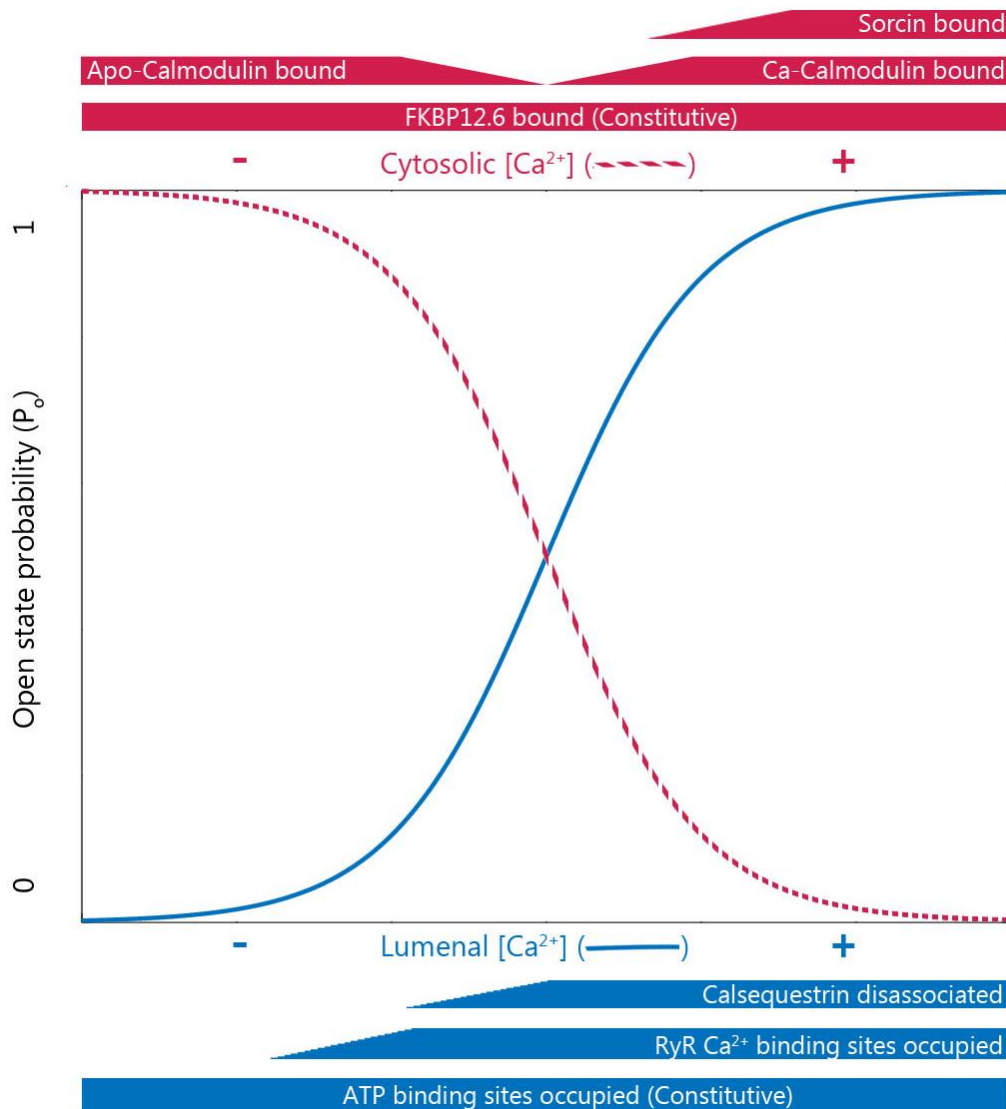


Figure 1.7. RyR2 channel opening is mediated by binding of regulatory ligands, which prevent ion ‘leak’ by stabilizing gating. P_o is a function of free $[Ca^{2+}]$ on both the luminal and cytosolic sides of the channel. As luminal $[Ca^{2+}]$ rises, calsequestrin (CSQ-2) Ca^{2+} sites, and those on the RyR itself, become occupied, leading to CSQ dissociation and channel opening. As cytosolic $[Ca^{2+}]$ increases, calmodulin (CaM) transitions from Apo- to Ca^{2+} -bound form, encouraging channel closure. At maximal cytosolic $[Ca^{2+}]$, sorcin binds to RyR to prevent channel re-opening.

four Ca^{2+} binding domains (Babu YS 1985), CaM increases channel sensitivity to $[free\ Ca^{2+}]$, increasing P_o at low cytosolic concentrations and decreasing P_o at high concentrations (Xu and Meissner 2004). Its role in limiting Ca^{2+} release and initiating channel closure is crucial for mammalian cardiac function (Yamaguchi et al. 2007). The binding domain sits in the cytosolic region, spanning amino acids 3583–3603 (hRyR2).

Calstabins aid in stabilisation of the receptor by increasing the probability of open or closed configurations. In the absence of calstabin binding, random

thermodynamic movements of the cytosolic cap translate to frequent, uncoordinated gating, resulting in 'Ca²⁺ leakage' which is associated with arrhythmias and heart failure in humans. The binding site of FKBP is known (Guo T et al. 2008), and it has been suggested that its stabilising effects are mediated by clamping two RyR domains thereby increasing the energy required for conformational change (Efremov et al. 2015).

1.5.6.4 Signal limit: Sorcin (closing after [Ca²⁺] overload)

Sorcin, like calstabin, helps to terminate Ca²⁺ release, by binding to RyR at high cytosolic [free-Ca²⁺] to initiate channel closure (Bers 2004; Rueda et al. 2006). In its Ca-bound configuration, this 21.6 kDa protein also interacts with other Ca²⁺ homeostatic components, possibly increasing the activity of SERCA and NCX pumps (Zamparelli et al. 2010).

1.5.6.5 Luminal regulation: The Calsequestrin Complex

Prior to muscular contraction, Ca²⁺ release must be delayed until SR storage is sufficient to allow a full CICR-mediated ECC response. Luminal regulation by the Calsequestrin (CSQ) complex achieves this. When Ca²⁺ is less than 100µM, two anchor proteins, Triadin and Junctin, bind CSQ to the RyR, minimizing P_o in the process (Zhang et al. 1997). As luminal Ca is restored, CSQ binding sites (up to 50 on a single protein unit) become occupied (MacLennan and Wong 1971). As Ca²⁺ ions flow back into the SR lumen, they are initially chelated by CSQ, with up to 50 Ca²⁺ sites on a single protein (MacLennan and Wong 1971). Once these binding sites are filled, the calsequestrin complex is disrupted, releasing triadin, junctin and CSQ from the RyR to facilitate channel opening.

1.5.6.6 Phosphorylation of RyR2 and regulatory ligands

Phosphorylation sites appear crucial for regulating RyR2 activity. In general, phosphorylation has been shown to sensitise Ca²⁺ release in cell lines, whilst in single channel studies P_o is increased in the presence of PKA (Valdivia et al. 1995). Studies on rabbit RyR2 have shown that phosphorylation and de-phosphorylation both have the potential to upregulate channel activity, for example causing failures and arrhythmias (Camors and Valdivia 2014).

The overall picture is complicated by the suspected presence of many, as yet, unstudied phosphorylation sites. Just three closely linked sites have been unambiguously defined, based on the impacts of knockout mutations at residues

S2031, S2808, and S2814, which have been shown to be phosphorylated by two kinases, PKA and CaMKII (Takasago et al. 1991). Of these, S2031 is an exclusive PKA site, phosphorylation of which is suspected to play a role in limiting cardiac cell proliferation. A non-phosphorylatable mutation at this position is associated with cardiac hypertrophy (Benkusky et al. 2007). A recent study found that an experimental reduction in RyR2 expression results in an increase in phosphorylation at this site, consistent with its function as a balancing mechanism (Guillén 2017). S2808 and S2814 are PKA- and CaMKII- dependent sites, respectively. These two sites are in close proximity and form a 'phosphorylation loop' on the protein structure and act to upregulate channel activity in the phosphorylated state (Wehrens et al. 2006). However, neither site is present in insects, which have a 48bp insertion that elongates the phosphorylation loop whilst potentially adding one novel phosphorylation site in place of the two that are missing (Xu and Yuchi 2019).

1.6 RyR Sequence, Structure and Function

The RyR, already critical to human medicine, is becoming an increasingly important model in agricultural entomology. Functional studies have traditionally relied on forward-genetic analysis of diseased states, complemented by reverse-genetic approaches. However, studies have long been hampered by a lack of information on the structure of this receptor.

The RyR is too large and complex to be studied by X-ray diffraction methods and as such cryo-EM is now the method of choice. In 2012, something of a paradigm-shift occurred, dramatically improving resolution of RyR imaging. Old 20Å images, struggling to resolve even the cytosolic cap, have been superseded by sub-4Å structures that resolve even the details of the channel core. Box 1.3 covers the history of RyR imaging and the sudden acceleration in imaging capacity.

Near-atomic resolution structures of the mammalian RyR1 (Yan et al. 2015) and RyR2 (Peng et al 2016) have now been captured. This was achieved initially with the channel in the closed state, bound by FKBP or ryanodine (Zalk et al. 2015), but since then structures in a variety of conformations have been published, all with sub-4Å resolution in the core regions (des Georges 2016). The capacity for functional study in mammals has consequently been revolutionised. Previous studies on RyR diseases have gained a new emphasis.

In contrast, insect structural studies remain limited. Just one partial cryo-EM has been achieved (Lin 2017), but this structure is of limited use without a map of the channel core. Until sufficient progress is made on imaging insect RyRs, mammalian structures may be used to predict those of insects. Protein alignments show that human and *Drosophila* channels are ~47% alike on average (Sattelle et al. 2008), with similarity increasing to >70% around the channel core (unpublished alignment). Recent attempts to extrapolate mammalian to (highly divergent) insect structures are not without risk or controversy (Lin et al. 2019).

This section comprises an overview of the channel's structural components, a description of the newly elucidated opening mechanism, and investigations into the function and location of small-molecule binding.

Box 1.3: Highlights of imaging studies

1987: First purification and visualisation of human cardiac RyR2 by staining, viewed from top down (Inui et al. 1987).

1992: First images of unstained channel in its entirety, in 3D, revealing 4-fold symmetry and a characteristic mushroom shape, with a small cylindrical TM domain (Radermacher et al. 1992).

1992-2005 hiatus: Orientation bias largely prevents improvements in structural imaging (because the protein predominantly lies either cap-side-up or cap-side-down). However, interaction sites for most, if not all, of the known RyR modulators were identified during this time e.g. sites for phosphorylation; redox modification; Calmodulin binding and FKBP12 (immunophilin) binding (see references in text).

2005: the first internal structural view of the protein achieved, using a perforated imaging grid to allow the protein to exist equally in all orientations (Samso et al. 2005). However, whilst this view allowed many of the cap structures to be elucidated – the structure of the channel core remained shrouded in mystery. The debate over the number of TM helices would not be solved for a further decade.

2012: the first study to report successful implementation of direct electron detection in cryo-EM (Bammes and al 2012). This is an example of a major technological leap immediately fuelling a flood of studies and progress in the field. Previously, each electron released from the analyte would strike a charged plate in order to be converted into a photon – however, electron impact usually results in release of multiple photons, causing

a loss of resolution as they pass through the CCD detector. Direct Detection Devices thus allowed a drastic improvement in resolution.

2014: Imaging at 6Å resolution allows deconstruction of the large-scale cap and arm movements involved with channel opening (Efremov et al. 2015).

2015: RyR1 imaging at sub-4Å resolution published by 3 separate labs in the same year. Images allow mapping of the channel core down to atomic scale, although more disordered regions of the structure still remain at poly-alanine-level resolution (Yan et al. 2015; Zalk et al. 2015).

2016: Full atomic structure of RyR2 published, along with description of gating mechanism on an amino-acid-level (Des Georges et al. 2016). highly detailed characterisation of RyR1 interactions, based on single particle cryo-EM analysis and amino-acid substitution of key residues.

2017: First partial crystal structure of an insect RyR, that of *Plutella xylostella* (Lin et al. 2018) resolving just the N-terminal domain.

1.6.1 General Structural overview

This substantial, mushroom-shaped channel measures 270Å across the top of a cap that represents 80% of its mass and which rests upon the SR lumen. The remainder of the channel's mass is buried within the SR membrane as a series of helices supporting the pore (Van Petagem 2014). Ligands, such as cellular modulators and other small molecules, generally bind to the large surface area provided by the cap region and enact conformational changes upon the cap structure. These changes are transmitted to the pore of the channel through complex allosteric coupling between the four protomers, which move relative to one another. Column-like helices in the central domain conduct these movements down into the channel core (Peng and al 2016).

The 2.2-megadalton RyR structure is organised hierarchically, with over ten distinct domains interlocking with one another. Functionally, the channel can be split into Core and Periphery. First, the central core, composed of the N-Terminal, Central and Pore-Forming Domains (NTD, CD and PFD), is approximately 100Å tall and projects out of the SR membrane. The Handle Domain (HD), which connects the Core regions, also leads outwards toward the second functional region, the Periphery. Two arms jut outward, at 90 degree angles from one another, together

forming extensive structures composed of Helical Domains (HD) on one arm and SPRY domains on the other (des Georges 2016). At the base of the central Core, the PFD is formed by six membrane spanning domains, which lead sequentially inward, finally terminating in the Pore itself, and linking back to the rest of the Core through the C-Terminal Domain (CTD).

The Pore, as an isolated unit, resembles channels of other families, such as the KcsA bacterial sodium channel (Balshaw et al. 1999), and the IP₃R, a related Ca²⁺ channel on the SR membrane. The Pore can be expressed autonomously, and maintains its function as a Ca²⁺ sensitive channel (Xu et al. 2000). At the extreme end of the Pore sequence, the last 15 amino acids are alone responsible for bonding the four protomers together into a homo-tetrameric unit (Gao et al. 1997).

Whilst the Pore can exist as an independent entity, the function of the Periphery, and the non-Pore remnants of the Pore, is regulatory – without it, pore function is heavily impaired, for example the channel does not close at high Ca²⁺ concentrations (Bhat et al. 1997). Of the channel modulators described in the section above ('Modulation of RyRs'), all bind within the cytosolic domain. The size of this domain, despite not being required for ion conduction, is testament to the sheer number of interactions taking place on this channel. Furthermore, the Periphery is responsible for organisation of the channel in space and time. Synchronisation between RyRs is crucial in order to raise cytosolic Ca²⁺ concentration by orders of magnitude in milliseconds. This synchrony is achieved by precise spatial organisation – where channels are allosterically linked to neighbouring channels to form an extensive array. Under such conditions it has been observed that two or more channels may open nearly simultaneously and spontaneously (Porta 2012).

The SPRY (SP1a/Ryanodine receptor) domains have long been known for their regulatory importance – and are linked to immune responses when present in other proteins (D'Cruz et al. 2013). In RyR1, the SPRY domain is responsible for direct Cav1.1 interaction after an action potential (Tae et al. 2009), however insect channels do not undergo direct Cav1.1 coupling, so their role here is not known.

1.6.2 Opening Mechanism: An Overview

In order to fulfil the various regulatory roles described previously, the RyR pore-opening mechanism must be able to respond to a wide variety of ligand binding

conditions. It is now known that the Pore, far from being a binary switch, is capable of taking up a variety of intermediate configurations, dependent upon which combinations of ligands are bound (Des Georges et al. 2016). Prior to discussion of such intermediates, a basic description of the 'channel opening', is valuable (Efremov et al. 2015).

Opening begins with the occupation of Ca^{2+} binding sites. Conformational changes follow, altering the positions of the transmembrane helices relative to the cytosolic cap and increasing the average gate diameter. This occurs in the following manner. Radial rotation of the Periphery occurs around an axis formed by the Handle Domain (Peng and al 2016), making a 'swirling motion' when viewed from above. This movement is transferred from the Central Domain (CD) through the O-ring (Peng and al 2016), a region in which CTD, S6, and the S2-S3 linker come together to form an O-like structure (see Fig. 1.8). Thus, swirling of the cap leads to coupled outward shifts of the entire pore-forming region, as well the transmembrane region more generally. The Periphery then tilts outward and downward, whilst the pore contracts vertically and expands outward. The Gate, which is formed by convergence of the four copies of a single residue, swings open (Des Georges et al. 2016).

Gating itself has been found to be both transitory and stochastic, effected heavily by random thermodynamic movements which occur independently of protein conformation. However, the above conformational changes cause large-scale shifts in apparatus, greatly altering P_o . The period of each 'opening event' is fixed (within a given cellular state), whilst it is the increased probability of such events occurring that leads to the rise in Ca^{2+} conductivity in response to action potential (Sitsapesan and Williams 1994). P_o ranges from near-zero to near-certainty ($P_o=1$), depending upon the combination of bound ligands and moderators which determine channel conformation.

1.6.3 Opening Mechanism: Detailed investigations

On the scale of the ion-conducting Pore region, some 100Å in height, the large-scale changes described above are focussed down to minimal, rotations and shifts. Only with the publication of near-atomic resolution structures has it become possible to speculate the opening mechanism, whilst extensive reverse-genetic studies have subsequently substantiated the available evidence. These studies have been

steadily taking place since the medical importance of the receptor became clear (see below 'RyR amino acid alterations in disease states'). However, studies of the receptor under normal functionality have accelerated in recent times and are summarised here. Contributions to the field having occurred on a variety of receptors including human RyR1, rabbit RyR1, mouse RyR2, and pig RyR2 and RyR3 however, for clarity, residue numbers are given based on human RyR2 (hRyR2) in this section and subsequently. All of the altered residues discussed in this section are conserved in insect RyRs, and indeed across invertebrate orders, providing further support of their functional importance (unpublished data).

The translation of large-scale into small-scale movements, descending top-downward through the channel, must logically occur at a fixed point – a Hinge – to mediate the see-saw motion. One such hinge is thought to reside at residue G4935 (TGQ hRyR2) (Mei et al. 2015). Around this point, which lies sequentially downstream of the pore, the S6 solenoid can be seen to pivot, in response to bowing of the Periphery, in order to enact pore closure (Des Georges et al. 2016). A second Hinge appears to lie upstream of the Pore, at position F4853 (FFV hRyR2) (Peng and al 2016) but it is unclear whether these two hinges operate in tandem, or whether each operates individually depending upon the conformational change underway.

Once structural changes have been transferred through the Hinge(s), they are conducted to the inner Pore through the S6 solenoid. Movements within the Ca²⁺ conducting channel occur on an atomic scale. Viewed from the inside, during open configuration, the walls of the Pore narrow gradually from top downward. This trend continues down through the transmembrane region until, at the base of the membrane-spanning region, the Pore reaches its narrowest point. This Filter determines which ions can pass through the channel. In hRyR2, the 2.5Å filter is formed by glycine residues converging from each protomer at position G4864 (QGL hRyR2). Macrostructural movements do not alter the G4864 position, but they do cause dramatic changes further upwards, to residue I4867 (IID hRyR2). This is the Gate, and the four identical residues at this position face outwards during channel conductance, to make a gap width of 4Å (far wider than the 2.5Å filter of its neighbouring residue). However, during channel closure, the four residues rotate and converge inward, dramatically reducing the gap to around 0.5Å, which is insufficient space for ion passage, thus closing the Gate.

It has been argued that a second site of selectivity exists higher up (more luminal) in the pore than the G4864 filter. A GGGIG group is present, which is known in similar channels to act as a selectivity filter for cations. In this case, the region is followed by an aspartate and a glutamate (D4829 and E4830, GGGIGDE hRyR2) residue, whose inward facing carboxyl groups limit the width of the channel significantly (Gillespie 2014). Topographies of the inner surface of the pore confirm the presence of this region. Furthermore, in Rabbit RyR1, G4894 (G4824, hRyR2, GGGIGDE) has been identified as the narrowest region in the open channel (Des Georges et al. 2016). If the position of this selectivity filter is variable between species and isoforms, the role of the I4867 as the Gate appears to remain constant, at least in mammalian channels.

1.6.4 Calcium and Caffeine: In search of a binding site

The RyR gating mechanism is controlled by binding interactions with small molecules. Ca^{2+} is the primary regulator, possibly requiring ATP, but caffeine, the much-used experimental modulator, can mimic the action of Ca^{2+} and is thus expected to partially share a binding site. Together, these molecules influence pore width. Site I4867 – the Filter – can be seen to open wider and wider as binding sites for these molecules fill up. In the presence of Ca^{2+} only, pore width increases minimally, suggesting a requirement for ATP binding in tandem. Caffeine binding is also known to have similar effects on pore opening: in the presence of caffeine but absence of Ca^{2+} pore width is similar to that in the Ca^{2+} -only state. Maximum pore-width is achieved by binding of Ca^{2+} , ATP and caffeine together, suggesting that all three have independent and additive roles to play in opening of the channel (Des Georges et al. 2016). For each of these molecules, arrays of interacting residues have been identified through reverse-genetic study. Only very recently have these studies, in combination with high-resolution imaging, allowed confident investigation of these sites. As will be seen, for all three molecules, residues of interest are clustered tightly around an area known as Thumb-and-Fingers (TAF). They therefore sit at the interface between CD and CTD, right at the heart of the integral O-ring region.

1.6.4.1 Calcium

Myofibril excitation-contraction-coupling requires rapid and synchronised release of Ca^{2+} from internal stores, triggered by minute increases in cytosolic free- Ca^{2+} , as brought about by channels on the cell outer membrane. Thus, cytosolic Ca^{2+} sensing

is of fundamental importance to channel function. Each protomer of the RyR contains an EF-hands (EF) group, situated close to the TAF, in the CD. This EF group is a well-known Ca^{2+} binding site on various proteins, including Calmodulin (Kuboniwa et al. 1995), and was thus unambiguously stated to be the Ca^{2+} sensor in RyR (Efremov et al. 2015). However, recent deletion of the entire EF motif (4026-4062, hRyR2) had zero impact on cytosolic Ca^{2+} activation (Guo et al. 2015). Two earlier studies had implicated a glutamate residue just upstream of the EF hands. Alteration of E3987 (LEG hRyR2) reduced sensitivity to cytosolic Ca^{2+} activation by a factor of 1000 to 10,000 (Chen et al. 1998; Li 2001). Recent atomic-scale imaging has now allowed pinpointing of this site directly on RyR1 (Des Georges et al. 2016). As shown in Fig 1.8(d) The carboxyl groups of E3893 (TEG) and E3967 (TEY), of the CD, press up against that of T5001, of the CTD (3848, 3922 and 4931, hRyR2). Interestingly, the previously identified site is not involved, despite the dramatic phenotype. This indicates again the importance of the CD-CTD connection in the O-ring domain, in that alteration of residues here annihilates channel function. Since then, the Ca^{2+} site has been clarified still further, with the investigation of W4645 (YWD hRyR2). This residue appears to act as a moveable lock, which mediates changes in Ca^{2+} binding probability under channel 'sensitization' (e.g. by caffeine) (Murayama, 2018).

Whilst cytosolic Ca^{2+} sensing is important for RyR opening, closing of the channel requires a luminal sensor to interact with CSQ and detect store depletion. A second function of this site is to detect store overload, which also has the capacity to stimulate channel opening. Logically, this site should be located on the luminal side of the channel and indeed recent studies focus on a region distinct from those above. E4872 (GEL, hRyR2) is now thought likely to play a role in luminal Ca^{2+} sensing. Firstly, ablation of this site abolishes luminal, but not cytosolic, Ca^{2+} activation of mouse RyR2. Further, swapping this residue for a histidine, which binds metal, converts RyR2 to a luminal Ni^{2+} -gated channel (Chen et al. 2014). Furthermore, mutation of a nearby residue, E4878 (QEQ, hRyR2), also reduces luminal Ca^{2+} activation. Channel movement during opening appears to show E4878 moving toward E4872 (hRyR2), suggesting that Ca^{2+} may initiate the structural transition by pulling this residue inward (Peng and al 2016).

1.6.4.2 Caffeine

Caffeine is an important experimental probe of RyR function, appearing to stimulate the receptor in a Ca^{2+} -like manner. This suggests it may occupy, at least partially, the Ca^{2+} binding site (Murayama 2018). In RyR2, D4868 and E4872 are known to interact with caffeine, based on mutation of these residues, which dramatically diminishes caffeine efficacy (Chen et al. 2014). Both of these residues are also implicated in cytosolic Ca^{2+} sensing. Mutations C4888H, C4891H, and H4908C also completely abolish the activation of RyR2 by caffeine, although it is thought that this has more to do with connectivity between the zinc-finger domain in the TaF region (Peng and al 2016). W4645 is a crucial site for Ca^{2+} binding, however alteration of this residue also affects potentiation by caffeine, which is thought to bind nearby. Binding of caffeine causes a change in orientation of W4645, such that the Ca^{2+} site becomes smaller, and more energetically favourable. High resolution images show, unambiguously, that this residue is included in the binding site, along with I4926 (LIN hRyR2) from the CTD.

1.6.5 RyR amino acid alterations in disease states: clues to function

Alterations to channel regions can provide clues to the function of that region. Such is the basis of reverse genetics (e.g Homem and Davies 2018), where alterations are generated deliberately. Sometimes, however, alterations arise naturally through amino acid substitutions, and these can be equally valuable. In the context of ion channels, and RyRs specifically, disease-causing alterations on the mammalian channel have long been the target of investigation. Lessons learnt from such studies are discussed briefly in this section, along with their implications for structure and function of the insect channel.

In humans, RyRs are much studied models for muscular and cardiac disease states, due to the integral role played by these channels. Three pathologies have received considerable study: Malignant Hyperthermia (MH); Central Core Disease (CCD); and Catecholaminergic Polymorphic Ventricular Tachycardia (CPVT). All three are associated with amino acid substitutions in the RyR. As will be seen, profound phenotypic effects arise due, often, to just a single point mutation. These cases represent an opportunity to dissect the function of the surrounding protein regions.

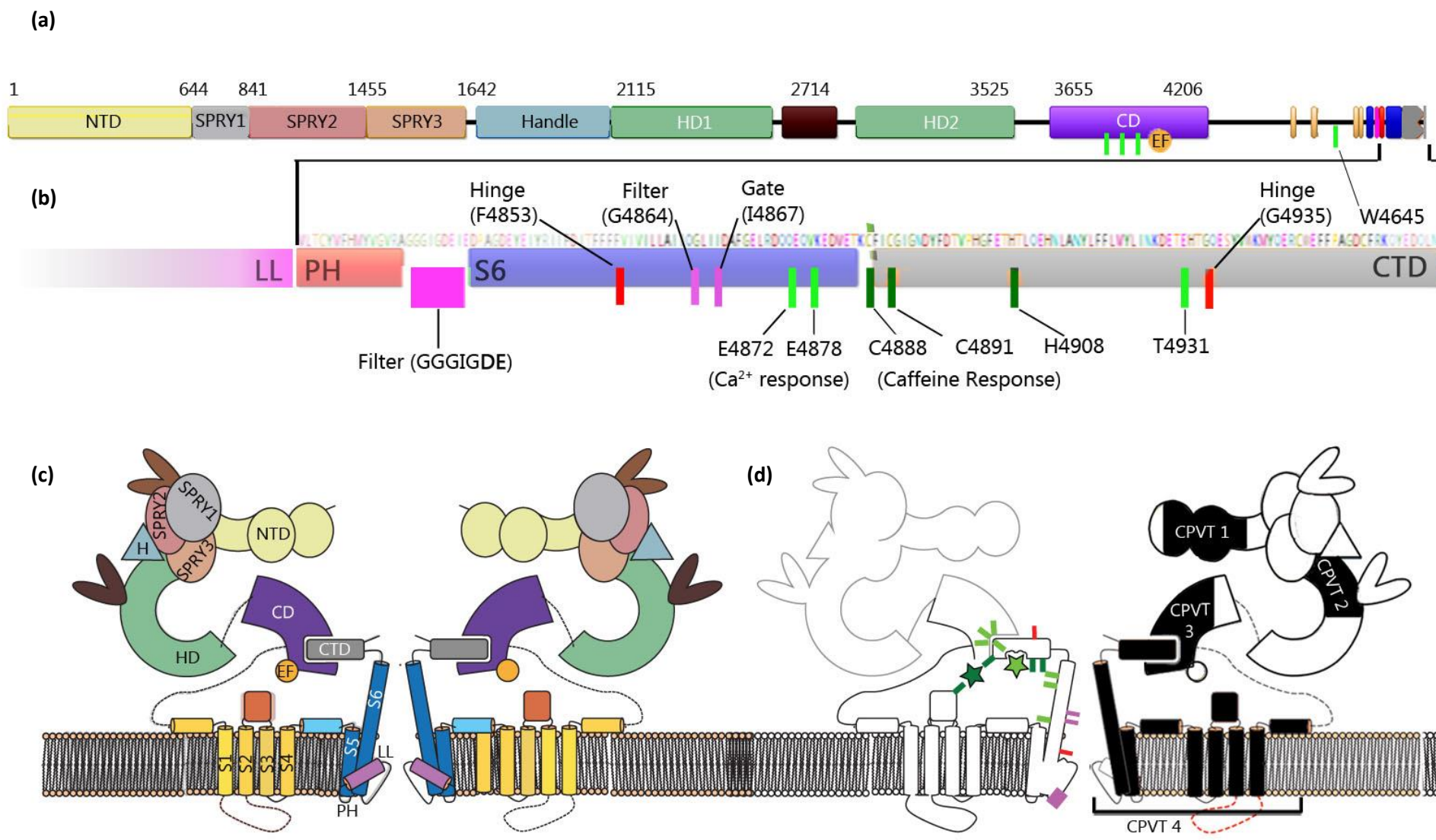


Figure 1.8. a) Amino acid sequence and key domains of rabbit RyR1, as recently resolved in Yan et al. (2015). NTD (N-Terminal Domain); SPRY1/2/3 (SP1a/Ryanodine Receptor); H (Handle); HD1/2 (Helical Domain); CD (Central Domain); EF (EF-hands);

b) Close-up of the pore-forming region, with key positions labelled: LL (Luminal Loop); PH (Pore Helix); S6 (Solenoid 6); CTD (C-Terminal Domain). Critical amino acids are labelled in pink (filter and gating); red (hinging); light green (Ca^{2+} sensing); dark green (caffeine sensing). See references in text.

c) Graphic representation of tertiary structure of two opposing RyR subunits, in dimeric formation. Structural components are labelled following notation in (A) and (B). Four subunits are required for RyR self-assembly, with portions of the CTD, S6, LL and PH regions converging along a central column to form the channel pore.

d) Two RyR subunits, displaying functionally critical amino acids and regions. LHS: Binding sites for Ca^{2+} (light green star) and caffeine (dark green star) recently visualised (Des Georges), can be seen to converge around a region called the 'O-ring'. Other critical residues labelled, following notation in (B). Lower RH panel: The four regions of medically important mutations are labelled (CPVT 1-4, Black). Mutations in these regions are associated with pore 'leak'.

MH is characterised by sustained and uncontrolled Ca^{2+} release from RyR1 within muscle cells, in response to volatile anaesthetics such as halothane. Locked into a semi-contractile state, muscle metabolism rises sharply, leading to build-up of heat and lactate (Larach et al. 2010). Homeostatic removal of lactic acid causes reductions in blood pH, or acidosis, which can be fatal. Mutations associated with MH are clustered in the NTD and have been shown to weaken the cohesion of the protein, with the resulting 'unzipping' of the structure, presumably allowing unregulated channel gating (Zvaritch et al. 2009). Such findings demonstrate the importance of NTD-CD connectivity in regulating channel gating. It has been suggested that the region forms a 'Gating Ring' around the crown of the RyR, with NTDs of the four protomers coming together to lock the channel into its closed state (Van Petagem 2014).

CCD is a rare disorder resulting in various degrees of muscle weakness during infancy, which may persist through adolescence. It is recognised by an altered morphology of muscle fibres containing "core" lesions, which can vary in intensity and localization. Lesions and the resulting weakness are associated with severe reductions in Ca^{2+} permeability, such that the ECC process is slowed or prevented altogether. In one case, a single point mutation, causing a I4895T substitution, was found to completely abolish Ca^{2+} permeation (Loy et al. 2010). It was later learnt that this residue is a key component of the selectivity filter (Gillespie 2014), and this position is very similar to filters in some bacterial potassium channels. Over 160

causative mutations have been identified for MH, and 100 for CCD (<http://triad.fsm.it/cardmoc/> (accessed 02/07/19)).

CPVT is characterised by a RyR-mediated Ca^{2+} leak from the SR during resting phase (Santulli et al. 2015). If the leak is severe, depolarisation of the muscle cell may occur arrhythmically and spread to neighbouring muscle tissue across the heart, causing potentially fatal cardiac arrest (Blayney and Lai 2009). The exact mechanisms behind this leak vary depending upon the mutation site. Advances in cryo-EM mapping allow the resolution of clusters of CPVT-causing mutations into four specific structural domains (see Fig 1.8d). In this case, and for all three diseases, mutations are clustered at interfaces between protomers (Tung et al. 2010; Van Petagem 2014), where they disrupt channel quaternary structure and thereby prevent proper regulation. Secondly, disease-related mutations are clustered at the activation domain, where they either disrupt Ca^{2+} sensitivity, or prevent necessarily modulation by accessory proteins. It has recently been shown, in RyR2, that the CPVT-disease mutations can almost all be explained in terms of disruption of intramolecular interactions. Those in CPVT1 tend to lie on connections between NTD and Handle, for example, whilst those in CPVT2 are between the CD and HD (Peng and al 2016). Domains with high inter-regional connection appear to contain the greatest share of disease-causing mutations across all RyR-related conditions. This is exemplified by the O-ring, which has more than 10% of recorded mutations, despite representing a tiny proportion of total channel mass (Fig 1.8).

Analysis of RyR disease mutations can play a key role in dissecting channel structure and function and has been the starting point for the majority of studies discussed in this section. For example, a previously characterised CPVT mutation, W4645R, was recently used as the springboard for an investigation that eventually uncovered part of the Ca^{2+} binding site, as well as the mechanism of channel activation by caffeine (Murayama 2018). Whilst disease-causing mutations have informed RyR channel studies in humans, channel studies in insects have been informed by a different type of amino acid change. Resistance to diamides is now known to be primarily mediated by amino acid changes occurring in a C-terminal location close to those hotspots described in Fig. 1.8. The remainder of this thesis will concern such resistance-causing mutations, their impact upon channel function in the presence and absence of diamide insecticides.

Chapter 2: Methods

2.1 General Methods

2.1.1 Genomic DNA extraction

The protocol for DNA extraction from *D. melanogaster* was modified from a Berkeley Drosophila Genome Project (BDGP) protocol. Centrifugation steps take place in an Eppendorf 5424 centrifuge at 12,000 rcf at RT for 15 minutes, unless otherwise stated.

Groups of 1-20 flies were frozen at -20°C in a microcentrifuge tube, and ground using a plastic mortar in 200µl Buffer A (see Recipes) until homogenous. The samples were incubated at 65°C for 30 minutes to allow for cell lysis and release of nuclear DNA into solution. DNA precipitation was achieved by addition of 400µl Buffer B solution, mixing, and incubation on ice for 10 minutes. The samples were centrifuged, and the supernatant transferred to a new microcentrifuge tube. In order to clean the DNA samples, 420µl isopropanol was added, followed by centrifugation, and disposal of the supernatant. For final rinsing, 1ml cold 70% ethanol was added, the samples incubated for 3 minutes at RT and centrifuged for 5 minutes, before disposal of the supernatant. This rinsing step was repeated. The final remnants of ethanol were removed with a 10µl pipette, and the samples incubated uncapped for 10 minutes to allow the pellets to air dry, before resuspension in 31µl ddH₂O.

2.1.2 RNA extraction

The protocol for RNA extraction from *D. melanogaster* was modified from a CGB protocol (Bogart and Andrews 2006). Centrifugation steps take place in an Eppendorf 5424 centrifuge, at 4°C and 12,000 rcf unless otherwise stated. Incubation steps are at RT, in a fume hood, for 5 minutes unless otherwise stated.

Groups of 5-10 flies were flash-frozen in a microcentrifuge tube, and ground using a plastic mortar in 200µl trizol for 3 minutes until homogenized. Incubation was followed by centrifugation for 10 minutes to pellet out the insoluble matter. The supernatant (~170ul) was transferred to a new microcentrifuge tube with 60µl chloroform and shaken vigorously by hand. Incubation was followed by centrifugation for 15 minutes to separate out the solution into a lower fat phase

and an upper aqueous phase. Using full aseptic technique and RNase free equipment, the aqueous phase was transferred to a new microcentrifuge tube, ensuring not to contact the fat phase. RNA precipitation was achieved by addition of 100µl isopropanol, followed by inversion, incubation and centrifugation for 10 minutes. The supernatant was discarded, 500µl cold 75% ethanol was added, and the sample centrifuged at 7500rcf for 5 minutes. The supernatant was again discarded and a 10µl pipette used to remove any remaining solution from the sample. The sample was incubated uncapped for 10 minutes to air dry and resuspended in 51µl RNase-free H₂O.

2.1.3 cDNA synthesis

Total RNA was used for cDNA synthesis using the Thermo Scientific SuperScript III First-strand cDNA synthesis kit. 0.5-5µg of template RNA (typically 3µg) was mixed with 1µl of oligo(dT)₂₀, 1µl of 10 mM dNTP mix (10 mM each of dATP, dGTP, dCTP, dTTP at neutral pH) and nuclease-free water (to make up to 13µl final volume) in a 1.5ml Eppendorf tube. The mixture was incubated at 65°C for 5 minutes and then placed on ice for 1 minute. 4µl of 5X First-Strand buffer, 1µl of 0.1 M DTT, 1µl of RNaseOUT Recombinant RNase Inhibitor (Thermo fisher Scientific) and 1µl of SuperScript III were added and mixed by gently pipetting up and down. The final 20µl mixture was incubated at 50°C for 1 hour. The reaction was inactivated by heating to 70°C for 15 minutes. cDNA was stored at -20°C.

2.2 Polymerase chain reaction (PCR)

All reactions took place in standard 0.5ml thin-walled PCR tubes, in a Bio-Rad C1000 Touch Thermal Cycler.

2.2.1 Primer Design

Primers were designed to have the correct melting temperature, molecular weight, % GC content and restriction sites. OligoCalc (in Genious) was used to ensure optimal parameters (Kibbe, 2007). The primers were usually 20-30 nucleotides in length with a GC content of 40-60% and a melting temperature (T_m) of 50-60 °C. All were synthesised by Sigma Aldrich.

2.2.2 Standard PCR

Standard PCR reactions utilised 12.5µl Thermo Scientific 2X DreamTaq with Taq polymerase, 1µl of dNTP mix, 1µl of 10 µM forward primer, 1µl of 10 µM reverse

primer, 1-2µl of DNA and sterile water up to 25µl. The cycling conditions varied depending on the primers and the length of the amplicon. Initial denaturation was carried out at 95°C for 1-2 minutes. This was followed by 25-35 cycles of denaturation (95°C for 30 seconds), annealing (55-65°C for 30 seconds) and extension (72°C for 1 minute/Kb). The final elongation was carried out at 72°C for 5 minutes.

2.2.3 High-fidelity PCR

High-fidelity PCR with BioLabs Phusion DNA Polymerase was used for long amplicons or when very accurate amplification of the DNA sequence was needed. The reactions were done in 0.5ml thin-walled PCR tubes and contained 4µl of 5X Phusion Buffer, 0.4µl of dNTP mix, 1µl of 10 µM forward primer, 1µl of 10 µM reverse primer, up to 250 ng genomic template DNA or 10 ng plasmid DNA, 0.2µl Phusion DNA Polymerase and sterile water up to 20µl. Initial denaturation was at 98°C for 30 seconds followed by 30 cycles of denaturation (98°C for 10 seconds), annealing (45-72°C for 30 seconds) and extension (72°C for 30 seconds/Kb) with a final elongation at 72°C for 10 minutes.

2.2.4 Site-directed Mutagenesis by PCR

Introduction of singular and multiple-nucleotide alterations upon DNA sequences, *in-vitro*, was achieved by PCR using the Agilent Site-Directed Mutagenesis QuikChange kit. Primers, containing the desired alteration, were designed manually according to the Agilent guidelines and were 25-45 bases in length. OligoCalc was used to avoid self-complementary sequences, to ensure GC content was at least 40% and the T_m was as close to 80°C as possible whilst staying within the above parameters.

PCR reactions occurred in thin-walled PCR tubes with 5µl of 10X Buffer, 100 ng double-stranded DNA template, 1.25µl each of forward and reverse primer (10 µM), 1µl of dNTP mix, made up to 50µl with sterile water. The mixture was then briefly vortexed and centrifuged before the addition of 1µl PfuUltra DNA polymerase (Agilent). The initial denaturation step was 95°C for 1 minute, followed by 18 cycles of denaturation (95°C for 50 seconds), annealing (60°C for 50 seconds) and extension (68°C for 1 minute/Kb) with for a final extension of 68°C for 7 minutes. For each reaction, the average T_m of the two primers was typically between 65-75°C. Following the PCR reaction, the plasmids were digested with

DpnI using 1µl/reaction at 37°C for 1 hour. This removed any parental, non-mutated, supercoiled dsDNA.

2.2.5 PCR product purification

PCR product purification was carried out using the Qiagen MiniElute kit by adding five volumes of Buffer PB to the PCR solution, mixing, applying to the QIAquick spin column and centrifuging for 1 minute at 10,000 x g. The DNA bound to the column was then washed with 750µl of Buffer PE and centrifuged. A further 1 minute in the centrifuge ensured the complete removal of wash buffer. 30µl ddH₂O was then added to the column and the DNA eluted by centrifugation.

2.2.6 Agarose gel electrophoresis

The size and quality of the PCR products were assessed by agarose gel electrophoresis. The gels were made by diluting Thermo Scientific agarose in 1X TAE (Tris-Acetate-EDTA) buffer (Appendix, Recipes). The mixture was heated to >85°C and maintained at an elevated temperature for >1min/100ml to dissolve the agarose, before being allowed to cool slightly prior to the addition of ethidium bromide to a final concentration of 0.4 µg/mL. The gel was set, using plastic combs to introduce wells for the nucleic acid samples. Samples were mixed with bromophenol blue dye (2µl of 6X loading dye, 2µl PCR product and 8µl sterile water) and run alongside a Thermo Scientific GeneRuler 1 Kb, or 100bp, DNA ladder (1µl of ladder with 1µl of 6X loading dye and 4µl of sterile water). Standard settings for a 5cm x 7cm 1% agarose gel were: 70mV; 100 mA; 45-minute run time. To visualise large bands >7kb, the agarose concentration was increased to 1.5-2%, whilst to visualise small bands <500bp the agarose concentration was reduced to 0.5-0.75%. The resulting DNA bands were visualised on a Gene Genius Bio-Imaging System using the Syngene UV transilluminator.

2.2.7 Extraction of PCR products from agarose gels

Gel extraction and purification of PCR products was done using the Qiagen QIAquick Gel Extraction Kit. The gel was placed on a UV light box and the DNA fragments were excised from the gel using a clean, sharp scalpel. The gel fragment was then weighed in a 1.5ml Eppendorf tube, 3 volumes of preheated Buffer QG were added (where 1mg equates to 1ml) and the tube incubated at 50 °C for 10 minutes with vortexing every 2 minutes to help the gel slice to dissolve fully. 1 volume of

isopropanol (corresponding to the weight of the original gel slice) was then added. The sample was pipetted onto the QIAquick spin column and centrifuged at 16,000 x g for 1 minute. The flow-through was discarded and a further 500µl of preheated buffer QG was added to remove any remaining gel. To wash the sample, 750µl of Buffer PE was applied to the column membrane and centrifuged for 1 minute. The sample was then centrifuged for a further 1 minute to remove any remaining wash buffer. 30-50µl nuclease-free water was added to the column and allowed to permeate the matrix for 5 minutes before centrifugation for 1 minute to elute the DNA.

2.3 Molecular Cloning and Transformation

2.3.1 Plasmid assembly by endonuclease digestion and ligation

DNA fragments, amplified by PCR and gel purified, were ligated into the appropriate plasmids, selected according to the subsequent use of the plasmid, the size of the insert (Kb) and the availability of complementary restriction sites. The plasmid vectors were linearised by digestion with appropriate restriction enzyme(s) using the ThermoScientific FastDigest system. For plasmid DNA, up to 1 µg plasmid was combined with 1µl of FastDigest (FD) enzyme(s), 2µl of FastDigest Green Buffer, the solution made up to 20µl with sterile water and incubated at 37°C for 30 minutes. For entire RyR plasmids, or >10kb plasmids, 0.5µg DNA/µl FD enzyme was used. For restriction digest of PCR products, 0.2µg DNA/µl FD enzyme was used. If required, the FD enzymes were subsequently inactivated by heating for 5 minutes at 80°C. The digested samples were analysed by gel electrophoresis and DNA bands of correct size extracted.

Digested vector and PCR fragments were ligated together as follows. 1µl T4 DNA ligase and 1µl T4 ligase Buffer were combined with the fragments to be ligated and the solution made up to 20µl with sterile water. Total DNA concentration in solution was maintained below 20ng/ul and a 1:1 molar ratio of vector: insert was ensured. Ligation occurred for 2h at RT and the new plasmid construct transformed immediately or refrigerated at 4°C overnight. Ligation of PxRyR-containing constructs fragments follows a modified protocol, as detailed in Section 2.5.

2.3.2 Concentration by Ethanol Precipitation

In some cases, concentration of the ligation reaction was required prior to transformation. 2µl sodium acetate (3M) was added to the 20µl ligation reaction

and mixed in gently. 60µl cold ethanol (99%) was added to the solution, the solution gently mixed and then incubated on ice for 15 minutes (or overnight, time permitting) to precipitate the DNA. The solution was then centrifuged for 30 minutes at 4°C and the resulting DNA pellet rinsed with the addition of 70% ethanol. The sample was centrifuged briefly to ensure pellet stability, the ethanol rinse discarded, and remaining ethanol removed with a 10µl pipette (being careful not to contact the, potentially invisible, pellet). The sample was incubated uncapped for 10 minutes to air dry, before resuspension in H₂O (volume dependent upon application).

2.3.3 Bacterial transformation

Ligated plasmids containing inserts were transformed into bacterial hosts using Agilent Technologies XL10-Gold Ultracompetent Cells (>10kb) or XL1 Blue Competent Cells (<10kb).

Transformation using XL10-Gold Ultracompetent Cells was according to the following steps: 1 round-bottomed 14ml falcon tube per transformation was pre-chilled on ice. The XL10-Gold cells were thawed on ice, and 25µl aliquoted into each falcon tube. 1µl of β-Mercaptoethanol was added to each tube and the tubes swirled gently. The cells were then incubated for 10 minutes, mixing gently every 2 minutes. 2µl of ligated plasmid was added to the tube and the tube incubated on ice for a further 30 minutes. The tubes were then heat shocked in a 42°C water bath for 30 seconds and placed directly on ice for 2 minutes. 500µl of pre-warmed LB medium was added and the tubes incubated at 30°C for 90 minutes with shaking at 225-250 rpm.

XL1 Blue competent transformation follows an identical protocol except that the duration of heat shock was 45s.

2.3.4 Transformation Validation and plasmid Propagation

Two LB plates, containing the appropriate antibiotic selection (ampicillin for PcDNA3.1; zeocin for pIZ/H5), were spread with 80µl and 200µl of the transformation solution, respectively, and incubated at 30°C for 18-24h (RyR-containing constructs) or 37°C for 12-16h, or until colonies were sufficiently established to visualise a range of colony sizes. Individual colonies were picked with a 2µl pipette tip. Colonies on 2µl tips were placed into tubes of 10µl ddH₂O and mixed via rapidly pipetting up and down using a 10µl pipette. 3µl of the colony-H₂O

was aspirated for further propagation, and the tip (with solution) placed in a 14ml falcon tube containing 4ml LB broth and 2µl 50mg/mL antibiotic. The propagate was incubated at 30°C for 18-30h, in a shaking incubator at 225-250 rpm, until sufficiently turbid that the 2µl tip was no longer visible when viewed side-on.

The remaining Colony-H₂O solution was used for PCR-validation, following the steps outlined above (2.2.2 PCR). Two to three reactions were prepared for each colony to be validated, with each reaction assaying for a different part of the RyR sequence, corresponding to the N-terminus, middle, and C-terminus (primer pairs 1, 7, 13 in appendix). For each reaction, 2µl of Colony-H₂O was added in place of the DNA addition step.

2.3.5 Plasmid purification

To isolate plasmids of high-purity from propagates of colonies validated to contain the correctly ligated sequence, the QIAGEN QIAprep Spin Miniprep Kit was used. After incubation, the bacterial overnight culture was pelleted by centrifuging in the falcon tube at 4000 x g for 20 minutes at 10°C. The supernatant was discarded, the pellet resuspended in 250µl Resuspension Buffer P1, and the solution vortexed thoroughly until the pellet was fully dissolved before being transferred to a 1.5ml Eppendorf tube. Cell lysis was completed using 250µl Lysis Buffer P2 and inverting the tube 4-6 times until the solution became clear and homogenous. The lysis reaction was allowed to proceed for 5 minutes and was then terminated by the addition of 350µl of Neutralisation Buffer N3, inverting the tube 4-6 times. The solution was then centrifuged at 16,000 x g for 10 minutes and the supernatant decanted onto a QIAprep spin column and centrifuged for 1 minute to bind the DNA. The column was then washed with 500µl of Buffer PB and centrifuging for 1 minute, and an additional wash with 750µl of Buffer PE / centrifugation for 1 minute. The column was then centrifuged for a further 1 minute at 11,000 x g to remove any residual wash solution and dry the membrane. To elute the plasmid DNA, the column was placed in a 1.5ml Eppendorf tube and 50µl EB Buffer was applied to the membrane, the column incubated for 1 minute at room temperature and then centrifuged for 1 minute to elute DNA into the tube. The quantity of the plasmid DNA recovered was determined using a spectrophotometer and the plasmid was stored at -20°C.

2.4 Final Product Validation and Sequencing

2.4.1 Restriction Fragment Length Validation

For rapid cloning validation, purified constructs were digested using restriction enzymes known to create a highly specific and easily recognisable band pattern (listed in table 2.3) on agarose gels. Digestion by endonucleases followed protocols described in 2.3.1.

2.4.2 Sequencing

All DNA sequencing was outsourced to Eurofins Genomics TubeSeq sequencing service. Samples were submitted premixed with the appropriate primer in a 1.5ml safelock Eppendorf tube. For PCR products up to 1000bp, 15µl of 5 ng/µl DNA was premixed with 2µl of 10 µM primer. For PCR products over 1000 bp, 15µl of 10 ng/µl DNA was premixed with 2µl of 10 µM primer. Analyses of the sequences was done using Geneious, the bioinformatics software platform supplied by Biomatters Limited.

2.5 Generating RyR mutant genotypes (with RFCLM as example) - specific cloning strategy for RyR mutagenesis and assembly

During this thesis, a total of 17 RyR coding sequence (CDS) constructs were created, in addition to the WT-PxRyR and G4946E-PxRyR constructs already available (Table 2.1). None of the modifications introduced into the WT-PxRyR cDNA were shown to affect the stability of the pIZ vector into which they were cloned, and in all cases, large quantities of pure plasmid DNA were obtained via these methods. This section contains a summary of the steps taken to create the modified RyR constructs, referring to RFCLM-PxRyR (Chapter 6) as an example. Throughout this section, references are made to the standard protocols (2.1 General Methods), however it was frequently necessary to modify the standard protocols when working with the full-length RyR, in order to improve the success rate, and such changes are detailed below.

Various complications are inherent during molecular work on the Ryanodine Receptor, due in part to the sheer size of the receptor. Whilst the genomic region itself is over 200,000bp in length, the 15,386bp CDS, in combination with a >3000kb vector, is still sufficiently long that it requires dividing of the CDS into smaller manageable cDNA fragments prior to any molecular work (most reverse

Table 2.1 List of RyR constructs generated during this PhD, and their usage herein

#	RyR-genotype	Vector	Usage
1	PxRyR-WT	Piz/H5	Studied Previously (Trocza 2015)
2	PxRyR-WT	pUAST	Stable <i>D.melanogaster</i> lines created
3	PxRyR-G4946E	Piz/H5	Studied Previously (Trocza 2015)
4	PxRyR-G4946E	pUAST	Stable <i>D.melanogaster</i> lines created
5	PxRyR-I4790M	Piz/H5	Diamide efficacy assessment by calcium imaging
6	PxRyR-I4790M	pUAST	Stable <i>D.melanogaster</i> lines created
7	PxRyR-I4790T	Piz/H5	None
8	PxRyR-G4946V	Piz/H5	Diamide efficacy assessment by calcium imaging
9	PxRyR-G4946V	pUAST	Stable <i>D.melanogaster</i> lines created
10	PxRyR-E1338D	Piz/H5	None
11	PxRyR-Q4594L	Piz/H5	None
12	PxRyR-DLM (Multi-mutant)	Piz/H5	None
13	PxRyR-K4700R	Piz/H5	Diamide efficacy assessment by calcium imaging
14	PxRyR-Y4701F	Piz/H5	Diamide efficacy assessment by calcium imaging
15	PxRyR-I4790C	Piz/H5	Diamide efficacy assessment by calcium imaging
16	PxRyR-S4919L	Piz/H5	Diamide efficacy assessment by calcium imaging
17	PxRyR-V4945M	Piz/H5	Diamide efficacy assessment by calcium imaging
18	PxRyR-RFCLM (Multi-mutant)	Piz/H5	Diamide efficacy assessment by calcium imaging
19	hRyR2	pUAST	None

transcriptases and polymerases have a reliable extension limit of <13kb). The separate DNA fragments must then be re-assembled after mutagenesis (section 2.5.3).

A second issue is cytotoxicity, which becomes problematic during propagation and sub-cloning of the RyR sequence in *E.coli*. Although *E.coli* theoretically lacks the transcription machinery to make use of the *OPIE2* promoter in the Piz/H5 insect RyR expression plasmid, circumstantial evidence in this PhD suggests that some expression does occur within the bacteria. Notably, bacterial transformations with PxRyR containing plasmids yield colonies that vary dramatically in their growth-rate. Screening colonies of varying size for the presence of the PxRyR plasmid revealed that those that grow quickest invariably do not contain the C-terminal, pore-forming region of the PxRyR sequence. RyR-containing colonies are invariably slow-growing, requiring longer incubation times. Plasmid yield is also reduced in

Table 2.2 Mutagenesis oligos

Mutation	Oligonucleotide 1	Oligonucleotide 2
G4946V	GGACGTGGCTGTTGTGTTCAAGACGTTGAGGAC	CTCAACGTCTTGAACACAACAGCCACGTCCAACAG
I4970M	GTATCGCTGGCTATGCTGATCGGGTACTACC	TAGTACCCGATCAGCATAGCCAGCGATACTATAGAG
Q4594L	GATAATGGACAAGTGCTGATAAAGCCCCACGAGTCC	CGTGGGGCTTTATCAGCACTTGTCATTATCTTCC
E1338D	CTGATGAAGGAGGCGAGCTGATGCCAGATGCCG	TGCGCCGGCATCTGGGCATCAGCTGCCTCCTTG
I4970T	GTATCGCTGGCTACACTGATCGGGTACTACC	TAGTACCCGATCAGTGTAGCCAGCGATACTATAGAG
K4700R	GTTCTACACCTTgCGTACGTGGCGCTGG	CCAGCGCCACGTACcgCAAGGTGTAGAAC
Y4701F	GTTCTACACCTGAAGTcGTGGCGCTGG	CCAGCGCCACGaaCTTCAAGGTGTAGAAC
I4790C	GTATCGCTGGCTgtCTGATCGGGTACTAGGATTGAAGG	CCTTCAAATGGTAGTACCCGATCAGacaAGCCAGCGATAC
S4919L	CTCTTCTGTACTtaCTGTGGTACTTCTCGTTCTGTGATGGGC	GCCCATCACAGAGAACGAGAAGTACCACAGtaAGTACAGGAAA GAG
V4945M	CGCTCATCTGTTGGACGTGGCTaTgGGGTTCAAGACGTTGAGG	CCTCAACGTCTTGAACCCcAtAGCCACGTCCAACAGATGAGCG
RFCLM	CCTCGCCAGGAAGTTCTACACCTTGAAGTACGTGGCGCTGGTGTGGCC GCACTCTATAGTATCGCTGGCTACTGATCGGGTACTACATTGAAGG TCCCGC	No reverse primer required in Lightning Multi Reaction
(MULTI)	CGATCACAGACAACTTTCTGTACTCTGTGGTACTTCTCGTTCTCTGT	

these colonies, by 50-75% compared to vector-only colonies (data not shown), possibly suggesting selection for lower plasmid copy-number.

As will be discussed later in this thesis, RyR-related toxicity problems are amplified within protein expression systems such as eukaryotic cells or entire organisms, where introduction of the RyR protein is expected to profoundly alter the Ca²⁺ homeostasis of the system, as well as introducing novel, bulky pores into internal lipid membranes.

2.5.1 Mutagenesis on individual PxRyR fragments

The PxRyR modifications introduced during this thesis are listed in Table 2.2, along with the oligonucleotide sequences used to introduce the change.

Prior to mutagenesis, the 18,177bp WT-PxRyR-pIZ/H5 construct was digested into five fragments (Fig 2.1) and each fragment was separately incorporated into a pcDNA3.1(-) vector. All but one of the listed changes in Table 2.2 are to the C-fragment, with E1338D being the exception.

During the latter stages of this PhD, prior to the creation of RFCLM-PxRyR, Agilent released their Lightning Multi kit, which allowed the introduction of up to five mutations simultaneously into an <8kb plasmid, thus vastly speeding up the mutagenesis process. The protocol for the Lightning Multi kit differs from the standard only in primer design, whereby two or more (up to five) primers are used, with each primer capable of introducing one or more changes. Uniquely, all five primers bind to one cDNA strand, with no complementary primer binding required; instead, the *Pfu* enzyme extends the sequence from each primer, in non-overlapping fashion, before knitting together the fragments to generate a single-stranded DNA plasmid for transformation.

2.5.2 fragment assembly into the plasmid and plasmid propagation

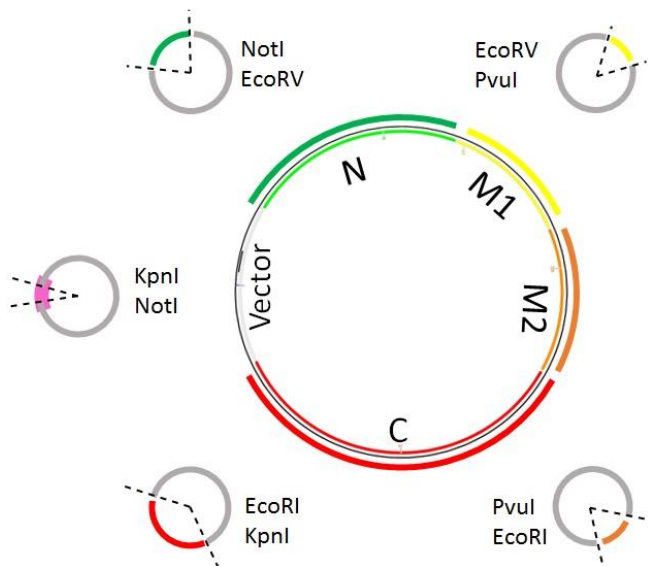


Figure 2.1 *PxRyR* construct, fragment assembly and restriction sites used for cutting out and re-ligating.

The WT-*PxRyR* sequence was digested into four fragments, as labelled in the diagram.

- N ('N-terminus', green) - 4061bp
- M1 ('Middle 1', yellow) - 2350bp
- M2 ('Middle 2', orange) - 2684bp
- C ('C-terminus', red) - 6326bp
- Vector (plZ/H5) - 2900bp

Having divided up the WT-*PxRyR* sequence prior to mutagenesis, the four fragments to be re-incorporated into the linearised plasmid vector required digestion from their respective pcDNA3.1 vectors and re-assembly into a whole intact full-length cDNA (Fig 2.1). However, this five-component ligation, with a final product size of 18,177bp (in plZ) or 23,876bp (in pUAST), had a low success rate under the standard ligation protocol. In particular, the EcoRV blunt end cut site (N - M1 fragments) was associated with inefficient ligation due to self-ligation. This, combined with the necessarily small quantities of each fragment in solution, frequently led to the presence either of construct sequences lacking one or more fragments (especially N or C) or to constructs containing additional copies of the N fragment. A protocol was therefore established in order to maximise

Table 2.3 Ligation ratios for RFCLM and other *PxRyR* assemblies

Fragment	Size Ratio (Moles)	Ligation Ratio
Vector	1	1
N	1.5	3
M1	1	2
M2	1	2
C	2	6

success, in which the total DNA concentration in the ligation reaction was maintained at ~10ng/ul. Equal fragment molar ratios were abandoned in favour of halving the vector concentration, thereby minimising the presence of vector-only colonies. C-fragment concentration was increased by an additional 50%, in order to account for the pore-toxicity mentioned previously (Table 2.3). The ligation solution was incubated at 50°C prior to addition of ligase, and the reaction was run overnight at 15°C and the solution maintained at this temperature until transformation, to

Table 2.4 MUTAGENESIS OLIGOS FOR PC/PIZ HYBRID PLASMID SYNTHESIS

Primer	Sequence	Tag	Restriction site addition
Pc/pIZ switch F	AAACGGGCCCTCTAGACTCG	TGA	AAGCTT (HindIII)
Pc/pIZ switch R	CTTGGTACCGAGCTCGGATC	TGA	ACGCGT (MluI)

maximise stability of the construct. Each ligation product was analysed by gel electrophoresis in 0.5% agarose, running at 60V for 90 minutes, against a 1kb ladder and a linearised full length WT-PxRyR.

It was also observed that the number of successfully transformed bacterial colonies could be increased by up to 10-fold by purification and concentration of the ligation reaction prior to transformation of the new plasmid construct into *E.coli*. In this case, 2µl of the non-purified ligation mix was set aside for control transformation, with the remaining 18µl undergoing ethanol precipitation (2.3.2), re-dissolving the DNA the pellet in 4µl H₂O. For transformation, 50µl of thawed XL10g cells were added directly to the 4µl purified ligation product.

2.5.3 *pcDNA3.1(-) / pIZ/V5-His modified plasmid creation, for fragment assembly*

In order to express PxRyR in Sf9 insect stem cells, a hybrid plasmid vector was created, composed of the multiple-cloning-site (MCS) from pcDNA3.1(-), plus the addition of two extra restriction enzyme cut sites, spliced into a pIZ/V5-His plasmid vector in place of the original MCS. To make this new hybrid vector, the pcDNA MCS sequence was first amplified by PCR, with the additional restriction sites added to the amplicon (primers in Table 2.4). The addition of HindIII and MluI cut sites at the 5' and 3' ends, respectively, allowed the amplified sequence to be digested ready for ligation into pIZ/V5-His.

2.5.4 *Plasmid Assembly Validation*

Transformed, purified PxRyR assemblies were validated for completeness via three steps: diagnostic digestion; complete amplification; and complete sequencing.

Diagnostic digests were carried out initially as a cheap and immediate method of validation. The PxRyR plasmid sample was incubated with the diagnostic

endonuclease of choice (Figure 2.2) for 1h, at a ratio of 0.5µg DNA to 1µl FD enzyme. Analysis was by gel electrophoresis in 0.5% agarose, running at 60V for 90 minutes, using a 1kb ladder and a co-digested sample of WT-PxRyR.

Plasmid assemblies indicating a correct fragment pattern on restriction digest were then amplified in their entirety, as a further check of integrity, in 13 1-2kb fragments (see index for primers) (Fig 2.3a). Finally, constructs positive for all 13 bands were sequenced in their entirety to confirm the faithfulness of the *Quikchange Pfu* enzyme, and rule out the possibility of inadvertent insertions during digestion and assembly (Fig 2.3b).

2.5.5 Transfer of Recombinant RyR constructs between vectors

Plasmid vectors used during this PhD include PcDNA3.1(-), pIZ/H5 (for Sf9 expression, Ch3,4,6) and pUAST (for *Drosophila* expression, Ch5), with recombinant mutagenized RyRs requiring to be transferred frequently between the three. The transfer strategy from PcDNA to pIZ/H5 has been covered above (2.5.3), whilst strategies for transfer of PxRyR and hRyR2 into pUAST will be covered here.

A shortcut was employed for switching the PxRyR cassette between insect expression vectors, based on the observation that two KpnI sites flanked the C-terminal fragment, 1798bp upstream and 1bp downstream, respectively. Simultaneous digestion of RFCLM-PxRyR-pIZ/H5 and WT-PxRyR-pUAST with KpnI, and electrophoresis in 0.5% agarose (60V, 1h) gave bands 8151, for the C-terminal fragment containing the mutation and either 10,020bp for the pIZ/H5-RyR or 15,729 for the pUAST-RyR. Purification and ligation of the mutation-containing fragment with the chosen backbone,, followed by *E.coli* transformation, yielded a much higher success rate than seen for the 5-fragment ligations detailed above. Given that all of the PxRyR constructs studied in this thesis contain alterations only to the C-terminal fragment (excepting E1338D which was created but not studied), this strategy was sufficient for all the required PxRyR transfers between the two plasmids.

(a)	PxRyR-pIZ/H5		PxRyR-pUAST	
	Apal	Sall	Mfel	KpnI + EcoRI
Fragment sizes (bp)	400	650	13661	8451
	1200	2550	5331	7275
	3300	6600	3981	6287
	4000	8300	833	1864
	9100			

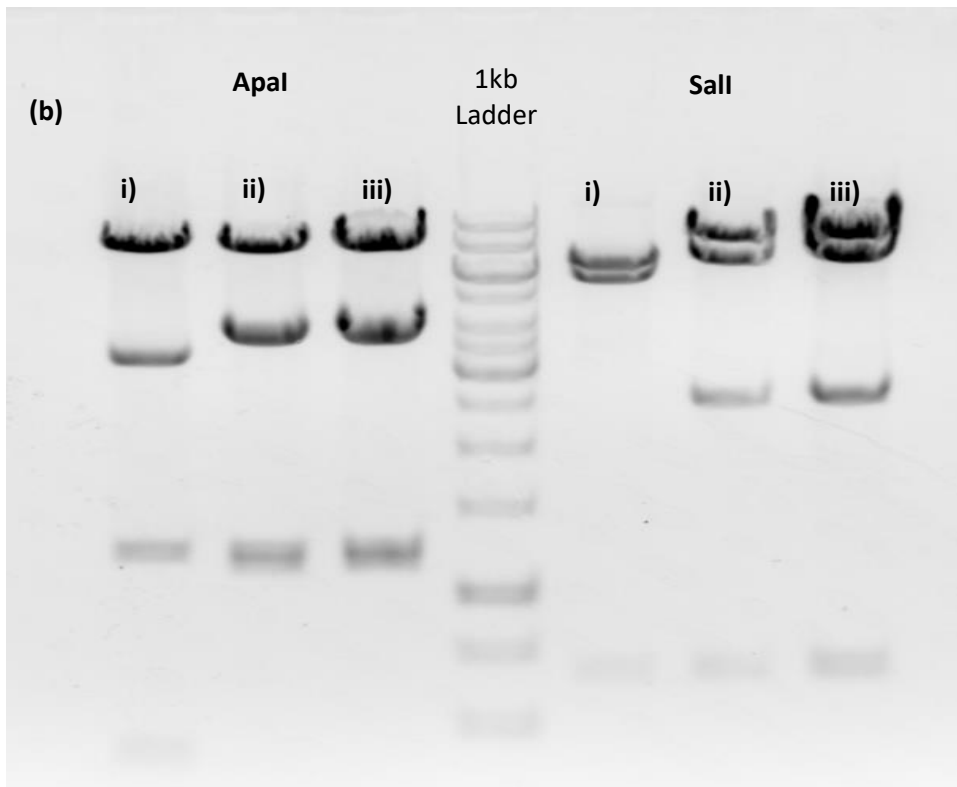


Figure 2.2 Confirmation of correct assembly of the RyR plasmid construct by diagnostic digestion, using one of a selection of endonucleases.

- (a) List of diagnostic enzymes and the expected fragment sizes for RyR contained in either pIZ/H5 or pUAST vectors
- (b) Example electrophoresis gel, showing Apal and Sall digests confirming the correct assembly of RFCLM-PxRyR in pIZ/H5, with i) Incomplete RFCLM-PxRyR construct (negative); ii) Complete assembly RFCLM-PxRyR; iii) WT-PxRyR (positive control)

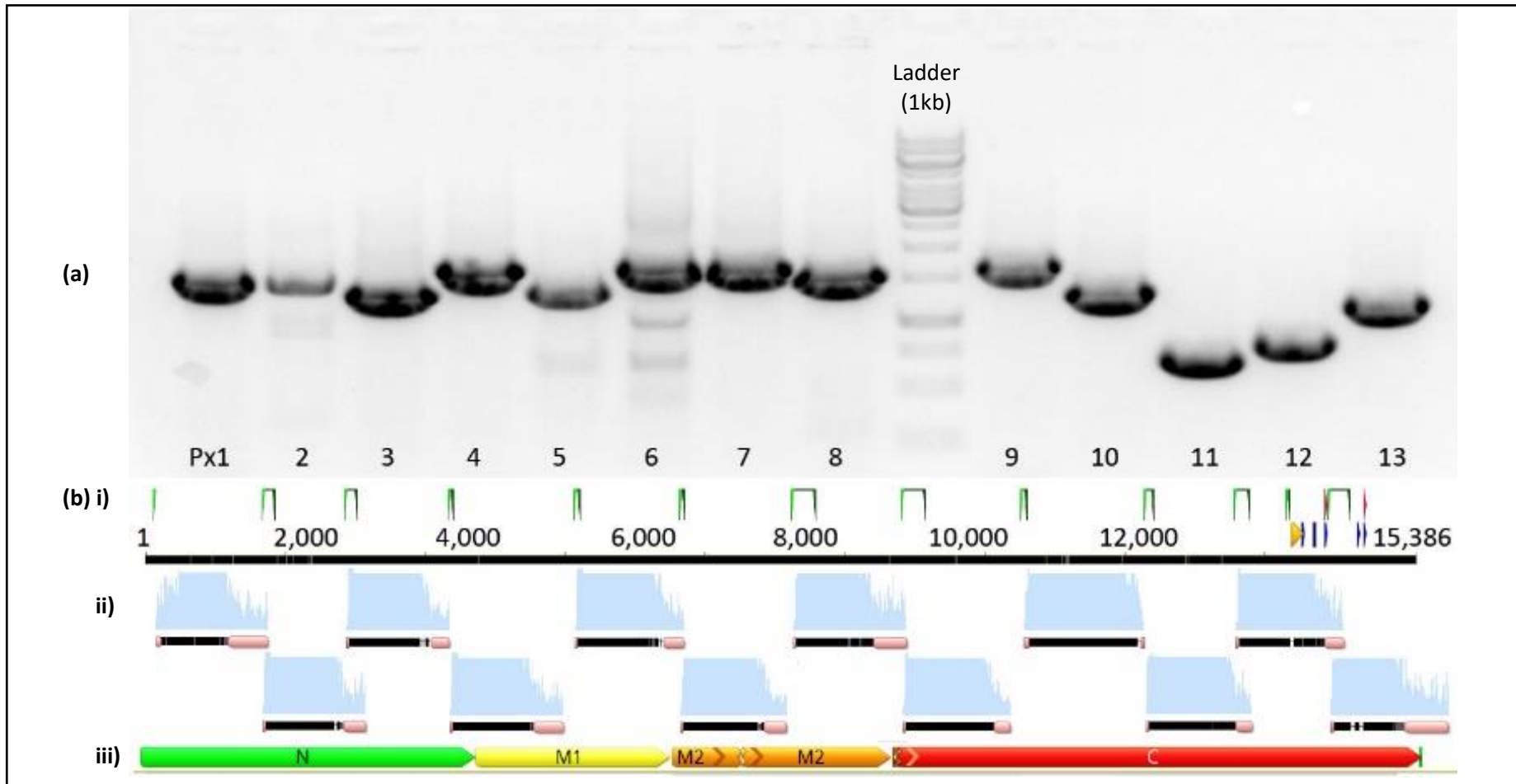


Figure 2.3 Validation of assembled PxRyR plasmids by amplification and sequencing. **(a)** Electrophoresis bands, following amplification of RFCLM-PxRyR by primer pairs Px1-Px13 (see appendix). **(b)** Graphical representation of each PxRyR sequence, with base-pair numbering **(i)** green arrows representing primer bind positions, corresponding to primer pairs Px1-Px13, **(ii)** sequencing traces and **(iii)** coloured schematic of the four PxRyR fragments, as referred to in mutagenesis and assembly protocols of this thesis (2.5.3).

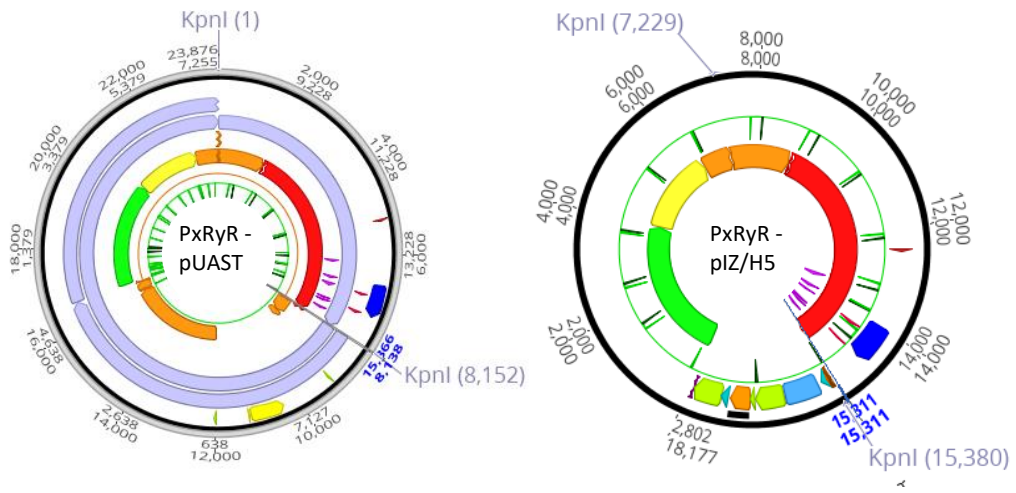


Figure 2.4 Rapid transfer of PxRyR C-terminal fragments between constructs of different vectors via straightforward KpnI digestion.

Chapter 3: Validation of the perfusion Calcium Imaging system for quantifying diamide response in Sf9 cells

3.1 Chapter Summary

The goal of this thesis is to establish differences in diamide insecticide susceptibility between sequence variants of the *P. xylostella* RyR (PxRyR). Accurate quantification of calcium responses in Sf9 cells for the same purpose has previously been achieved using FLIPR on cell lines stably expressing PxRyR constructs (Troccka 2015). This Chapter describes the development and validation of a high-throughput Ratiometric Imaging Perfusion system (RIPS) approach to enable a more rapid assessment of PxRyR responses in Sf9 cells transiently expressing PxRyR.

First covered is a determination of the conditions required for optimal PxRyR channel expression, maximising the number of functionally responding cells. This is followed by an assessment of the caffeine response, selection and processing of adequate responses (as defined below), and a determination of the degree of variation in response between experiments and between sequence variants. The method employed for diamide response quantification is discussed and diamide responses of the wild-type PxRyR (WT-PxRyR) construct under this experimental setup are compared to those established in previous studies. Finally, a second experimental setup, the Absolute Calcium Imaging system (AIS), is considered and compared to the standard RIPS setup in terms of the diamide concentration-responses generated.

3.2 The need for a novel method for rapid in-vitro investigation of insecticide resistance mechanisms

A primary objective of this thesis is to establish the contribution of RyR mutations, which have been found in various moth populations worldwide, to the diamide resistant phenotype. In order to do so, it is necessary to quantify the effect of each of the individual amino acid substitutions found in these diamide resistant moths on diamide-mediated activation of (moth RyR-containing) Sf9 cells. One method of

achieving such a goal is to study intracellular Ca^{2+} signalling mediated by recombinant RyR channels. Such a study should ideally be achievable over a time-scale of months, rather than years, to address the continuing emergence of novel resistance-associated amino acid alterations in moth RyRs (See Ch4+Ch6).

Previous published attempts to express insect RyR (from the model species *Drosophila melanogaster* and *Bombyx mori*) were carried out using HEK293 cells, using the pcDNA vector family (Kato et al. 2009; Xu et al. 2000). These examples built on protocols established by study of the human hRyR2 channel in heterologous mammalian cell lines (George and Lai 2002; George et al. 2004). However, a previous student at Rothamsted (Troccka, 2013 - PhD thesis) found that the HEK293 cell line gave a level of *P. xylostella* RyR expression which was inadequate to be used for functional characterisation. Furthermore, it was found that higher transfection loads caused HEK293 cell death by lysis, possibly due to the absence of insect RyR accessory proteins in this mammalian cell line. By switching to using Sf9 cells, which derive from the fall armyworm, *Spodoptera frugiperda*, functional characterisation of the *P. xylostella* RyR channel was shown to be feasible (Troccka, 2013 - PhD thesis).

Rabbit RyR1 protein expression had been achieved previously in Sf21, via baculoviral transfection. Sf21 is an older *S. frugiperda* cell line which generally gives slightly higher expression than its Sf9 counterpart (Antaramian et al. 2001). However, for a more consistent and reliable intracellular functional characterisation, a non-lytic system was required. InsectSelect (Invitrogen) was developed to contain promoters OpIE2, OpIE1 of the baculoviral system, but circumvented use of the virus itself. Use of such a non-lytic system for insect RyR expression in Sf9 cells was first documented briefly in a DuPont patent (Casper et al. 2010), and more recently in a peer reviewed paper (Troccka et al. 2015). The latter reports the generation of WT-PxRyR and G4946E-PxRyR stable lines of Sf9 cells expressing PxRyR. The cells, which are monoclonal and thus, in principle, near-identical to one another, were able to be analysed en masse on the imaging platform FLIPR (Fluorometric Imaging Plate Reader) in order to precisely quantify response to diamide insecticides.

Chapters 2 and 4 of this thesis aim, once again, to establish quantitative differences in the impact of diamide insecticides upon cellular-scale RyR-mediated response to caffeine in modified PxRyRs expressed in Sf9 cells compared to Sf9 cells expressing

the WT-PxRyR. Preliminary studies indicated that the magnitude of such differences, in terms of cellular fluorescence responding to diamide application, may vary from 1000-fold in some cases down to 2-fold in others. It was therefore necessary to design an experimental system capable of resolving such phenotypic variation. In this case, however, the methodology was also constrained by a second factor, that of time - specifically the time required to generate a relatively large number of PxRyR variants, all successfully expressed in an intracellular location, in order to characterise receptor functionality and diamide response. Whilst previous studies (Troccka et al. 2015; Casper et al. 2010) opted to generate Sf9 cells constitutively expressing a PxRyR protein-coding sequence in order to characterise in high detail singular sequence variants, attempts to repeat the same methodology here were not considered practical, since this thesis reports upon the generation of 13 recombinant PxRyR constructs, reflecting either genetic variants identified in field-studies, or 'artificial' variants, the partial functional characterisation of which will be reported in the following Chapters. As generation of a single monoclonal stable line takes between 3-9 months [Troccka, pers. comm.], assuming optimal success rate, generation of stable lines for all 13 PxRyR variants would alone consume the entire duration of this PhD.

The primary reason that previous studies employed monoclonal stable lines for RyR intracellular studies is for the consistency in expression level that this methodology allows. As will be discussed in detail below, transient transfection of Sf9 cells is associated with variation in:

- i) levels of protein expression
- ii) cell viability
- iii) Fura-2-AM dye loading
- iv) RyR distribution within the Sf9 cell
- v) RyR functionality in response to caffeine, diamides and other applied agonists.

This variation occurs above and beyond variations that derive from the fluorescence quantification system employed, examples of such systems being FLIPR; the Ratiometric Imaging Perfusion system (RIPS) employed here; or the Absolute imaging system (AIS) also employed here (Section 3.5).

The study of Biology is often a continuous exercise in minimising all variables but one: in this case, the Ca^{2+} signals of cells transiently expressing insect RyR. This Chapter details a series of experiments undertaken to characterise sources of variation inherent in attempts to quantify RyR functionality in transiently transfected Sf9 cell lines. Where possible, sources of variation are mitigated. In order to further reduce within-treatment variation, a novel protocol for classification and sorting of cells by response-mode is established. All experiments in this Chapter are undertaken on the *P. xylostella* Wild-Type RyR (WT-PxRyR), with baseline responses to caffeine and diamide being characterised for subsequent comparison to other PxRyR variants.

3.3 Chapter Specific Methods

3.3.1 Overview of the experimental system

PxRyR cds are expressed transiently in Sf9 cells, the cells seeded on glass cover slips and imaged with an inverted fluorescence microscope. The cells are first impregnated with a fluorescent Ca^{2+} indicator and then exposed to RyR-activating concentrations of caffeine, as well as to the diamide insecticides CLR and FLB. Cellular fluorescence, upon the release of Ca^{2+} from its intracellular stores, is recorded and plotted as a function of time. Cells expressing sequence variants of

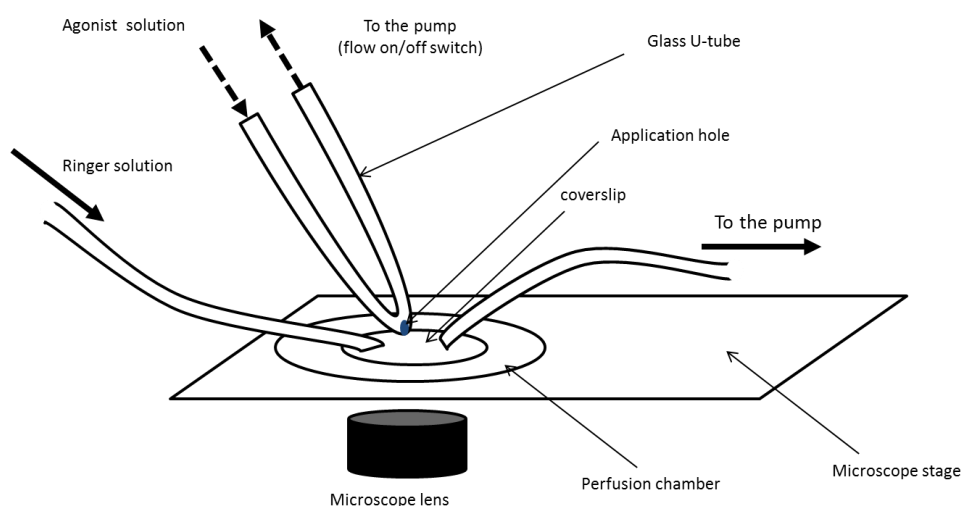


Figure 3.1 (Provided by Troczka) Perfusion chamber setup with a metal U-tube applicator for recording of multiple agonist applications. Black arrows indicate flow of a Ringer solution. Agonist solutions flow directly through the metal U-tube under force of gravity, with peristaltic pumping ensuring negative pressure within the U-tube, relative to the bath solution. Electronic closure of the pump out-flow causes tube pressure to rise, releasing agonist into the bath solution.

the PxRyR are compared in their relative responses to caffeine, and in their relative responses to the diamides.

The Ratiometric Imaging Perfusion System ('RIPS') utilises an inverted microscope to image cells at 20x magnification ($n=200-300$ per FOV). Cells are seeded upon a 14mm diameter glass slip placed within a perfusion chamber. The RIPS' allows confocal imaging of hundreds of cells simultaneously, with highly localised and temporally precise application and evacuation of agonist via the U-tube Reverse Flow technique (Ebbinghaus-Kintscher et al. 2007), whilst continuous perfusion of Ringer's medium prevents local depletion of dissolved Ca^{2+} ions (Fig 3.1). The intracellularly loaded Fura-2-AM fluorescent dye (ThermoFisher) is excited by an alternating 340/380nm LED beam, and is measured by a photodiode detector mounted on the inverted microscope with a fura filter set. Calculation of ratiometric fluorescence intensity across the two excitation wavelengths allows quantification of fura-bound vs unbound Ca^{2+} .

The Absolute Imaging System ('AIS') utilises an inverted microscope and a Hamamatsu OR CA detector enabling imaging at 10x magnification ($n=3000-5000$ per FOV). Cells are seeded upon a 5mm diameter glass slip placed within a Compton perfusion chamber (Fig 3.2). Agonist application is via bolus drop and rapid removal from solution was not possible, although continuous perfusion of Ringer's does take place. Intracellular Fluo4 (Thermo Fisher) is excited by a continuous 488nm LED beam and absolute cellular fluorescence calculated.

3.3.2 Insect cell husbandry

Frozen stocks of Sf9 cells (Life Technologies) were stored under liquid nitrogen, in 1.5ml aliquots of approximately 1.5×10^7 cells re-suspended in Sf-900 II SFM media containing 10% FBS and 10% DMSO. To initiate new cultures, a frozen stock aliquot

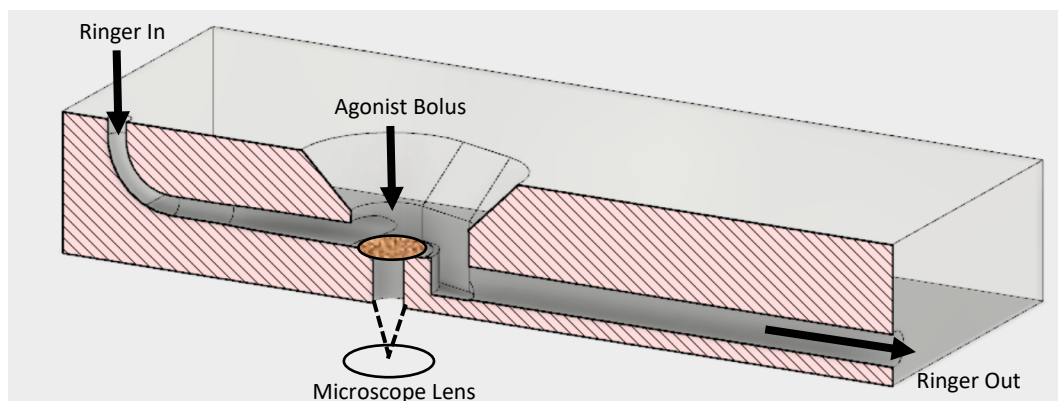


Figure 3.2 The Compton Perfusion Chamber used with the Absolute Imaging System.

was gently thawed at 37°C and transferred to T-25 culture flasks. Flasks were placed in a 27°C incubator and left for 1 hour for cells to attach to the bottom surface. The SFM medium containing DMSO was then removed and replaced with 5ml of fresh pre-warmed SFM media containing 10% FBS and 50µl of a penicillin-streptomycin cocktail (50U/100µg/ml). The cells were kept in the flask until they reached confluence. The cells were then passaged as described below, halving the FBS concentration until it reached 0.6% and the cells were ready to use for downstream applications. Sf9 cells were maintained in a sterile dedicated incubator at a constant 27°C.

The media in near confluent (90-95% cell coverage) T-25 flasks was removed and 4ml of fresh Sf-900 II™ media added. Cells were detached from the bottom of the flask by sloughing and tapping the side of the flask. 1ml of the detached cells was transferred to a new T-25 flask containing 5ml of fresh media containing 0.6% FBS. Near confluent cell cultures were passaged every 2-3 days, with the typical number of passages not exceeding 30. To scale up the cell cultures 3ml of detached cells from the T-25 flask were seeded into a T-75 flask containing 12ml of fresh Sf-900 II SFM media and the desired concentration of FBS.

New stocks of low passage cultures were made by collecting cells from near confluent T-75 flasks into fresh media and transferring the detached cells from each flask into a 50ml tube (Greiner Bio-One, Kremsmünster, Austria). The number of cells present was determined by transferring 10µl of the cell suspension to a hemocytometer for counting. The 50ml tube was then centrifuged at 500g for 5 minutes, the supernatant removed, and the cell pellet gently re-suspended in Sf-900 II media containing 10% FBS and 10% DMSO, at a density of 1×10^7 cells/ml. These cells were split into 1.5ml aliquots and placed in a -80°C freezer for 24h before being transferred to liquid nitrogen in a storage container for long term storage.

3.4 Characterising PxRyR-expressing Sf9 cells response to caffeine and diamides using the Ratiometric Imaging Perfusion Rig

3.4.1 Identification of the caffeine 'type-response' and cellular selection

Throughout this thesis, caffeine was used to activate recombinant insect PxRyR channels, via increased sensitivity to cytosolic $[Ca^{2+}]$, as is common practise (Thomas et al. 2004). Although caffeine activation does not reflect physiological activation of RyR in native insect muscle, it nonetheless triggers $[Ca^{2+}]$ -mediated Ca^{2+} release that is both transient and (somewhat) repeatable, without apparent cytotoxic effects over an experiment's duration. Specifically, caffeine is used to check and standardise the RyR functionality of each cell, in order to qualify that cell for further experimentation. It was thus first necessary to examine variation in the response of recombinant PxRyR-expressing Sf9 cells to caffeine, and to determine which response mode should be treated as a 'type-response'.

Exogenous RyR-expressing cells generally exhibit intercellular variation in RyR activation Ca^{2+} flow dynamics (George et al. 2003b). This may be because inherently RyR-null cells typically used in these types of studies do not possess the requisite Ca^{2+} -handling machinery, that are endogenously expressed in native nerve and muscle cells, needed to regulate RyR Ca^{2+} release. Such receptor dysregulation is expected to increase between-cell variation, whilst also potentially mediating cytotoxicity (George et al. 2003b). One method of reducing cytotoxicity and variation is to form monoclonal stably expressing cell lines (as mentioned in Section 3.2) which, by definition, are capable of consistent, long term protein expression without cytotoxic effects (George and Lai 2002). However, for the reasons described above, all experiments in this thesis were instead conducted on transiently-transfected cells, and therefore awareness and mitigation of between-cell variation became a critical component of the thesis.

One critical observation that was made at an early stage in this PhD Studentship was that application of caffeine (10mM) to a field of view (FOV) containing hundreds of Sf9 cells produces an array of transient responses (Fig 3.3). In order to make sense of such variation, responses were categorised based on the shape of their curve. It was observed that cells broadly divide into one of three response categories:

Logistic rise, logistic fall (Cat A)

Logistic rise, plateau (Cat B)

other (Cat C)

Category A is identified as the 'Type-response' (Fig 3.3, blue response curves), meaning that cells exhibiting this response to caffeine will be selected for further downstream analysis. The majority of past studies also focus on this response mode when studying RyR-functionality, with the logistic rise portion of the response an robust index of Ca²⁺ release from the ER into the cytosol (Thomas et al. 2004). The duration of the the Ca²⁺ release is also determined by RyR intracellular regulation (section 1.5.5) as well as NCX/SERCA Ca²⁺ pump activity. Cardiac RyR2 transients, in ventricular myocytes, are tightly regulated, and have an approx. 1s duration, suggesting that, in an *in-vitro* context, shorter transients may be associated with healthier, more '*in-vivo*-like' cells (Li et al. 2017). Cat A Ca²⁺ responses to caffeine typically reach a maximum within 1-5 seconds.

Category B (Fig 3.3, red response curves) probably also reflects an appropriate CICR response, and thus viable expression of RyR. However, the lack of Ca²⁺ homeostasis is problematic in an experimental analysis that relies on sequential application of caffeine before diamide (see Fig 3.7).

3.4.1.1 A leaky pipeline

In fig 3.3, 371 cells are present in the FOV (brightfield, not shown), of which ~70% have been successfully loaded with Fura 3-AM and are emitting sufficient 340nm fluorescence to be visible in this image. At all points during this thesis, the term FOV refers to the total population of cells visible under the objective during calcium imaging analysis.

- 8.85% ($\pm 6.7\%$, n=4) of these cells, when exposed to 10mM caffeine, exhibit a response that would be categorised as a caffeine response based on prior literature (e.g. for native cells expressing RyR or stable cell lines, (Ebbinghaus-Kintscher et al. 2006). 0% of the untransfected cells responded to caffeine.

- Of these responding cells, 5.9% ($\pm 3.2\%$) exhibited the Cat A response (red), allowing further downstream experiments on those cells. 2.8% exhibited a Cat B response (blue), indicated by failure to return to close to basal fluorescence level within the 30s allotted time.

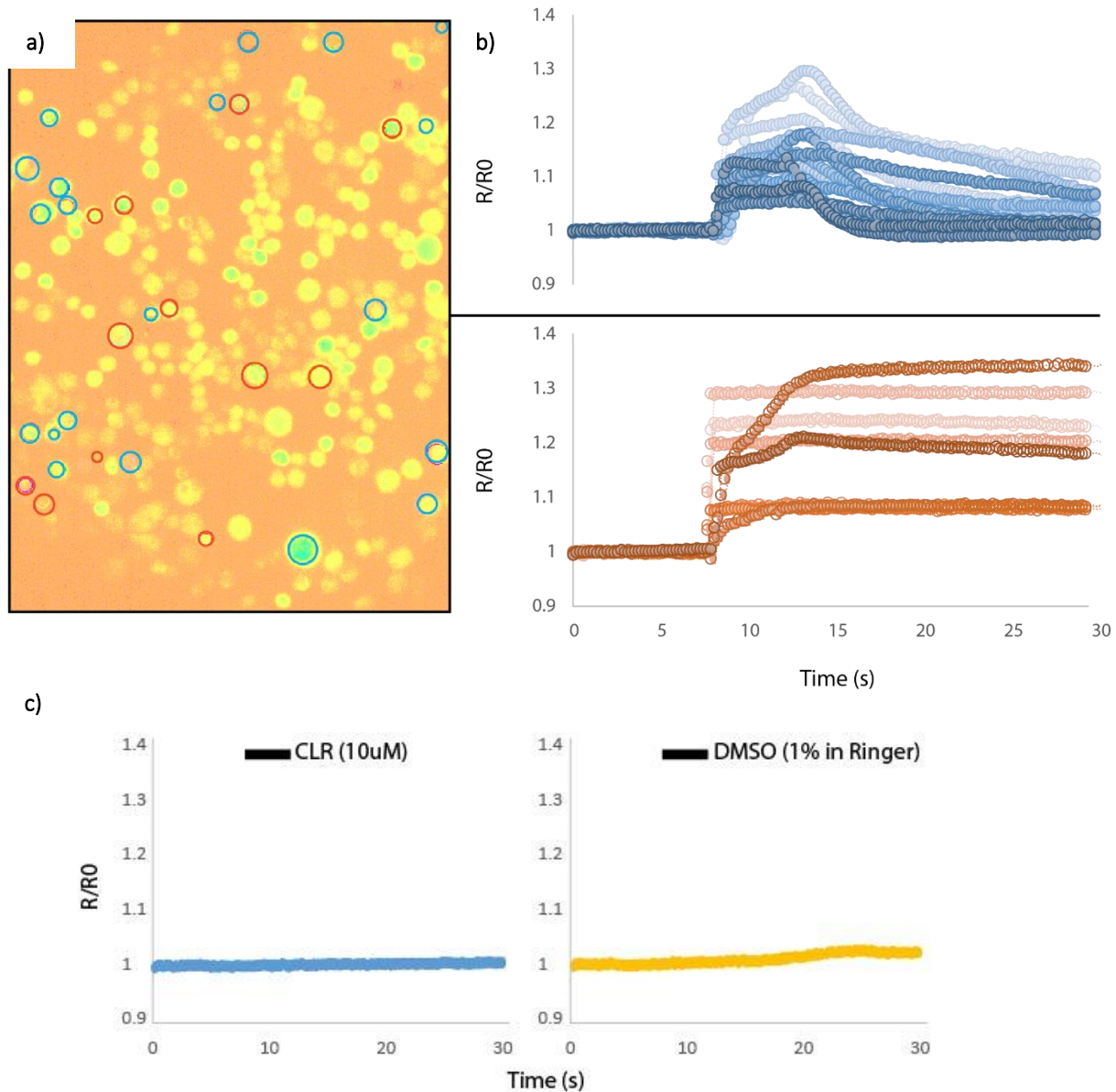


Figure 3.3 Visualisation and processing of caffeine responses in transiently PxRyR-expressing Sf9 cells. The scale bar in this image indicates 100 μ m. PxRyR constructs are expressed in Sf9 cells under standard conditions established in this Chapter. **a)** Responding cells are selected as Regions of Interest, where 'response' to caffeine is defined as a shift in ratio of >0.1 over the 30s period (n=4 slips). **b)** Responders are then grouped by response-mode into Category A - logistic rise, logistic fall (blue traces); B - logistic rise, no fall (red traces); or C - other. Where 'logistic fall' is very broadly defined as any cell that experiences greater than 50% reduction in fluorescence within the 30s period. **c)** Null-transfected cells did not respond to caffeine stimulus (blue) but did respond to DMSO (yellow).

- On average, 86.5% ($\pm 14\%$, $n=4$) of the cells exhibited an increase in fluorescence when exposed to a high concentration of CLR (10 μ M). Null (mock) transfected Sf9s registered no visible response to CLR (Fig 3.3c)

Thus, whilst a high proportion of cells exhibited diamide responsiveness, it is notable that just 1-9% of cells in this FOV exhibit the caffeine-response characteristics that point to PxRyR expression, and the majority of cells display no visible response to 10mM caffeine. Selection of cells with 10mM caffeine (Box 3.1) is thus acknowledged to reduce downstream sample size by a factor of 50- to 250-fold, relative to the total number of CLR-responding cells. However, it was observed that caffeine response co-varies with diamide response within a given cell, such that variation in the former will amplify variation in the latter (Fig 4.5, Chpt 4). It was therefore considered worthwhile to only analyse a consistent sub-population (Cat A) in order to minimise downstream variation.

3.4.1.2 Physiological underpinnings of the observed variations remain unknown

In all the experiments detailed here, Sf9 cells vary dramatically in their response to caffeine (Fig 3.3). Whilst that variation has been successfully quantified and categorised, its meaning in terms of cell physiology and RyR regulation is not clear.

An improvement to this study would be to determine which of the above response types definitively correspond to PxRyR expression, and whether expression location and magnitude varies between cells. GFP-tagging the PxRyR protein would allow visualisation of the proteins location in cells, and crude quantification of the amount of protein being expressed (e.g. see Troczka, 2013 – thesis). Alternatively, immunochemical localization of the PxRyR protein (Niu and Ashley 2000; Baumann 2000) using lobster RyR antibody may be possible. In the absence of such expression characterisations, data on variation in response to 10mM caffeine is a ‘functional surrogate’. Whenever ‘expression’ is mentioned during this Chapter, it is referring to ‘functional response’, with the assumption that response to caffeine indicates expression (because non-transfected cells have been shown not to respond).

3.4.2 Protocol optimisation to maximize the cat A response in PxRyR transfected cells

A series of experiments were undertaken in an attempt to achieve a caffeine response which was reproducible on every level, including:

- within the same cell across multiple caffeine applications
- across multiple cells within the same caffeine application, and across multiple caffeine applications
- across multiple cells within different experiments, and different transfection events.

The variation in response to caffeine within a single FOV (Fig 3.3) can be partially mitigated by response categorisation and selection, as in the protocol described above. However, such variation can be further mitigated by first identifying the cause, and then controlling it. The experimental procedures were therefore examined with the goal of maximising the proportion of cells exhibiting 'Cat A-response'. In tandem with these optimisation experiments, the sources of variation in caffeine response were gradually identified.

3.4.2.1 Optimising cell growth and seeding

During the investigations in this thesis, the following parameters were observed to co-vary with variations in response to 10mM caffeine: Cell density (cells/mm²); Transfection load (μl/cell CF); Viability (%); Proliferation rate (cells/cell/day); and Basal Cellular Fluorescence (pixel intensity).

Preliminary studies of Sf9 cell growth and transfection with PxRyR revealed that wells of cells seeded at an initially uniform density of 400cells/mm², after growth (24h), followed by transfection with 0.02ul/ml of Cellfectin (4h) and further incubation (44h), varied in density at the 48hr time point from 0 to >800 cells/mm² (counting only viable cells). During the initial 24h, migration and cellular proliferation result in non-uniform cell distribution at the point of transfection. During the transfection incubation, cells in patches of local low-density were prone to lysis. During the final 44h, cells in different parts of the plate proliferate at different rates, presumably due to local density and transfection conditions.

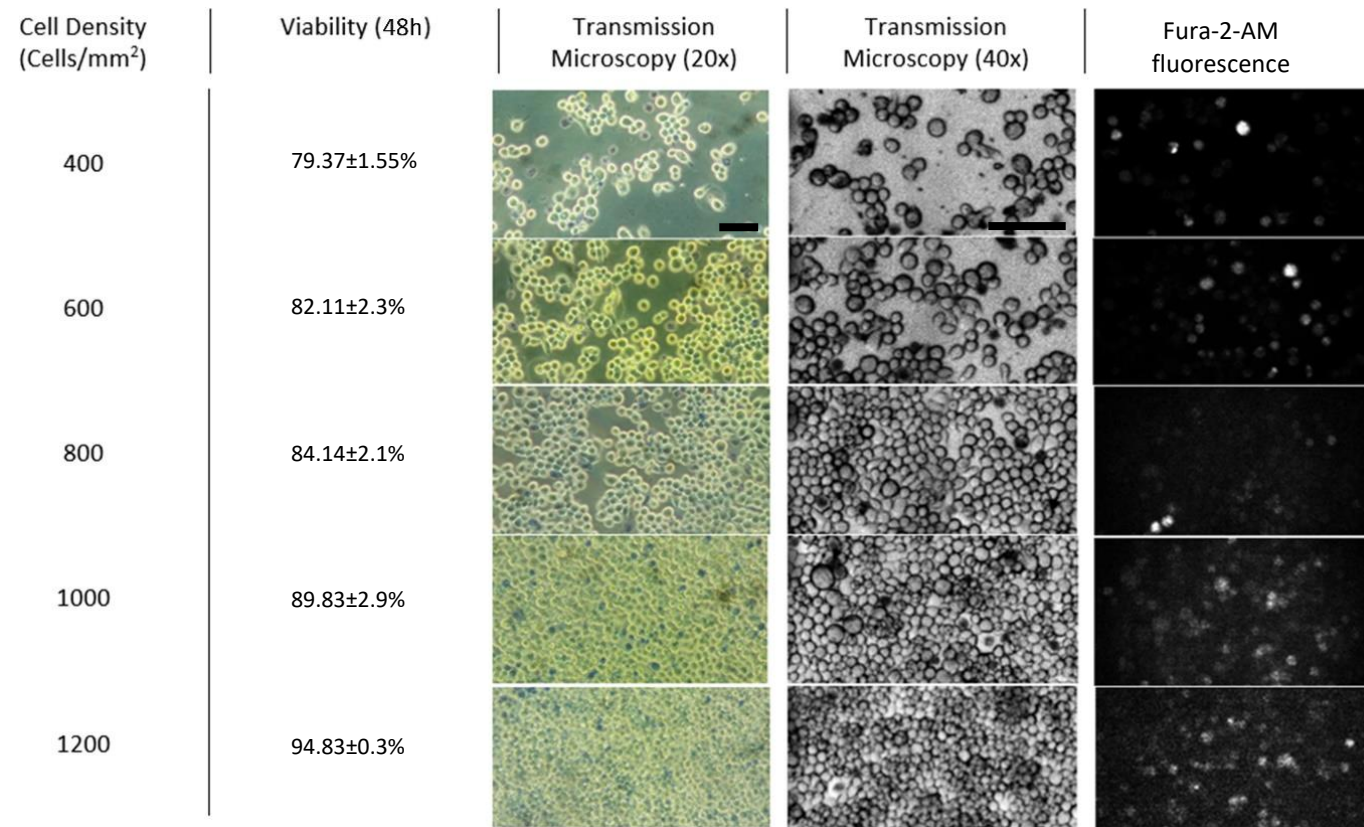


Figure 3.4 Cell culture optimisation – Growth conditions to maximise a Cat A caffeine response. Scale bar 100µM. The 20x and 40x images are taken of different FOVs upon the same coverslip. Trypan-blue stained cells are displayed as Transmission Microscopy images obtained with a 20x objective lens (LH panels). Further bright-field magnification of the FOV allows detailed assessment of cellular phenotype (centre panels). The Fura-2-AM stained cells are visualised down a 40x objective under a 380nm LED beam (RH panels).

In an attempt to optimize the seeding density, Fig 3.4 displays the growth of monolayer cell culture preparations seeded at densities of between 400 and 1200 cells/mm². Cell density was measured at the point of seeding, determined by the number of cells transferred into the culture well.

Cell viability was measured after 48 hours of growth. Trypan blue permeates ruptured cell surface membranes as a consequence of necrotic cell death. Non-permeable cells are therefore assumed to be viable (i.e. have an intact surface membrane). Trypan blue assays indicate that cell viability increases dramatically with density. Reduced cell viability (Trypan test) corresponds with reduced cell density after 48h (Fig 3.4).

Higher magnification analysis of unstained, undamaged cells under bright-field illumination (Fig 3.4 centre panels) shows that cell diameter decreases with density, with cells at the highest density being 27% smaller on average than those at the lowest density. At the optimal seeding concentration of 800 cells/mm², only 5-15% of cells are visibly damaged – i.e. display membrane blebbing; a rounded shape; poor adhesion; positive for trypan blue staining.

Cells were also loaded with Fura-2-AM in order to determine effects of density on the fluorescence signal (Fig 3.4 RH panels). Average cellular fluorescence decreased slightly from 1238 at 400cells/mm² to 989 at 1200cells/mm², but variation (standard deviation) in fluorescence between cells decreased dramatically from 702 down to just 288, suggesting that higher densities could reduce variation in background signal. However, density was limited on the upper end by the requirement to avoid cell overlap in order to define clearly the fluorescence response of a given cell during experimentation. Average cell confluency must therefore remain below 90%.

The results presented in Fig 3.4 suggest that increasing the seeding density is beneficial for cell health, and gives more dense cultures at the 48h timepoint, but the overall rate of growth and proliferation of cells prescribes a maximum seeding density of 800 cells/mm² in order not to exceed the approximate 90% confluency boundary. This is the equivalent of 150,000 cells in the 1.9cm² well. This was adopted as the ideal density for all the remaining experiments in this thesis.

3.4.2.2 Optimising Transfection

Cellfectin (CF) is a cationic lipid-mediated transfectant which functions by wrapping individual DNA molecules in unilamellar micelles to facilitate their uptake into cultured cells. The reagent has a phosphatidyl head group which binds to the negatively charged DNA, whilst its fatty acid side chain facilitates uptake of the molecule into the cell, possibly via endocytosis. Because it functions by surrounding the DNA, the concentration of the reagent must be optimised in relation to the amount and size of the DNA molecule (see Fig 3.5), according to recommendations in the manufacturer protocol.

PLUS is a surfactant which aids formation of CF:DNA complexes under some circumstances, although its precise mode of action has not been specified by the manufacturer (Thermo-Fisher Scientific). All transfections in this thesis use the manufacturer recommended concentration of PLUS reagent, of 0.0045ul per ul Sf900II medium.

Fluorescence of (Fura-2-AM loaded) cells in response to caffeine agonist was used as a proxy indicator for PxRyR protein expression (as detailed in section 3.4.1.2). The total number of responding cells increases with CF concentration, but the number of Cat A cells plateaus at 0.02 μ l CF/ul medium, whilst cell viability decreases concurrently (Fig 3.5). Taken together, these results indicate that future transfections should occur at 0.02 μ l CF per μ l medium, in order to maximise expression levels at minimal cost to cell health. Such optimisations are repeated for each PxRyR sequence variant studied in this thesis, with the ideal CF concentration varying between 0.015 – 0.025. An identical concentration of CF when applied in the absence of complexed DNA did not cause measurable reduction in cell viability. Furthermore, no Cat A responses were detected after transfection with PLUS and DNA in the absence of CF.

In conclusion, cell seeding density and the concentration of transfection reagent cumulatively affect cell viability and hence the caffeine response.

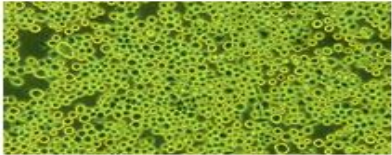
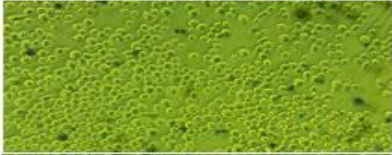
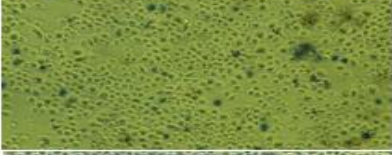
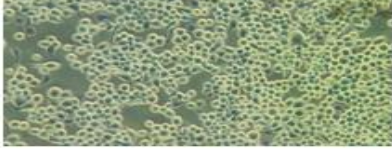
Cellfectin volume (per μ l medium)	Amount of DNA (per μ l medium)	Amount of PLUS (per μ l medium)	Viability (48h)	% Responding Cells	Transmission microscopy image (20x)
0 μ l	3.25ng	0.0045 μ l	99.61%	0/50	
0.01 μ l	3.25ng	0.0045 μ l	92.47%	0/50	
0.015 μ l	3.25ng	0.0045 μ l	84.14%	12%	
0.02 μ l	3.25ng	0.0045 μ l	83.42%	18%	
0.025 μ l	3.25ng	0.0045 μ l	81.20%	22%	

Figure 3.5 Transfection optimisation – ideal transfection reagent composition for transient transfection. The effects of different concentrations of transfection reagent on cell viability and PxRyR protein expression is shown. Transfection occurs in 200 μ l medium, with Cellfectin (CF) concentration varied according the manufacturer’s recommendations. Amounts of DNA and PLUS reagent used were constant, such that the key variable is the ratio between CF:DNA. Viability was measured with the Trypan-blue cell viability test (see text) at 48 hours after searching for responding cells. Cells reared at 800cells/mm² density (as per Fig 3.4). Images taken 48h after transfection. Experiments were undertaken to determine how to minimise death whilst maximising Cat A response frequency. N=1 coverslip, 50 cells, calcium imaging carried out following protocols in detailed in Fig 3.3.

3.4.2.3 Optimising transfection incubation times

Other transfection parameters were modified as per manufacturer suggestion, to maximise the frequency of Cat A responses. Initial incubation of CF solution and DNA solution individually was maintained at 5 minutes, sufficient time for solution homogenisation. Transfection reagent incubation with the DNA (30 minutes), before application to cells, is designed to allow the formation of CF micelles containing PxRyR DNA. Incubation of Sf9 cells with transfection reagent for <2h was insufficient to yield any Cat A caffeine response in the subsequent cell culture. Experiments in this thesis therefore follow a 4-hour incubation with CF, chosen as the optimal period that yields sufficient numbers of Cat A responding cells needed for experimentation whilst minimising the amount of time spent in potentially toxic conditions. However, it was noted that when the cell transfection incubation time was increased up to a maximum of 24 hours there was no observed change in cell viability, on the other hand neither was there an increase in PxRyR expression. After the 4h transfection, cells are returned to 'conditioned medium' with addition of 0.6% BCS in order to promote cell health and proliferation.

In terms of post-transfection incubation, the response of cultured cells to caffeine was quantified at 24h, 48h, 72h, 96h in WT-PxRyR. The total number of responding cells increased over time and was highest at 96h, however Cat A responses were most frequent at 48h.

3.4.2.4 Fura 3-AM intensity is problematically high in damaged cells

Fura 3-AM was used as a ratiometric Ca^{2+} indicator due to its high dynamic range and long window of effect due to slow compartmentalisation, and slow decline in fluorescence. A Ca^{2+} binding affinity for this dye of $K_d=335\text{nM}$ compares favourably to the free cytosolic $[\text{Ca}^{2+}]$ of healthy cells, which is typically around 50-100nM. However, basal cellular fluorescence varied from ~200 to ~2000, with the value shown to negatively correlate with cell *density* (cells/mm²) and *viability* (trypan blue test) (Fig 3.4). In the case of damaged cells, the increased fluorescence may be due to a failure of Ca^{2+} homeostatic mechanisms in the cell, allowing uptake of Ca^{2+} from the media, which has a comparatively high Ca^{2+} concentration of 2mM. In all cases, a 10-fold variation in basal fluorescence threatened to be problematic if it would push the brightest fluorescing cells close to the dye's upper limit of fluorescence. Past authors have indicated the maximum saturable range of this dye is 1000nM

(Thomas and all 2000) which would put the brightest resting cells during these experiments far above the upper limit of fluorescence. In order to sidestep the problem of variable fluorescence, brightly fluorescing FOVs of cells (representing low viability or unhealthy cells) were avoided during all experiments, and individually brightly expressing cells were excluded from downstream analysis.

3.4.2.5 The Final optimised Transfection Protocol

Sf9 cells were grown at 27°C in Sf900 II SFM supplemented with FBS. Transfection of cells with the Piz/H5 PxRyR expression plasmid and Cellfectin ('CF', transfection agent) was performed according to the manufacturer's (Thermo Fisher Scientific) instructions. Glass coverslips (1cm² diameter glass) coated with Poly-L-lysine (Sigma, MA, USA) were placed in a 4 well plate. Each well was then filled with 500µl of Sf-900 II medium and each coverslip was seeded with 150,000 cells, for a density of 800 cells/mm², giving 90% average confluency. Cells were allowed to attach to the coverslips for 16h and then were transfected in 4 well plates. Transfection solution was composed of: 3.25ng PxRyR-piz/H5 plasmid DNA dissolved in water; 0.0045µl PLUS detergent; 0.02µl CF; per 1ml of fresh Sf900II serum-free medium. CF and DNA:PLUS solutions were individually mixed and incubated for 5 minutes, before combination and incubation for 30 minutes. Cells were removed from their media and washed twice, prior to addition of transfection solution. Transfection incubations proceeded for 4 hours, before the cells were washed and returned to 30% conditioned SF900 media, with 0.6% FBS. Post-transfection, cells were incubated at 27°C for 40-52h. Cells were then loaded with Fura-2-AM prior to imaging, as outlined in the following section.

3.4.3 Calcium Imaging

In PxRyR-transfected Sf9 cells, caffeine- and diamide-mediated activation of the RyR is thought to result in a flow of Ca²⁺ from the endoplasmic reticulum (ER), leading to rapid increase of free cytosolic calcium concentration ([Ca²⁺]_c) which is bound by the Ca²⁺- sensitive reporter dye and visualised as an increased fluorescence signal intensity (based on in-vivo studies (Ebbinghaus 2007)).

The experimental calcium imaging methodology for this study is based upon previous work (Trocza 2015) but required adaptation for use on transiently transfected, rather than stably transfected, cell lines. One novelty is the approach of relativizing cellular response to diamide application against prior response to

caffeine application, which is detailed in Box 3.1. Standardised caffeine concentration was reduced from 30mM to 10mM in order to allow consistent response to repeated applications upon the same cell (Fig 3.7d). Other changes have been discussed throughout section 3.4.2. The resolved experimental method is as follows:

3.4.3.1 The Final calcium imaging and data collection protocol

Fura 3-AM dye was used for monitoring calcium release in Sf9 cells transfected with recombinant PxRyR. 48h post transfection cells were loaded with 1mM of Fura 3-AM. Cells on coverslips in 4 well plates were first put into 500µl of fresh SF-900 II medium and then 2µl of the dye stock solution (5mM) was added. Cells were left to incubate at 27°C for 45-60 minutes, followed by 3 washes with 500µl of fresh un-supplemented Sf-900 II medium. Prior to imaging, coverslips with Fura-2-AM loaded cells were placed in standard Ringer's solution, with 2mM [Ca²⁺] (CaCl₂). All experiments were carried out in an air-conditioned room maintained at approximately 25°C.

Unless otherwise stated, data collection for all the calcium imaging studies reported in this thesis took place on the RIPS system. This system uses an Axio Vert.A1 microscope with a LD Plan-Neofluar x10/0.4 lens (Zeiss, Oberkochen, Germany), measuring the ratio of excitation at 340/380nm (calcium free/calcium bound indicator) every 180ms and capturing emission at 510nm. Cells on the coverslip were placed into a perfusion chamber of approximately 0.5 ml volume (Fig 3.1) mounted on the microscope stage. A peristaltic pump drives continuous unidirectional flow of Ringer through the bath. Caffeine and diamide agonists were applied using 3 seconds bursts via a metal U-tube. Fluid dynamics were measured using a solution of red amaranth dye, diluted 1:20 in Ringer. Perfusion flow rate was 49µl/s. Agonist solution travel time from U-tube to bath was 21s. Agonist release formed a constant and repeatable teardrop shape in the bath, of radius 1.3mm. From point of trigger to expansion into final radius took ~0.15s. No admixture of dyed-agonist solution with bath-solution was apparent, with the dye-solution forming a clearly visible boundary at the edge of its radius, when viewed at 4x magnification. After trigger release, evacuation of agonist was mostly via the U-tube, and the majority of dye-solution was evacuated within ~0.25s, however a small proportion of the solution avoided U-tube evacuation and instead mixed with the bath solution.

Experiments upon fields-of-view (FOVs) of cells consisted of multiple agonist applications, with the order and timing of applications dependent on the experimental aims. Recording begins at T=0s, with application of 10mM caffeine at 7-10s, followed by a 140s delay, during which period, the caffeine application recording is viewed in order to highlight respondent cells. During range finding experiments (Fig 3.8a), iteratively increasing diamide concentrations are applied, with a delay of 30s between applications. During concentration-response experiments (Fig 3.9), a single caffeine application is followed by a single diamide application at 150s. Experiments were recorded using VisiView® (Visitron Systems, Puchheim, Germany) software. Raw video capture on the software was used to identify responding cells and crudely assess response mode. Outputted numerical pixel intensity data were analysed using Microsoft Excel and SigmaPlot v.12 (Systat Software).

3.4.4 Characterisation of the recombinant WT-PxRyR Caffeine-response in Sf9 cells

It was necessary to fully characterise the caffeine response of recombinant PxRyRs because caffeine response is used as a baseline against which to assess the diamide response. Relative shifts in caffeine response between cells are used to calibrate measurements of diamide response between those same cells. Characterisation of WT-PxRyR in terms of caffeine and diamide response will also be used as a baseline against which to compare other recombinant PxRyR sequence variants.

The data in Fig 3.6 comprises caffeine applications (10mM) across 5 FOVs across 3 experiments (Fig 3.6). Caffeine response was shown to be broadly comparable between cover slips and between experiments, utilising the RIPS system and the standardized methodologies described above. Each FOV of cells yielded between 5-22 Cat A respondant cells. 'R/R0' refers to the absolute increase in fluorescence in response to agonist application (maximum amplitude of each cell), expressed as a ratio of cell baseline fluorescence. The highest recorded response of any single cell in this experiment was 1.45, indicating a maximum fluorescence increase of 45% against the baseline fluorescence of that cell. For the majority of FOVs measured, an average R/R0 between 1.1-1.3 was recorded. Thus in general, caffeine signals observed here are small in comparison to those of other cell types studied in the literature (Thomas 2004), but in many cases the signal-to-noise ratio is extremely good.

Within a given FOV, interquartile variation in caffeine response can be as low as 0.05, or as high as 0.18. Interestingly, between different cell FOVs, interquartile variation is no higher than that between cells on a single FOV. Similarly, interquartile variation between experiments is not higher than that between FOVs in a single experiment (Fig 3.6), all together suggesting that the majority of fluorescence variation occurring in these experiments is physiological (derived from within the cell) rather than due to abiotic variations occurring across the coverslip or across different experiments.

The rest of this section will therefore discuss steps taken to ensure that variation in caffeine response between cells on the same FOV, and between those on different FOVs and different experiments, does not translate to variation in diamide response measurements.

3.4.4.1 Cellular characterisation of Caffeine-release

The amplitude, wavelength and minimum period of caffeine-evoked Ca^{2+} release transients were characterised in single WT-PxRyR expressing Sf9 cells (Fig 3.7). Within a single FOV of cells, amplitude of fluorescence signal caused by Ca^{2+} -release transient is shown to increase with increasing concentrations of caffeine agonist

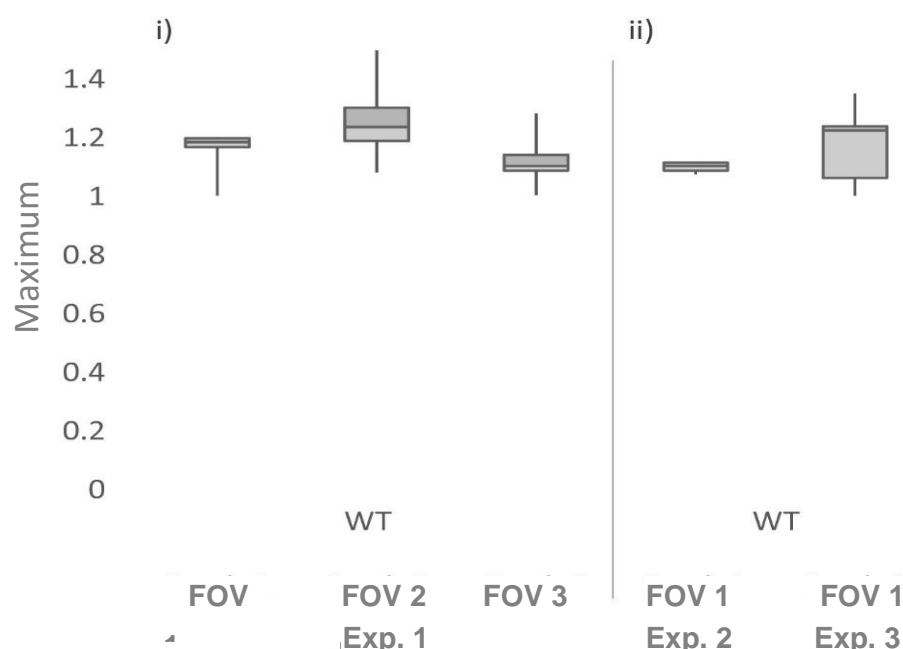


Figure. 3.6 Boxplot of transient amplitude in response to 10mM caffeine, showing variation in caffeine response across i) multiple FOVs on the same coverslip ii) FOVs on coverslips over different experiments

(Fig 3.7c). The signal amplitude directly measures increase in Ca^{2+} in the cell – hypothetically caused by Ca^{2+} released during gating of the population of PxRyR channels in the cell (i.e. one CICR cycle). Normally, *in-vivo* Ca^{2+} release is tightly controlled by a series of RyR-modulating proteins (see Introduction Chapter). CICR only occurs once a series of conditions are met, including correct store-filling, ATP availability, and cytoplasmic Ca^{2+} evacuation, which ensures that the Ca^{2+} efflux is approximately constant across multiple release events. In this thesis, the RyR-modulating machinery is lacking from the cellular (Sf9 cell) environment, and RyR regulation is thus achieved primarily by varying caffeine concentration, whereby caffeine increases the sensitivity of the channel to luminal Ca^{2+} . The increase in signal amplitude with increased caffeine application (Fig 3.7c) appears to have an approximately linear relationship between caffeine concentrations in the range 1mM to 30mM, indicating that an appropriate level of control over RyR opening is achieved through this methodology. 10mM caffeine appears to lie well within the linear portion of the concentration-response graph, eliciting an approximately half-maximum (EC50) response, on average, in these cells. The results therefore support the adoption of application of 10mM caffeine as the standard sub-maximal activating concentration for recombinant PxRyR-expressing Sf9 cells during the experiments discussed in this thesis. Regarding the concentration-response curve itself (Fig 7c) it should be noted that this data represents only that from a single FOV of 17 responding cells, under a protocol of sequential addition of increasing concentrations of caffeine to the same cells. Whilst it is not valid for drawing detailed conclusions on the nature of caffeine activation outside of this lone FOV, the graph nevertheless permits comparison with previous studies. Casper et al (2010) previously reported a sigmoidal relationship for other insect RyR-expressing Sf9 cells in response to caffeine, broadly similar to that described here but with an approximate 10-fold reduction in the EC50 (i.e. increased sensitivity to caffeine). If the RIPS methodology employed herein reports lower- than-expected sensitivity, this should be attributed to the rigorous selection procedure (Fig 3.3) which by selecting for a given response mode may inadvertently select for a given response magnitude. In any case, the experimental format is designed for comparison of diamide-response between PxRyR sequence variants studied within this thesis, rather than with other publications which occur on unrelated experimental setups (see conclusion of this Chapter for further discussion).

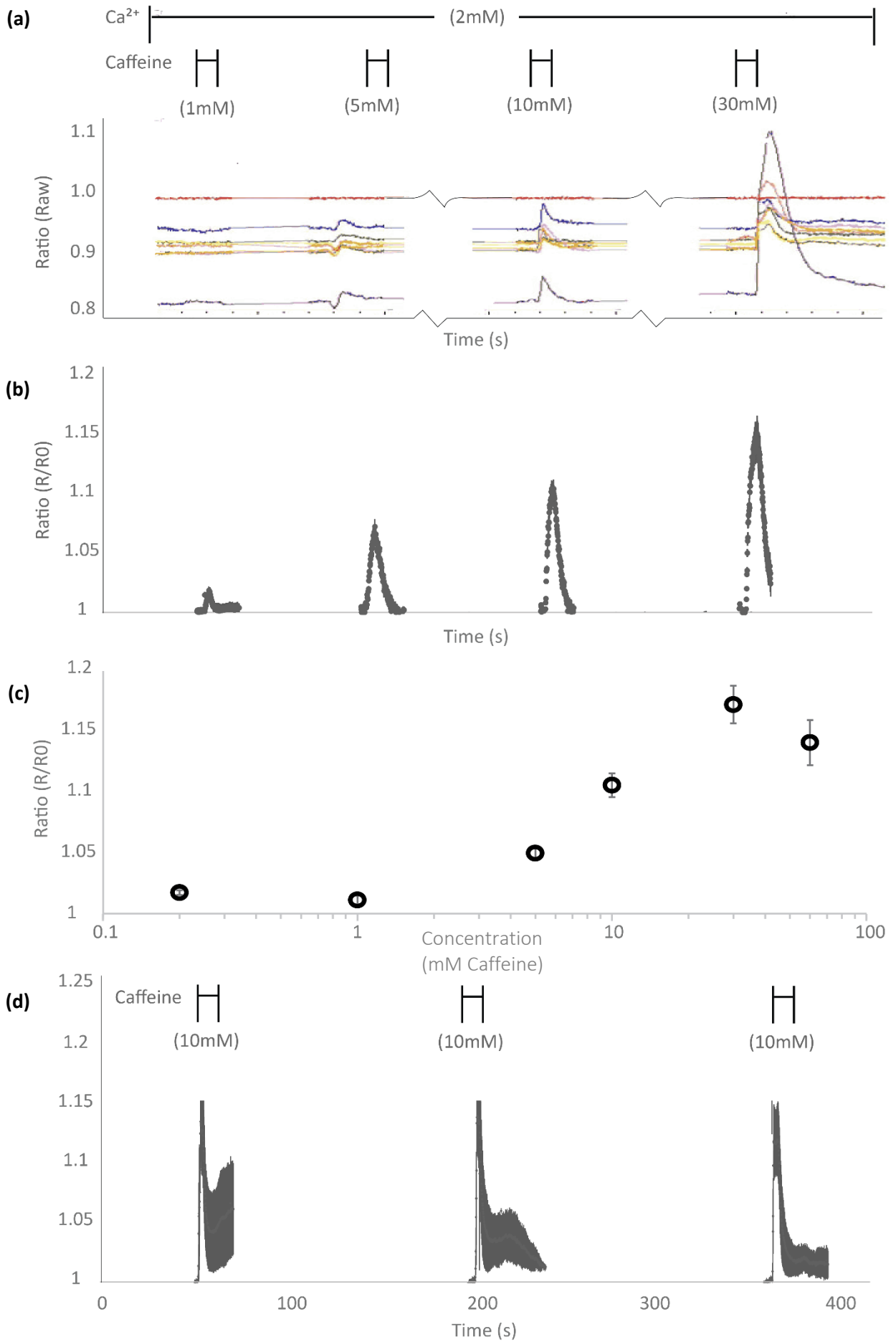


Figure 3.7. Characterisation of variation in caffeine response at increasing caffeine concentrations, and across time at constant dose

- (a) Example of raw fluoresce data from Sf9s expressing WT-PxRyR exhibiting calcium signal transients in response to increasing concentrations of caffeine. 10 cells were selected for raw data acquisition, one of which lacks a caffeine response (top, red) and is used for 'non-responder baseline removal', as per box 3.1.
- (b) Application of successively increasing doses of caffeine on Sf9 cells expressing WT-PxRyR
- (c) Data from (b) represented as concentration-response for clarity.
- (d) Repeated application of 10mM doses of caffeine, with rest period of 30s. WT-PxRyR expressing cells show consistent caffeine response over time and return to near resting Ca^{2+} concentrations within 30s. By contrast, cells exposed to 30mM caffeine required at least 150s to return to a resting state and failed to exhibit consistent response (data not shown).

Experiments were also conducted to determine the minimum resting period that would ensure complete calcium store renewal after caffeine exposure. Lumenal Ca^{2+} store volume is the primary driver of Ca^{2+} release amplitude, where higher store volumes create a higher concentration gradient, allowing more Ca^{2+} release within a fixed CICR period. Tight control of calcium store volume in experimental cells should therefore be a priority. Fig 3.7d shows that, at 10mM, 100s of resting period was required before a second transient, identical in amplitude to the first, could be elicited. A shorter resting period was associated with iterative reductions in transient amplitude, for example 30s resting period gives response of 1.08 ± 0.03 . At 30mM, a resting period of 500s was often not sufficient to allow elicitation of a second identical transient, suggesting that this concentration of caffeine perhaps alters the physiology of the cell. Such observations are critical to this thesis, where almost all *in-vitro* experiments on diamide activation require sequential application of caffeine before diamide (see Box 3.1).

Transient calcium signal duration did not increase meaningfully with increased caffeine concentration within the same cell, or between cells of the same FOV. Differences in transient signal duration are largely mediated by other cellular factors outside of the RyR, such as the relative activity of the various pumps (NCX, SERCA, etc) as well as titres of lumenal and cytoplasmic Ca^{2+} buffer and chelator proteins ((George et al. 2003a), and would therefore not be expected to respond to caffeine concentration.

3.4.5 Characterisation of the recombinant WT-PxRyR diamide-response in Sf9 cells

The primary aim of this thesis is to determine the impacts of lepidopteran RyR amino acid variants upon diamide insecticide efficacy. In the remaining portion of this Chapter, the response of recombinant WT-PxRyR transfected Sf9 cells to the diamides FLB and CLR will be characterised.

The recombinant PxRyR response to caffeine was characterised previously, in terms of its variation within a FOV (Fig 3.3), variation across experiments (Fig 3.6) and physiological properties over a range of caffeine concentrations (Fig 3.7). These characterisations served two purposes within the wider thesis, firstly acting as an experimental template upon which to conduct the diamide experiments and secondly by closely defining 'physiological normality', in order to pre-define which cells are suitable for inclusion in diamide experiments. Going forward, the standard protocol for diamide experimentation will involve pre-application with 10mM caffeine, a step which itself serves multiple purposes:

1. Identifying appropriately responding cells (c.f. Fig 3.3)
2. Quantifying the relative responsiveness of each individual cell

The assumption of point 2. is that individual cellular caffeine response co-varies with individual cellular diamide response (within a given PxRyR variant of recombinantly expressed PxRyR). This was shown to hold true in subsequent work (Ch4, Fig 4.6). The diamide response can thereby be relativized, based on first relativizing the caffeine response (See box 3.1 for how this Proportional Normalised Response (or PNR) is calculated).

To calculate the Proportional Normalised Response (PNR), raw data was first normalized using the equation: F/F_0 , where F is a fluorescence ratio value recorded for an individual cell upon each individual time point and F_0 is an average fluorescence ratio calculated over the first 5 seconds prior to addition of the agonist. The maximum response amplitude is taken as the maximum fluorescence signal outputted by the cell across all frames.

Final amplitude data was presented as a mean value and the standard deviation of the mean. In all concentration-response plots in this thesis, response data was expressed as a percentage of the highest response registered within the graph. In the case of diamide studies, normalized diamide response data was relativized

against prior caffeine response data of that same cell (in the RIPS system, 10mM caffeine application always occurs 150s before diamide application). Data points are presented as the mean values for each individual experiment and standard errors compared to the mean.

3.4.5.1 Agonist Diluents and Background Fluorescence

Due to their low solubility in water, stock P_xRyR agonists used in this study were dissolved initially in DMSO and then diluted into the Ringer's medium at a dilution factor of 1:100. For example, stock solutions of 1, 10, 100 μ M FLB sulfoxide were made up in 100% DMSO, and immediately prior to application, diluted 1:100 in medium. 1% DMSO was found to elicit low amplitude linear responses in some Sf9 cells (both transfected and non-transfected). In the context of prior 10mM caffeine activation, these DMSO-mediated responses were comparatively small, but however still large enough to impact response readings in the pre-linear (<EC₅₀) portion of the concentration-response relationship. As such, the fluorescence amplitude of 'non-responsive' cells (those exhibiting no change in fluorescence in response to caffeine) was measured during each diamide measurement, and then subtracted from the fluorescence of each responding cell (see Box 3.1) in order to remove DMSO-mediated fluorescence from further analysis.

Changes in background fluorescence due to application of agonist frequently occur in non-ratiometric calcium imaging, either due to changes in solution viscosity or due to poor dissolution of agonist in the media. In this present case, use of a ratiometric dye mostly removes the issue of background disturbance, and the effects occur equally at both ratiometric wavelengths, and therefore cancel each other out. Any remaining noise is ameliorated by the 'non-responder' subtraction mentioned above.

Despite introduction of the above steps to remove agonist application background noise, as FLB has a notoriously very low water solubility (around 0.03 mg/l), particles are still visible when diluted from DMSO into Ringer's medium at concentrations above 5 μ M. In all cases in this thesis therefore, the more soluble sulfoxide form of FLB was used for experiments. This compound differs only by the removal of one double-bonded oxygen from the terminal sulfur moiety, and was shown previously to illicit a very similar response in *Heliothis* neurons (EC₅₀ 0.61 μ M (FLB sulfoxide vs 0.91 μ M for FLB (Ebbinghaus-Kintscher et al. 2007)). Additionally,

pluronic F68 was added to the final solutions of all agonists (including caffeine) at 0.003% concentration, in order to aid the solubility of diamide compounds (following Ebbinghaus-Kintscher et al. 2007).

3.4.5.2 Absolute $[Ca^{2+}]$ was not measured

In this thesis, no attempt is made to quantify the absolute concentration of Ca^{2+} present within a cell. Instead, relative changes in Ca^{2+} -mediated fluorescence are quantified as a ratio of the maximum measured fluorescence (i.e. 'normalised to the maximum') and expressed on a relative scale. This methodological approach means that results are only comparable between experiments conducted on an identical experimental system.

It should be noted that even if the absolute concentration of Ca^{2+} present had been quantified, this approach is also not ideal. The equation $[Ca^{2+}] = K_d((F - F_{min})/(F_{max}-F))$ has

Box 3.1. Calculating Proportional Normalised Response to diamide insecticides

Data analysis pipeline:

- Identify caffeine-responsive cells
- For each cell, measure the caffeine response as follows:
 - Calculate 'average fluorescence prior to application': F_0
 - Calculate 'normalised fluorescence score at each timepoint' for responding cells: F/F_0^{response}
 - Calculate and subtract 'cellular background': $F/F_0^{\text{total}} = F/F_0^{\text{response}} - F/F_0^{\text{non-response}}$
 - Calculate 'maximum fluorescence amplitude': $\Delta F/F_0$ [Caffeine] = $\text{Max}(F/F_0^{\text{total}}) - 1$
- Similarly, measure response to diamide as follows:
 - Calculate F_0
 - Calculate F/F_0
 - Calculate $\Delta F/F_0$ [Diamide]
- For each cell, divide $\Delta F/F_0$ [Diamide/Caffeine] to get the '**Proportion of Normal Response**' (PNR) triggered by diamide
 - Repeat the above for all cells in the FOV, for the given dose
 - Take the mean average PNR across all cells in the FOV
- Repeat the above for all doses in the dose-response
- Plot the 'PNR' (Relativized Response) against diamide dose

been used by previous authors to measure absolute $[Ca^{2+}]$ (Grynkiewicz et al. 1985). Application of ionomycin is used to induced saturating levels of Ca^{2+} by collapsing the integrity of the surface membrane (Kato et al. 2009), whilst calculation of F_{\min} requires EDTA calcium chelation to effectively determine the intensity of the dye in zero-free $[Ca^{2+}]$. However, both F_{\min} and F_{\max} observations appear likely to cause damage or non-physiological alteration to the cell. Furthermore, the result is a standardised $[Ca^{2+}]$ figure that appears to encourage comparison between studies employing the same calculation, despite the fact that such comparisons are rendered foolhardy by the methodological chasms that generally exist between studies (e.g. different cell systems, different dyes, different agonist application systems, different imaging systems).

3.4.5.3 A Method for Maximising the Speed and Accuracy of Diamide Concentration-Response Quantification

This thesis aims to assess the diamide responsiveness of a large number of recombinant PxRyR wild-type and PxRyR sequence variants, and it aims to create a protocol by which the effects of future novel diamide resistance linked mutations can be characterised as quickly and accurately as possible.

A two-step process was resolved in order to achieve this goal:

1. Range-Finding (Fig 3.8a) upon a single FOV of cells
2. Detailed characterisation upon multiple cover slips over multiple experiments

3.4.5.3.1 Range-Finding

Previous characterisation of lepidopteran diamide resistance associated mutations in Sf9 cell lines (Trocza et al. 2015) showed response amplitude variation across a nM to mM diamide concentration range. Here, in the present study, range-finding was used prior to detailed characterisation, in order to quickly establish an approximate minimum and maximum effective concentration of agonist (EC_{min} / EC_{max}), within which range to conduct full concentration-response characterisation. Range-finding was conducted upon a single FOV of cells, following the normal protocols established above, beginning at [FLB]=1nM or [CLR]=0.1nM as the respective lowest effective concentrations noted in the literature for the two diamides (Trocza et al. 2015). Diamide concentration was raised iteratively by a factor of 10 (e.g. Fig 3.8a), until a response was elicited (EC_{min}). Diamide concentration was then raised by the same factor once more, in order to potentially elicit a higher response (EC_{max}) (Fig 3.8b). The diamide concentration used to elicit the two responses generated by this method inform the parameters of 'Detailed Characterisation', below.

Data acquired under the range-finding protocol were not used for concentration-response calculation. Diamide binding is known to be irreversible, such that repeated applications on the same cell may alter apparent response. Furthermore, the effects of diamide binding upon Sf9 cell physiology outside the 1200s experimental window are unknown. Irreversible diamide binding may mean that each sequential application affects the cell additively, as the agonist fills further RyR binding pockets within the cell, or alternatively it may mean that Ca^{2+} release occurs slowly and constantly from the point of first addition, such that

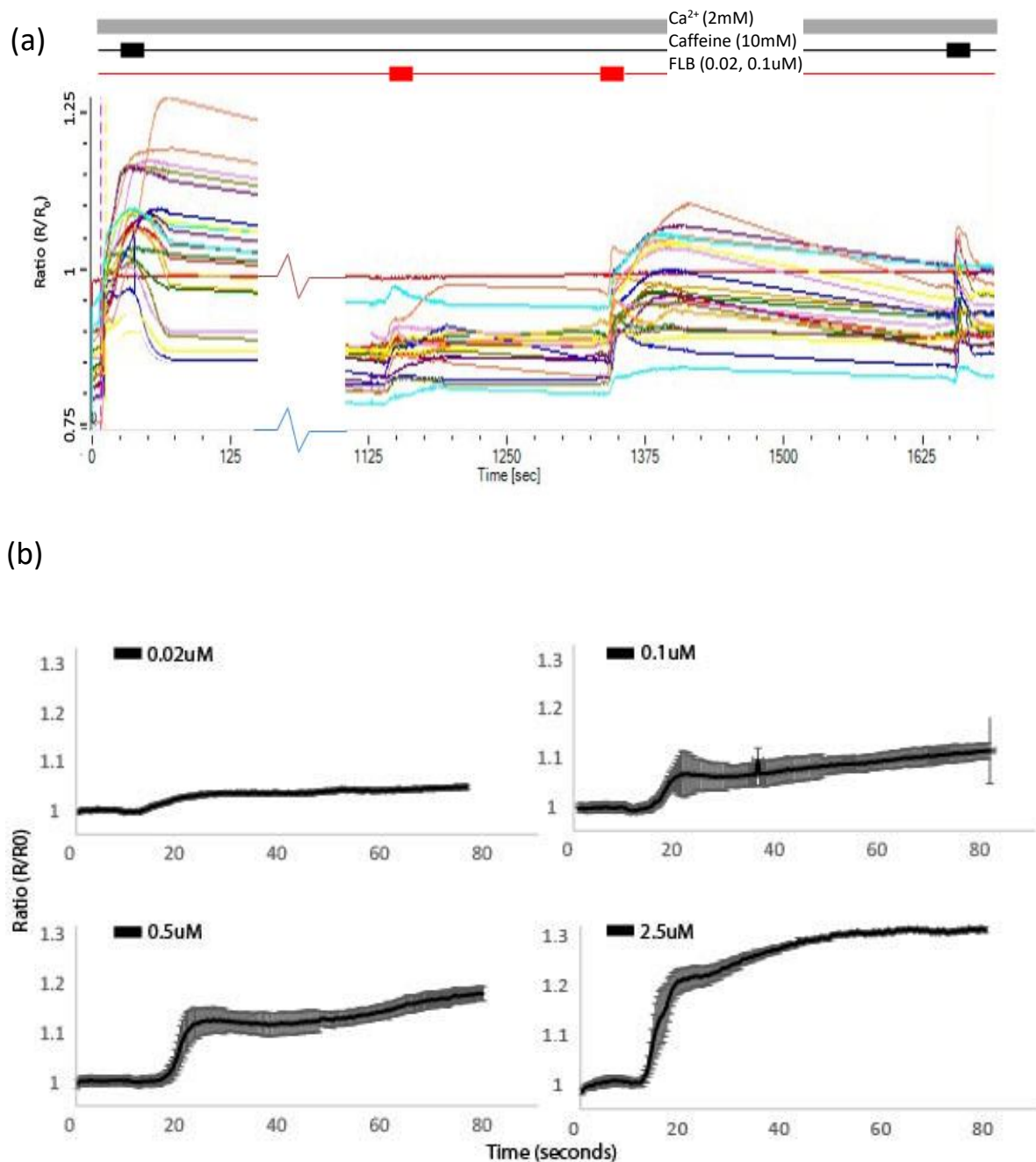


Figure 3.8 Characterisation of response variation with increasing concentrations of diamide insecticide

- Raw traces show application of caffeine followed by application of iteratively increasing concentration of diamide (in this case FLB sulfoxide). Gradual increase in FLB-sulfoxide application on the same cell allows quick qualitative establishment of EC_{\min} and approximate EC_{\max} response (where in this instance, EC_{\max} is taken as the point at which diamide response is equal to the prior applied caffeine response)
- Individual cellular responses after application of increasing concentrations of FLB-sulfoxide upon 'fresh' FOVs. Such responses are collated to form a detailed quantitative assessment of the diamide dose-response relationship.

increased dosage is required for further activation due to depleted Ca^{2+} stores. Complete characterisation of such physiological responses to diamide in Sf9s was not within the scope of this thesis, although RyR-expressing CHO cells (Ebbinghaus-Kintscher et al. 2006) were able to respond repeatedly to diamide application if given sufficient time to recover between applications. As noted previously, diamide application did not elicit response in non-PxRyR expressing cells (apart from DMSO creep-response), suggesting that the insecticides have minimal non-RyR mediated effects. Furthermore, maximum amplitude of diamide response was found to be similar to maximum amplitude of caffeine response (~25% increase in basal fluorescence, in all cases), which potentially indicates that the diamide induced Ca^{2+} release is remaining within the same physiological limits as the caffeine-induced Ca^{2+} release.

3.4.5.3.2 Detailed Characterisation

In order to characterise a concentration-response relationship for diamide activation of PxRyR, experiments were conducted following the protocols established in this Chapter. Cells were treated sequentially with 10mM caffeine (4 seconds) followed by diamide (4 seconds). Cellular diamide response amplitude was normalised to the prior caffeine response to create a response ratio, which was then normalised against the maximal caffeine responses of the given receptor type (in this case, WT-PxRyR) to generate a PNR score.

Such a method was employed here to generate concentration-response relationships for WT-PxRyR under exposure to CLR and FLB agonists (Fig 3.9). When PNR was plotted against agonist concentration, for both agonists a classic sigmoidal relationship is apparent in which low concentrations illicit minimal response up until an inflection point, after which increases in concentration result in a rise in PNR. In the case of CLR, concentrations below $0.01\mu\text{M}$ were not tested as previous studies showed a lack of response below this concentration. Response to FLB (Fig 3.9, orange data points) appears to increase linearly between $0.1\text{-}1\mu\text{M}$, as is typical in a sigmoidal relationship, whilst FLB concentrations above that fail to illicit considerable increases in response magnitude. CLR response was also plotted against a sigmoidal pattern (Fig 3.9 blue data points), although the fit is less convincing, with a lack of data coverage on the linear portion of the relationship, and considerable variation, especially at concentrations of 0.01 and $0.02\mu\text{M}$.

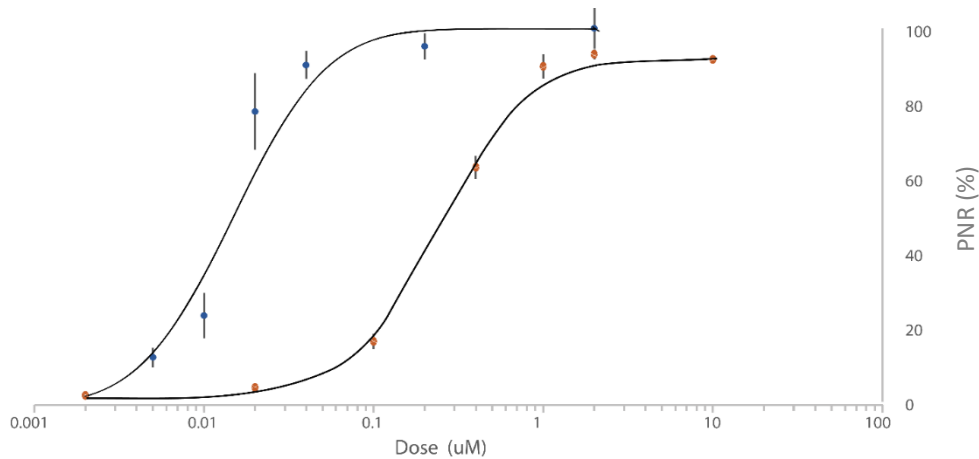


Figure 3.9 Concentration - response curves showing the normalised response of WT-PxRyR expressing cells to stimulation by CLR (blue) and FLB (orange), acquired via the RIPS system described in this Chapter. All calculations as in the Box 3.1 pipeline.

In order to reduce variance generally, all concentration-response data for a given agonist (against a given RyR-expressing cell population) were collected on the same day. As a result, it was not possible to collect further data to fill gaps within the linear portion of the graph. An additional shortcoming of the experiment is the lack of technical replicates at each concentration. The undertaking of Range-Finding studies can be described as a poor man’s technical replicate; however, these studies give no indication as to what variation in measurements would be encountered upon a repeat of the experiment. A lack of duplication and paucity of concentration data-points can be attributed to the slowness or inefficiency of the experimental setup. This aspect will be discussed further below, in the context of weighing up the costs and benefits of the ‘RIPS’ system.

Despite the shortcomings of this specific dataset, individual data-points acquired by this system appear reliable, with generally low variance (average response measurement error: 2.6%). An EC50 of 0.0148 for CLR and 0.27 for FLB are comparable to those generated by previous authors (Trocza WT EC50s = 0.016µM for CLR; 2.5µM for FLB).

3.5 Absolute Ca²⁺ Imaging: An alternative method of diamide response quantification

The RIP system described throughout this Chapter was found to be an effective method of diamide response quantification. However, its drawbacks include low sampling rate and poor control of abiotic factors. Parallel experiments were

undertaken via a separate methodology, referred to here as Absolute Ca^{2+} Imaging (named for the use of an absolute calcium indicator, Fluo4, in place of a ratiometric indicator, Fura-2-AM). In this method, cells were cultured and transfected following protocols identical to those described for RIPS but scaled down to take place in the individual wells of a 96-well plate. Coverslips of cells were removed from the 96-well plate and placed in a Compton Perfusion Chamber, a purpose-built 3D-printed design (Fig 3.2) (Paul Compton – Rothamsted Research). Ringer's solution flows continually over the cells, driven by a Scientifica Bath Perfusion Tool. Imaging of individual wells was captured by a Hamamatsu QE180 ORCA detector, mounted upon an axiovert 135M inverted microscopy and viewed down a 10x magnification eyepiece, utilizing an absolute Ca^{2+} indicator, Fluo4. Agonist was applied to the well as a whole, in bolus release from a pipette, and any change in fluorescence intensity recorded. Images containing 3000-5000 cells (Fig 3.10a) were analysed in terms of the baseline (before addition of agonist) and maximum fluorescence (after agonist addition) of each cell.

An automated pipeline (see Box 3.2) was developed for this study in order to first identify individual cells and secondly record fluorescence data across each frame of the video.

The system design was heavily influenced by a previous study concerning the role of hRyR2 mutants in cardiac death (Thomas et al. 2004), in which HEK cells transiently transfected with recombinant hRyR2 mutants were found to vary in their Ca^{2+} release physiology. Fluorescence of every cell ($n \sim 5000$) in the FOV is measured before and after agonist application, resulting in millions of data-points per individual micro-well. Manual analysis of each well is then required to remove background noise, segregate cells by response type (responders vs non-responders), and accrue final amplitude data from each individual cell. Regrettably, the system lacked one important functionality of the RIPS method: agonist evacuation was not possible, and therefore pre-application of caffeine agonist before diamide was not possible, with the result that individual cells could not be characterised in terms of their general physiological response to caffeine.

Theoretically, the system might have allowed precise quantification of diamide response with high sampling rate and excellent control of abiotic conditions. The 96-well format offers the possibility of high throughput data acquisition (if only a high throughput data analysis could be realised), whilst the confocal imaging

system possesses a bespoke climate control chamber, such that light, temperature and humidity are closely controlled. However, despite its promise 'on paper', the Absolute Imaging system utilised for Sf9 cells, against diamides, produced an unsatisfactory output in comparison to the RIPS system and previously published work. Application of iteratively increasing concentrations of CLR against WT-PxRyR expressing Sf9 cells produces a sigmoidal relationship (Fig 3.10b). However,

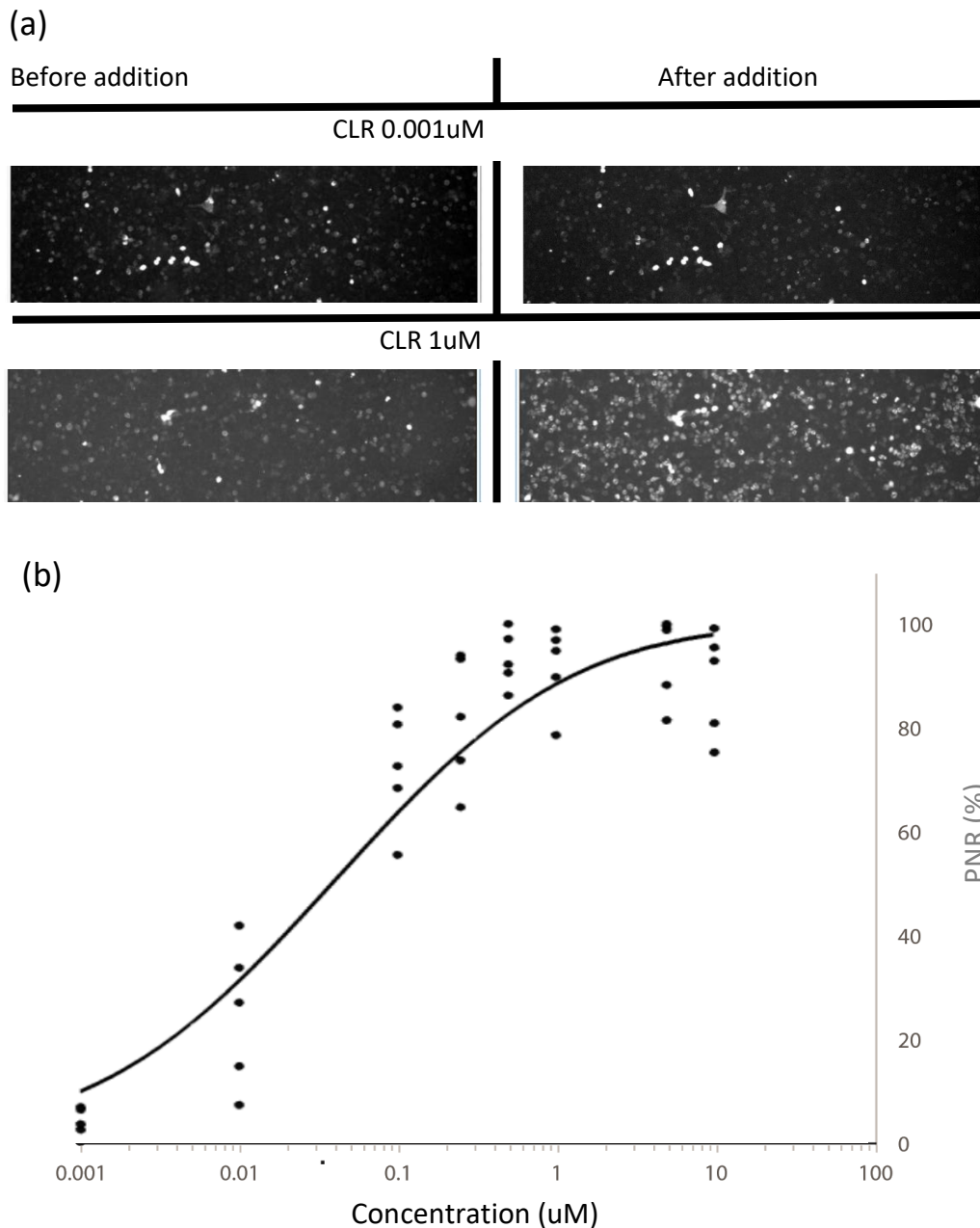


Figure 3.10. Comparison of concentration response to CLR achieved via the alternative experimental setup, Static Ca²⁺ imaging, described briefly below. Data points correspond to peak amplitude (mean ± SEM) of 10-30 cells measured over 1200s, relativized to the individual response obtained for caffeine and normalised to the maximum response.

variation in response is as high as 40% of maximum value within a single application (e.g. at 0.01 μ M). Although this variation compares favourably to raw data from RIPs (e.g. >50% variation, Fig 3.8a), relativization of cellular diamide responses with caffeine responses, on the RIP system, is responsible for reducing such variation markedly (average 12.2% variation, Fig 3.9). A sigmoidal curve has been plotted to the data in Fig 3.10b for comparison to other concentration-response curves in this thesis. The reasons for the variation seen in this graph are discussed below.

3.5.1 Drawbacks of the Absolute Imaging system

3.5.1.1 Absolute vs. Ratiometric fluorescence measurement

The benefits of ratiometric dye (e.g. Fura-2-AM, used throughout this Chapter) compared to absolute dye, are well documented. Most inherent sources of fluorescence (e.g. NADH, actin) are removed from further consideration by

Box 3.2 Pipeline for cell identification and fluometric analysis, following Absolute Ca²⁺ imaging

Initial Cell Identification and fluorescence quantification by CellProfiler

- Video loaded and background identified based on corresponding transmission microscopy image.
- Cells are screened for change (or non-change) in fluorescence, relative to background, between initial and final frame. Non-changing cells are removed from further analysis.
- Pixel intensity values are measured during each frame of the video for background and foreground (each cell a separate foreground object)
- Results are converted into .CSV format via an R script

Data selection and processing

- Background values removed from cellular fluorescence (pixel intensity) value for each cell
- Cellular fluorescence was compared just for the initial 100 and final 100 frames of each video
- Change in fluorescence averaged across cells in FOV
- Maximum change in fluorescence (amplitude) plotted vs concentration of applied agonist.

ratiometry. By comparison, absolute dye, such as the Fluo4 used here, captures every source of fluorescence within the 300-330nm range, including much abiotic noise, and much biological interference.

3.5.1.2 Agonist application issues

Diamides are poorly soluble in aqueous solution. This is partly what lends them an excellent eco-toxicological profile as insecticides, preventing them from readily contaminating water sources. During the RIPS experiments in this Chapter, diamide is pre-dissolved in a Ringer solution containing 1% DMSO and 0.003% Pluronic acid (final concentrations v/v), before addition to the Sf9 cells via a pressurised application system which ensures the complete replacement of the original 'bath solution' with applied 'agonist solution' in the local area of the cell (see Fig 3.2). By comparison, bolus agonist application into a microwell (on a 96 well plate) requires that the agonist solution disperses from the surface of the bath solution in the well down to the base of the well where the cells reside. Irreproducible bolus delivery by pipette results in variation in the location of bolus addition to well. Assuming a 10m/s Brownian dispersal of agonist, time to reach base of well ought to be minimal (height of solution is 5mm). Solubility is a compounding issue under these conditions, because the requirement of agonist-solution to mix with bath-solution creates a situation where diamide often falls partially or completely out of solution.

3.5.1.3 Atypical transient shape due to failed Ca^{2+} reuptake

The RIPS system has been shown to illicit typical and reproducible Cat A type Ca^{2+} release transients in response to caffeine application (Fig 3.7). By comparison, in PxRyR-expressing Sf9 cells, no Cat A responses were recorded under the Absolute Imaging system. Instead, responding cells exhibited irreversible increases in fluorescence in response to 10mM caffeine, and failed to return to basal fluorescence within 1h of agonist application. This despite previous authors demonstrating the validity of a very similar system in HEK cells expressing hRyR2 (Thomas et al. 2004). Without the ability for application of 10mM caffeine prior to diamide stimulus, the protocol of PNR relativization touted here was not applicable. Cells instead segregated into just two categories, 'responders' (which empty their stores entirely) or 'non-responders' (which exhibit zero or negative Ca^{2+} efflux). Consequently, non-typical responders bring a large amount of biological variation into the data. At the same time, measurable variation (in terms of the fluorescence

change triggered by agonist addition) is also reduced, because cells are unable to register sub-maximal responses to intermediate agonist dosage.

3.6 Conclusions

This Chapter has outlined the development and evaluation of a methodology aimed at rapidly quantifying the effects of PxRyR amino-acid substitutions on diamide efficacy. Such evaluations should ideally be done in the context of previous studies; however, such are the differences in methodology, and the variation in response to those differences, that contextualisation is difficult. Here it is shown that transiently expressing Sf9 cell lines produce differing responses under two separate experimental systems, where the principal difference is in agonist delivery and evacuation (EC50 for CLR by RIPS: 0.015 μ M vs AI: 0.033 μ M). Certainly, comparison of the data presented here with different experimental set-ups, often using different cell lines, would be unwise. Caffeine release dynamics of insect RyR expressed in Sf9 cells (Sattelle, 2009) vary considerably from those on CHO cells (Ebbinghaus-Kinscher et al. 2007) and HEK cells (Kato et al 2009), as expected due to differences in cell size, physiology and Ca²⁺ handling. More fruitful is an evaluation of this methodology in terms of its real-world utility, i.e. in its ability to rapidly characterise newly discovered diamide resistance related target-site mutations. Firstly, it is clear that the method is laborious for detailed phenotypic characterisation. FLIPR on stably expressing cell lines (Trocza, 2015), is capable of producing a diamide concentration-response curve similar to that reported here (Fig 3.9) in a single day of measurements (Peter Luemmen Pers. Comm). By comparison, to obtain a concentration-response curve using RIPS requires at least five days of measurements, with the whole experimental protocol requiring a period of a month to accommodate the prerequisite laboratory steps (culture, transfection, incubation). However, it is hoped that this disadvantage in speed of analysis is compensated for by time-saving due to the absence of the requirement for stable cell-line generation. Recent advances in plasmid mutagenesis, allowing up to five nucleotide/amino acid alterations to be introduced simultaneously (Agilent lightning), combined with highly efficient golden-gate cloning, ensures that even large, multi-substitution recombinant PxRyR constructs can be generated in a matter of weeks. Chapters 2 and 4 of this thesis will each analyse large numbers of recombinant constructs, in order to determine if this methodology is of practical value.

Chapter 4: Target-Site Resistance to Diamide Insecticides

4.1 Chapter Summary

Resistance to diamide insecticides in Lepidoptera is known to be caused primarily by amino acid changes on the Ryanodine Receptor (RyR), otherwise known as Target Site Resistance (TSR). Recently, two new target site mutations, I4790M and G4946V, have emerged, and both have been shown empirically to decrease diamide efficacy. A detailed understanding of the effects of these mutations on diamide efficacy *in-vitro* is as yet lacking.

In the previous Chapter, an experimental system was established to quantitatively assess the impact of TSR mutations on diamide efficacy *in-vitro* using transiently transfected Sf9 cell lines. In this Chapter, this Sf9 system is employed to quantify the impact of these two novel mutations on diamide activation.

The results help to further define the ‘diamide resistance region’ within the insect RyR transmembrane domain, and the location of a possible site of diamide interaction, as visualised on a 3D PxRyR model, and are additionally discussed in terms of future diamide resistance monitoring.

4.2 Introduction

4.2.1 Target Site Resistance

Just 18 months after their market debut, resistance to diamide insecticides emerged in the Philippines in a population of DBM (*P. xylostella*) and was quickly followed by further episodes in nearby locations (Troccka et al. 2012). Partial sequencing of the resistant *P. xylostella* populations soon revealed a commonality; a polymorphism, G4946E (DVAVG/E), located close to the C-terminus of the RyR. An earlier study had shown the importance of this region of the receptor in diamide efficacy, with C-terminal-ablated channels failing to bind the insecticide (Kato et al. 2009). The following five years would see numerous studies reporting the presence of the mutation in resistant DBM populations from divergent locations (see references in Table 4.1). As the G4946E mutation spreads worldwide its importance became clear, from functional evidence in insect cell lines, to binding studies on native membranes (Troccka et al. 2015; Steinbach et al. 2015). The G4946E

mutation continues to emerge in new localities, with near-fixation of the mutation recently reported in South Korea (Kang et al. 2017).

The differing coding triplets for the glutamic acid residue found in different populations (GAG for the Thai strain and GAA for the Sudlon (Philippines) strain) imply that this mode of resistance has evolved at least twice in *Plutella* (Troczka et al. 2012), whilst its incidence in at least 10 countries, spread across 3 continents, strongly suggests at least one more evolutionary event (Steinbach et al. 2015). An alternative substitution, G4946V, at this position has recently been characterised in *P. xylostella* populations from Guangzhou and Zhencheng in China, where the population make-up is split 70:30, G4946E to G4946V (Qin et al. 2018). Additionally, mutation at this G4946 residue (*P. xylostella* numbering) has been implicated in resistance in other insect pest species. A glutamic acid rather than glycine is reported as being present in resistant *C. suppressalis* populations in China (Yao and et al. 2017), whilst both G4946E and G4946V substitutions have been implicated in diamide resistance in European populations of *T. absoluta* (Roditakis et al. 2017). Taken together, resistance-conferring changes at this position have emerged on a total of 8 separate occasions in the past decade, in each case rising from an allele-frequency of near zero and progressing to near-fixation.

Whilst the S4-S5 linker as a whole has been shown to be critical to channel gating (Ramachandran et al. 2013), non-conserved changes at the 4946 position, which have been selected for as a response to diamide exposure, appear to confirm that standing variation at this interface position between helix and linker can be maintained in the insect pest population. In support of this theory, fitness costs associated with the G4946E mutation have been shown to be moderate, with some populations retaining the mutation without diamide selection (Troczka et al. 2016) (although see Ch5 for an investigation of this point). However, sequencing of

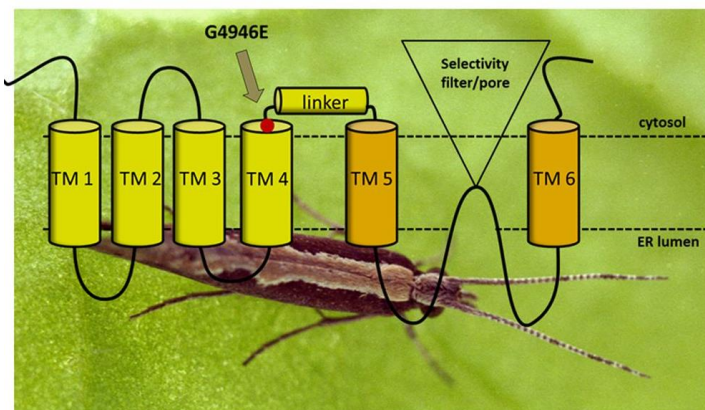


Figure 4.1. Transmembrane protein topology of the C-terminal domain of the *P. xylostella* RyR based on the crystal structure of rabbit RyR1 (Yan et al. 2015). The region containing the G4946E substitution (position G4900 in published sequence (Troczka et al. 2012), accession number JX467684) links transmembrane domains TM4 and TM5. Image © Rothamsted Research Ltd and Troczka et al., 2015.

weakly resistant lepidopteran populations frequently fails to detect G4946E, suggesting that residual mutant allele frequencies are below the 2-5% detection thresholds (Roditakis et al. 2017; Guo et al. 2014b; Troczka et al. 2012). Thus, for the resistant allele to rise to fixation from such depths requires that it provide a sufficiently large selective advantage. An overview of the past decade of scientific literature does indeed suggest that, in the presence of diamide selection, survivorship (i.e. RR) of G4946E/V mutants over wildtype is frequently increased >3000-fold (References in Table 4.1).

4.2.2 I4790M— A novel cause of resistance in diverse lepidopteran pests

Diamide resistance is no longer exclusive to *P. xylostella* but is now also present in diverse populations of *T. absoluta*, *S. frugiperda*, *S. exigua* and *C. suppressalis*. Unsurprisingly, this diversification is coupled to the emergence of new genotypic mechanisms. One RyR amino acid residue in particular, I4790M (VSLAI/M), is implicated in resistance within all of the species listed. Detected in resistant lepidopteran pests from Brazil, Florida, Europe, Israel, China and Korea, this residue is developing a global importance to rival that of the G4946 locus.

The I4790M change was first detected in a Chinese population of *P. xylostella*, one of a combination of four mutations identified in the RyR channel of this particular diamide-resistant strain, conferring potent (>2000-fold) CLR resistance (Guo et al 2014). Despite a lack of experimental validation, correlative evidence of I4790M conferring resistance is plentiful, as the mutation hitch-hikes its way across the globe. Its impact was first clearly shown in a Sicilian population of *T. absoluta*, in 2015, which exhibited 180-fold CLR resistance at a mutant-allelic frequency of close to 100% (Roditakis et al. 2017). It is now known to be fixed in various populations across Italy and Greece, where it appears to ‘compete’ with the G4946 mutations – the two changes almost never appearing in the same organism, with almost all local populations fixing for one or the other (Roditakis et al. 2017). I4790M has also been detected in South American populations of *S. frugiperda*: the Puerto Rican and Brazilian populations are described as distinct, although gene flow between the two is not unlikely (Nagoshi et al. 2017). The Brazilian population developed I4790M-mediated resistance in early 2016, whilst the Puerto Rican population exhibited 160-fold (CLR) and 500-fold (FLB) resistance but has not been genotyped for presence of the mutation. Interestingly, laboratory selection of the Brazilian population with CLR led to slight increases in CLR resistance (237-fold), but dramatic

increases in FLB resistance (>42,000-fold) (Bolzan et al. 2019). Another noctuid pest, *S. exigua* also carries the equivalent of I4790M, which is present in almost all surveyed Chinese populations and is associated with 150-fold CLR resistance. The mutation is also fixed in certain Chinese populations of *C. suppressalis*, associated with 250-fold CLR resistance (Sun et al. 2018). As all of these recorded episodes closely associate with CLR resistance, I4790M does certainly appear to be conferring resistance, although not to as high a degree as G4946E. However, as seen in Table 4.1, I4790M resistance is certainly sufficient to cause control failure once it spreads to fixation.

Table 4.1 Summary of major global diamide resistance occurrences, detailing geography, severity and mechanism of resistance

a: CLR = chlorantraniliprole; FLB = flubendiamide;

b: Lethal Dose, in mg/L

c: LD expressed as ‘% of Recommended Dose’, where RD is 48mg/L for FLB and 82.5mg/L for CLR

d: converted from ug/cm² (Cho and et al 2018)

Studies on laboratory-selected resistant strains were left out of this table, as their relevance to control-failure in the field is limited. Studies reporting low to medium resistance ratios (RR<50) were left out of this table as this range falls within the spectrum of population variation (Following (Nauen and Steinbach 2016)).

Further information on calculations made in this table is provided in Methods.

Common	Species	Location	Compound ^a	LD50 ^b	Slope	LD80 ^b	% of RD ^c	RR	Mechanism	Source	
Rice Stem borer	<i>C. suppressalis</i>	China	CLR	214	1.94	437	530%	153	Unknown	Yao et al. 2017	
			CLR	-----Resistance Status: Some Evidence-----							G4946E
			CLR	108	1.97	218	264%	250	I4970M +/ Y4667C/D		Sun et al. 2018
Tea Tortrix	<i>A. honmai</i>	Japan	CLR	99	2.48	173	210%	77	Unknown	Uchiyama + Ozawa 2014	
			FLB	161	3.11	251	523%	105			
Fall Armyworm	<i>S. frugiperda</i>	Brazil	CLR	2.6	2.66	4.38	5%	237	I4790M	Bolzan, Boaventura et al 2019	
		Puerto Rico	FLB	1.5	1	6	13%	500	Unknown	Gutiérrez- Moreno et al. 2019	
			CLR	0.16	1.1	0.56	1%	160			
		Europe, Africa, India, China	-----Resistance Status: Unknown-----						N/A	Stokstad 2017	
Beet Armyworm	<i>S. exigua</i>	South Korea	CLR	>25		Unknown		>2,500	Unknown	Cho et al. 2018	
			FLB	>100		Unknown		>100,000	Unknown		
		China	CLR	4.93 ^d		Unknown		154	I4790M	Zuo 2017	

Tomato leafminer	<i>T. absoluta</i>	Brazil	CLR	650	1.2	2063	2501%	3095	Unknown	Roditakis et al. 2017	
		Italy	CLR	838	1.38	3399	-	2704	G4946 E/V I4790 M/T		
		Greece	CLR	>1000	N/A	N/A	>1666%	>3200	G4946 E/V		
		Spain	CLR	0.12	1.25	0.6	1%	1	N/A	Roditakis et al. 2018	
		Israel	CLR	6998	2	17,438	21,137%	22,573	Unknown		
		Sub-Saharan Africa, West Asia, East Asia			-----Resistance Status: Unknown-----					N/A	Biondi et al. 2018)
Diamond-back moth	<i>P. xylostella</i>	Thailand	FLB	175		Unknown		775	G4946E	Troczka et al. 2012	
		Philippines (Sudlon strain)	CLR	>1000		Unknown		>10,000	G4946E	Steinbach et al. 2015	
			FLB	>1000				>10,000	G4946E		
		China	FLB	265		Unknown		2000	G4946E	Troczka et al. 2016	
		China	CLR	23	2.83	37.5	78%	2128	E1338D, Q4594L, I4790M	Guo et al. 2014	
		India, Japan, USA			-----Resistance Status: Some Evidence-----					G4946E	Steinbach et al. 2015
		Brazil	CLR	204	3.06	321	669%	27,739	Unknown	Ribeiro et al. 2014	
		South Korea	CLR		-----Resistance Status: Some Evidence-----					G4946E	Kang et al. 2019
FLB											
		CLR	36	1.43	95	115%	1196	Unknown	Cho et al. 2018		

4.3 Methods

4.3.1 Concentration-response assays

Throughout this thesis, diamides are dissolved in a final solution comprising 1:100 DMSO:H₂O. Diamide solubility in DMSO is not listed on the compound data sheets, however solubility in dimethylformamide, which is a very similar solvent*, is known to be ~1000x higher than the value for distilled water, so it is probable that the DMSO:H₂O solution increases solubility. Preliminary solubility tests (eyeball-test) in this thesis indicate that precipitate starts to be visible at concentrations of CLR above 150µM, and concentrations of FLB above 75µM (indicating that the presence of DMSO may raise FLB solubility above the 58µM maximum).

*([https://www.gaylordchemical.com/innovation-center-2/using-superior-solvents/replace-dmf-with-dmso/](https://www.gaylordchemical.com/innovation-center-2/using-superior-solvents/replace-dmf-with-dms/))

4.3.2 In-silico analysis methods

4.3.2.1 Computational modelling

Taking into account the publication of Yan *et al.* (Yan *et al.* 2015) who described the (closed-state) conformational model of the European rabbit RyR1 in complex with FKBP12 at 3.8 Å resolution determined by single particle cryo-electron microscopy (cryo-EM), a multiple amino acid alignment of the RyR wildtype sequence of *P. xylostella* (UniProt G8EME3; Guo *et al.*, 2012) and the rabbit structure (PDB 3J8H) was used to map the known mutation sites linked to diamide resistance (Trocza *et al.* 2012; Guo *et al.* 2014b; Guo *et al.* 2014a). As PDB 3J8H does not cover the complete sequence of the rabbit RyR1 (due to structural disorder), another but complete sequence of *Oryctolagus cuniculus* RyR1 (UniProt P11716) was added to the pairwise alignment to map the gaps in the structure determined by cryo-EM. A homology model for the *P. xylostella* RyR was constructed using the Advanced Homology Modeling tool within the software suite Maestro (Maestro 2019). To correct for vdW clashes and distortions in the local structure, the raw model was subjected to an energy refinement procedure with the macromodel minimization (LBFGS method, 5000 iterations). The illustrations from the resulting 3D models shown in this thesis were generated from the Maestro modeling suite.

4.3.2.2 Assessment of diamide resistance

Within this chapter, two scores are used to assess diamide resistance episodes: Resistance Ratio (RR) and %_{RD}. Each provides unique information on the nature of the resistance episode.

RR is a common assessment of resistance, an indication of the efficacy of the insecticide against a resistant strain in comparison to a baseline efficacy in an insecticide susceptible reference strain that pre-dates resistance (Lethal Ratio Test (Robertson 2007)). RR indicates the scale of insecticide resistance that is taking place within the organism, information that is particularly valuable in combination with a biochemical understanding of resistance mechanisms. However, reliance on baseline toxicity measurements makes RR a poor quantifier of absolute insecticide resistance. Baseline measurements are variable within populations of a species, and even more so between different species, and such variation becomes problematic when it is amplified 100- or 1000- fold during calculation of RR. This can result in dramatic misdiagnosis of resistance severity, as shown in table 4.2, in which the Brazilian *P. xylostella* population registers a lower CLR LD50 than the Chinese *C. suppressalis*, whilst comparison by RR alone would suggest that the *P. xylostella* is experiencing a considerably more severe resistance.

When the goal of resistance monitoring is to predict control failure, this chapter utilises %_{RD}. As outlined in previous studies (Silva et al. 2011; Guedes 2016), this score is based upon comparing the LD80 (lethal dose for 80%) of the population with the Recommended field Dose (RD) of the insecticide. %_{RD} is therefore an expression of the “LD80 as a percentage of the RD”, and gives a direct estimation of the probability of control failure. If the estimated LD80 is higher than the label rate of the commercial formulation, control failure will probably take place. Such a score has basis in European and Brazilian law, where new synthetic insecticides are required to kill >80% of their target population at their prescribed RD. On this scale, if a population registers a %_{RD} <100% against a given insecticide, this is an indication that control is currently effective; it matches or exceeds the minimum expectations of European and Brazilian insecticide registration requirements (Silva et al. 2011). A score of >100% indicates a significant risk that control failure will occur, based on the assumption that non-controlled (resistant) phenotypes will proliferate and increase within the population.

Table 4.2. Comparison of CLR resistance across field strains from three lepidopteran species (from Table 1, above).

Species	Location	Compound	LD50	Slope	LD80	% of RD ^c	RR
<i>T. absoluta</i>	Israel	CLR	6998	2	17,438	21,137%	22,573
<i>P. xylostella</i>	Brazil	CLR	204	3.06	321	669%	27,739
<i>C. suppressalis</i>	China	CLR	214	1.94	437	530%	153

4.3.2.3 Calculation of RR and %_{RD}

Calculation of %_{RD} is via the following equation:

$$\%_{RD} = (LD80 / RD) \times 100$$

Where LD80 is the Lethal Dose for 80% mortality of the insect population, and RD is the recommended field dose. Where LD80 is not listed in the literature, it is calculated via the following equation (GraphPad 2019):

$$EC_F = \left(\frac{F}{100 - F} \right)^{1/H} \cdot EC_{50}$$

Calculations of LD80 were validated against studies of known LD80, e.g. (Roditakis et al, 2018). Calculated values are generally much lower, at just 60-80% of actual values, such that likelihood of control failure is expected to be far higher than reported here. Disparities between calculated and actual values are likely to be caused by early plateau of the logarithmic phase of the concentration-response curve.

Resistance Ratios, described above, were extracted from the literature, and required no further calculation. 'RD', recommended dilutions were extracted from the insecticide labels for FLB (BELT©) and CLR (Coragen©) (table 4.3). For simplicity's sake, the RD is taken to be that of the 'Lepidopteran Dilution'. and is used as such throughout this chapter. BELT values calculated based on the given recommended spray values of 75-150ml/Ha of 480g/L BELT formulation. CORAGEN values calculated based on the given recommended spray values of 0.046 - 0.098lb/acre. The lepidopteran pest dilution for CLR has been calculated based on the median spray, 82.5g/Ha. For comparability with the literature and with FLB, this

value was converted to 82.5mg/L following the arbitrary conversion listed in the BELT480 product label, i.e. 48g/Ha: 48mg/L. It should be recognised that spraying practices and guidelines vary between localities, crops and pests. Although they are unlikely to exceed the spray limits listed here, the (mal)practise of under-dosing is common in some regions (Trocza et al. 2016), such that control failures may be significantly more likely than reported here.

Table 4.3. CLR and FLB spray dosage information.

Compound	FLB (BELT)	CLR (Coragen)
Minimum spray (g/Ha)	31	55
Maximum spray (g/Ha)	72	110
RD (mg/L)	48	82.5

4.4 Results

4.4.1 Generation of novel PxRyR constructs

The three novel mutations E1338D, Q4594L and I4790M were originally discovered in Yunnan province, China, in *P. xylostella* individuals displaying a 2128-fold resistance to CLR (Guo et al. 2014a). Documentation of this resistance episode was a key prompt for the conception and initiation of this PhD. Therefore, PxRyR constructs incorporating E1338D, Q4594L and I4790M individually, and in various combinations matching those found in the original field study, were created (Fig. 4.2). However, it soon became apparent that I4790M was of much greater relevance than the other two mutations, emerging autonomously in various lepidopteran species and isolated populations. Investigations into I4790M-mediated resistance were therefore prioritised, whilst investigations into combinatorial constructs involving the other two residues were put on hold.

The first year of this PhD also saw reports of a *T. absoluta* outbreak in Europe, accompanied by the sequencing of the novel diamide resistance-associated variant, G4946V (Roditakis 2016). Investigation of this novel amino acid variant at the G4946 position was therefore also prioritised.

In this Chapter, comparison of the novel PxRyR constructs is made against two previously created constructs, WT-PxRyR and G4946E-PxRyR (made available courtesy of Bartek Troczka). Characterisation of WT-PxRyR was completed in Ch3 following a novel methodology developed for this thesis. Characterisation of G4946E is undertaken as part of this Chapter, in order to evaluate the methodology further.

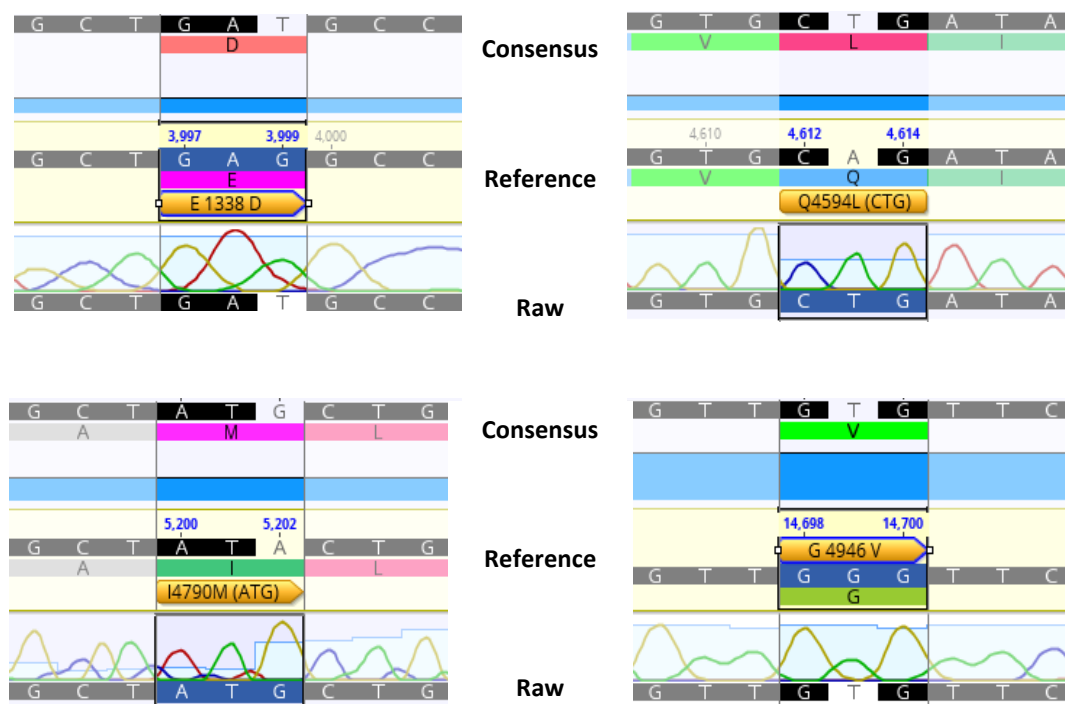


Figure 4.2: Sequence comparison of mutated nucleic and amino acid positions for each PxRyR construct created. Mutations were generated by site-directed mutagenesis upon fragments of the PxRyR. ‘Consensus’ displays the successfully implemented alteration, whilst ‘Reference’ bears the original Wild-Type genotype. ‘Raw sequence’ data is also provided. Mutagenized fragments were reassembled into full-length PxRyR following the cloning strategies detailed in the Methods Chapter.

4.4.2 Functional Expression of modified PxRyR constructs

4.4.2.1 Preliminary Diamide Dosing

Modified PxRyR constructs were expressed in Sf9 cells following the protocols established in Ch1. Preliminary experiments with 10mM caffeine exposure indicate that the constructs form functional PxRyR channels (Fig 4.3). Subsequent dosing of the same cells with 5µM CLR reveals that I4790M-PxRyR expressing cells are susceptible to this concentration, as is the WT-PxRyR, but that G4946V-PxRyR cell line registers no Ca²⁺ release. Repeated dosing with caffeine failed to provoke Ca²⁺

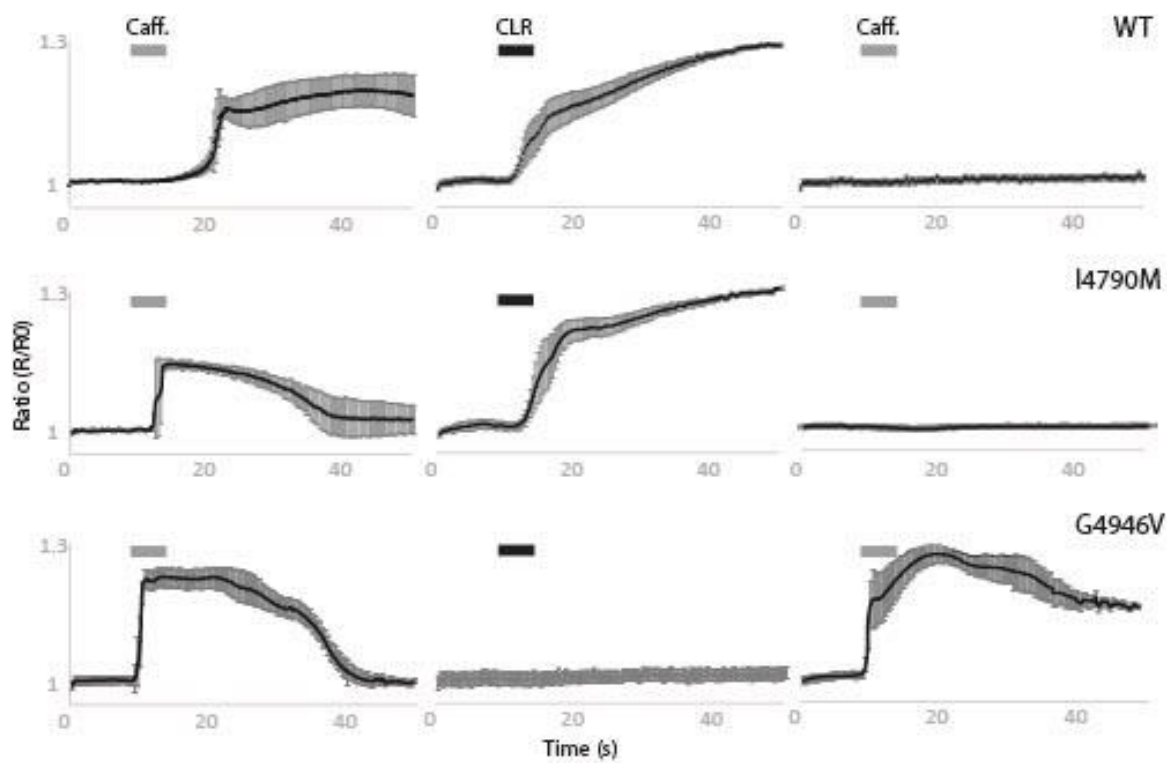


Figure 4.3 Recombinant PxRyR mutants expressed in Sf9 cells, dosed sequentially with 10mM caffeine (grey) and 5µM CLR (black).

release in those cells which had previously been activated by the diamide, but successfully provoked Ca^{2+} release in cells expressing G4946V-PxRyR.

4.4.2.2 Differences in Ca^{2+} handling between WT and modified constructs

Temporal and amplitude properties of caffeine-evoked Ca^{2+} transients were characterised in Sf9 cells expressing WT and G4946E-PxRyR. The amplitude of Ca^{2+} release evoked by caffeine is critically dependent on the filling status of the ER Ca^{2+} store. Importantly, average cellular resting fluorescence of PxRyR-transfected cells of each genotype do not differ significantly (G4946E, 1.80 ± 0.32 ; I4790M, 1.51 ± 0.74 ; G4946V, 1.15 ± 0.21) when compared to the ER Ca^{2+} load determined in cells expressing WT-PxRyR (1.00 ± 0.38), indicating that genotypes have approximately the same resting Ca^{2+} store capacity. Comparison of the peak response at each concentration (Fig. 4.4) suggests no significant functional heterogeneity exists between the two genotypes, under these conditions.

Time constraints prevented a caffeine concentration-response relationship to be generated for each of the recombinant PxRyR constructs. Instead, the recombinants are compared in their response to a single (10mM) dosage of caffeine (Fig. 4.5a), as this falls well within the linear portion of the WT-PxRyR response curve. Measurements were taken for all three constructs in a single day, in order to minimise methodological variation, with between 6-25 cells responding for each construct. This preliminary investigation indicated that neither G4946E-PxRyR nor G4946V-PxRyR produce a caffeine-stimulated peak significantly different in amplitude to that of the WT-PxRyR construct (Fig 4.5b, $P > 0.05$). However, the I4790M-PxRyR produced a significantly higher peak (Average: 1.31; $P < 0.05$). Even accounting for variation in measurements between experiments (see Ch3, Fig 3.6) the difference recorded is robust. I4790M-expressing Sf9 cells were also observed to respond more readily to caffeine compared to WT (i.e. more Cat A and B responses - see Ch3, Fig 3.5).

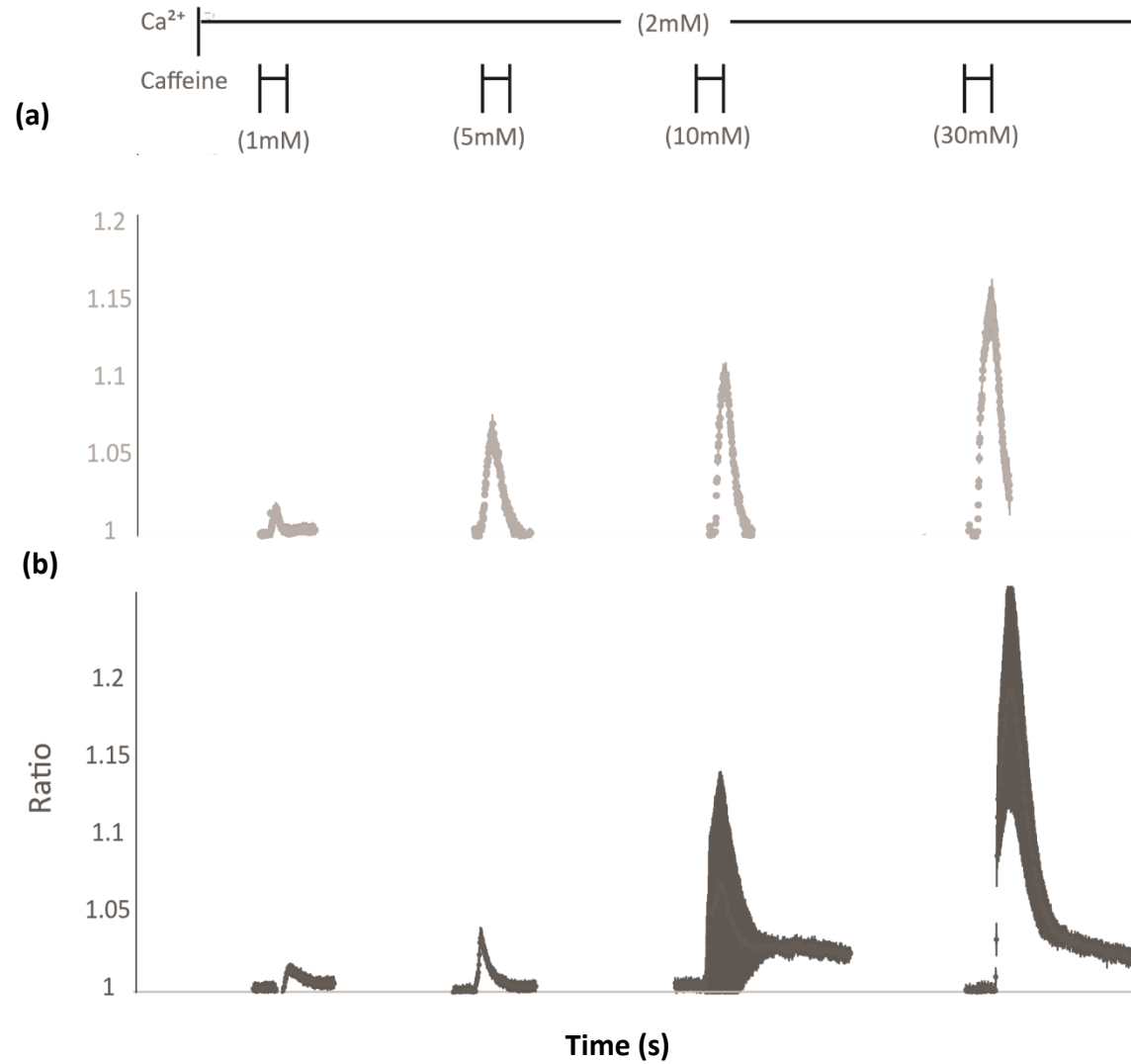


Figure 4.4 Response of a) WT, b) G4946E to increasing concentrations of caffeine

Data for WT PxRyR was previously displayed in Ch1 and is redisplayed here for comparison only.

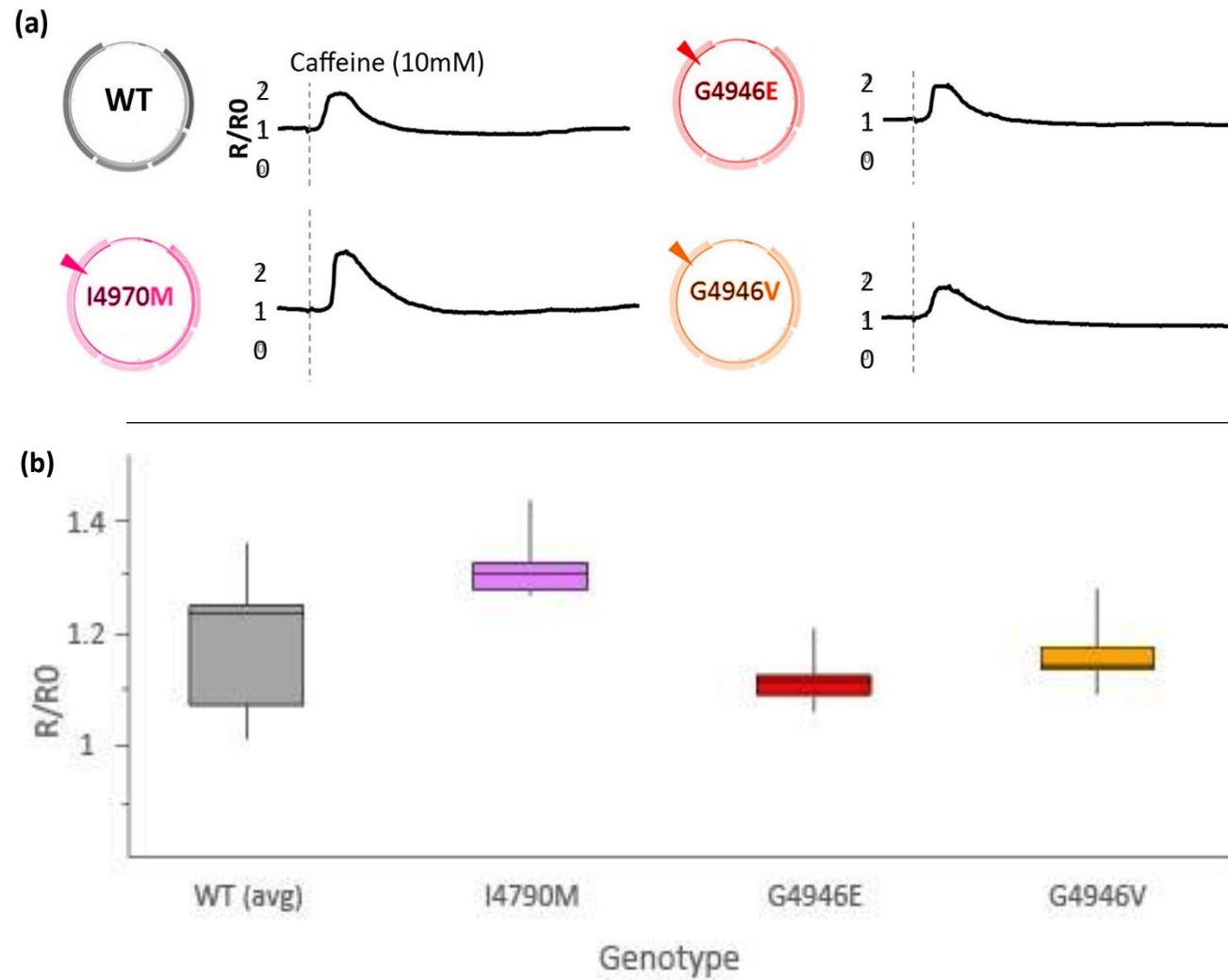


Fig 4.5 Caffeine response comparison between modified PxRyR constructs.

A hypothetical 3D structural model (Fig. 4.6) of the PxRyR protein suggests an $\sim 30\text{\AA}$ distance between I4790M and the caffeine binding site (as defined in (Murayama 2018)), implying that interaction between the two regions is unlikely. Again, lack of any substantial investigation into calcium handling differences between the constructs hinders further physiological discussion of this observation.

In the context of this thesis, the more important point is that the I4790M construct may register reduced Proportional Response (PNR) to diamides due to a relatively increased caffeine response (median response 24% higher than WT response, fig 4.4, b). Due to the calculations performed during concentration-response analysis (Box 3.1), this would result in an apparent 24% reduction in the recorded diamide response vs the theoretical expected response. Therefore, during the analysis for Fig 4.7, I4790M-caffeine responses were each reduced by a factor of 1.24 to compensate for this discrepancy.

4.4.2.3 Variation in caffeine-response correlates with variation in diamide response, across all three PxRyR variants

It was previously shown that cells vary in their general physiological ability to conduct calcium in response to caffeine application (Fig 3.6). An assumption of this thesis is that caffeine response and diamide response covary. That is, cells that exhibit a higher than average response to caffeine are expected to exhibit a higher than average response to diamide application. If the assumption is true, it justifies the technique employed throughout Ch 3+4+6, in which cellular response to diamide is first normalised against a baseline, and then relativized against the caffeine response of that same cell (see Ch3, Box 3.1).

Scatter plots of caffeine response against diamide response (Fig 4.7) corroborate a potential association, but that the relationship begins to break down at high concentrations of diamide (i.e. R^2 is reduced). The steepness of the plotted line in Fig 4.6 indicates the relative response of the construct to caffeine vs diamide, with an incline of ~ 1 indicating equal responsiveness to both compounds. R^2 indicates the extent to which variation in caffeine response (x) predicts variation in diamide response (y) (the value is literally determined by the distance of outlier values from the trendline of the graph). Strong correlations are observed for WT ($R^2=0.89$),

G4946V ($R^2=0.56$) and I4790M ($R^2=0.60$) when tested at concentrations close to their EC50 (see Figs 4.8-4.10). I4790M-RyR expressing cells exposed to a much higher concentration of diamide (25 μ M) exhibit a markedly increased variation in response amplitude, weakening the relationship ($R^2=0.23$). By comparison, variation in caffeine response remains very similar between experiments, and across different genotypes (the caffeine concentration remains at 10mM in all cases). Whilst at diamide concentrations above the linear portion, it was found that caffeine and diamide response correlate poorly or not at all.

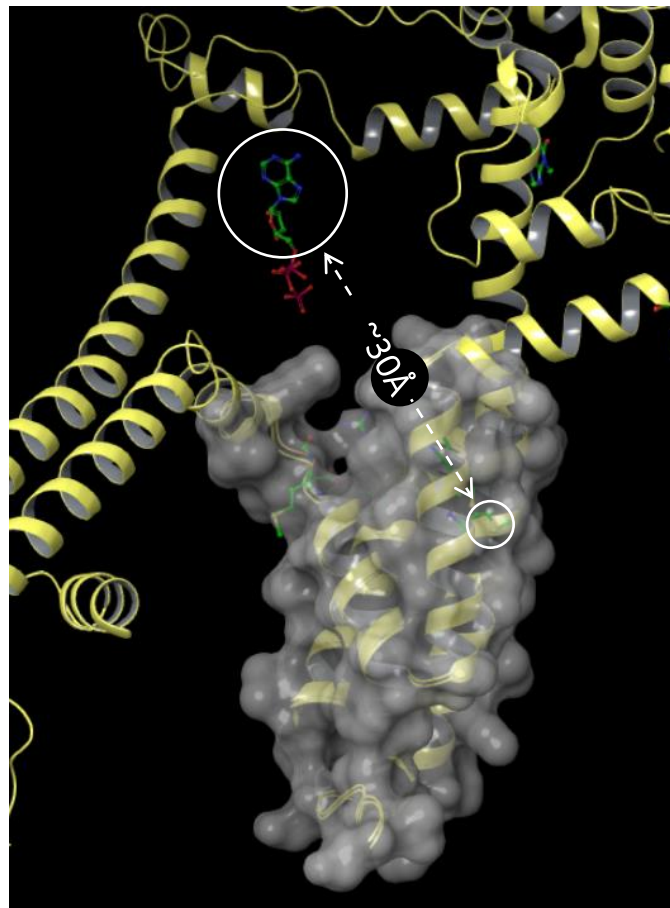


Figure 4.6. PxRyR homology model, indicating position of caffeine binding site (large circle) relative to position of I4790M mutation (small circle).

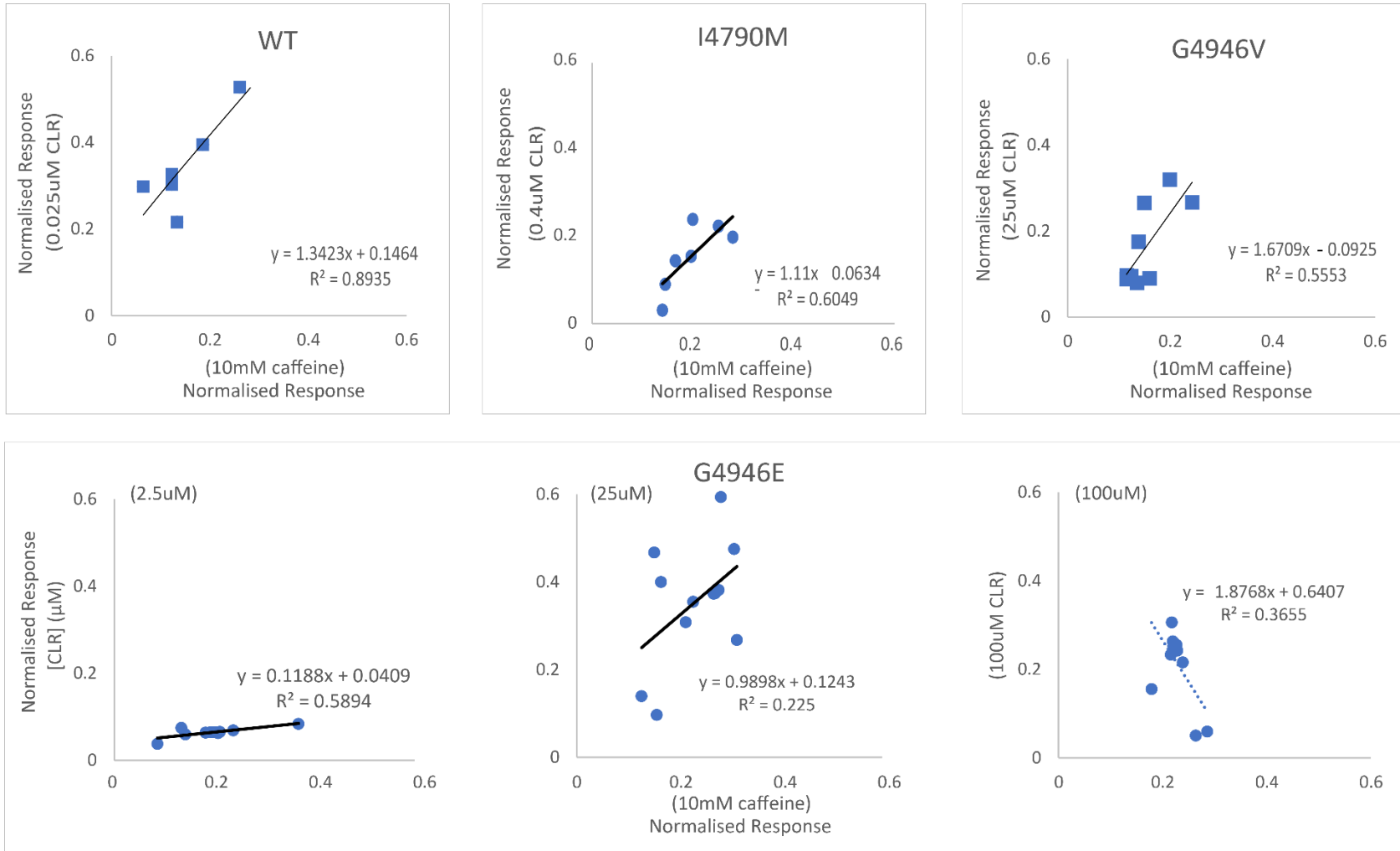


Figure 4.7. Normalised response to 10mM caffeine (x) vs normalised response to varying concentrations of CLR (y). Each plot represents a patch of PxRyR-expressing Sf9 cells exposed to caffeine and then diamide stimulus.

4.4.3 Quantifying the impact of field-derived mutations on PxRyR stimulation by diamides

By successive application of caffeine and diamide, following the protocol outlined in Ch3, Box3.1, the recombinant PxRyR constructs G4946V-PxRyR and I4790M-PxRyR were characterised in terms of their responsiveness to increasing diamide concentrations. Concentration-response relationships are displayed, with comparison to WT-PxRyR, for CLR and FLB in each case. For each concentration point, n = 5-8 patches of cells, where a patch of cells contains between 5-32 Cat A responding cells.

4.4.3.1 G4946E – the root of resistance

Diamide resistance associated with G4946E in the field varies from ~2000-fold for FLB in China, to ~10,000-fold to CLR in the Philippines (references in Table 4.1). Over the past decade, the role of G4946E in diamide resistance has been extensively characterised *in-vitro*. Sf9 cells expressing a non-resistant WT-PxRyR channel exhibited non-transient gating and calcium store emptying in response to 100nM FLB application, whilst those expressing the G4946E channel were refractory to such effects up to (and most likely beyond) the limit of solubility of the compound (Trocza et al. 2015). For CLR, a more complete concentration-response profile was achieved for both the WT-PxRyR and G4946E-PxRyR constructs, with the EC50 increasing from ~0.017µM to around ~3.7µM, implying a RR of 218-fold. Similarly, native membrane preparations containing PxRyR from a resistant moth strain exhibited 450-fold (FLB) and 159-fold (CLR) reduced binding when compared to membrane preparations from a susceptible strain (Steinbach et al. 2015).

The results presented in Fig. 4.8 broadly agree with past studies, cited above, reiterating the reduction in diamide efficacy due to the G4946E change. The RRs recorded here of 100-fold for CLR contrasts to the 218-fold resistance reported in (Trocza et al. 2015). In this case (and in Figs. 4.8 and 4.9), quantification of a resistance ratio for FLB was not possible, due to the inability to reach a plateau in the FLB-response prior to the limit of solubility.

4.4.3.2 G4946V – a new locus of resistance in *Tuta absoluta*

Populations of *T. absoluta* with diamide resistance ratios of ~2700-fold or >3200-fold were recorded in Italy and Greece (respectively), as of 2017. The associated

G4946V mutation characterised in the resistant *T. absoluta* populations has not yet been identified in other species (at the time of writing). It was necessary therefore to experimentally validate the role of this mutation in the observed resistance episodes. The mutation is also interesting in the context of achieving a better understanding of the nature of G4946E-mediated resistance. The valine (V) substitution in the *T. absoluta* populations has no charge, compared to the strong negative charge on the glutamic acid (E) substitution. If both cause an equal level of resistance, this might indicate that the associated decrease in diamide efficacy is due to binding site obstruction rather than changes in chemical interaction.

The results presented in Fig. 4.9 indicate that the G4946V substitution does mediate substantial resistance to both FLB and CLR. A calculated RR of 144-fold to CLR indicates more potent resistance effects than those seen for G4946E in this study. However, caution should be exercised in comparing the resistance profiles of the two constructs given that, as discussed previously, detailed analysis of cell physiology was not made in this study.

Since the collection of this data, other authors have made parallel attempts at characterisation. *T. absoluta* membranes harbouring G4946V-RyR have >300-fold reduced FLB binding (Roditakis et al 2017). G4946E, inserted by CRISPR/Cas9 transgenesis into an otherwise susceptible genetic background, exhibits a resistance of 223-fold to CLR in beet armyworm (Zuo et al. 2017).

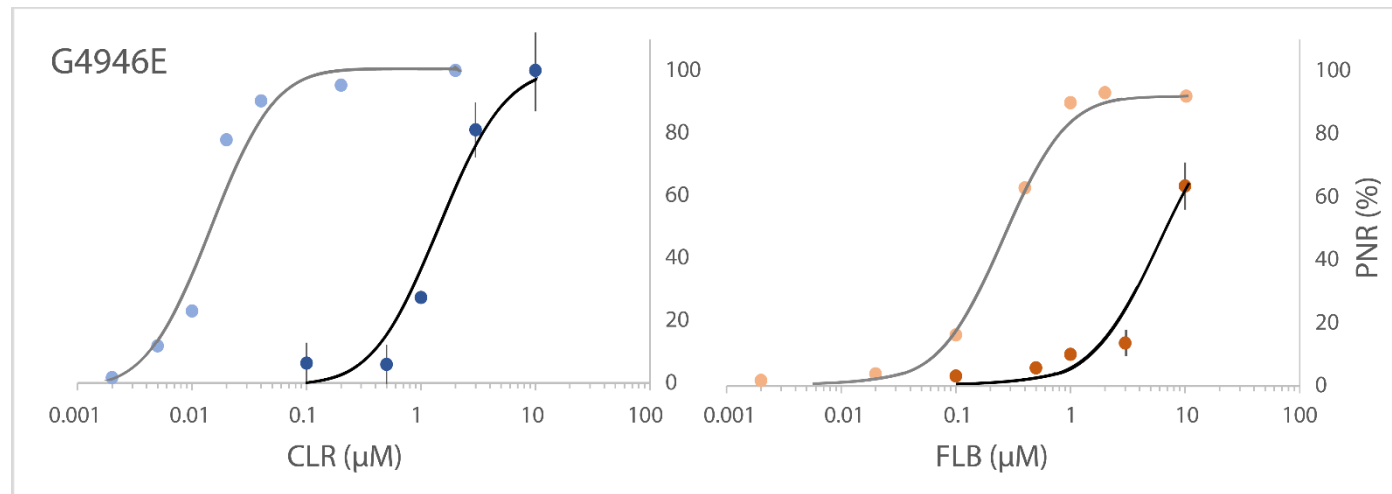


Figure 4.8. Dose-response relationship of G4946E -PxRyR (dark fill) to CLR (blue) and FLB (orange) with WT-PxRyR (light fill) response included for comparison

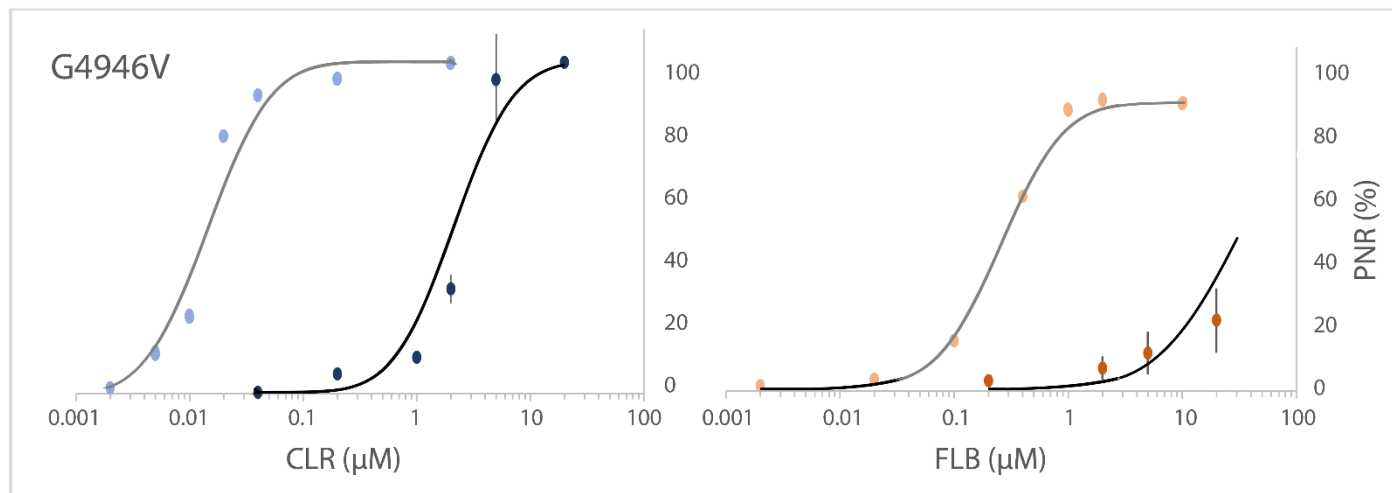


Figure 4.9. Dose-response relationship of G4946V -PxRyR (dark fill) to CLR (blue) and FLB (orange) with WT PxRyR (light fill) response for comparison

4.4.3.3 I4790M – A novel cause of resistance in diverse lepidopteran pests

The potential significance of the I4790M residue is immediately clear when one looks at an alignment of insect RyRs (Fig 4.10), as almost all insect orders are wildtype methionine (M) whilst Lepidoptera are distinguished from other orders by having an isoleucine (I). It seems highly plausible that the methionine at this position is therefore a selectivity switch, responsible for the relative ineffectiveness of diamides, particularly FLB, on non-lepidopteran pests (Steinbach et al. 2015). Such a theory is supported by reverse genetic studies in *Drosophila*, which naturally have methionine at this position and exhibit low diamide susceptibility. Substitution with isoleucine conferred a 7.5-fold increase in CLR efficacy and a 15-fold increase in FLB efficacy (Douris 2017). Anthranilic acid diamides such as CLR are thought to bind at a separate, albeit coupled, location from the phthalic acid diamide FLB, potentially explaining this discrepancy in susceptibility in the engineered *Drosophila* strain (Isaacs et al. 2012; Qi and Casida 2013). A recent backcrossing experiment in *S. exigua* found that introgression of the I4790M mutation caused approximately 20-fold resistance to both diamides (Zuo and al. 2019).

Functional biochemical studies on I4790M are severely lacking and we still don't fully understand why this mutation causes diamide resistance. Homology protein modelling of the *P. xylostella* RyR has shown that this residue lies just 13Å from G4946 in the 3D structure, with suggestions that the two residues may form part of the diamide binding pocket (Steinbach et al 2015). However, attempts to use a fluorescent CLR tracer to measure thoracic membrane binding failed to draw any meaningful conclusions (Guo et al. 2014b). A similar attempt using radiolabelled-CLR suggests a 4790M-mediated reductions in binding, although the presence of 4946E in the membrane preparations prevents a clear interpretation of the results (Roditakis et al. 2017).

Fig. 4.11 indicates that I4790M does indeed confer a degree of resistance to diamide insecticides. For CLR, the calculated RR is moderate, at just 10-fold (comparing to RR of 100-fold for G4946E in this study). A slightly higher resistance is apparently conferred to FLB, with estimates between 20-fold and 35-fold, depending on the line steepness calculated. As previously, limitations of solubility prevent accurate quantification of FLB resistance.

			4786	4787	4788	4789	4790	4791	4792	4793	4794
Insecta	Lepidoptera	<i>P.xylostella</i>	V	S	L	A	I	L	I	G	Y
	Lepidoptera	<i>T.absoluta</i>	V	S	L	A	I	L	I	G	Y
	Lepidoptera	<i>C.suppressalis</i>	V	S	L	A	I	L	I	G	Y
	Diptera	<i>D.melanogaster</i>	V	S	L	A	M	L	I	A	Y
	Coleoptera	<i>T.castaneum</i>	V	S	L	A	M	L	I	A	Y
	Hymenoptera	<i>A.mellifera</i>	V	S	L	A	M	L	V	A	Y
	Hemiptera	<i>M.persicae</i>	A	S	L	A	M	L	I	A	Y
Crustacea	Cladocera	<i>D.pulex</i>	I	S	L	F	M	L	I	A	Y
Arachnida	Araneae	<i>C.salae</i>	I	S	F	C	M	L	I	A	Y
	Acari	<i>T.urticae</i>	L	A	V	F	M	L	I	G	Y
Nematoda	Chromadorea	<i>C.elegans</i>	T	S	F	A	L	L	V	S	F
Mammalia	Primates	<i>H.sapiens</i>	V	A	F	L	C	I	I	G	Y
Mammalia	Lagomorpha	<i>O.cuniculus</i>	V	A	F	L	C	I	I	G	Y
Aves	Passeriformes	<i>T.guttata</i>	I	S	F	F	C	I	I	G	Y
Actinopterygii	Lepisosteiformes	<i>L.oculatus</i>	I	S	F	F	C	I	I	G	Y

Figure 4.10. Lepidoptera segregate from other invertebrate and vertebrate species at the 4790 position on the RyR

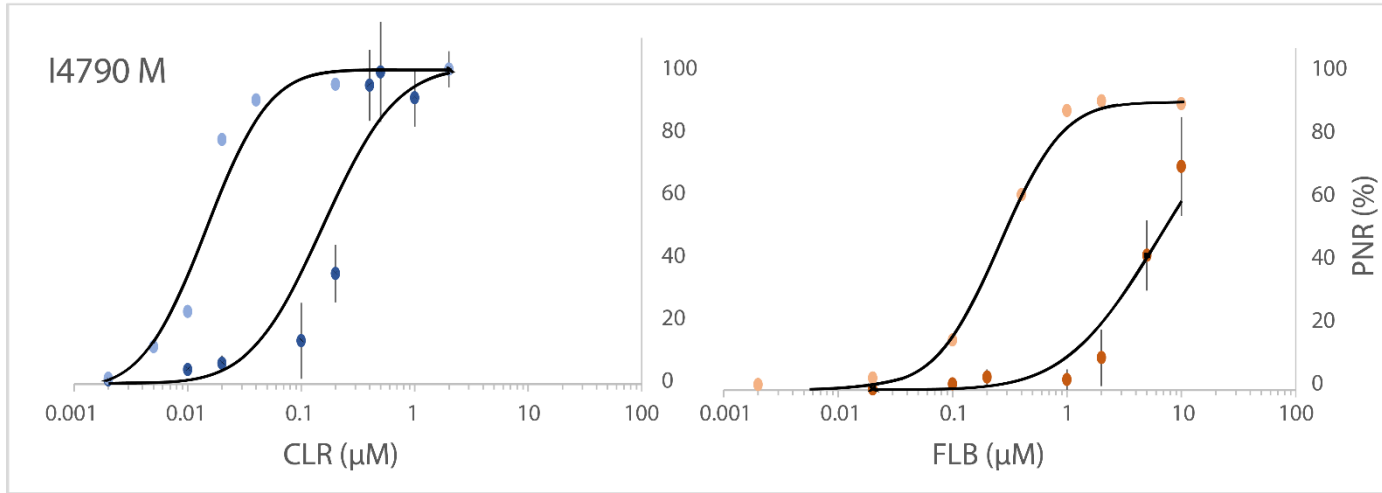


Fig 4.11. Dose-response relationship of I4790M -PxRyR (dark fill) to CLR (blue) and FLB (orange) with WT- PxRyR (light fill) response shown for comparison

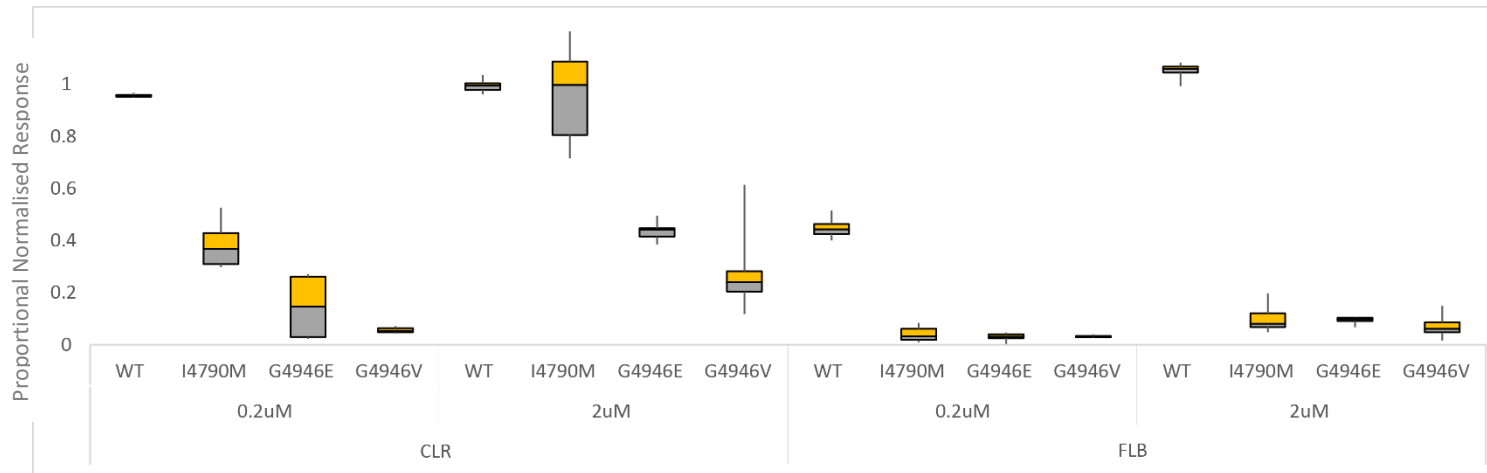


Figure 4.12. Boxplot comparison of all resistant PxRyR mutant responses to diamides CLR and FLB

4.5 Discussion

It has been noted previously (Thomas et al. 2004) that heterologous expression of RyR in cells that contain neither the native RyR nor its native regulatory environment may yield channels that behave entirely dissimilarly to those *in-vivo*, bringing into question the relevance of the results in the context of insecticide resistance in the field. Channels produced in null-cell systems may not exist in a macromolecular organisation, since many of the accessory proteins are absent (Macrill 1999). Three points offer evidence to the contrary, however. The first is that this study addresses just one characteristic of the RyR channel; the release of Ca^{2+} due to agonist binding. Such a mechanism has been shown not to require additional accessory proteins, and indeed not even to require the majority of the protein to be intact (Xu et al. 2000). Secondly, the mutations studied here might be expected not to illicit strong functional differences, because these exist and even spread throughout populations, as opposed to those pathological mutations cited in medical studies (e.g.(George and al 2007)). Indeed, the mutations are not expected to illicit functional difference at all because they lie in a region quite distinct from the Ca^{2+} , caffeine, ATP-binding region (Fig 4.6). The third point is that numerous studies have now made use of such heterologous expression systems to study lepidopteran RyR *in-vitro*. This study draws on these previous studies, and its strength is in comparison to those previous studies, rather than requiring comparison to *in-vivo* results. Furthermore, the comparison is made between genetically very similar recombinants, varying by just a single amino acid alteration, as opposed to the work of others ((Kato et al. 2009; Tao et al. 2013)) which compare drastically different constructs. The benefit of *in-vitro* studies such as these are to allow a 'reductionist' environment to look at individual channel changes out of the context of the compensatory mechanisms that might exist *in-vivo*.

4.6 Conclusion and future work

The results in this Chapter (summarised in Fig 4.12) have shown that alterations of residues G4946 and I4790 on the PxRyR cause a severe reduction to the diamide effect in PxRyR-expressing cell lines. Comparison of the results presented here with those of other studies reveals that resistance ratios vary dramatically between *in-vitro* and *in-vivo* studies, even when mediated by the same cause. For example, whilst the G4946E change produces a 10,000-fold reduction in CLR efficacy in the field, the same change produces a mere 100-fold change in this study. Similar

findings in other cell line and ligand binding studies support the point (Trocza et al. 2015). The simplest explanation is that in field populations, multiple sources combine to aggravate the phenotype. Possible mechanisms include cuticular changes affecting insecticide penetration; behavioural adaptations for avoidance; metabolic upregulation to speed up detoxification and removal; and target-site alterations to reduce insecticide efficacy (IRAC 2019). Alternatively, the disparity may be attributable to other aspects of the genetic background. In complex organisms, any phenotype is determined by the overlapping effects, or epistatic effects, of multiple independently acting genes. Previous studies document examples of a genetic alteration increasing fitness in the presence of an insecticide, in a genetic-background-dependent fashion (Smith 2011).

The I4790M change was found here to mediate a 10-fold reduction in CLR efficacy, whilst in the field its presence is associated with ~150-fold change (Gutierrez-Moreno et al. 2019). This result also supports the role of I4790M as a diamide 'selectivity switch' between lepidopterans and other insect classes – partially explaining the major reduction in FLB-response outside of the Lepidoptera. I4790M-mediated FLB-resistance was comparable to the other two resistant constructs. Referring to Figs 4.8-4.10, 10 μ M FLB elicits a response magnitude of 63% (I4790M); 20% (G4946E); 78% (G4946V), respectively, whilst resistance to CLR conferred by I4790M is much less potent than that of the G4946 alterations. Certainly, the FLB-resistance conferred by I4790M in this study is much less severe than the resistance ratios calculated between Lepidoptera and other insect orders, which can reach a magnitude of 10,000- or 100,000-fold difference (Hall 2007), even accounting for the observation that field-study resistance ratios tend to be much higher than lab-study ratios. If the I4790M is a selectivity switch, it is surely one of many which combine to make such a wide selectivity difference between the classes.

Whilst the proliferation of target-site resistance is cause for alarm in terms of reduced defence against lepidopteran insect pests, it may also hold clues to reversing resistance. Analysis of the resistance-associated mutations described above, combined with empirical studies on the RyR channel, bring ever closer the goal of pinpointing the diamide binding site. A list of additional candidate mutations was compiled (Fig 4.13) based on the correlation of known diamide susceptibility with the occurrence of residue changes across an alignment of 44 insect and non-

insect RyR sequences. Residues that segregate between lepidopterans and other insects represent candidate resistance-associated mutations. The presence of a residue in other insects is evidence of functional compatibility, hence the assumption is that residues present in other insects are more likely to reoccur in Lepidoptera in the field.

Mapping of the *P. xylostella* TM region on to the available 3D structure of closed-state rabbit RyR1 (Yan et al. 2015) shows a very close proximity of G4946E and I4970M. At approximately 13Å distance, they face each other from either side of a Voltage Sensor Domain-like cavity (pVSD), a highly polar region whose homologues in other channels are known sites of ligand interaction. The role of the pVSD in diamide binding is supported further by a series of reverse genetic studies, as will be discussed further in Ch6, where it will inform an effort to define the position and extent of the diamide binding site.

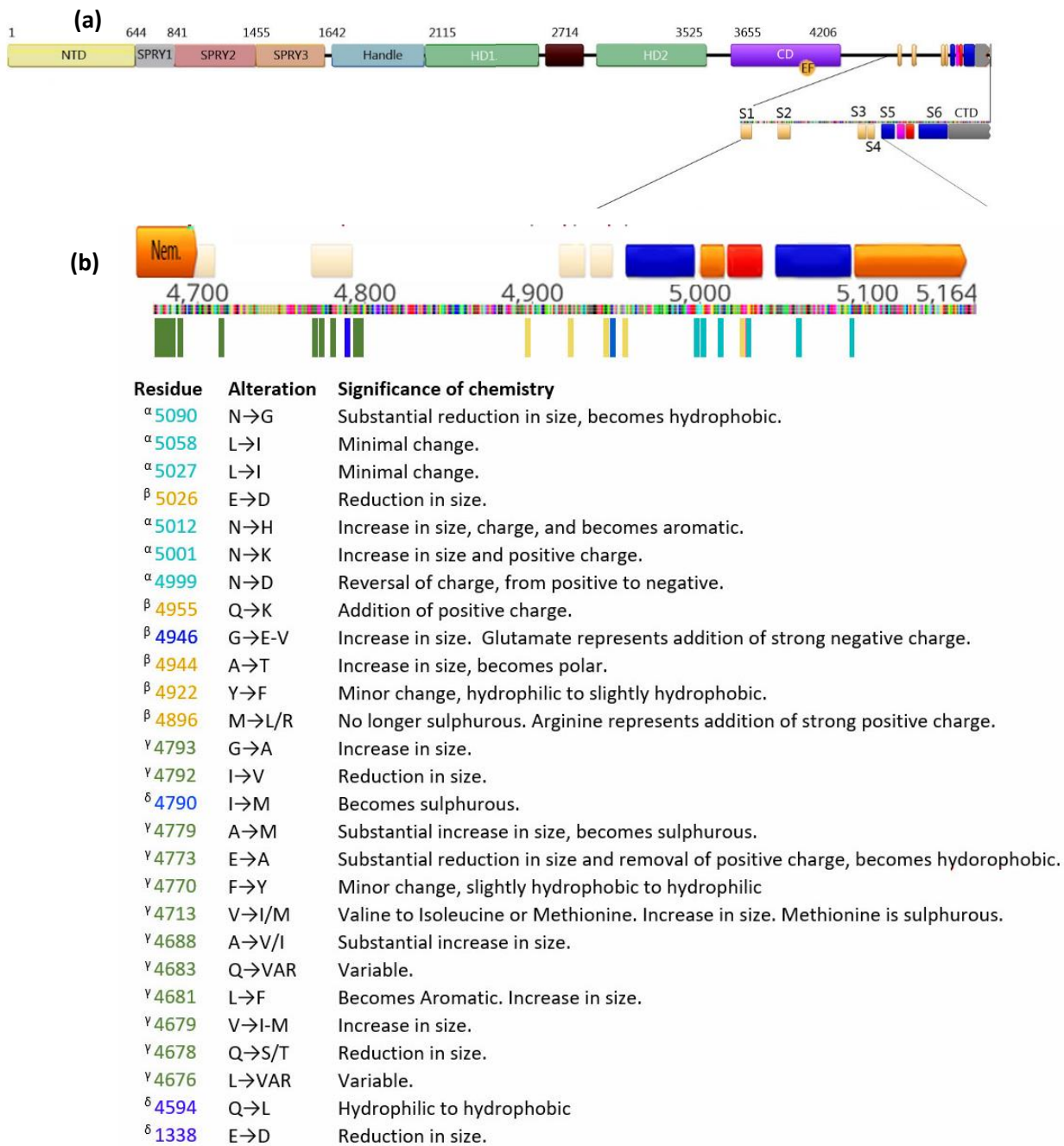


Figure 4.13 Additional candidate mutations that may alter RyR channel sensitivity to diamide insecticides. Alterations are listed by position, and the significance of the alteration in terms of local chemical interactions is described. Changes in size are expected to alter the size of cavities, which can impact ligand binding. Changes in charge may alter the local hydrophobicity, changing what type of ligands can bind. Sulphurous amino acids have the capacity to form di-sulphide bonds with other sulphurous amino acids, which can drastically alter the shape of the protein. Hypothetical residue changes based on: α , Wang et al 2012; β , Daniel Cordova pers. comm; γ , residues identified in this study based on alignment of 43 insect RyR sequences.

Chapter 5: *In-vivo* investigations of Diamide Resistance

5.1 Chapter Summary

5.1.1 *An in-vivo model of diamide resistance*

The previous Chapter investigated two novel RyR mutations and concluded their probable role in reductions of diamide control efficacy in lepidopteran field populations. However, resistance is a field-condition and should be studied in settings as close as possible to those of insects in the field (Ffrench-Constant and Bass 2017). The goal of isolating the RyR sequence variants within Sf9 cells (Ch4) was to show beyond reasonable doubt that the individual mutations linked to diamide resistance are responsible for alterations in diamide interaction with the receptor. Having done so, it is now important to corroborate these findings by showing that reductions in diamide efficacy *in-vitro* are mirrored by the same reductions *in-vivo*. To that end, this Chapter details the integration of the previously studied PxRyR and amino acid variants of PxRyR into *Drosophila melanogaster*, followed by a toxicological impact assessment of the diamides CLR and FLB upon those fly lines.

5.2 Chapter Introduction

5.2.1 *Resistance, but at what cost*

It has been shown, over the past decade, that the spread of diamide insecticide resistance (see Ch1) represents (in most cases) the spread of allelic variants of the RyR gene, encoding proteins of altered structure that exhibit reduced diamide interactions. Armed with this knowledge, the spread of resistance is countered by a strategy of insect resistance management (IRM) mode of action (MoA) rotation, as advised by the Insecticide Resistance Action Committee (IRAC). The basal theory behind this MoA rotation is one of fitness costs: a phenotype is shaped by the selection pressures of its environment, bringing it ever closer to optimality in that environment, such that alterations to the environment, for example, by introduction of synthetic insecticides, predators, or competitors, necessarily reduces the fitness of this phenotype (Coustau et al. 2000). The upshot is that each resistance-causing allele can be described to suffer from a *cost* in the absence of

insecticidal pressure. Knowledge of such costs can potentially be employed to *predict* the probability of existing target-site mutations spreading through populations, in order to enact IRM protocols in advance of invasion. Population genetics defines the probability of a given resistance allele spreading through a population as a function of three variables (e.g. Wilson and Rannala 2003):

- *Benefit* provided by the allele, in terms of increased survival and reproduction in the presence of insecticide pressure
- *Cost* inflicted by the allele, in terms of reduced survival and reproduction in the absence of insecticide pressure
- *Heritability* of the allele, or the effective dominance of its phenotype, in a heterozygous context

(Where all three variables are calculated relative to the non-resistant wild-type (WT) allele).

The cost outcome depends entirely on whether the resistance is metabolic (a quantitative trait) or TSR (a discrete trait). In the case of metabolic resistance, the cost may be a straightforward trade-off between resource allocation into xenobiotic/toxin detoxification or allocation into nutrient metabolism. Transcriptome profiling of CLR-exposed *C. suppressalis* shows that, whilst detoxification related genes are up-regulated, the flipside is a downregulation of general metabolism genes (Meng X et al. 2019), with the accompanying metabolic reductions expected to negatively impact development rate. Indeed, *Culex pipiens* mosquitoes which over-express esterases were shown to contain on average 30% less lipids, glycogen and glucose than their wildtype counterparts (Rivero et al. 2011).

In the case of target-site resistance, the cost is less predictable. Indeed, no studies have succeeded in measuring the fitness costs due to specific target site (amino acid) changes on the RyR (to the author's knowledge). Theoretically, such costs may derive from potential alterations to the function of the protein itself, and the biochemistry surrounding that. If functional effects of the acquired mutation are significant, then the cost of resistance will be high. *Plutella* exhibiting 22,700-fold CLR resistance exhibited profound costs in absence of CLR exposure (Ribeiro et al. 2014). Relative to a field-derived reference strain, they produced fewer, smaller

larvae, which took longer to develop and were less likely to successfully pupate. However, any accompanying metabolic differences between the resistant and susceptible strains were not established, so it is not known whether the costs are attributable to the target-site alteration, or to other causes. Indeed, another study indicates that the cost of diamide target-site resistance is low or non-existent. The Sudlon strain of *Plutella*, collected from the Philippines during an early resistance outbreak, carrying the G4946E mutation, shows only mild resistance-costs, in terms of a 7-14% delay in development across various larval and pupal stages (Steinbach et al. 2017). Indeed, the strain continues to display high levels of resistance without further diamide selection (Steinbach et al. 2015), suggesting that such costs are not sufficient to reduce the prevalence of the resistant allele in the population. However, this second study also suffers from an identical flaw – lack of genetic investigation beyond the RyR locus hinders understanding of the fitness cost of the G4946E mutation on its own. Much of the variation seen between these studies should be attributed to the lack of precise genetic investigation. This Chapter therefore reports upon *in-vivo* experiments to corroborate the *in-vitro* resistance effects reported in Cht 3+4 and briefly assesses the impacts of that resistance upon indicators of fitness.

5.3 Methods

5.3.1 *D. melanogaster* rearing

D. melanogaster strains were maintained in standard 25x95mm polystyrene vials (Genesee) with 5ml of fly food (Nutri-Fly® Bloomington formulation). Fly stocks were kept at 19°C and transferred to fresh vials every 4 weeks. Virgin female *D. melanogaster* for crosses were collected within 8 hours of emergence.

5.3.2 The germline transformation strategy, and generation of the injection line

The ϕ C31 integrase system uses *P*-element-mediated germ-line transformation to integrate exogenous DNA sequences into the *D. melanogaster* genome. ϕ C31 integrase is an enzyme that mediates recombination between attP docking sites in the genome and an attB-containing plasmid, pUAST, leading to the integration of the whole plasmid into that site in the genome. In this case, the system will be used to integrate the PxRyR CDS.

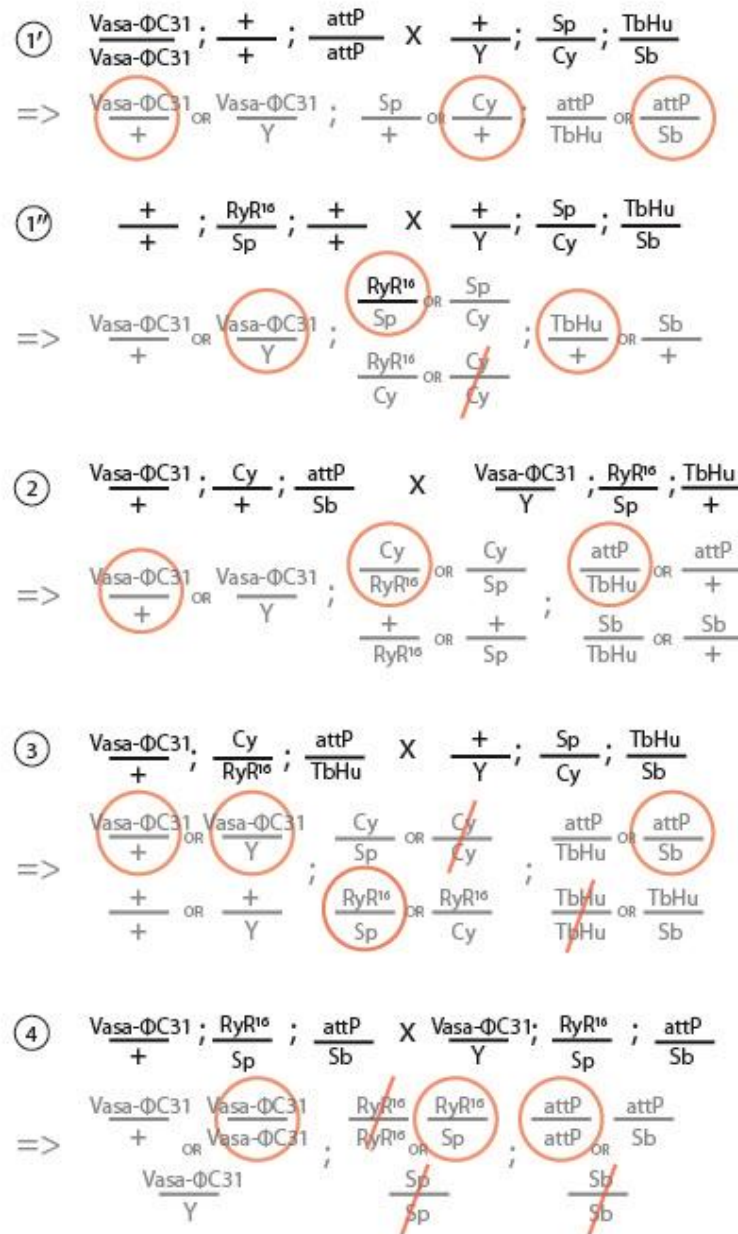


Figure 5.1 Iterative crossing with a double-marker line is used to combine two Bloomington stock lines, in order to create an injection line that expresses ϕC31 by the *vasa* germline promoter (Chromosome 1), the RyR^{16} knockout (Chromosome 2) as well as the *attP* sequence for UAS-mediated genomic integration (Chromosome 3). Red circles indicate the genotype that has been selected for further crosses. Red strikes indicate a non-viable genotype.

An *attP* integration strain carrying a truncated *RyR* allele (hence forward referred to as *RyR16.attP* strain) was generated by replacing chromosome 2 from strain $y[1] M\{\text{vas-int.Dm}\}ZH-2A w[*]; M\{3xP3-RFP.attP\}ZH-86Fb$ by chromosome 2 from strain $y[1] w[*]; \text{RyR}[16]/\text{CyO}, y[+]$. Both strains were acquired from the Bloomington Drosophila Stock Centre (reference numbers #24749 and #6812, respectively). A crossing scheme detailing how this strain was generated is shown in Fig 5.1. The

RyR16.attP strain expresses the ϕ C31 integrase under the control of the *vasa* promoter, allowing for efficient transformation just within the germline cells. Upon the second chromosome, it carries a null-functional RyR mutated allele over a balancer. And upon the third chromosome, an attP integration site, position 86F8, where the inserted *PxRyR* sequence will land.

5.3.3 Generation of UAS-*PxRyR* genome modified *Drosophila* lines

~150 female and ~150 male flies of the RyR16.AttP strain were transferred to a cage with an egg-laying plate made using FlyStuff grape agar mix (FlyStuff laboratory equipment) streaked with a yeast paste (RedStar). The adult flies were added to the cage 2 days prior to embryo injection and left at 25°C to allow the flies to acclimate, and the food was changed 2-3 times a day. On the day of injection, the grape agar plate was changed at 2 hours, 1 hour and 30 minutes before egg collection to empty females of old embryos. The embryos were rinsed off the grape plate into a mesh basket and washed with water, with an egg collection every 30 minutes to ensure injection was carried out using embryos in which blastoderm cells had not formed. Embryos were transferred to a 2 x 2 cm square glass cover slip and aligned, using a fine sable paintbrush, with the dorsal side face up and the posterior end of the embryo ~2 mm from the edge of the coverslip in a line. Exact drying time mediated high injection survival: lines of embryos were dried until the aqueous meniscus between eggs was on the verge of disappearing (30s-5min). To halt the drying process, halocarbon oil 27 (Sigma-Aldrich) was applied sparingly to the embryos. Prior to injection, embryos were incubated for a further 5 minutes to allow the halocarbon oil to penetrate between the chorion and vitelline membrane. During which time, embryo developmental stage became apparent, and overaged embryos were sacrificed by deep insertion of the needle. The needle was then opened via anteroposterior abrasion along the embryo chorion, whilst applying >2000kPa solution pressure.

For UAS-*PxRyR* integration, the Φ C31 recombination system was used, whereby integrase catalyses recombination between an attB site (present in the UAS-*PxRyR* vector) and an attP site (present in the genome of the RyR16.attP strain) in a non-reversible manner, integrating the entire vector into the fly genome (following (Bischof et al. 2007)). The UAS-*PxRyR* vector was created via traditional enzymatic cloning (Ch2, section 2.5). *PxRyR* CDS had previously been cloned from the in-house 'Roth' strain of *P. xylostella* (Trocza 2013) and inserted into the backbone of the

pUAST-AttB plasmid, which contains a white-eye colour marker (*w*) for screening. The required PxRyR mutations were introduced into the UAS-PxRyR plasmid via site directed mutagenesis, as described in Cht 2.

UAS-PxRyR altered constructs were microinjected into non-decorionated syncytial blastoderm embryos using an inverted microscope (Eclipse TieU, Nikon, Japan) equipped with a 10x/0.25 (magnification / aperture) lens, 10x/22 eyepiece and fluorescence illumination. The injection solution contained 150ng/μl UAS-PxRyR plasmid and 100ppm fluorescent dye (fluorescein isothiocyanate dextran, Sigma-Aldrich) in injection buffer (Table 5.1). Solutions were delivered into the embryo by a FemtoJet express microinjector (Eppendorf, Hamburg, Germany) controlled by a

Table 5.1 Optimal Injection conditions. Excellent transformation efficiency was achieved for the G4946V-PxRyR construct, following these conditions

Condition	Notes
Humidity	60% - and eggs remained in contact with H ₂ O at all points during alignment
Temperature	21°C
Egg age	50 mins (30 min laying time, 20 min alignment)
Egg oil	Halocarbon 27
Injection solution	150ng/μl DNA; 0.5μl fluo buffer; 0.5μl injection buffer; spun at 22,800 RCF for 10 minutes, and supernatant taken
DNA Preparation	Excellent DNA purity, confirmed via Qubit, Nanodrop, sequencing and diagnostic digestion
The Needle	'Program 5' - Heat 800; Fil 4; Vel 60; Del 145; Pul 175 (See image below – shorter needle tip length allows consistency of solution flow)
Injection Pressure	1500kpa//800kpa - Allowed constant flow from needle
Injection Method	- Probe to find easiest point of insertion - Needle on the <u>lower</u> half of the egg (find centre and then lower needle) - In cases of injection in between two egg-layers, simply waited for inner layer to expand out, and then inject again

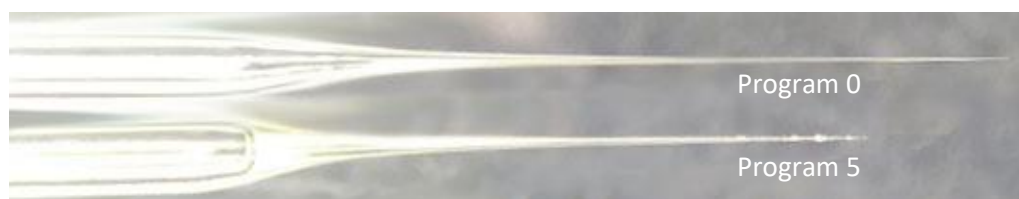


Figure 5.2. Specific needle and injection parameters, contributing to the high-quality injections achieved for Injection of G4946V-PxRyR-PuAST in to line vasa; RyR16/Sp; attb

Needle Program 0 - Heat 700; Fil 4; Vel 60; Del 145; Pul 175

Needle Program 5 - Heat 800; Fil 4; Vel 60; Del 145; Pul 175

motorised TransferMan NK2 micromanipulator (Eppendorf, Hamburg, Germany). Injection needles were prepared from quartz capillaries (WPI, D=1mm, L=100mm) using an P-2000 micropipette puller (Sutter Instrument Co, Novato, USA). Needle pulling conditions are listed in Fig 5.2. The injection needle was back-filled with 0.5µl of injection solution and aligned to the embryo posterior.

Table 5.1 and Fig 5.2 detail the conditions used to achieve the highest quality injections (based on adult survival and successful transformation). Injection solution was delivered into the embryonic posterior, with approximate injection volume identified by brightness of fluorescence, as viewed under unfiltered mercury fluorescence (Nikon IntensiLight Illuminator). Injection volume was maintained at an arbitrary level (determined by eye), found to maximise post-injection survival under these conditions. Specifically, injection volume was minimised to the point that embryonic cytoplasmic leakage from the injection site did not occur, whilst maintaining sufficient volume to visualise fluorescence.

Once the embryos were injected, the coverslip was prepared for incubation by draining the halocarbon oil, rinsing with 70% ethanol, rinsing with water and gently drying with tissue. The coverslip was then slotted into a food vial with 5ml of Nutri-Flyfood (Genesee), in which the food had been scored by forceps to create a rough surface and supplemented with 5-10 grains of dry yeast (RedStar). One coverslip was placed per vial, ensuring the embryos remained close to but not immersed in the food, and the approximate number of intact embryos recorded on the vial. Embryo vials were incubated at 25°C at 90-100% humidity and transferred to 50-70% humidity at 48h. Pupae were transferred to new vials and F0 virgin females and males were collected and isolated as they emerged.

5.3.4 Screening of UAS-PxRyR flies

Four strains were generated; one integrated with the wildtype PxRyR sequence; a second containing the G4946E mutation; a third containing the I4790M mutation detected in *P. xylostella* and *T. absoluta*, and the fourth containing the G4946V mutation found in *T. absoluta*. Surviving embryos (F0) were reared at 25°C to adulthood and backcrossed with non-injected flies of RyR16.AttP. F1s were scored for the expression of the *mini-white* (*w*) marker in their eyes. Successful integration of pUAST constructs at the intended genomic locations produces F1 flies with red-*ish* eyes. Homozygotes were generated by inter-crossing positive F1s and selecting

F2s (males and virgin females) with darker red eyes. These were inter-crossed to establish the homozygous stock (Fig 5.3)

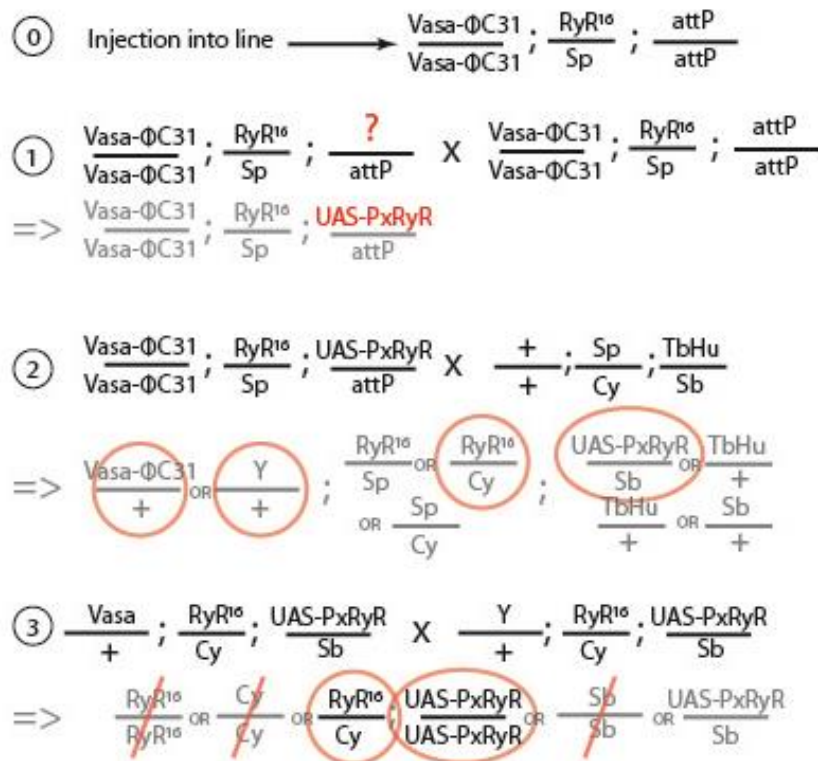


Figure 5.3 The RyR16.attp line is injected with UAS-PxRyR plasmid DNA to achieve integration of the construct. Integrated F0 lines are back-crossed to the RyR16.attp line to form heterozygous PxRyR (F1). Chromosomal swapping via the double-marker strain is used to generate homozygous PxRyR lines. The inserted PxRyR sequence is not expressed in this line due to the absence of a Gal4 driver sequence. Instead, the endogenous DmRyR sequence (carried by the Cy (straight wing) allele marker) is expressed.

5.3.5 Driving Expression of UAS-PxRyR

The UAS-Gal4 system was used to drive the expression of PxRyR in *Drosophila* (following Brand and Perrimon 1993). The inserted pUAST-PxRyR plasmid contains an Upstream Activation Sequence (UAS) prior to the start of the RyR CDS. The UAS sequence is under control of the GAL4 transcription factor, a protein not present in the wildtype *Drosophila* genome. Thus, the UAS-PxRyR containing line must be recombined with a Gal4-containing line, such that the GAL4 transcriptional activator is expressed and activates the UAS enhancer. This was achieved following a series of crosses as detailed in Fig 5.4.

The driving line employed in that crossing pattern is Bloomington Stock 67480, genotype $y[1] w[*]; Mi\{Trojan-GAL4.0\}RyR[MI08146-TG4.0]/SM6a$, generated by

Lee et al (Lee et al 2018). This trojan-Gal4 was designed in a way that once it is integrated in the genome it “hijacks” the transcription profile of the upstream regulatory region, whilst a poly-adenylation sequence after the Gal4 halts transcription of the downstream region. Thus, knockout strains are generated that express GAL4 under the control of the regulatory elements of the knocked-out genes. In this case, the Gal4 has been inserted at base number 18,477 of the endogenous DmRyR genomic sequence, meaning that the Gal4 (and thus its UAS-enhanced PxRyR sequence partner) is regulated by the same transcription factor machinery that regulates the endogenous DmRyR, whilst at the same time knocking out transcription of that endogenous DmRyR gene. Additionally, the RyR¹⁶ allele (recombined into the injection strain, Fig 5.1) is a deletion of the first intron of the DmRyR gene, thought to prevent functional channel formation (Sullivan et al. 2000). Thus, two different null-RyR variants in combination are employed in order to knock out the endogenous protein.

The rationale behind the rescue strategy is that a Trojan-GAL4-RyR/RyR16 hemizygous strain is null, not viable and can only survive if a functional UAS-RyR transgene is provided. Both Trojan-GAL4-RyR/Cy and RyR16/Cy are also homozygous lethal strains and only survive as heterozygotes because the balancer chromosome marked with Cy (straight wing phenotype) carries an intact DmRyR allele. Crossings between the RyR16.attP strain generated previously ($\gamma[1] M\{vas-int.Dm\}ZH-2A w[*]; RyR[16]/CyO; M\{3xP3-RFP.attP\}ZH-86Fb$) and the Trojan-GAL4 mentioned above, as expected, only generated flies with Cy wings (Fig 5.5). These results indicated that non-Cy Trojan-GAL4-RyR/RyR16 hemizygotes flies were indeed RyR-null and not viable.

Notably, a series of other Gal4 driver lines were tried, prior to the availability of this line in late 2018, but each was incapable of ‘rescuing’ the lethality caused by the lack of a functional DmRyR. The lines tested were:

- Brain, muscle, Cardia-Gal4 (#8182, genotype **P{GawB}DJ752**) (to direct expression of PxRyR to muscles, cardia and nervous tissue, corresponding to the endogenous DmRyR expression pattern)
- Tubulin-Gal4 (#5138, genotype **P{tubP-GAL4}LL7**) (to direct expression of PxRyR to muscles)

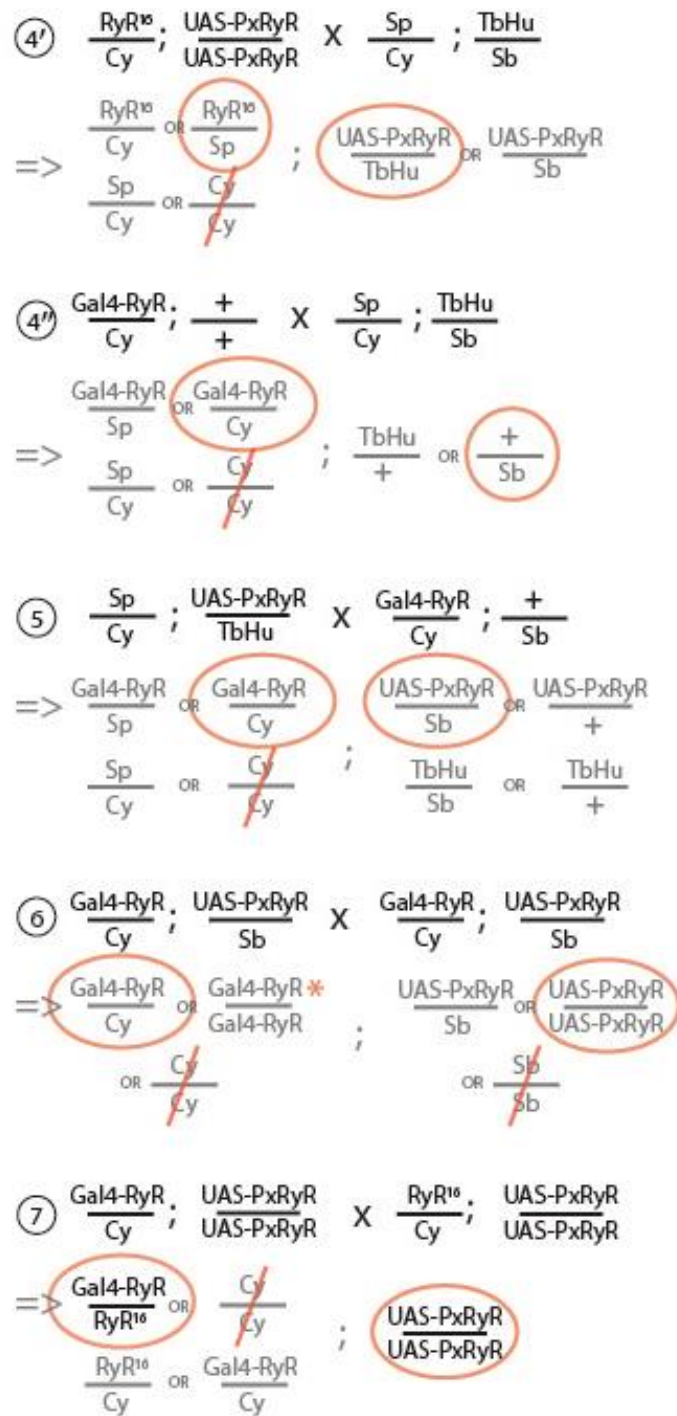


Figure 5.4 A series of crosses the double marker line was used to recombine the inserted UAS-PxRyR into a line that also expresses the Gal4 promoter. Further crossing leads to the removal of the Cy marker, and with-it removal of the endogenous DmRyR expression. The asterisk (*) in panel (6) indicates the 'stable line' genotype that is yielded only at development temperatures below 17°C.

- HSP-Gal4 (#1799, genotype **P{GAL4-Hsp70.PB}89-2-1**) (body-wide expression, with the ability to regulate expression level based on temperature)

By comparison, expression of UAS-PxRyR via the RyR-Gal4 driver was shown to successfully rescue the lethality caused by the lack of a functional DmRyR. This,

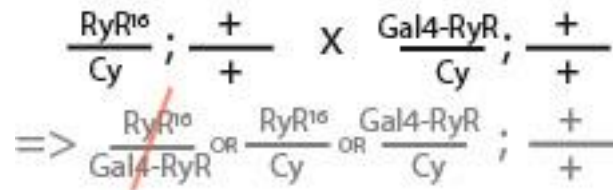


Figure 5.5 Attempted recombination of RyR¹⁶ and RyR-Gal4 null alleles into the same line. Flies fail to develop past larval stage L1.

however, was only achieved when crosses were kept at 17°C and moved to 25°C in the 9th day of development. Crosses kept at 25°C did not generate any rescued individuals. Maintaining the fly crosses at a lower temperature until the 9th day of development helped to overcome this lethality and allowed for the selection against the Cy (curly-winged) phenotype, which is not detectable at low temperatures. Non-Cy, DmRyR null flies rescued from lethality by the expression of PxRyR genes (Fig 5.6a i) were selected for bioassay (see Section 5.3.1 for details of adult bioassays) and also used to generate stable fly strains (Fig 5.6a ii).

5.3.6 Confirming Knock-in and Driving of PxRyR

Confirmation of successful knock-in of PxRyR variants was via cDNA sequencing (Fig 5.6 b). Adult *Drosophila* RNA was extracted (Ch2, 2.1.2) and 750ng used for cDNA synthesis using Superscript III (Life Technologies) and random hexamers (Life Technologies, CA, USA), according to the manufacturer's recommended protocol. The region of cDNA containing the mutation was amplified using primers PxRyR 11-13 (listed in table S2, appendix). The sequenced region is divergent from that of *Drosophila* RyR and sequencing traces indicated that no amplification of *Drosophila* RyR cDNA took place.

5.3.7 Experimental Methods on PxRyR-containing Fly Models

5.3.7.1 Larval bioassays and fecundity assessment

Larvae for bioassay and fecundity assessments were reared under the following conditions, carefully controlling for larval density. 30 adult virgins and 30 adult males of each strain were anaesthetised and placed into 8oz *Drosophila* Stock Bottles (Genesee) (one bottle per strain), 17 days prior to bioassay. Bottles were incubated at 25°C and adults allowed to lay for 48h, before being removed. After a further 9 days at 25°C, emerging adult males and virgins were selected from each

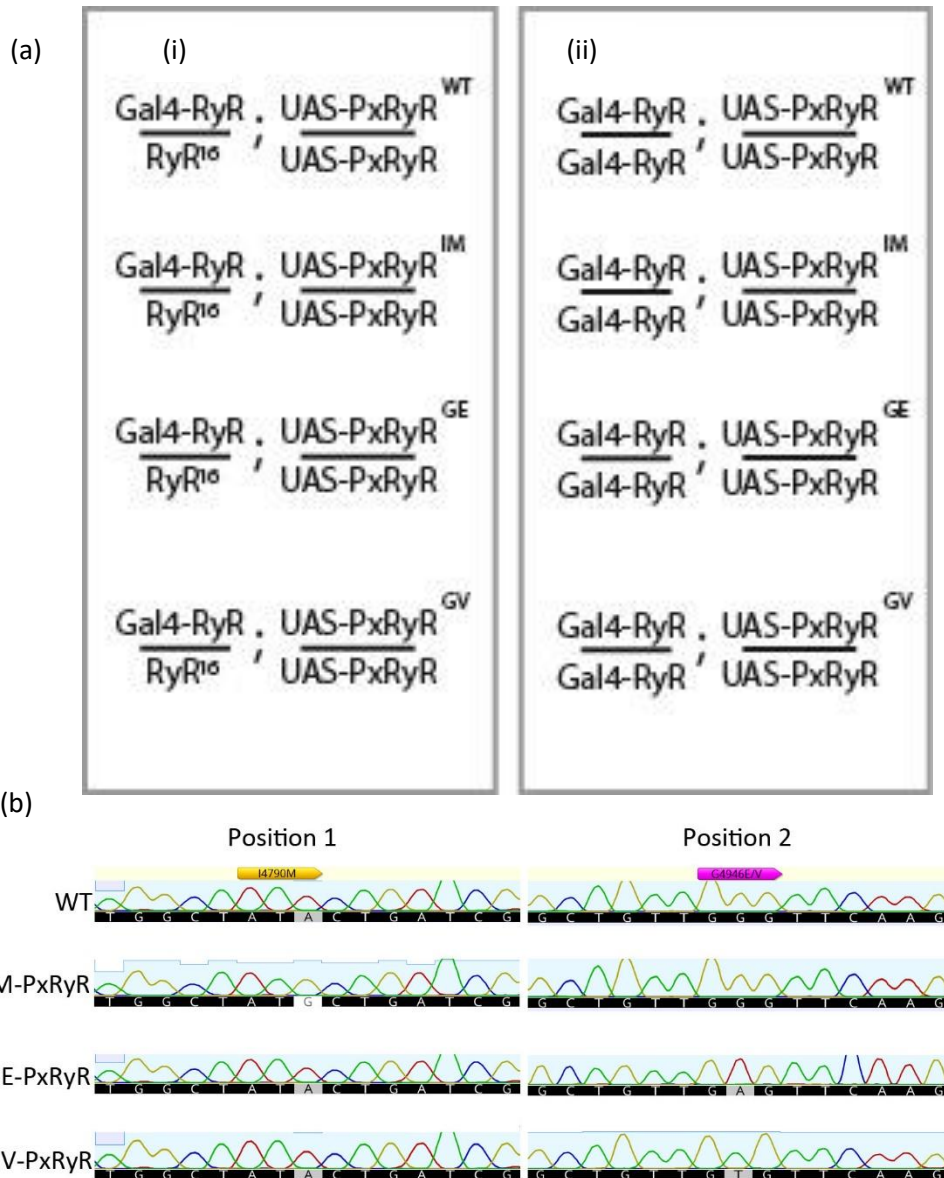


Figure 5.6 a) *Drosophila* lines generated for this Chapter. Stable lines (panel i) were used during all experiments detailed here, except for adult bioassays in which the RyR¹⁶ lines (panel ii) were used. Experiments on G4946E and G4946V fly lines are planned but had not been completed at the time of writing.

b) sequencing trace confirmation of successful integrations in the F2 generation.

strain.100 virgin females and 75 males of each genotype were placed into separate embryo collection cages (Genesee 59-101) with molasses agar plates (see Recipes, Appendix) supplemented with yeast paste to encourage egg-laying. Flies were allowed to adapt in cages for a period of 48h before beginning experimentation. After this point, eggs were extracted every 12h by removal of the used egg-plate from the cage and replacing with a new plate. Cages were maintained at 25°C, and egg extraction continued for 3d. The used egg- plate was labelled and incubated at

28°C for 22h to allow time for the fertilised eggs to hatch. Fecundity (#eggs) and fertility (#hatched/#unhatched) were quantified for each plate of eggs. After quantification, egg-plates were supplemented with additional yeast paste and returned to the incubator to develop into larvae. The incubation temperature was altered, in order to achieve developmental synchrony prior to bioassay, where necessary (development at 19°C is slowed by approximately half relative to development at 25°C). L2 larvae were used for larval bioassays, following the instructions below. Excess larvae, not required for bioassay, were reared at 25°C until larval stage 3 (L3) (72h) in order to conduct crawling speed assay.

Stock solutions of CLR and FLB were made up at 2000mg/L in 100% acetone. Stocks were diluted 1:50 to make up the first concentration (40mg/L) and diluted serially thereafter, at a ratio of 1:3, with all dilutions made in ddH₂O containing 2% acetone. For the non-insecticide control, ddH₂O containing 2% acetone was used. Narrow vials (Fly-Stuff laboratory equipment) were pre-prepared with 0.8g dry fly diet (Flystuff - Nutri-Fly Food, Instant Formulation) per vial, with 3ml of the relevant insecticide/control solution applied and incubated overnight for absorption of solution into the food and evaporation of acetone. The next day, the egg-plate (now containing L2 larvae of 48-60h age) was removed from the incubator and the larvae rinsed with tap water into a fine mesh sieve. Yeast paste on the plate was also removed and rinsed in the sieve in order to extract all burrowed larvae. The recovered larvae were transferred to an empty petri dish and 20 larvae were sorted using a fine sable paint brush and transferred to each bioassay vial. After transfer, 500µl ddH₂O was applied by pipette to rinse the larvae into contact with the insecticide impregnated food. In some cases, where development rate was variable between larvae, it was necessary to select larvae by size during this transfer stage. Each vial was scored for pupation (T+9d) and eclosion (T+13d).

5.3.7.2 Adult insecticide bioassays

3-5-day old adult non-virgin females were used in insecticide bioassays to assess the susceptibility of different fly strains to technical compounds. The flies were subjected to the insecticide in a contact/feeding bioassay. Standard *Drosophila* vials were filled with agar solution (4ml/vial) containing 2% w/v agar (Dutscher Scientific), 1.2% w/v food grade sucrose and 0.4% v/v glacial acetic acid. Insecticide solution was formulated in 100% acetone and diluted by 50% into ddH₂O and diluted serially thereafter at a 1:5 ratio. Individual concentrations were pipetted in

100µl volume onto pre-made agar vials, which were manually tipped and rotated in order to allow the solution to cover the surface homogenously. For each concentration, vials were prepared in duplicate for each fly strain with flies anaesthetised with CO₂ and 20 female flies added to each vial. The vials were kept upside down until all flies became active to avoid flies getting trapped in agar.

'Mortality' and/or 'efficacy' was assessed after 24h, 48h and 72h, where compound 'efficacy' indicates the number of flies lacking movement or ability to remain vertical, whilst 'mortality' indicates the number of flies that are deceased. Data was analysed using Genstat (2019) software package, with LC50 values calculated by dose-probit analysis.

5.3.7.3 Crawling Speed Assay

Larvae, collected as described above, were placed in the centre of a molasses agar dish and subjected to 11W halogen light, at a distance of 15cm from dish edge. Negative phototaxis was recorded for 1 minute, on a Sony HandyCam, 30fps, mounted 50cm above the dish. A virtual grid of 1mmx1mm squares was placed over the recorded video using DaVinci (DaVinci Resolve 15, 2019) video editor. The path of the larvae was manually tracked, and the number of squares passed through by each of the larvae was counted. Data was analysed by ANOVA and Least Significant Difference in Excel (Microsoft Excel, 2019).

5.3.7.4 Climbing Assay

Groups of 10 adult male flies (reared as in Section 5.2.4.1) were transferred into standard vials of fly food (as in Section 5.2.4.1) and incubated at 25°C for >24h. Flies were then transferred to empty fly vials, via tapping (without the use of CO₂) in preparation for climbing assays.

The climbing (negative geotaxis) assay was performed with the use of an automated fly climbing system adapted from a previously described Hillary climber set up (Willenbrink et al. 2016). The system employs a two-storey acrylic tube rack (measuring 550 x 400 x 50mm) capable of holding 20 standard *Drosophila* vials (Fig 5.7). The rack rests upon a horizontal camshaft, bearing asymmetrical cams that cause the rack to rise and fall within a 4mm travel as the shaft rotates. The shaft itself is driven by a Marelli Motori MAA 63MB6 electric motor, at a rate of approx. 200rpm, resulting in a violent and consistent shaking of the vials. The rack is marked

with a horizontal line, at a height of 6cm from the base of each vial, in order to assess fly climbing ability.

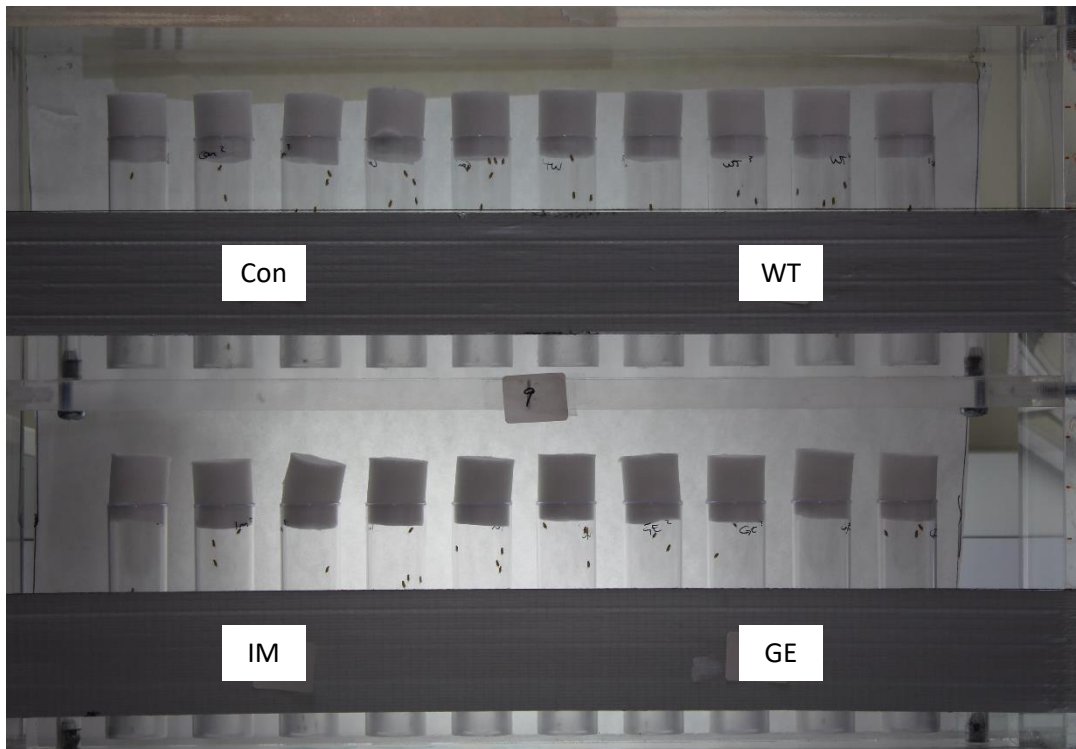


Figure 5.7 The fly climber apparatus (an adaptation of the Hillary climber). The proportion of flies successfully climbing to a height of at least 6cm within each vial within 8 seconds is recorded on camera and manually counted.

Vials of flies were loaded into the climbing assay tube rack. The climbing assay itself involved: 5 seconds of vial shaking; 8 seconds for climbing; image capture; 45 seconds resting, repeated 13 times during a single experiment. No data was collected during repeats 1-3 to allow for habituation before data collection. Images were captured with a Canon EFS digital camera with an 18-55mm lens, positioned on a tripod at a height level with the centre of the climbing system. Captured images were manually scored. The number of flies above the 6cm line in each vial was determined, and the score for each vial averaged over the 10 data-points. Data was analysed by ANOVA and Least Significant Difference in Excel (Microsoft Excel, 2019).

5.4 Results

5.4.1 Insecticide Bioassays

A list of fly lines generated in this thesis is provided in Fig 5.6. Susceptibility of the fly lines to diamide toxicity was assessed by contact bioassay on adult flies. Newly emergent females from the RyR¹⁶ lines (Fig 5.6ai) were selected based on the non-Cy (straight wing) phenotype and segregated into agar vials surface-coated with the insecticides CLR or FLB.

No significant difference in mortality to CLR was found between WT and I4790M adults (LD50 29±9mg/L vs 19±8mg/L). By comparison, mortality to FLB did differ between the strains, with I4790M being significantly less sensitive than WT. However, with an RR of just 3.6-fold (LD50 11.15±3mg/L vs 40±5mg/L), the magnitude of the difference is far smaller than that recorded by previous authors. The total lack of I4790M-mediated resistance to CLR, and minimal resistance to FLB, came as a surprise. Of further concern was the high dosage required to kill even the WT PxRyR-expressing fly line. A CLR concentration of 29mg/L, the LD50 value for the WT line in this study, is >100-fold higher than the CLR concentration required to kill populations of moths extracted from the field. A further drawback of the adult bioassays was the failure to generate lines carrying the G4946E mutation. Under the conditions of rearing employed in this methodology, the RyR16/RyR-Gal4; GE-PxRyR/+ represented just 0.1% of emerging flies (compared to an expected 33%). By comparison, WT and I4790M flies emerged at a proportion of 24% and 29% respectively. The indication is that the G4946E substitution causes some impact on survivability during development.

Following further crossing experiments, stable lines (Fig 5.6aai) became available, opening up the possibility of larval bioassays, which had previously been shown to be more applicable and more sensitive in terms of quantifying diamide efficacy (Douris 2017). Almost all bioassays against moths in the literature are performed on L3 larvae, the same stage chosen here in the 'pestified' *Drosophila*. Diamide usage in the field is designed to target moth larvae through coating of leaves with the insecticide, leading to ingestion of the compound during feeding. By comparison, the previously attempted adult bioassays relied primarily on contact and uptake through the integument.

In larval bioassays, the WT and I4790M lines displayed a large discrepancy in mortality when challenged with either FLB or CLR. Concentration-response calculations (Fig 5.8) indicate a concentration lethal to 50% of the WT population ($LD50^{WT}$) at $0.047\mu\text{g/L}$ ($0.0176\text{-}0.115$) CLR. By comparison, CLR $LD50^{IM}$ is $9.3\mu\text{g/L}$ ($3.5\text{-}24$), equivalent to a resistance ratio (RR) of 198-fold for CLR. WT larvae respond

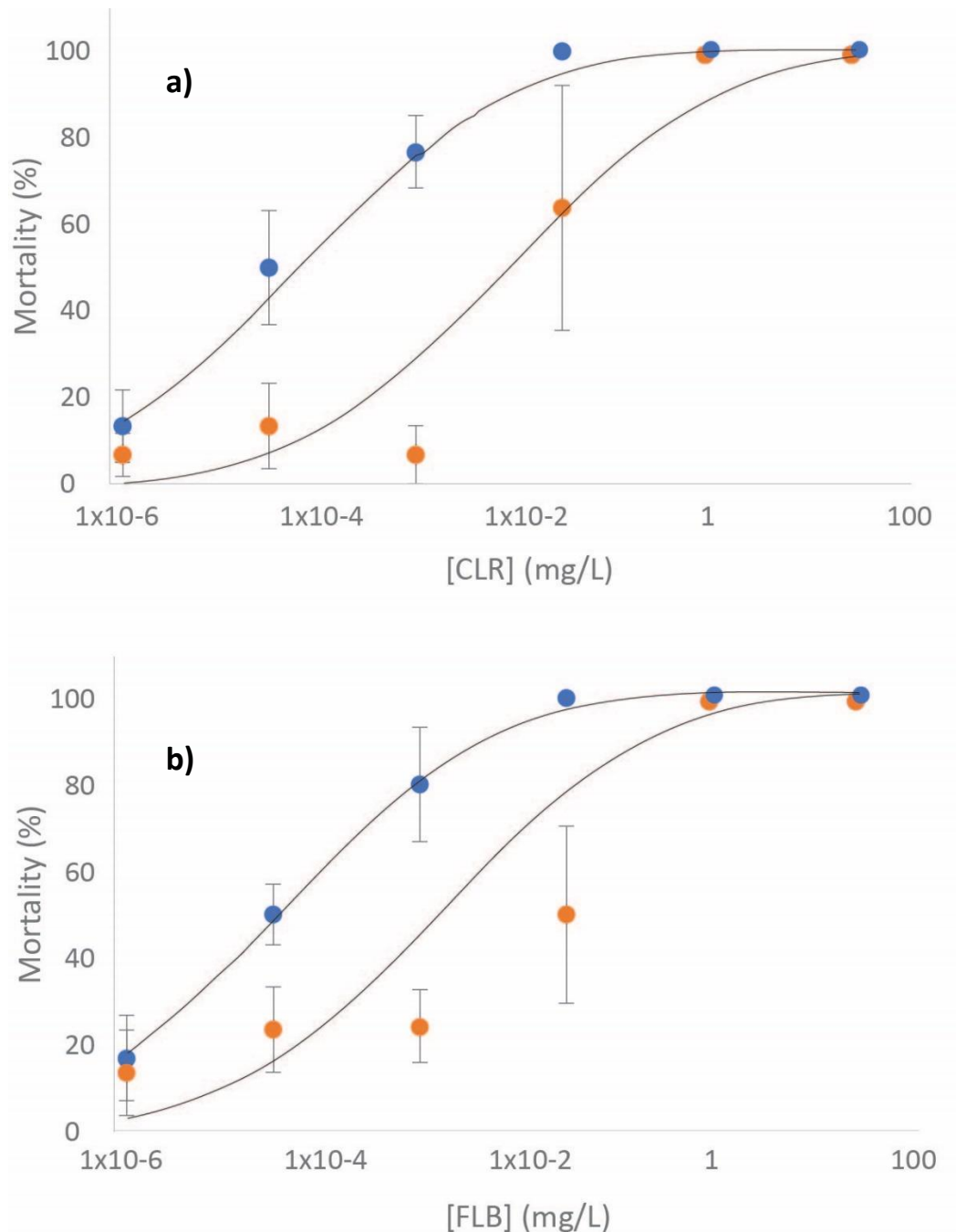


Figure 5.8 Larvae of the drosophila lines WT-PxRyR (blue) and I4790M-PxRyR (orange), exposed to dietary diamide, and assessed for larval mortality, where mortality is taken as failure to enter the pupation phase. Larval mortality increases in a concentration-responsive manner when exposed to (a) CLR and (b) FLB. Error bars indicate standard deviation of mortality averaged over three repetitions.

similarly to FLB as to CLR, with LD50^{WT} at 0.037µg/L (0.013-0.091) FLB. Whilst LD50^{IM} is 3.6 (1.2-11) µg/L, equivalent to a RR of 97-fold for FLB.

These results are notable for a number of reasons:

First, that they differ substantially from bioassays conducted on adults, with lethal dosage reduced by up to five orders of magnitude. An LD50^{WT} of 0.037µg/L FLB for *Drosophila* larvae expressing WT-PxRyR is >100-fold lower than that recorded for 3rd instar *P. xylostella* larvae against this compound (4 µg/L (Hirooka et al. 2007)).

Secondly, variation in response is large, especially in the I4790M line, where the number of dead larvae in a vial varies at a given insecticide concentration by up to 50% of the maximum. And this variation exists even at the lowest concentrations of insecticide applied.

Third, and as a result of the previous point, the response curve is poorly resolved. An ideal curve will see approximately zero larval mortality at low insecticide concentrations, followed by a rapid increase in concentration-related mortality. The poor resolution of the curve suggests a heterogeneity in the response of larvae within each assay vial. Such heterogeneity can be mitigated by a larger *n* (more larvae per tube).

Survival of control (no insecticide) larvae was 65-72% (no significant difference between lines), compared to >90% survival for undisturbed larvae raised from eggs under the same conditions. This suggests the method of transferring larvae to the vial by brush should be substituted for a less invasive method, in future. Stochastic pre-adult mortality is very likely to have contributed to the variation observed in this bioassay (Fig 5.8).

The results of the larval bioassay on G4946E-PxRyR larvae are displayed in Fig 5.9. This line has displayed a particularly strange phenotype, in which average mortality was very high, even at low insecticide concentrations which are non-lethal to the WT, but mortality did not increase in a concentration-responsive manner. Given the inability to plot a concentration-response curve on this graph, calculation of LD50 for this strain is not meaningful (indeed, there is no recorded insecticide concentration at which fewer than 50% of insects die). The rest of this section will instead discuss why no concentration-response relationship is seen here, and how to remedy it in future work.

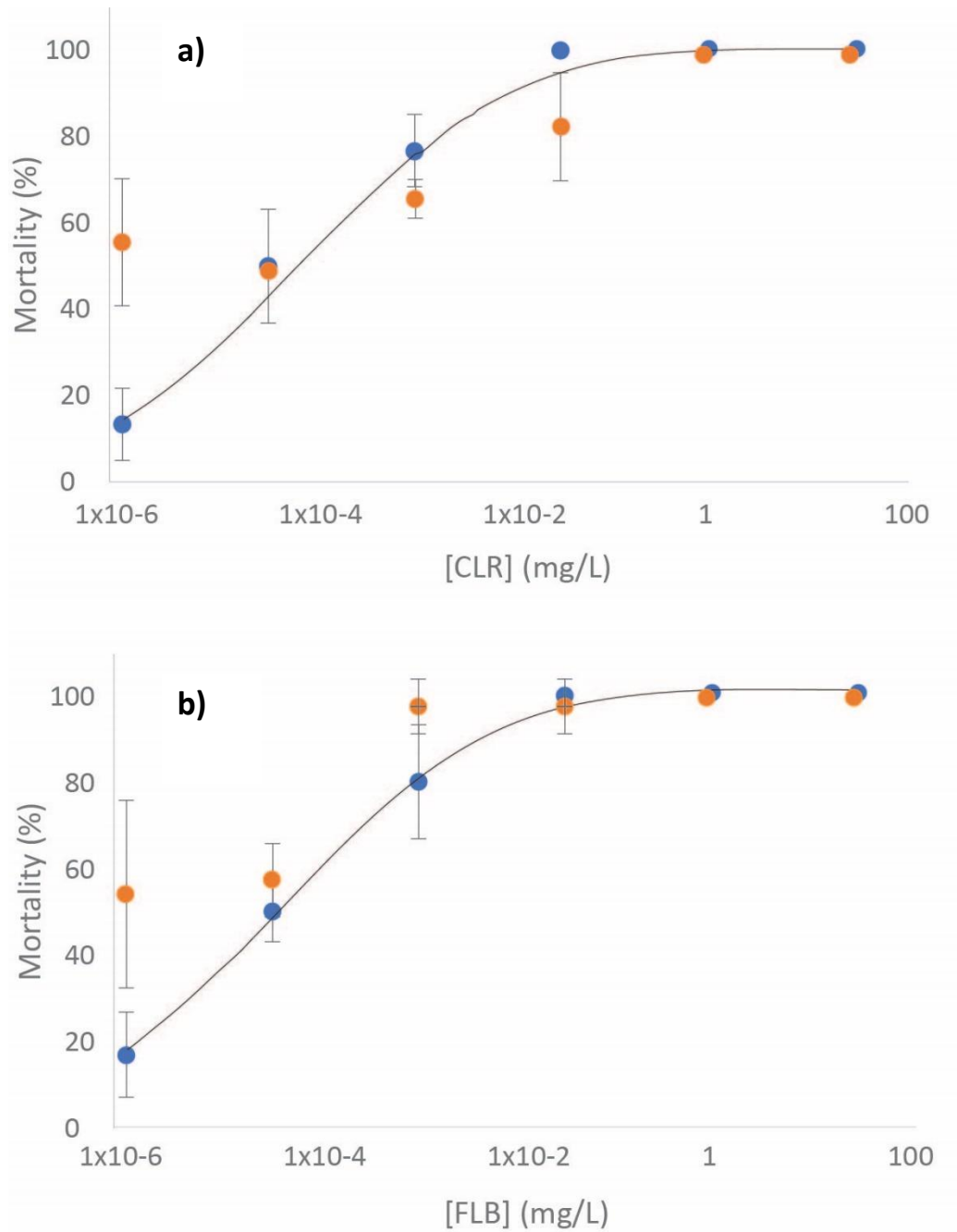


Figure 5.9 Larvae of the drosophila lines WT-PxRyR (blue) and GE-PxRyR (orange), exposed to dietary diamide, and assessed for larval mortality, where mortality is taken as failure to enter the pupation phase. G4946E-PxRyR larval mortality does not increase in a concentration-responsive manner when exposed to either (a) CLR and (b) FLB. The plotted line is fitted to the WT-PxRyR data. Error bars indicate standard deviation of mortality averaged over three dosage repetitions.

The G4946E RyR alteration has been shown previously to be lethal when applied to the *Drosophila* endogenous RyR (Douris et al 2017). This study employs the *P. xylostella* RyR protein in an attempt to sidestep that lethality. Indeed, G4946E PxRyR larvae in untreated vials do not experience higher mortality than those of

I4790M or WT larvae. However, the G4946E alteration does affect fly physiology. As discussed above, pre-adult mortality in the G4946E RyR¹⁶ line was so high as to prevent adult bioassays on G4946E PxRyR flies entirely.

5.4.2 Fitness costs of PxRyR alteration

Having determined the impact of the I4790M and G4946E mutations on diamide efficacy in drosophila larvae and adults, an unanswered question was to understand whether the altered response to diamide was coupled to any other physiological alterations. In the context of field control, decreased mortality during insecticide exposure, as conferred by the I4790M or G4946E mutations, converts into a selective advantage for the individual, compared to WT individuals. However, as discussed in Section 5.2, fitness benefits in the presence of insecticide treatment are expected to be balanced against fitness costs in a null-insecticide environment.

To investigate the possibility of fitness costs resulting from the PxRyR alterations generated here, we studied two aspects of fitness:

1. Reproductive success, measured by adult fecundity and fertility and larval developmental success
2. Vigour, measured by adult climbing speed and larval crawling speed

Fecundity and fertility and developmental success are key components of lifetime reproductive success. These two parameters were studied for each genotype under non-competitive conditions (i.e. genotype alone in cage). However, because the fecundity/fertility was a non-competitive assay, it doesn't consider the potential impact of the mutation upon competition for limited resources including a) adult nutrition b) competitive mating success c) competitive laying d) larval nutrition. In order to attempt to account for the impact of the mutations upon competition, we chose two indicators of vigour: larval movement speed and adult climbing ability. The hypothesis is that success (in most aspects of competition, listed above) is mediated by the ability to move, be that moving toward a food source, toward a potential mate, or toward an optimal laying location.

5.4.2.1 Indicators of reproductive success: Fecundity and Fertility

No differences were found in indicators of reproductive success between the fly lines (Fig 5.10). WT flies lay a median 60(±10) eggs per hour, compared to I4790M (59±3 eggs/h) and G4946E (69±2 eggs/h) (ANOVA, F-crit=9.1, F=0.51). Fertility varied between 75%-85% successfully hatching eggs across all three lines. Hatched

eggs were followed through development, reared under conditions identical to those of the larval bioassay (Section 5.3.1). There was no significant difference in the proportion of larvae successfully pupating (WT, 72±13%; I4790M, 65±14%; G4946E, 65±14%) (ANOVA, F-crit=5.4, F=2.6) nor in the proportion of pupae successfully eclosing (WT, 69±19%; I4790M, 77±11%; G4946E, 72±14%) (ANOVA, F-crit=5.4, F=1.9). All parameters were studied at 25°C, following the methodologies listed in this Chapter.

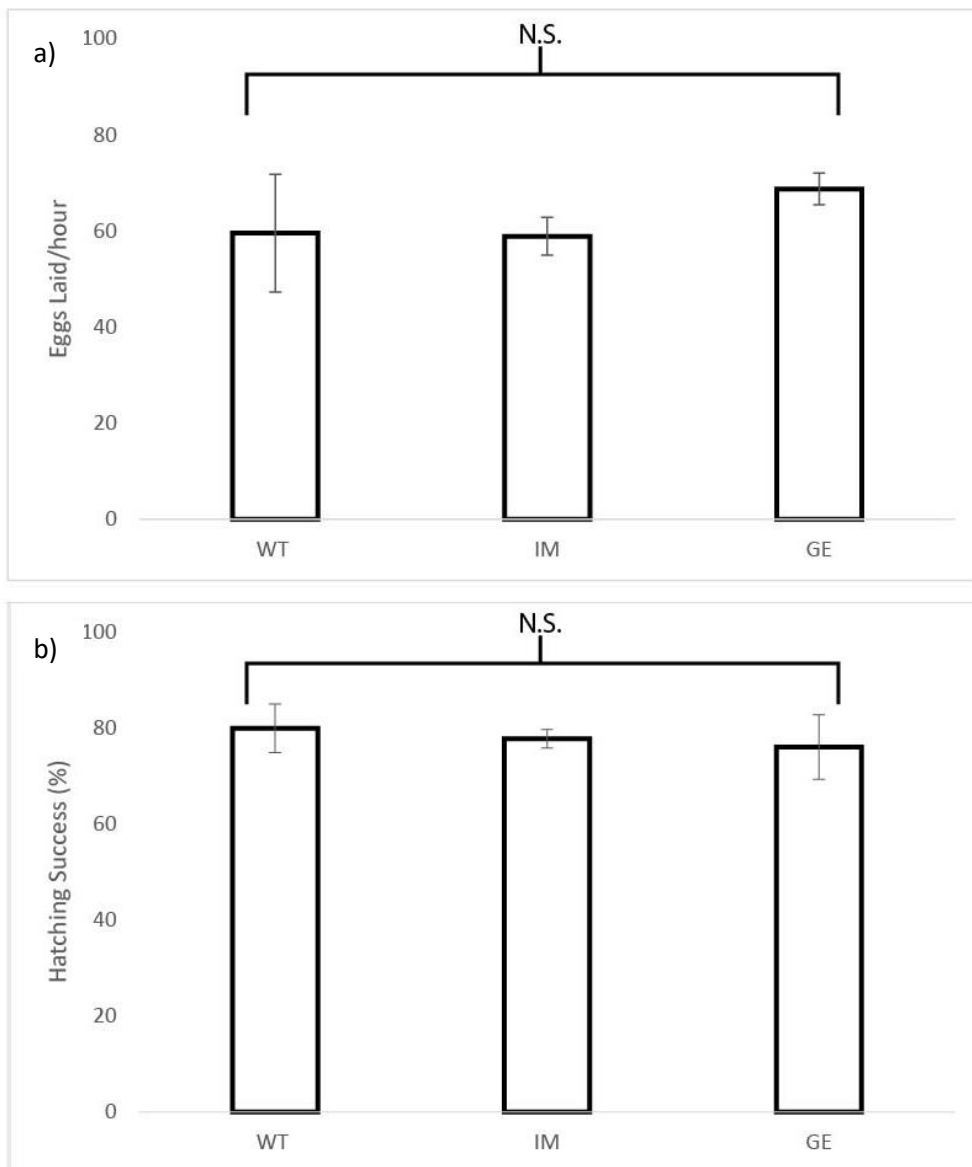


Figure 5.10 Diamide resistant drosophila lines do not differ in fecundity or fertility compared to their WT counterpart. Bar graphs of a) total fecundity and b) proportion of eggs hatching within 24h. n=3 plates, from cages of 175 flies. Error bars indicate standard deviation, or the range within which 95% of samples taken of the population at random are expected to sit

5.4.2.2 Indicators of vigour: Crawling speed and Climbing ability

Indicators of vigour were found to differ very significantly between the fly lines, with the G4946E and I4790M lines showing signs of reduced movement relative to the WT flies.

L3 larvae have well developed crawling musculature and naturally exhibit migratory behaviour as they search for a suitable location for pupation. Accordingly, larvae were placed in an environment of high light intensity, no food availability, and no shelter, encouraging migratory behaviour, which was measured for three minutes. The maximum speed achieved by each larvae during the time window (averaged over a 15-second period) is plotted (Fig 5.11a). WT larvae crawl at a velocity of 0.21 ± 0.05 mm/s, more than double the maximum velocity of I4790M (0.10 ± 0.06) or G4946E (0.09 ± 0.06) larvae. The average speed is the total distance travelled during the 3 minute period (Fig 5.11b). In this measure, too, the difference between lines is marked, with WT larvae averaging 0.14 ± 0.06 mm/s, more than double the distance of I4790M (0.06 ± 0.05) or G4946E (0.06 ± 0.03) larvae.

Adult cohorts from each genotype were raised in identical conditions (the same conditions used for the fertility/fecundity assays, Section 5.3). Adults were tapped into vials, shaken and knocked to the base of the vial, using the Hillary climber apparatus, before being allowed to climb the vial walls. The proportion successfully climbing above a 6cm threshold after 8s was recorded (Fig 5.12). WT adults successfully climbed above the threshold 40-70% of the time (Median 53%). Whilst I4790M and G4946E adults managed the same feat less than half as frequently (median 12% and 21%, respectively).

In summary, the results indicate that whilst the PxRyR alterations appear to bear no fitness costs in terms of reproductive capacity in a non-competitive environment, they bear potentially major impacts on the individuals ability to move. The indication is that, if placed into a competitive ecosystem, diamide resistant individuals are likely to suffer a considerable fitness cost.

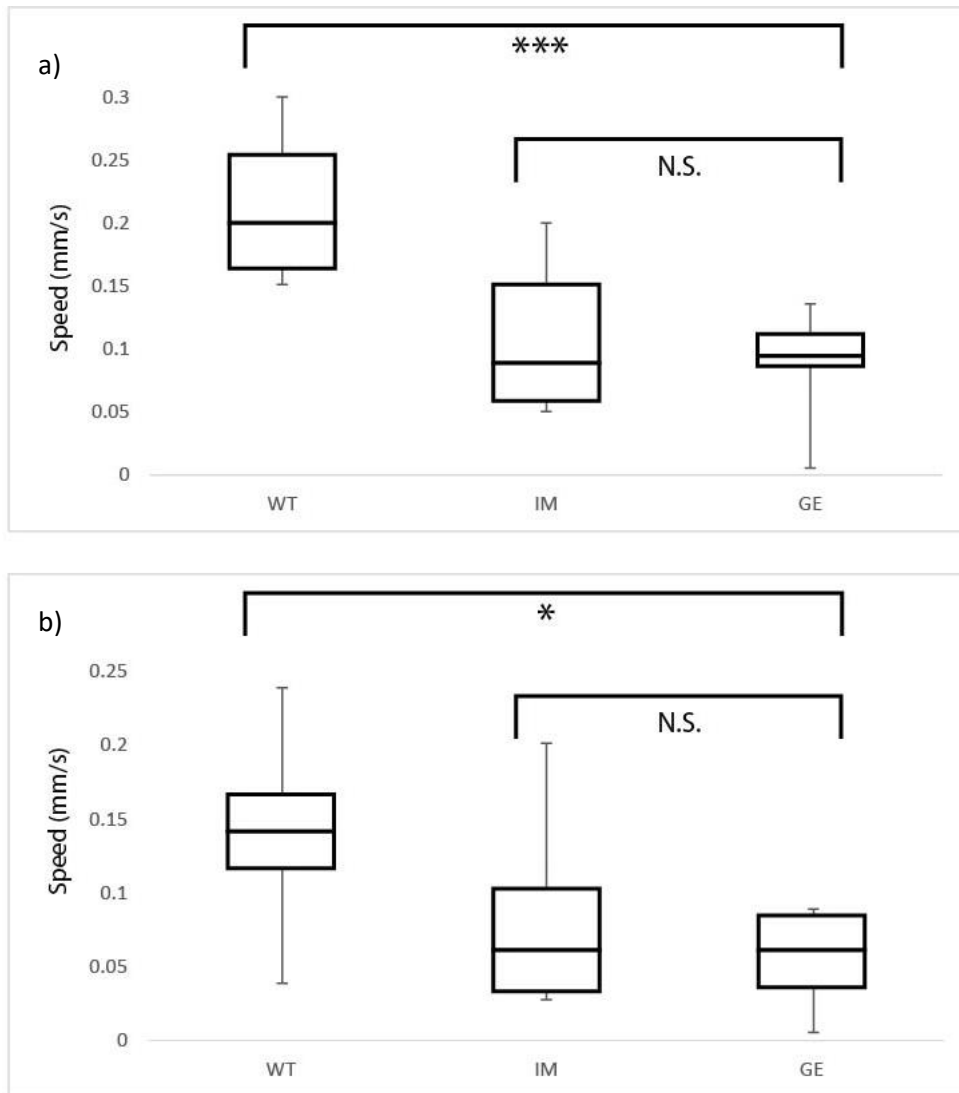


Figure 5.11 Diamide resistant *Drosophila* larvae crawl significantly more slowly than their WT counterpart. Boxplots indicating a) maximum and b) average crawling speed. *** indicates a statistically significant difference ($P < 0.001$); * indicates difference ($P < 0.05$); N.S. indicates a non-significant difference as determined by ANOVA and LSD. $n = 20$ larvae per genotype; the experiment was replicated, and similar results were obtained. Within a box plot, the error bars indicate the minimum and maximum values in the dataset, whilst the three lines of the box itself indicate the lower, median and upper quartiles of the data.

5.5 Discussion

5.5.1 What is the value of 'pestified' *drosophila*

At the start of this PhD, diamide resistance associated RyR target-site mutations were yet to be isolated and characterised *in-vivo*. To do so was an important goal, in order to confirm the participation of these amino acid alterations (on the RyR) in conferring the diamide resistance phenotype. Since the inauguration of this project,

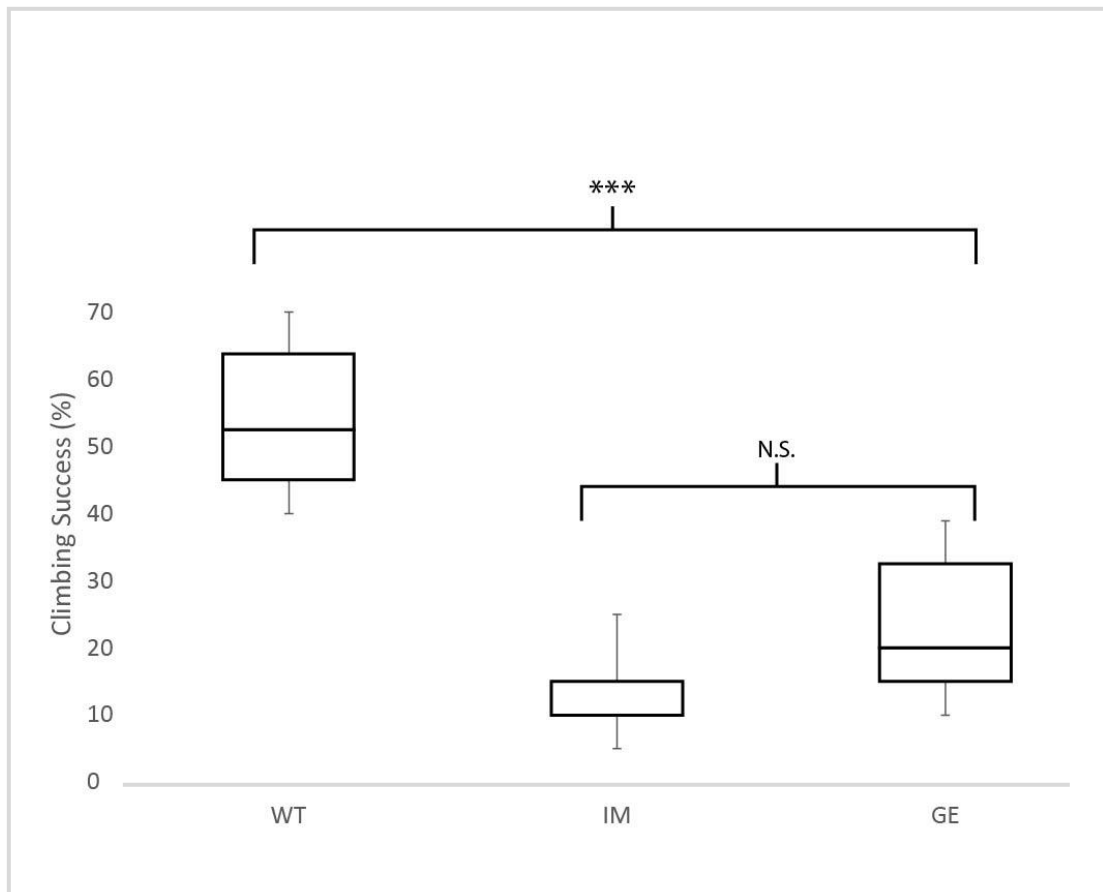


Figure 5.12 Boxplot of climbing success between three PxRyR-expressing *Drosophila* lines. Diamide resistant *Drosophila* genotypes climb significantly more slowly than their WT counterpart. *** indicates a statistically significant difference ($P < 0.001$) as determined by ANOVA and LSD; N.S. indicates a non-significant difference. $n = 40$ flies per genotype; the experiment was replicated and similar results were obtained.

other authors have succeeded in demonstrating resistance phenotypes conferred by these alterations *in-vivo*. Notably, Douris et al, using reverse genetic studies in *Drosophila*, substituted the naturally occurring methionine at position 4790 of the drosophila RyR with isoleucine (M4790I), which conferred a 7.5-fold increase in CLR efficacy and a 15-fold increase in FLB efficacy (Douris et al. 2017). Other studies have focussed on altering the pest of interest directly. A recent backcrossing experiment in *S. exigua* found that introgression of the I4790M mutation caused approximately a 20-fold resistance to both CLR and FLB (Zuo and al. 2019). A CRISPR/Cas9 study in beet armyworm, inserting the G4946E mutation into an otherwise susceptible genetic background, created an armyworm strain that exhibits a potent resistance of 223-fold to CLR (Zuo et al. 2017).

Here, a novel approach has been taken, in which the entire lepidopteran coding sequence, of resistant and non-resistant isoforms from *P. xylostella*, is inserted into

Drosophila. This is the first report of an entire RyR sequence being cloned and inserted into a different species. *Drosophila* and *Plutella* have a coding nucleotide sequence identity of 71% and have been on separate evolutionary paths for >250 millions years (Grimaldi and Engel 2005). The ‘pestified’ fly lines created here corroborate the impact of the I4790M mutation upon diamide efficacy. Notably, however, resistance ratios reported for I4790M in this study are generally much higher than those reported in past studies.

5.5.2 Are these lines good models of fitness costs associated with TSR?

Uniquely, the fly lines generated here were also used to investigate the fitness costs associated with the RyR mutations, and in doing so, revealed a tantalising picture that deserves further investigation. The RyR is an essential protein responsible for converting nervous stimulation into muscular contraction. Changes to the protein were found to significantly hinder larval crawling ability, and significantly slow adult climbing speed. However, it should be noted that these effects are recorded in a *Drosophila* model expressing the *Plutella* RyR – it is not clear whether *P. xylostella* expressing the G4946E alteration will also suffer from reduced movement ability. Future work could potentially involve assessing the fitness of genome-edited *P. xylostella* strains that had their RyR modified (e.g. [Zuo et al](#)) in order to quantify the effects of this mutation on the fitness of the moth.

It would also be interesting to compare the phenotype of the fly lines generated here against those generated by *Douris et al*. It seems feasible that the lines generated here will exhibit a diamide-phenotype more similar to lepidoptera, and thus is more ‘realistic’, due to possession of the lepidopteran RyR. The effects of individual mutations on diamide interaction obviously depend heavily on the actual structure of the RyR and the way that structural folding is changed by the sequence alteration. However, it is also possible that these lines are made less ‘realistic’ due to the complexity of the alteration - primarily, the requirement of driving the expression with RyR-Gal4 introduces an unknown. RyR-Gal4 is activated by the endogenous RyR transcription machinery in this case, so the inserted PxRyR should be expressed in an identical pattern and magnitude to the endogenous DmRyR. However, Gal4 is likely not 100% efficient as a driver, resulting in probable reduction in RyR expression in the altered fly line relative to unaltered flies. It is also suspected to alter the expression of off-target sequences in the fly genome (Liu

2008). Future work should quantify RyR expression in altered vs unaltered flies in order to rule out this possibility.

5.5.3 A future model of resistance spread?

No study has yet succeeded in modelling the ability of diamide resistant genotypes to spread through a population. However, as discussed herein, all necessary pre-conditions to such modelling have been met, with individual estimates of resistance cost, benefit and heritability having already been determined. One recent study in diamide resistant *Tuta* studies *heritability* in the context of insecticidal exposure *cost* and *benefit* to show that the 'Effective Dominance' of the diamide resistance phenotype increases with decreasing insecticidal concentration (Silva and al: 2018). Such findings show empirically the importance of maintaining spray concentrations at recommended levels, but the findings also indicate the benefit that could be derived from a future empirically supported modelling effort. Such a study might involve two laboratory populations, each initially composed of 50% wildtype and 50% TSR individuals, with one population receiving periodic diamide dosage. Frequent genotyping would allow detailed understanding of the *cost* and *benefit* of TSR over many generations, which would then inform a population genetic model of resistance dynamics which could be applied to potentially predict resistance spread in the field.

5.5.4 A Limitations and future work required

A further step in this study would be to employ qPCR to quantify expression of the introduced genes across the three *Drosophila* lines created here. This would allow the author to be sure that differences in phenotype are not attributable to variations in channel expression between these lines. As it stands, the author has made attempts to ensure equality of channel expression by utilising a near-identical genetic background between the lines (Fig 5.3 and 5.4). However, genetic drift within laboratory populations may cause even identical lines to diverge over time in terms of channel expression, hence the requirement for a qPCR expression test.

5.5 Conclusion

Integration of a 24,982kb sequence into *Drosophila* is not elementary. Expressing the gene is harder still, given its essential role in development and normal bodily function. Survival and reproduction of transformed flies is surprising, in this case. Whilst recent reverse genetic *in-vivo* transgenic studies of other authors have

provided insight into the impact of RyR mutations on diamide resistance *in-vivo*, this study corroborates previous findings and is the first that studies in detail the impact of those mutations on aspects of the individual's fitness.

Chapter 6: Chimeric investigations into the diamide binding site on the lepidopteran RyR

6.1 Chapter Summary

Identification of the diamide binding site is a crucial step, both toward generation of novel diamide chemistries (where the shape of the binding pocket informs which chemical leads should be developed) and toward monitoring and tracking of diamide resistance (where the impact of novel arising substitutions on diamide control can be predicted). However, a lack of published insect RyR C-terminal structure greatly hinders identification of the binding site. In such circumstances, phenotypic studies of genetic mutants are the principal mechanism by which the binding site can be identified.

Previous studies have demonstrated that a portion of the RyR close to the TM1 region mediates loss of diamide interaction (discussed further below). At the same time, naturally occurring RyR C-terminal substitutions have been shown to cause potent reductions in diamide interaction (see Ch4). This present Chapter first summarises all available knowledge on binding of diamides to RyR, in order to identify a 'diamide-resistance region'. A series of residues worthy of further investigation are subsequently identified (based on amino acid alignments between resistant and susceptible species, and amino acid chemistry), whose alteration may help to pinpoint a diamide binding site upon the RyR. Editing of five amino acid positions to match those found in the skeletal RyR1 of humans (hRyR1) results in a human-Plutella chimeric construct, which forms the basis of novel investigations into the diamide binding site.

6.2 Introduction

6.2.1 Diamides are highly selective against mammalian RyR

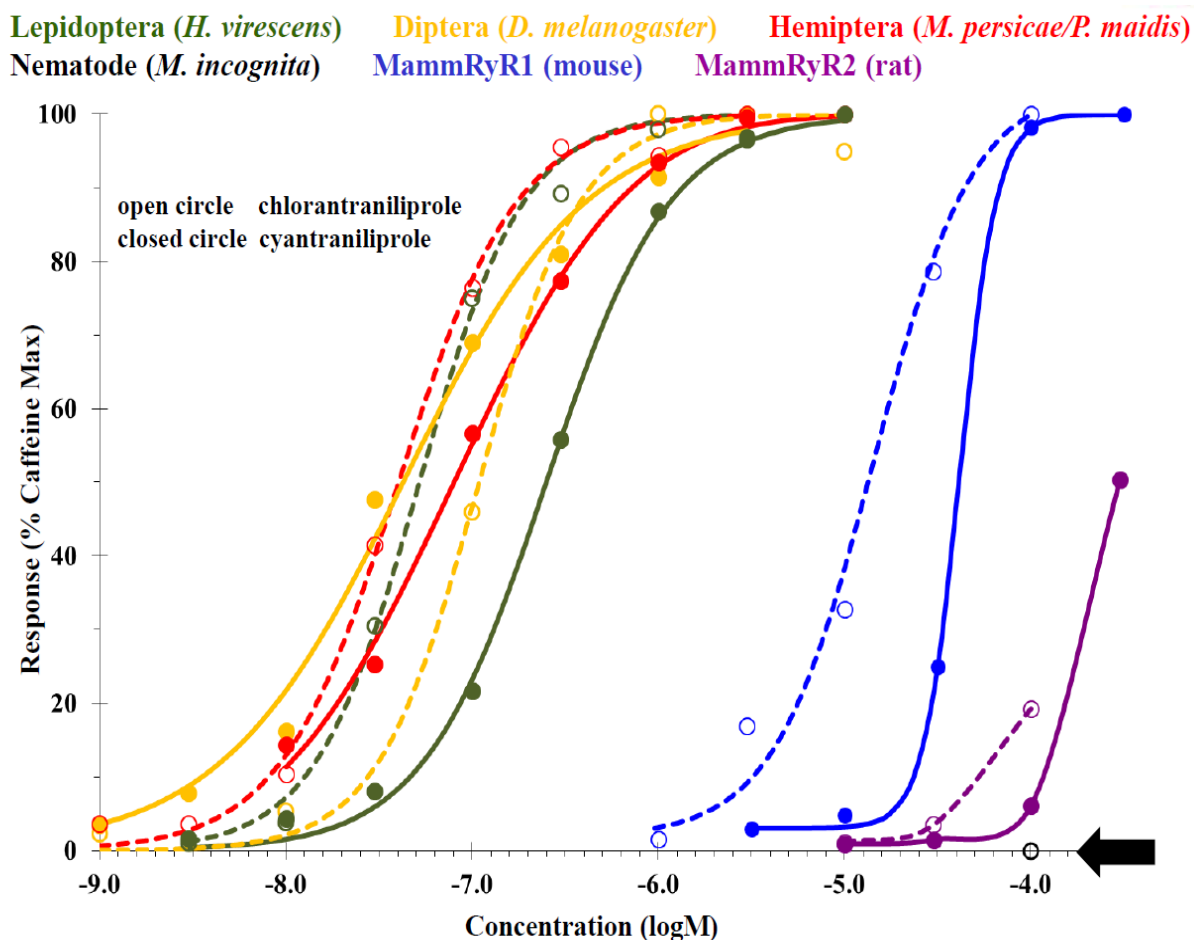


Figure 6.1 Summary of data obtained by various authors showing a lack of CLR (diamide) efficacy on non-lepidopteran RyR channels. Kindly provided by Daniel Cordova.

During their development, diamide insecticides were shown to activate lepidopteran RyR channels at very low concentrations, as well as *Drosophila* RyR channels expressed in CHO cells (Ebbinghaus-Kintscher et al. 2006). However, rabbit RyR (rRyR3), when expressed in the same system, was found to be refractory to FLB activation, even beyond the theoretical limit of solubility of the compound (30 μ M). Indeed, FLB was tested upon various mammalian primary cell cultures, including rat ganglia, skeletal muscle, heart muscle and neuron-like cells, registering a negligible response in all cases (al 2006; Ebbinghaus-Kintscher et al. 2006). Similarly, characterisation of the concentration-response relationship on various mammalian cell lines expressing RyRs and recombinant cells expressing insect RyRs (Fig. 6.1) indicated CLR to be some 300-fold less potent against mouse skeletal muscle RyR (RyR1) and >1000-fold less potent in rat heart cells (RyR2) compared to lepidopteran and dipteran RyR-expressing cells (Lahm et al. 2007).

Meanwhile, tests in an ecological context indicated that FLB is effectively non-toxic in terms of its potential passage through the food-web. With FLB residue on insects peaking at 5.59mg/kg, a large (200g) adult rat would be required to eat >70kg of maximally dosed insects within a 14-day period in order to reach their acute EC50. Similar quantities of diamide residue were stipulated for the various bird and fish species tested (Hall 2007). Metabolic studies in rats indicated that CLR breakdown occurs primarily by a multi-step oxidation of the methyl groups, followed by glucuronidation (WHO 2007). After ingestion, 24-36% of the compound is taken up from the rat gut into the bloodstream, with the rest being excreted directly. After 48-144h, 90% of the absorbed diamide was found to have been excreted.

A recent set of publications have reported single-channel studies investigating the binding dynamics of CLR on mammalian (rabbit) RyR1, following the claim that there existed “severe concerns about the safety of this chemical” (Magyar et al. 2019). Whilst such a claim is entirely unsupported by the evidence published within these studies, the findings are nonetheless enlightening in the investigation of RyR-diamide interaction. Chen et al report that, in rabbit RyR1-expressing sarcoplasmic reticulum (SR) vesicles, concentrations of 30-150 μ M CLR resulted in a small transient Ca²⁺ release response similar in amplitude to the CICR response elicited by Ca²⁺, and the amplitude increases slightly in a concentration-dependent manner (Chen et al 2018). Similarly, Truong et al studied 5-minute single channel recordings to show that P_o increases in the presence of 10 μ M CLR, resulting in a brief 65-fold increase in Ca²⁺ conductance compared to the baseline ‘closed’ state (Truong and Pessah 2019). The reported 65-fold increase almost exactly reiterates a previous finding by Cordova, who employed CYA instead of CLR (conf. proceedings). To summarize, these results indicate that CLR is capable of eliciting a small transient (i.e. non-disabling) response when applied at a very high concentration of 150 μ M, which is >1000-fold higher than the EC50 for lepidopteran RyR channels measured in cell lines, as reported here and elsewhere. In order to confirm that this reduction in CLR-activation is due to a reduction in binding, measurements of K_d were undertaken. A minimum CLR K_d of ~1.51 μ M (rising to 4.67 μ M in the closed state) was recorded on the rabbit RyR channel (Chen 2018), approximately 50 to 150 -fold higher than that previously recorded in cockroach, *Periplaneta americana*, leg muscles (Cordova et al. 2006). Such differences in K_d indicate that binding is a major

factor in determining diamide non-efficacy against mammalian RyR. The rest of this Chapter will discuss the causes of that discrepancy in diamide binding.

6.2.2 What is the cause of the discrepancy in binding and activation

Differences in diamide efficacy between mammals and insects are suspected to be attributable to differences in the structure of the diamide binding site on the RyR. Over the past decade, binding site studies on the RyR have taken one of two approaches: either a comparison of the relationship between ryanodine (Ry), phthalic diamide and anthranilic diamide binding, or attempts to directly pinpoint the approximate location of the binding region.

Isaacs (Isaacs et al. 2012) synthesized tritiated (radioactive) [³H]CLR, enabling the quantification of bound CLR to the house-fly (*Musca domestica*) RyR under various conditions, to determine its relationship to Ry and FLB binding. Ca²⁺ (which promotes the open-state of the channel (Mugherjee et al 2012)) was found to increase [³H]CLR binding, as is expected if CLR preferentially binds to the open channel. Other anthranilimides, such as CYA or CLR itself, inhibited [³H]CLR binding by competing for the same site. By contrast, FLB did not inhibit [³H]CLR binding, leading to a hypothesis that no competition exists between FLB and CLR due to there being two distinct, but allosterically coupled, binding sites for the two classes of diamides. The same result was reported by (Qi and Casida 2013), employing very similar methodology. However, it was also shown that FLB (applied at <1fmol [³H]FLB/mg protein) does not bind to the *Apis Mellifera* and *M. domestica* channels investigated, suggesting that an FLB binding site is not present, hence providing a more parsimonious explanation for the lack of competition. In contrast, CLR and FLB were found to compete, and in a concentration-dependent manner, in the lepidopteran species (*Agrotis ipsilon* and *Heliiothis virescens*) studied, suggesting that the binding sites of the two diamides are likely not distinct in moth species. The study also uncovered major differences between lepidopteran and non-lepidopteran channels. Whilst in the Hymenoptera and Diptera (*A. mellifera* and *M. domestica*) CLR is shown to bind preferentially to the open-state channel, the opposite may be true for lepidopteran species, since FLB binding was found to be unstimulated, or reduced, by Ca²⁺/ATP, and majorly reduced by Ry, strongly suggesting preferential binding to the closed channel state. Similar results, but to a lesser degree, were also reported for CLR. Thus, the FLB and CLR sites are thought to be closely coupled, but not identical. However, attempts to distinguish FLB and

CLR binding effects are confounded by the distinct differences between lepidopteran and non-lepidopteran RyR channels, as the non-lepidopteran channels studied to date are not a viable system for FLB experimentation. Such differences may partially be attributable to segregation at amino acid residue 4790 (Isoleucine (I) in Lepidoptera, methionine (M) in all other insects) as studied in Chpt 4. However, the contrast between the channels in the Casida studies suggest major structural differences at the protein level which would be unlikely to be caused by a single residue change.

6.2.3 The diamide interaction site

The actual position of the binding region (as opposed to the exact binding site(s)) was elucidated progressively following on from the above studies, primarily as a byproduct of investigations into incidences of field-resistance to diamides uncovering a selection of closely located, causatively linked, point-mutations on the RyR. Most of these investigations were reviewed in detail in a previous Chapter (Ch4) and discussions on this are not recapitulated here. However, one study in particular (Tao et al. 2013) bears further detailed discussion, as it has been instrumental in pinpointing the diamide binding region. By creating a chimeric RyR channel, composed of *D. melanogaster* and root knot nematode (*Meloidogyne incognita*) RyR sequence, a region within the C-terminus was found to be critically involved in formation of the diamide binding, in line with the findings of a previous study (Kato et al. 2009). A defining shorter chimeric segment within this C-terminal region, consisting of a 45aa region of the nematode sequence, located just prior to the start of TM1 (*P. xylostella* aa 4659 – 4703), produced a channel that was entirely refractive to CLR (up to 30 μ M). Of the 45 amino acids replaced, most are unlikely candidates to be involved in diamide interaction. The first 30 aa lie in a zone of high divergence, even within insects, hence conservation of a diamide binding site here would seem improbable given the variation. The last 10 amino acids, by contrast, are highly conserved, likely due to being at the start of the TM1 membrane spanning domain. Six of these amino acids are identical between humans and insects, leaving just K4695N, K4700R, Y4701F and V4702L (*P. xylostella* numbering) as possible loci of this major difference in diamide binding efficacy. Intriguingly, the latest episodes of resistance in *C. suppressalis* add further support to the Tao et al study. Unpublished reports from 2013 suggested a host of mutations associated with diamide resistance in this pest in China (Cordova pers. comm.). These included

G4946E, as well as a novel find, Y4701D (PxRyR numbering). A recent publication confirms this as a resistance locus, with alleles 4701C and 4701D found (alone) in a resistant population of *C. suppressalis* in Jiangxi, China (Sun et al. 2018).

For the purposes of the current study, probable diamide interacting residues identified in previous studies were cross-compared in an alignment of 44 arthropod, nematode and vertebrate RyR amino acid sequences. Highly conserved residues, whose alteration correlates with diamide resistance, were considered candidates for further study (Fig. 6.2). Almost all the resistance-associated mutations discovered to date are concentrated within a 250aa region close to the C-terminus of the protein (Fig. 6.2c), which in the 3D structure is located within the TM domain, peripheral to the channel pore (Fig. 6.2a,b). This 250aa region, which is similar in structure to the voltage sensor domain of voltage-gated channels such as the bacterial *KcsA* potassium channel, is referred to here as the 'diamide resistance region'. Candidate amino acid substitutions for binding site studies, when plotted onto the 3D structure, can be seen to form a ring-like pattern across the crown of the pVSD (Fig. 6.2d). Although it is tempting to pinpoint the diamide binding site to the 'diamide resistance region' identified here, such conclusions may not be entirely valid. 3D RyR models in insects are currently based on homology models of the lepidopteran RyR generated by overlaying its sequence onto the published mammalian RyR1 (closed-state) structure. Whilst recent imaging of the PxRyR N-terminus (Lin et al. 2018) and SPRY domain (Xu and Yuchi 2019) represents an enormous leap forward, sequence dissimilarities at the C-terminus still prevent confident predictions. Shortly prior to completing the investigations described in this Chapter, Lin et al published a controversial attempt to computationally predict FLB docking upon the RyR homology model (Lin et al. 2019). It is widely acknowledged that the predictive power of a docking study is highly dependent upon the resolution of the available protein model, in this case the study was conducted in the absence of any such high-resolution model. Hence, the investigations reported in this Chapter may be an important experimental validation of predictions made by Lin et al (discussed further in Ch7).

In summary, combining all the knowledge accumulated to date, some logical stipulations can be made regarding the nature and location of the phthalic/anthranilic diamide binding site(s). Firstly, that they are located somewhere within close proximity to the 'diamide resistance region' identified in

Fig. 6.2. Secondly, investigations on the G4946 residue indicate the binding sites are sufficiently close to each other that mutations at this position confer equal resistance to both CLR and FLB across a variety of tested pest species. Thirdly, that I4790 (investigated in Ch4) is located in close proximity to G4946 in the 3D structure and is most likely involved in diamide binding.

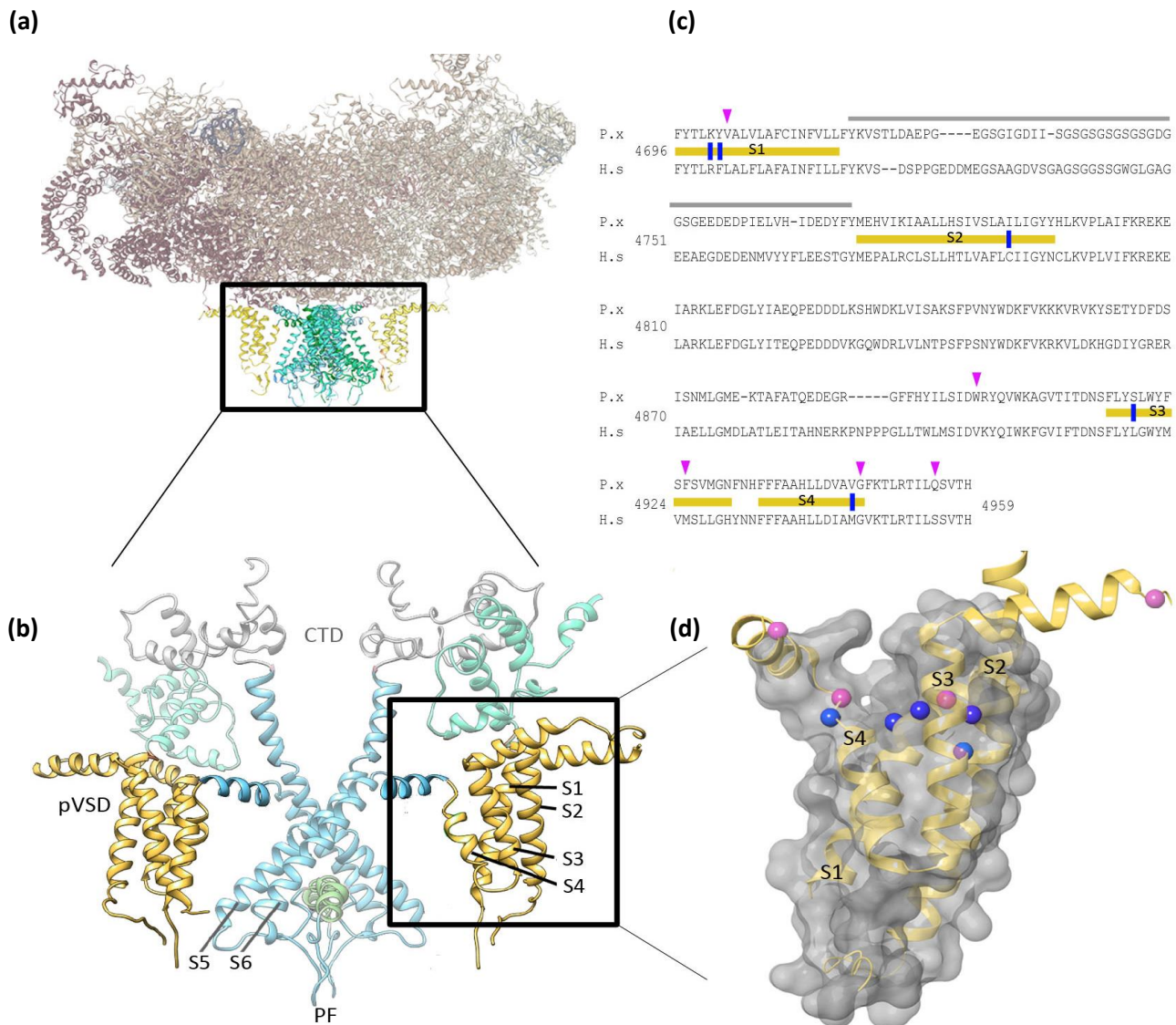


Figure 6.2 The ‘diamide resistance region’ in lepidopteran RyR.

(a) Crystal structure of rabbit rRyR1 in the closed state (Yan et al 2015, PDB 3J8H), with the transmembrane region boxed and highlighted (b) PxRyR-rRyR1 homology model* showing two isomers in dimeric formation, with the pore region shown in blue (PF, Pore Forming; CTD, C-terminal Domain; pVSD, Voltage Sensor Domain) and TM regions, S1-4 shown in yellow (boxed and highlighted) (c) Alignment of PxRyR (P.x) and human hRyR1 (H.s) amino acid sequences, (TM regions S1-4 (shown in yellow); divergent region (grey); aa residues investigated in this Chapter (blue); aa residues earmarked for future investigation (pink)) (d) PxRyR-rRyR1 homology model of the pVSD (labeled as in (c)), displaying a ring of amino acids implicated in diamide binding.

*All work is the author’s own. The PxRyR homology model was generated in collaboration with Oliver Gutbrod (Bayer CropScience), using Pymol and Schrodinger software.

6.3 Results

6.3.1 RFCLM: A chimeric RyR channel combining moth with mammal

The purpose of this Chapter (Ch6) is to further define the ‘diamide resistance region’, with the eventual aim being to define the diamide binding site. Since we are lacking a crystal structure of the PxRyR protein, this goal can only be achieved by a combination of homology modelling and reverse genetic experimentation to identify the amino acids critical for diamide interaction. The methodology for this Chapter closely follows that of Tao et al (cited and described above), in which Sf9 cells are transiently transfected with human/moth RyR chimeras in order to iteratively refine the residues and locus most responsible for diamide insensitivity in the mammalian channel. Following the protocol established in Ch3, and optimised further in Ch4, five PxRyR recombinant constructs were expressed in Sf9 cells and evaluated in terms of diamide effect relative to WT.

In the first instance, rapid mutagenesis (Agilent Lightning) and vector construction (Gibson) was used to create a chimeric construct composed of the WT-PxRyR with all five amino acid alterations, edited to match those residues present in human or rabbit (*Oryctolagus cuniculus*) RyR1. The chimeric construct is referred to as RFCLM-PxRyR, reflecting the five alterations: K4700R; Y4701F; I4790C; S4919L; V4945M (Fig. 6.3). Whilst the overall amino acid sequence identity between rabbit/human RyR1 and DBM RyR is just 42%, the changes implemented here lie within the ‘diamide resistance region’ (Fig 6.2). which has a much higher sequence identity of 73%, most likely due to the need to maintain the integrity of the RyR transmembrane domains and the channel pore. The amino acids chosen for

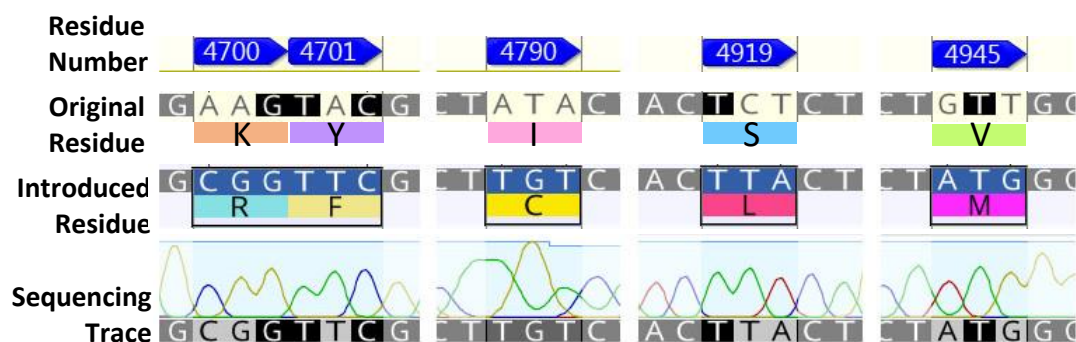


Figure 6.3 The five aa residue changes studied in this Chapter: K4700R; Y4701F; I4790C; S4919L; V4945M

modification all lie within conserved aa hotspots, according to an alignment of 43 RyR protein coding sequences. The exchanged residues, and the justification for their selection, are summarised in Table 6.1.

6.3.1.1 Brief characterisation of RFCLM caffeine-response

Following the protocols established in Ch3, the RFCLM-PxRyR construct was expressed in Sf9 cells and assessed in terms of its response to increasing dosage of caffeine. The response is found to increase with increasing caffeine concentration (Fig. 6.4). Comparison to the WT construct is important here, in light of the major difference in diamide-response recorded between the genotypes (Fig 6.5). Fig 6.4b indicates no substantial difference in signal amplitude between the two expressed constructs, in response to caffeine at any concentration. However, any firm conclusions are hindered by a substantial variation in response between cells. Furthermore, as explained in Ch3, sequential caffeine application on the same cell

Table 6.1 PxRyR amino acid positions altered to resemble rRyR1. Residue at each position noted for susceptible (insect, arthropod) and non-susceptible (vertebrate, nematode) species.

Position of modification*	Residue in susceptible species	Residue in resistant species	Additional justification for selection of residue
4945	Valine (V) in susceptible insects, arthropods;	Methionine (M) in vertebrates; Leucine (L) in nematodes;	Sequentially adjacent to G4946E (See Ch4)
4919	Serine (S) or Asparagine (N) in susceptible insects, arthropods;	Leucine (L) in vertebrates; Arginine (R) in nematodes;	
4790	Isoleucine (I) in susceptible insects, arthropods;	Leucine (L) in vertebrates; Cysteine (C) in nematodes;	Methionine (M) at this position shown to confer diamide resistance (See Ch4)
4701	Tyrosine (Y) in susceptible insects, arthropods;	Phenylalanine (F) or Methionine (M) in vertebrates; Lysine (K) in nematodes;	Terminal residue of the Tao chimera (Tao et al 2013)
4700	Lysine (K) in susceptible insects, arthropods	Arginine (R) in vertebrates; Glutamate (E) in nematodes;	Penultimate residue of the Tao chimera (Tao et al 2013)

*Amino acid numbering from PxRyR

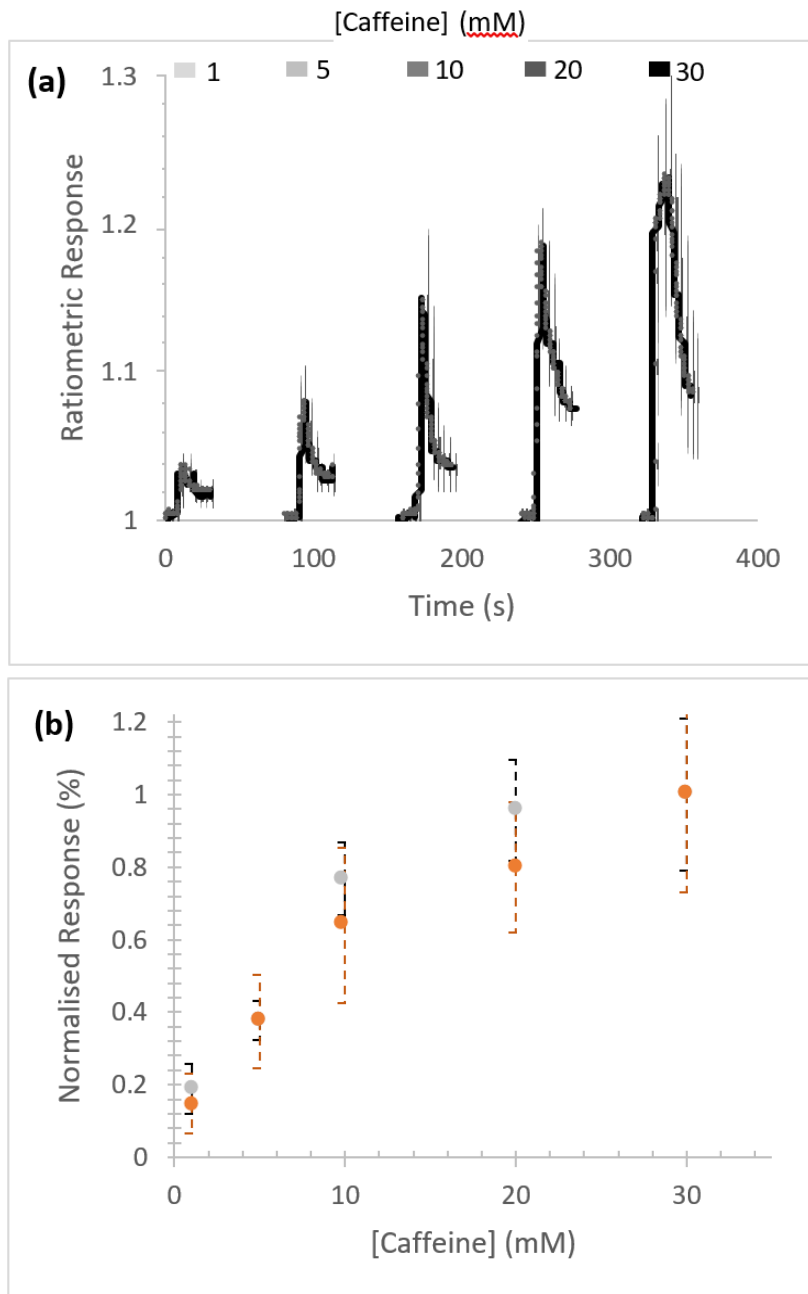


Figure 6.4 Response of RFCLM-PxRyR to increasing dosage of caffeine **a)** a recording of a single FOV of cells over time **b)** normalised, relativized responses of those same RFCLM-expressing cells (orange) compared alongside WT-expressing cells (grey)

patch is a method susceptible to misinterpretation due to uncharacterised effects of caffeine on cell physiology.

6.3.1.2 Characterisation of RFCLM diamide-response

Following the protocols described in Ch3, concentration-response experiments were conducted for RFCLM-PxRyR against CLR and FLB. RFCLM-PxRyR demonstrated a decreased sensitivity to CLR compared to the WT-PxRyR construct,

and near elimination of FLB-responsiveness (Fig 6.5a). For reasons of solubility discussed previously, the maximum applied concentration for both diamides was 50 μ M. In the case of CLR, this maximum concentration was apparently insufficient to enter the plateau phase of the concentration-response relationship. In the absence of such a plateau, 'relativisation' (Chpt 3, Box 3.2) of the response is problematic. Therefore, in this instance, the response magnitude elicited by 50 μ M CLR was treated as the maximum response amplitude for this sequence variant, to allow representation of the data for this variant in the same concentration-response format used for the other variants discussed in this thesis. A maximum response amplitude of 1.139 at 50 μ M is comparable to the maxima of other constructs in this thesis (IM, 1.182; GV, 1.127), lending support to this decision. Furthermore, additional concentrations of CLR, applied beyond the solubility limit, gave similar responses, each falling within one standard deviation of the 50 μ M response (1.39 \pm 0.23). Nonetheless, calculation of an exact resistance ratio is problematic. A 'minimum resistance-ratio' can be ascertained by comparison of WT-PxRyR EC50 (0.015 μ M) with the 'minimum EC50' of RFCLM-PxRyR (20.4 μ M), giving a RR=1360-fold to CLR [where the assumption is that the actual EC100 dose for RFCLM-PxRyR is greater than, or equal to, the hypothetical EC100 (50 μ M) used here].

In the case of FLB (sulfoxide form), responses were small and transient up to and beyond the limit of solubility of the compound (Fig 6.5a). RFCLM-PxRyR expressing cells did at no point display a typical, irreversible activation response to FLB (e.g. Ch4, Fig 4.2). The closest approximation to an RR calculation can be made by comparing the FLB concentrations required to illicit 10% responses of WT and RFCLM constructs in Fig 6.5. The EC10 for WT reads as 50nM, whilst that for RFCLM is at 50 μ M, giving an approximate RR of 1000-fold.

The impact of these five amino acid changes upon diamide efficacy is shown to be extreme, where diamide interaction is all but abolished, creating a channel similar in diamide-interaction properties to the human hRyR channel itself (RFCLM EC50: 20.4 μ M to CLR, which is comparable to studies in mice, Fig 6.1). The result appears to confirm the location of the diamide interaction site as being within the Voltage Sensor-like Domain (pVSD). Fig 6.5b indicates the positions of the five modified residues in the pVSD region, with an electro-static potential surface overlay indicating positive and negative amino acid moieties. The centre of this structure

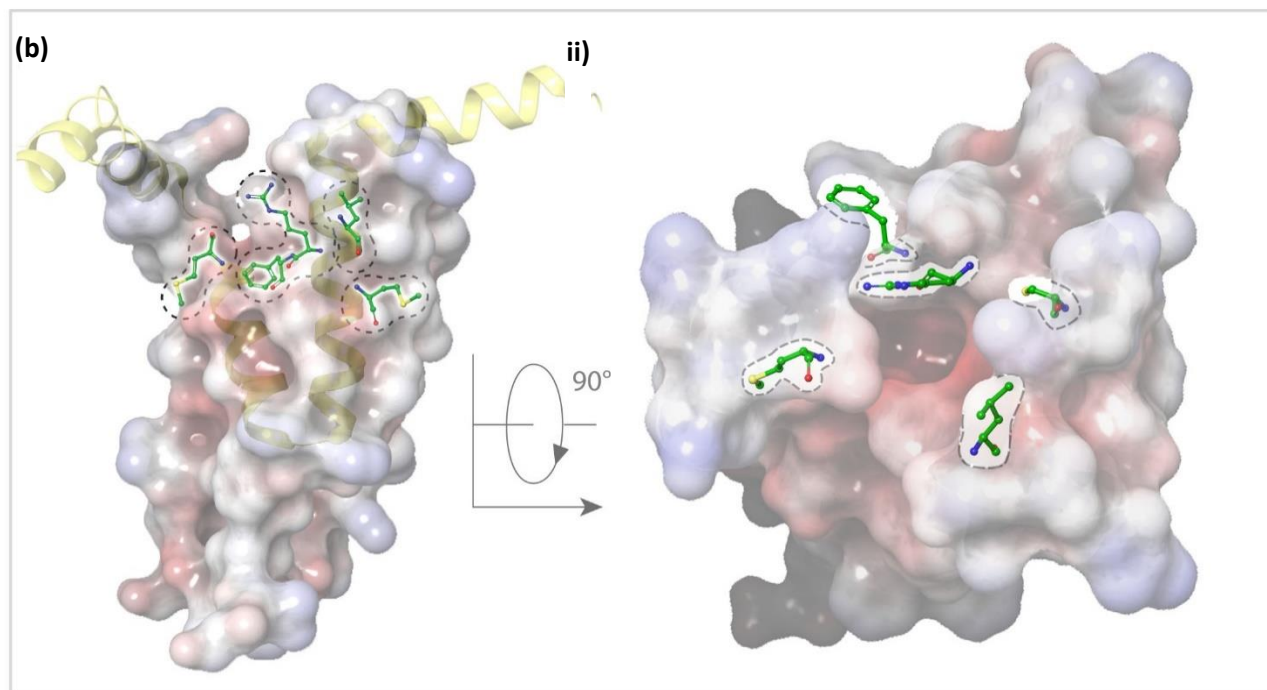
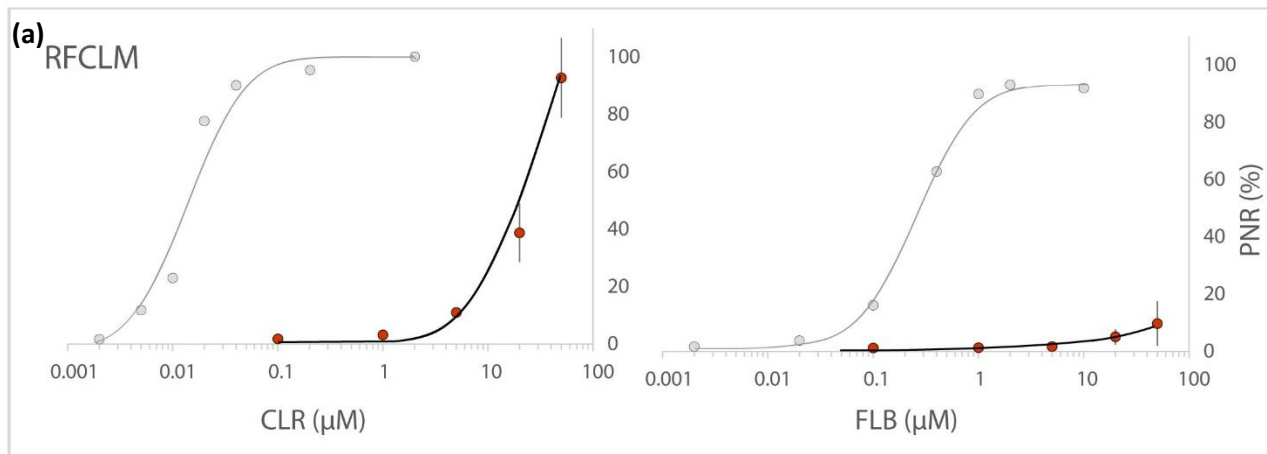


Figure 6.5 RFCLM-PxRyR is only activated by CLR at very high concentrations but is not activated by FLB at its limit of solubility.

(a) Dose-response relationship of RFCLM-PxRyR (red fill) to CLR and FLB (with WT PxRyR (grey fill) response for comparison)

(b) Homology model* of the RFCLM-PxRyR pVSD, displayed in **i**) longitudinal and **ii**) transverse orientation. Positions of the five amino acid substitutions are marked; dotted lines indicate that the residue is hidden within the structure.

*All work is the author's own. The homology model was generated in collaboration with Oliver Gutbrod (Bayer CropScience), using Pymol and Schrodinger software.

contains a cavity of high electronegativity (red), which is flanked by the five altered residues.

6.3.2 Unpicking the RFCLM modification

In pursuit of identifying which of the five amino acid residues in WT-PxRyR contributes most significantly to the lepidopteran RyR susceptibility to diamides, the five amino acid substitutions RFCLM were added individually, and in pairs, into novel PxRyR constructs.

6.3.2.1 Brief characterisation of RF-PxRyR chimera caffeine-response

Of the five altered aa residues, the K4700R-Y4701F (RF-PxRyR) combination was considered a strong candidate to be mediating the observed effects, based on the previous work by Tao et al. This combination was expressed, as before, against an otherwise WT-PxRyR background, in Sf9 cells. Comparison was then made between the RF-PxRyR and the RFCLM-PxRyR expressing cells in terms of caffeine and diamide responses, in order to validate that the constructs gave functional RyRs. Both constructs display an ability to respond to caffeine, and the amplitude of this caffeine response correlates with their response to CLR in both cases. A concentration of 20 μ M CLR was used, known to activate both RFCLM-PxRyR and RF-PxRyR to around 20-50% maximum amplitude. For RFCLM-PxRyR, the correlation coefficient between caffeine and CLR is strong (Fig 6.6a), indicating that the established method of relativizing diamide response with caffeine response is likely to resolve around 80% of the variation in Ca²⁺ responsiveness for this genotype. The correlation for RF-PxRyR is less strong (Fig 6.6b) but remains within the range of that seen for the other sequence variants studied in this thesis. The implication, therefore, is that the RF construct will display a considerable amount of variation to diamide dosage.

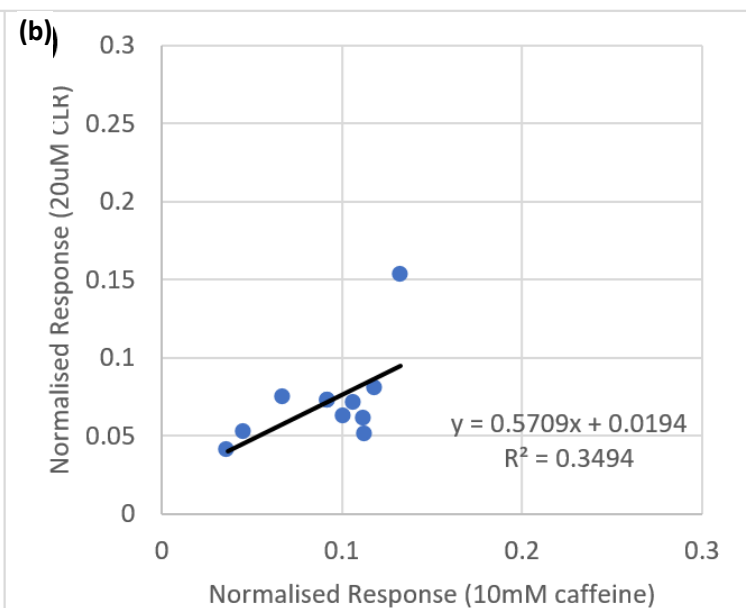
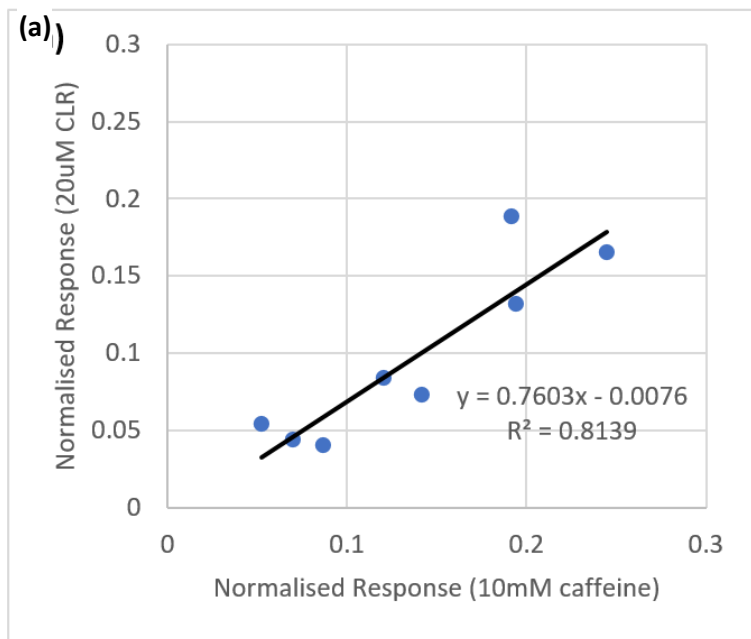


Figure 6.6 Correlation between caffeine and diamide responsiveness for (a) RFCLM -PxRyR and (b) RF-PxRyR

6.3.2.2 Characterisation of RF-PxRyR response to diamide

With insufficient time remaining for comprehensive concentration-response characterisation of each individual construct, a series of method changes were introduced:

- In a pairwise setup, referred to as a ‘discriminating dose’ experiment, sequence variants were exposed to identical concentrations of agonist, to compare the magnitude of response to that concentration.
- Characterisation of CLR susceptibility was prioritised over FLB susceptibility. Non-responsiveness of RFLCM-PxRyR to FLB, at any concentration, prevents meaningful comparison between this variant and others.
- The sequence variants were assessed in their order of hypothesised resistance, studying first those variants most likely to confer resistance.

RF-PxRyR when expressed in Sf9 cells shows an extreme reduction in CLR response relative to WT-PxRyR (Fig 6.7, Table 6.2). The magnitude of the difference is similar to that between RFCLM-PxRyR and WT-PxRyR. LSD consists of a pairwise comparison of mean average response amplitude between the constructs, compared to the standard deviation of all groups combined. An insignificant difference between RFCLM-PxRyR vs RF-PxRyR in relation to CLR efficacy suggests that the two amino acid alterations, K4700R and Y4701F, are responsible for mediating the majority of the RFCLM-PxRyR phenotype. The phenotype of this RF chimera was found to be as equally profound as that of the original RFCLM chimera, indicating that one or both of these residue positions is critically important for RyR interaction / non-interaction with diamide insecticides.

6.3.2.3 Characterising the effects of individual residue-changes on diamide response

In order to further break-down our understanding of the binding pocket, the K4700R, Y4701F and I4790C substitutions were added individually to the WT-PxRyR background construct. A preliminary assessment was then made of the caffeine responses for each of the novel variants. Due to severe time constraints, an assumption was made that given the previously recorded lack of difference

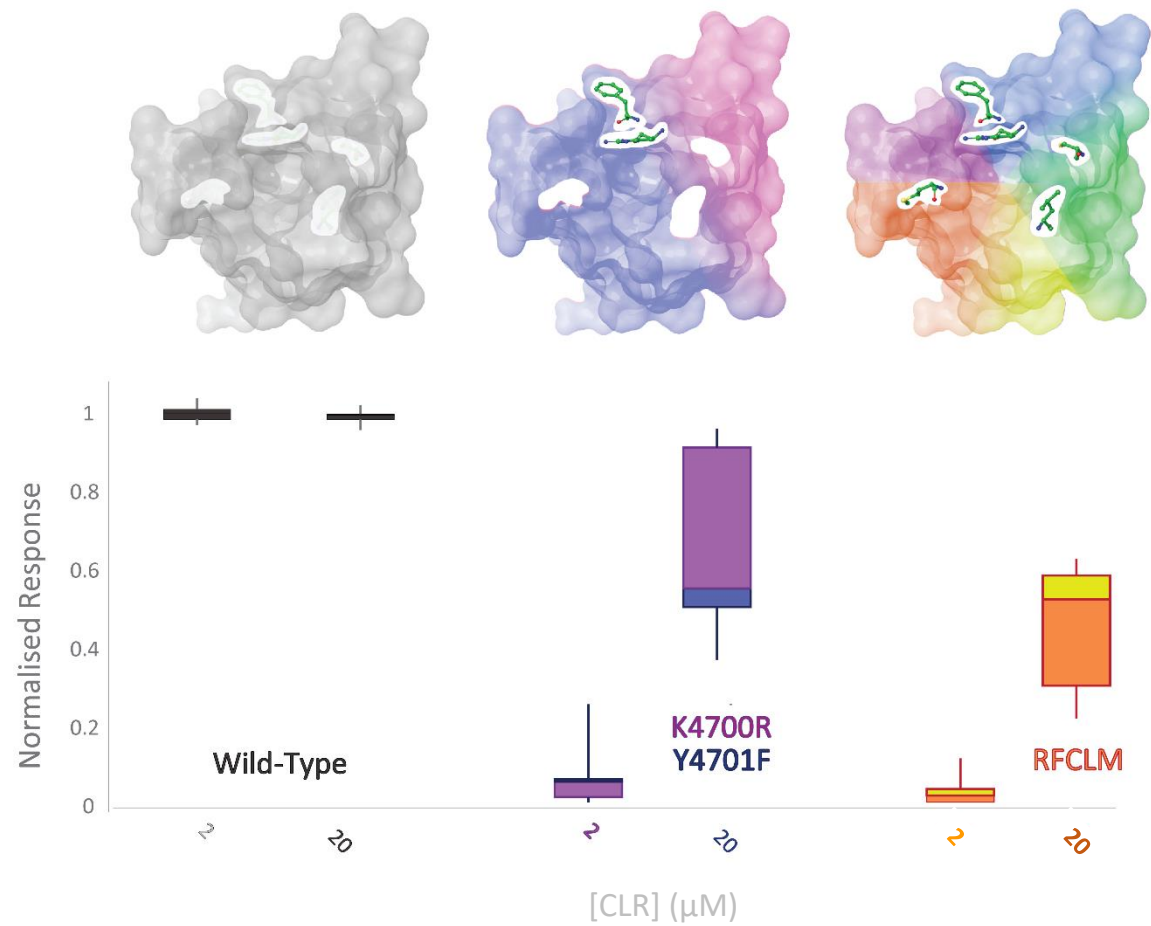


Figure 6.7 RF-PxrRyR and RFCLM-PxrRyR share a similar phenotypic response to CLR exposure. Sf9 cells (n=8-17) expressing either Wild-Type (Grey), RF (Blue-Purple), or RFCLM (Yellow/Orange) PxrRyR were exposed to 2 μM and 20 μM concentrations of CLR. All diamide responses were normalised against a prior caffeine response and relativized against the maximum WT-PxrRyR response.

between WT-PxRyR and RFCLM-PxRyR constructs in terms of caffeine response, constructs containing the same mutations expressed singularly would also be unlikely to vary significantly from the WT in caffeine response amplitude. Therefore, detailed characterisation of caffeine concentration-response, and caffeine-diamide response correlations, were not carried out. Instead, all the constructs were simply expressed on the same day, and each dosed once with 10mM caffeine. In defense of this approach, the study design is based upon a previous study, Tao et al, 2013, published in a major (and reputable) journal. Tao did not characterise caffeine response, nor response to any ligand but diamide. The current results (below) indicate the potential cost of their methodological omission.

Fig 6.8 indicates that all three RyR variants, K4700R, Y4701F and I4790C, were capable of responding to 10mM caffeine. However, there was considerable variation in caffeine response both between cells of the same variant, and across variants. If this caffeine response variation translates to diamide response variation, it may impact apparent responses by up to 3-fold. Although this represents a considerable variance, it can be considered as being acceptable in the context of the 1000-fold differences seen between the WT-PxRyR and RFCLM-PxRyR diamide response. If recombinant constructs are found to differ in diamide response by less than 10-fold, the veracity of this difference must be called into question.

All three novel variants, K4700R, Y4701F and I4790C, were found to confer a significant reduction in diamide response amplitude at the four 'discriminating doses' of CLR tested (Fig 6.9). However, the effect magnitude of each individual change was 50-100 times less severe than the synergistic effect of all five changes combined (in the RFCLM-PxRyR construct).

[Note: Analysis of the differences between variants in this thesis is based on the assumption that there is no significant difference in the maximum diamide response amplitude between the variants under comparison. This assumption has been tested variously in Chapter 4 (Figs 4.8 - 4.10) and in other publications (Trocza 2015), and it has been repeatedly shown that there is no significant difference in maximum amplitude between the variants so far studied. Analysis of differences between the K4700R, Y4701F and I4790C constructs here is thus made

under the assumption that these variant receptors also do not vary in their maximum response amplitude. With hindsight, this is an assumption that should have been validated experimentally.]

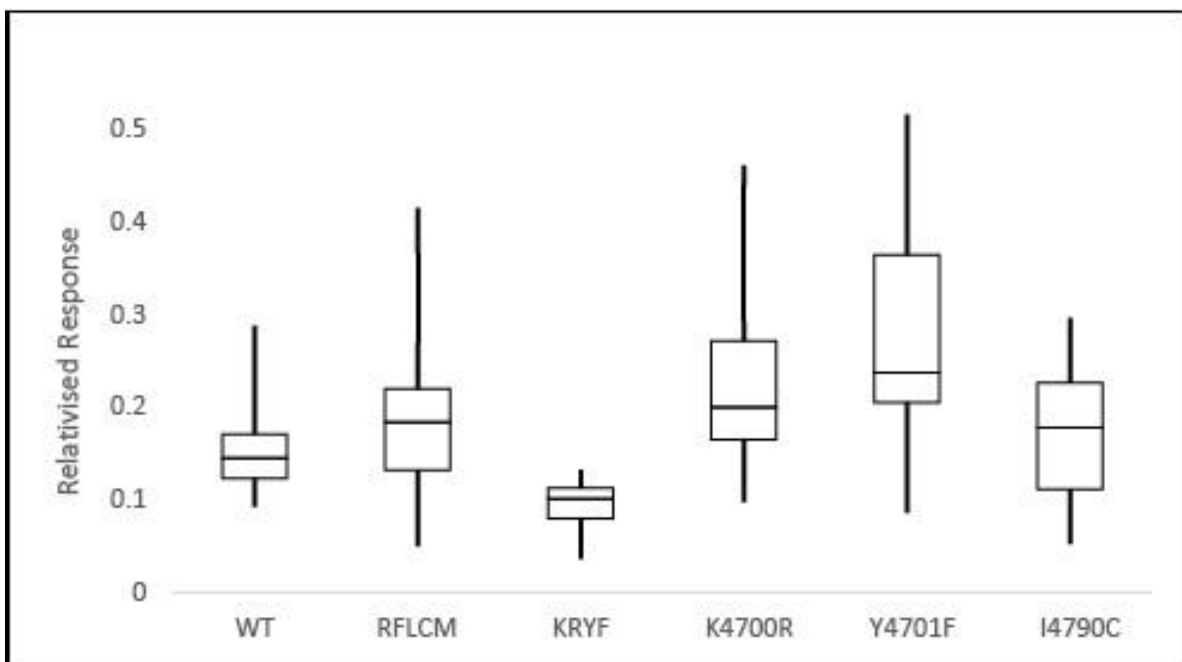


Figure 6.8 Comparative response to 10mM caffeine of all the recombinant constructs. Transfected Sf9 cells were imaged on the same day, one FOV per construct (n = 4-37 Cat A responding cells).

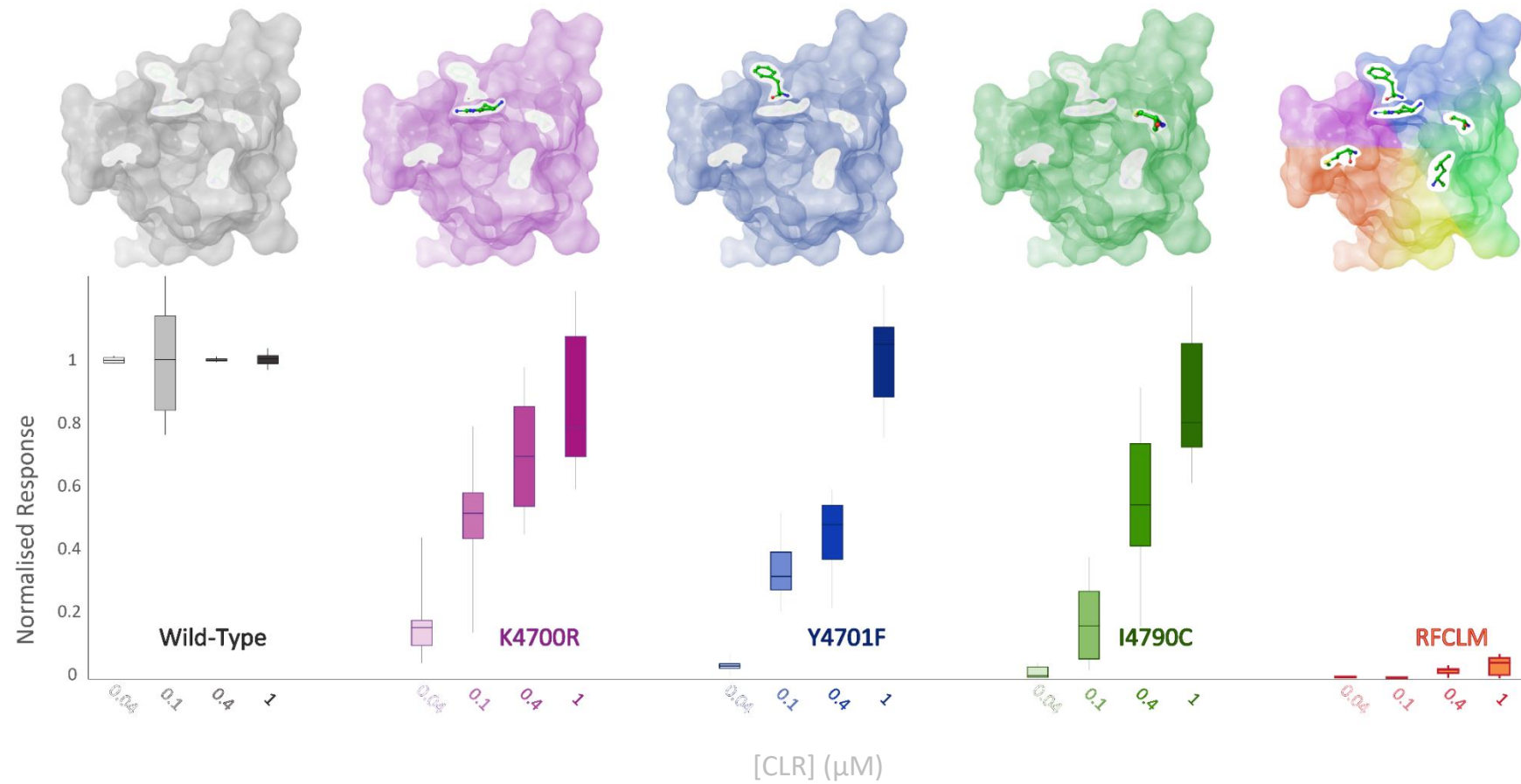


Figure 6.9 PxRyR variants exhibit differing response to increasing concentrations of CLR. Sf9 cells (n=5-26) expressing either Wild-Type (Grey), K4700R (Purple), Y4701F (blue), I4790C (green) or RFCLM (Orange) -PxRyR were exposed to increasing concentrations of CLR. All the diamide responses were normalised against prior caffeine response and relativized against the maximum WT-PxRyR response.

Table 6.2 Comparison of the responses of PxRyR sequence variants to discriminating CLR concentrations (Sub Tables a-d). Grey boxes list average response of that construct (relativized to WT). White boxes display indications of significance, based on LSD comparisons of amplitude between the variants. N.S = Not Significant; * = P<0.05; ***= P<0.001.

a) 0.04 μ M CLR					
	WT	K4700R	Y4701F	I4790C	RFCLM
WT	1	***	***	***	***
K4700R		0.20	***	***	***
Y4701F			0.039	N.S.	N.S.
I4790C				0.021	N.S.
RFCLM					0.0061

b) 0.1 μ M CLR					
	WT	K4700R	Y4701F	I4790C	RFCLM
WT	1	***	***	***	***
K4700R		0.51	*	***	***
Y4701F			0.33	*	***
I4790C				0.18	*
RFCLM					0.0038

c) 0.4 μ M CLR					
	WT	K4700R	Y4701F	I4790C	RFCLM
WT	1	*	***	***	***
K4700R		0.69	*	N.S.	***
Y4701F			0.43	N.S.	***
I4790C				0.55	***
RFCLM					0.025

d) 1 μ M CLR					
	WT	K4700R	Y4701F	I4790C	RFCLM
WT	0.99	N.S.	N.S.	N.S.	***
K4700R		0.96	N.S.	N.S.	***
Y4701F			1.039	N.S.	***
I4790C				0.89	***
RFCLM					0.042

Result Highlights (Table 6.3):

- The minimum CLR concentration tested here is 0.04 μ M, as this was the minimum concentration at which any of the modified PxRyR's registered a response. Despite that, the dose is far above the EC50 of the WT-PxRyR (0.015 μ M CLR).
- K4700R responds to the lowest (0.04 μ M) CLR concentration. Y4701F and I4790C do not respond at this concentration (their response is no different from that of the RFCLM-PxRyR variant). The magnitude of the K4700R response is 10-20% compared to the WT response.
- K4700R responds to a concentration of 0.1 μ M CLR with an average of 51 \pm 6% amplitude. This is comparable to an EC50 response and when compared to that of the WT (0.015 μ M), yields a resistance ratio of 6.67-fold.
- Y4701F (43 \pm 5%) and I4790C (55 \pm 16%) both reach an approximate EC50 response at 0.4 μ M CLR, translating to a calculated resistance ratio of 26-fold.
- The introduction of K4700R is associated with a minor reduction in CLR-mediated activation; the introduction of either Y4701F or I4790C is associated with a more significant reduction in CLR efficacy. It is significant that despite its constituent parts (K4700R and Y4701F) giving just 6.67-fold and 26-fold reduction in efficacy respectively, when the two substitutions are combined, the resulting RF-PxRyR bears the same diamide-resistant phenotype as RFCLM-PxRyR (RR>1000-fold).

[Note, the variance in these measurements is large. This was predictable due to the lack of preparatory work, as has been discussed above. However, the effect-

magnitudes at play are also sufficiently large that patterns are clearly demonstrable in this data.]

6.3.2.4 Assessing the contribution of Y4701F on flubendiamide (FLB) efficacy

The remaining efforts in this Chapter were directed towards resolving the contribution of Y4701F to the observed diamide resistance phenotype. Y4701 alterations have been found in resistant populations of *Chilo suppressalis* and are apparently increasing in frequency (Sun et al 2018). Bioassays of these populations indicate that this residue is involved in 250-fold resistance to CLR. This amino acid change was therefore hypothesised to play a central role in the RF phenotype (Fig

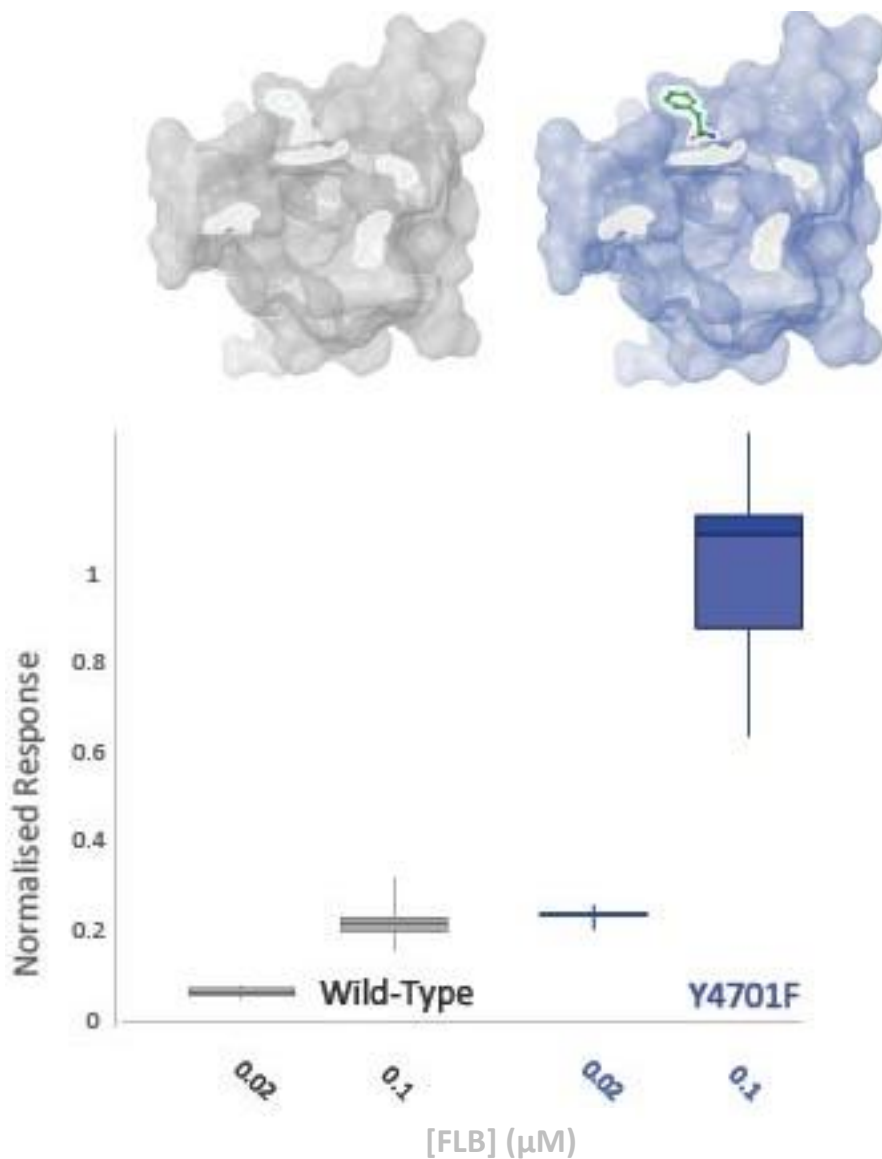


Figure 6.10 WT-PxRyR and Y4701F-PxRyR exhibit comparable responses to a low dosage of FLB. All responses were normalised against a prior caffeine-response and relativized against the maximum Y4701F response.

6.7). Indeed, it has been shown that the residue plays a far greater individual role in CLR resistance than its neighbour, K4700R (Fig 6.9, Table 6.3). Field studies also indicated that Y4701F might have differential effects vs CLR and FLB (Huang 2019, Unpublished). Given that the purpose of this study is to inform efforts to locate the binding site(s) of anthranilic and phthalic diamides, any recorded differences in response is potentially valuable information. Accordingly, the impact of the residue upon FLB efficacy was tested. As displayed in Fig 6.10, the Y4701F residue surprisingly does not confer resistance to FLB. Indeed, the alteration may confer an increase in FLB susceptibility, by up to 5-fold.

6.4 Discussion

Experiments in this Chapter have identified five amino acid substitutions, referred to as RFCLM, singled out for their dramatic impact upon diamide efficacy when added in concert to an otherwise WT-PxRyR construct and transiently expressed in Sf9 cells. These five alterations were mapped on to a homology model of the RyR protein and found to be located in close proximity to one another, as well as to the resistance-associated mutations studied in Ch4, and all lie within the previously defined 'diamide resistance region'.

6.4.1 Why is there a disparity between the effects of residue changes in isolation, and their effect in combination?

Further investigations indicated that two of the initial five residues, K4700R and Y4701F, were together responsible for a reduction in diamide resistance of approximately equal magnitude to that generated by the five residues (RFCLM) in concert.

However, investigation of the two substitutions in isolation, each expressed separately against an otherwise WT-PxRyR background, found that neither conferred a resistance ratio of greater than 26-fold to CLR, in comparison to >1000-fold resistance conferred by the RFCLM-PxRyR.

It seems clear, from these results, that the resistant phenotypes associated with each individual change combine synergistically (perhaps factorially) when placed together. That is, if we assume that K4700R and Y4701F cause reductions in CLR efficacy due to their **individual** effects on CLR binding or on CLR activation of the

protein, perhaps these two mechanisms multiply the effects of one another (6.7-fold resistance multiplied by 26-fold might create 175-fold resistance, for example).

Previous authors have shown that resistance-associated point mutations can create non-additive phenotypes when expressed in the same background. Such an epistatic interaction was found by Zimmer et al whilst studying P450s in the brown planthopper (Zimmer 2018).

Polypeptide folding during RyR formation is not well characterised, even in mammals, and changes to the sequence may impose dramatic alterations to this process. More investigations are perhaps required into this topic of interest.

6.4.2 What is the mechanism of the observed resistance effects conferred by Y4701F?

This investigation has found that Y4701F simultaneously confers resistance to CLR (26-fold) but, uniquely, also confers slight susceptibility to FLB.

Firstly, in terms of CLR-resistance, it is not clear why Y4701F would change the CLR binding site sufficiently to cause such a potent phenotype. The residue faces outward (abaxial) from the pVSD pocket (Fig 6.11), away from the hypothesised centre of the binding site (Fig 6.5). The change represents the loss of a polar interaction, raising the possibility that interaction with other nearby polar charges could be responsible for some kind of electrostatic alteration of the surrounding topography to affect a change in the binding pocket. However, the homology model indicates a total absence of other charged groups within 5Å proximity of the residue.

One possible explanation of this finding is that the CLR binding site extends over the 'anterior' (Fig. 6.11) lip of the pVSD, to contact the Y4701 residue.

In terms of the conferred FLB-susceptibility, it is notable that Y4701F-PxRyR is the only construct investigated in this thesis that has shown greater susceptibility to FLB than to CLR. By comparison, the WT, I4790M and G4946V are all activated by a concentration of CLR >20-fold lower than their FLB activating concentration. The RFCLM-PxRyR completely avoids activation by FLB.

6.4.3 Limitations

This Chapter represents a preliminary investigation into a series of amino acid changes potentially critical to the integrity of the diamide binding site in PxRyR. The Chapter builds upon the methodology of Tao *et al*, albeit focusing on substitution of individual amino acid residues rather than larger protein fragments, providing a greater level of fine detail than is available within that publication. Large phenotypic differences between the WT and modified PxRyR constructs ensures that this piece of work, although preliminary, nonetheless makes a meaningful and valuable contribution to resolving the position and extent of the diamide binding pocket. This study focusses on CLR because FLB was found to be completely ineffective against RFCLM-PxRyR and therefore rendered futile any quantitative comparisons between constructs' response to both drugs. CLR was also what Tao *et al* used for their assays. These results can legitimately therefore be considered as the logical continuation of the Tao study, further resolving the resistance region identified there.

Due to time constraints, the experiments performed were not sufficiently detailed to draw conclusions relating to the exact nature of the diamide binding site. It was particularly regrettable to run out of time before characterising S4919L and V4945M, as the K4700R and Y4701F substitutions were prioritised for obvious reasons, and there was a concomitant lack of previous knowledge being available on S4919L and V4945M. Further work in this area should focus on characterising the PxRyR alterations generated here in greater detail, especially in terms of their individual impact upon general physiology and response to caffeine, which in the present study varied considerably between constructs. Only thereafter will it be possible to effectively characterise the impact of these amino acid substitutions upon CLR and FLB efficacy.

A major flaw of this Chapter is an inability to express human RyR in Sf9 cell lines, since hRyRs are notoriously difficult to work with (Chris George, pers comm). Attempts were made to do so during this current investigation, but time limitations prevented its completion. Therefore, an assumption is made that mammalian RyR, when expressed in Sf9 lines, would yield a diamide insensitive phenotype comparable in magnitude to that seen in the studies detailed in Fig 6.1. This assumption is supported by experiments on the RFCLM-PxRyR chimeric construct (Fig 6.5) which itself displays a diamide insensitive phenotype comparable to those

studies, despite containing just five amino acid alterations derived from the mammalian receptor.

Despite its shortcomings, the results presented in this Chapter hint at the toxicological relevance of a selection of amino acid residues around the putative diamide binding site, further defining the 'diamide resistance region' and delineating a series of amino acids highly likely to be involved in diamide interaction.

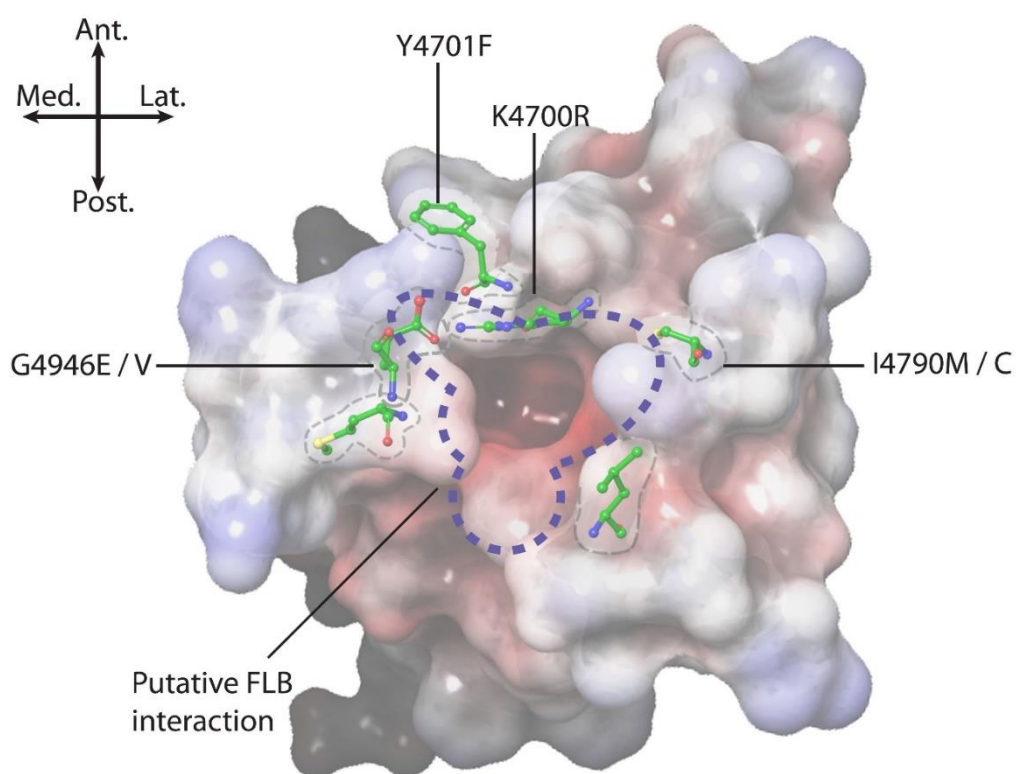


Figure 6.7.11 Positional summary of all of the amino acid residues studied in this thesis. Electrostatic potential: positive (blue) neutral (white) and negative (red). The putative FLB interaction site (Blue dotted ring) is that described by Lin et al 2019.

6.4.4 A hypothetical channel structure

Chapters 4 and 6, in combination, have defined a series of amino acid residues in terms of their alteration of diamide efficacy. Clearly visible in the centre of the pVSD (Fig 7.1) is a region of high electronegativity (red), surrounded by an opening of neutral and electropositive residues. This is a common feature of voltage-gated ion channels, frequently representing the site of ligand interaction (Gutbrod, pers. comm). The amino acid residues 4946, 4790, 4700 and 4701 partially encircle this region. In this thesis, the impact of changes to these four residues upon diamide interaction has been characterised, in an attempt to define the position and extent of the diamide binding site.

The four amino acid residues studied in detail appear to form a crescent across the anterior side of the pVSD (Fig. 7.1), with alterations of each (alone or in combination) producing substantial phenotypic effects upon interaction with at least one of the two diamides. Moving along the crescent, from the medial to the lateral side, an appreciation of the effects of each residue in isolation can facilitate the drawing of substantial conclusions regarding the binding site as a whole. The implications of each alteration will be discussed in detail over the following sections, taking into consideration the findings of the recently published, and highly controversial, homology model of the FLB-binding region upon the RyR (Lin et al 2019) (marked upon Fig 7.1).

The following assertions can be made based on the information from this thesis:

- • The G4946 position is almost certainly part of both FLB and CLR binding sites. It may represent a narrow point within the site, hence why longer sidechains cause obstruction here.
- • The Y4701 position is almost certainly a part of the CLR binding site but may potentially not be involved in FLB binding.
- • In combination, K4700R and Y4701F create a dramatic change in CLR efficacy, difficult to explain given their individually minor impacts.
- • The I4790 position likely plays a part in both CLR and FLB binding sites but may occupy a more dominant position in the latter.
- • That the 4790 and 4701 sites both exhibit differential effects between the diamides may indicate that the binding sites are non-identical (in support of Casida 2013)
- • However, since both compounds are equally affected by G4946E/V alterations strongly suggests at least partial overlap of binding.

6.5 Conclusion

Definition of the binding pocket has been a partial success, but further work remains. The 4700R-4701F combination must be characterised in much greater detail. In particular, computational analysis should be applied to understand the topological and electrostatic differences between the WT PxRyR residues (K, Y) and their mammalian counterparts (R, F) individually, as well as in combination. The profound phenotype of these two substitutions in combination, against the relatively insignificant phenotype of the two individually, demands explanation. Unfortunately, it was not possible to study residues V4945M and S4919L individually, for lack of time. The positions of these residues on either side of the pVSD should provide valuable information as to the anterior extent of the binding site.

Efforts to define the internal organisation of the diamide binding site in greater detail requires a change of approach away from individual residue analysis, instead targeting collections of residues as part of 'functional units' within the binding pocket. Field-derived, resistance-causing mutations such as G4946E, I4790M, Y4701C/D/F (Sun et al. 2018) seem likely to mediate their dramatic effects through topographical alterations to the pVSD environment – that is they change the interaction surface of the local area. Such changes provided useful information, in terms of identifying the extent/perimeters of the binding area. However, within that binding area, it is important to identify the residues responsible for forming inter-molecular forces (IMFs) with the diamide ligand.

Taking the previous two points into account, future studies might employ 'alanine scanning', or a similar approach, to rigorously characterise the binding pocket, targeting units of 5 contiguous amino acids and knocking out their binding potential by converting all five residues to alanine. Such combinatorial changes are expected to generate more substantial phenotypes compared to single alterations. Albeit, they do so at the cost of creating 'artificial' changes, rather than biologically relevant changes. As this study has shown, large phenotypic effects can be characterised quickly and crudely even in the presence of considerable sampling variation. Having established a phenotype for the combinatorial construct, alanine scanning on an individual-residue basis should follow, in order to determine the 'function' of each residue in diamide binding.

Two strings of residues stand out as candidates for alanine-scanning binding site analysis: 4918-4922; and 4942-4945. The former represents a high concentration of polar hydrogen-bond acceptors and represents a series of probable diamide-interacting residues. The latter contains the positively charged D4942 in a position close to the hypothetical 'entrance' of the FLB site (Fig. 7.1), as well as V4945, whose candidature has already been discussed at the heading of this Chapter.

Future students of RyR physiology should take heart from the present study, especially the results reported in Ch6, showing that dramatic changes to the pVSD can be achieved without fear of removing channel function. In this case, total ablation of FLB binding in the RFCLM and K-F constructs is paired with a mere 1.7-fold difference in caffeine response relative to the WT (Fig 6.8).

Ch7: General Thesis conclusion

The problem of insecticide resistance is at least a century old (Guedes 2016), but a perfect storm of recent factors has exacerbated the rise of resistance to diamides in Lepidoptera. South-East Asian *P.xylostella* populations provide a worst-case-scenario of how failed IRM can rapidly produce resistance, via lack of crop rotation, and overreliance on a single MoA (Trocza et al. 2016). A slowing down of new MoA discovery (Sparks and Lorschbach 2016), combined with increased regulatory pressure, further inhibits insecticide MoA rotation, whilst globalisation increases the likelihood of novel pest invasions, and climate change expands their invasive range (Chapman et al. 2017).

In this context, there is value in lengthening the 'shelf life' of an insecticide class, by combatting the development of resistance. Such was the aim of this thesis, in relation to the diamide class of insecticides. Herein, the problem of diamide insecticide resistance is approached from multiple sides:

1. Confirmation of target-site resistance observed in the field, as caused by point mutations to the RyR. Wherein, these mutations are now trackable, by population-scale PCR methods. Frequency of these mutations should inform the insect control strategy used, including the removal of diamides from rotation when frequencies are high.
2. Binding site studies presented here go some way to defining the interaction site of diamides on the RyR, which may inform efforts to design improved diamide chemistries.

7.1 A Rapid TSR diagnostic method facilitates improved IRM

7.1.1 *The theory*

Resistance, or the reduction in control efficacy of a synthetic compound, is caused by repeat application of the compound over multiple generations of an insect population (Guedes et al 2019). Genes for resistance mechanisms, already present within the population, increase in frequency due to the relative prosperity of their bearers. Target-site resistance (TSR) is a major form of insecticide resistance, and has been the focus of this thesis. The frequency of target-site mutations, which cause resistance, can be tracked in a population in order to predict the probability of control failure (Guedes et al 2019).

By avoiding application against populations registering a high frequency of resistance mutations, further resistance build-up is avoided. Moreover, switching to an alternative form of control, such as an insecticide of a separate mode of action can theoretically cause resistance to decrease over time (Guedes et al 2019).

It follows that, in theory, monitoring of resistance mutations in pest populations should create an early-warning, or ‘resistance surveillance’ system preventing insecticide resistance from developing.

7.1.2 In practise

The author has been able to find no evidence of such a complete resistance surveillance system in operation. Genotyping is becoming cheaper each year, so the possibility of large-scale tracking is there. However, the identification of TSR mutations is currently occurring far too slowly to be of any value. Additional resistance mutations are continually emerging (e.g. Sun et al 2018, Y4701C/D). In the past, characterisation of diamide resistance-associated mutations has taken 3-5 years (as with G4946E, I4790M, G4946V) (Trocicka et al 2017). Such lengthy characterisation-times can allow the resistance mutation to spread widely before tracking even begins. For example, 5 years was sufficient to see the G4946E mutation spread to populations in every continent on the globe (Steinbach et al 2015).

7.1.3 Work in this thesis heralds a more rapid mode of characterisation

The insecticide industry is not releasing new modes of action as quickly as resistance is developing to those modes of action. In the context of rising insecticide development costs (averaging \$250million USD (Sparks and Lorschach 2016)), falling profit margins and increasingly long development times (Ch1, Fig 1.2a), the agricultural community urgently needs to turn the tides on resistance.

This thesis has advanced the ability to diagnose TSR mutations, making for a quick and cheap method that fits into the fast pace of IRM. Following the ‘semi-quantitative’ protocol detailed in Ch6, a host of potential resistance-causing mutations can be evaluated by one worker within a six-month period.

Resistance validation is only one part of the IRM process. Here’s how the new method fits in. An idealised Target-site Resistance Management strategy involves a number of steps, and not necessarily in this order:

1. Track resistance-associated mutations
 - a. Population genotyping. If a region of interest (less than 1kb) is known, population-scale sequencing of this region can reveal SNPs. If one particular SNP appears to be rising in frequency across multiple sequencing events, this is an indication of selective pressure (Wilson and Rannala 2003, Kimura 1968), which in turn indicates a likelihood that this SNP will impact insecticide efficacy.
 - i. A method of population genotyping without sequencing was recently developed by Boaventura et al. Called allele-specific PCR, it is a cost-effective manner of identifying the frequency of sequence variants in a population (Boaventura et al. 2019).
 - b. Resistance-associated point-mutations identified during population sequencing require validation. The rapid, semi-quantitative mode of validation employed in Ch6 of this thesis is sufficient to determine whether a point-mutation causes high or low levels of resistance. More detailed studies, (e.g. Troczka 2015), have fundamental value but are not necessary in order to draw practical conclusions regarding the impact of a given mutation.
 - c. Once validated, population genotyping continues, monitoring the spread of those identified mutations.
2. Adjust spray rotations accordingly
 - a. Where mutation validation has shown a potent resistance-causing effect, and where population sequencing has shown that the mutation is present locally at a frequency capable of causing a >10% drop in insecticide efficacy, spraying of that insecticide class must be suspended
 - b. Once resistance-associated mutations have disappeared from the population, as confirmed by further sequencing, application of the given insecticide class should continue

This monitoring protocol should be mandatory and enforced by insecticide producers with the backing of national governments, due to its benefit to the producer and for the world alike, in order to combat resistance.

7.1.4 Caveats to such a resistance surveillance strategy

Target-Site Resistance is only one cause of insecticide control failure – others include metabolic resistance, behavioural resistance and cuticular resistance (reduced penetration). The above protocol is primarily effective against TSR, although could be adapted for Metabolic Resistance. To monitor all forms of resistance requires toxicological assessment (bioassay) of a representative sample of the population on at least a yearly basis. This is an expensive process, as insects must be collected and reared for at least one generation, and because

representative sampling of a population of billions of insects (for example across pests of maize in China) requires sampling of huge numbers of insects in order to actually detect any low-level resistance. The method of resistance tracking based on population sequencing is thus preferable where-ever possible.

7.1.5 Future Steps toward a better surveillance strategy

7.1.5.1 Does Resistance have a cost?

A major tenet of the above IRM strategy is that insecticide resistance will subside in the absence of insecticide application. The basal theory behind this assumption is that of fitness costs: a phenotype is shaped by the selection pressures of its environment, bringing it ever closer to optimality in that environment, such that alterations to the environment, for example, by exchange of one insecticide for another, reduces the fitness of this phenotype (Coustau et al. 2000). On a genetic level, this is the reason that each resistance-causing allele can be described to suffer from a Cost in the absence of insecticidal pressure.

In this this thesis I show that resistance to diamide insecticides does have a cost, when studied in ‘pestified’ *Drosophila*, modified to express the *P.xylostella* RyR in place of their own. Pestified *Drosophila* carrying resistance mutations, G4946E or I4790M, experienced dramatic reductions in flying and crawling speeds in comparison to pestified *Drosophila* wild-type at both positions. If such costs are found to exist in populations of insects ‘in the field’, it will be further evidence to support the implementation of the resistance surveillance strategy as discussed.

7.2 Diamide binding and the search for novelty

7.2.1 Running to stay still

The ongoing battle against insecticide resistance necessitates continuous development of novel compounds in order to maintain capacity for MOA rotation (CropLife, 2012). But demands on the industry are going through a major shift toward increased regulatory oversight focussed on minimising human and environmental health risk. For example, in Japan, as of 2014, just 10% of marketed agrochemicals were categorised as Poisonous Substances, in comparison to around half in the 1960s (Hirooka, 2018). In the EU, safety and environmental impact assessments are now (since 2011) ‘hazard-based’ rather than ‘risk-based’ (Nishimoto 2011) contributing to the decline in new registered products.

Environmental safety concerns now govern an insecticide's shelf life, as occurred in the case of the three neonicotinoid insecticides banned in 2019 (EU Official 2019), where concerns centred around effects on wild bee colonies.

Against such a backdrop, development of novel insecticides, of which diamides are a major example, must attempt to combat insecticide resistance whilst maintaining a low toxicity to beneficial insects. New diamide development is ongoing process, as exemplified by the recent market release of Tetraniliprole by Bayer CropScience.

7.2.2 What this thesis has done, and how this contributes to better insecticidal design

This thesis aimed to increase the rate at which novel diamide insecticides could be developed. taking into account the following four-step overview of the lead development process (Whitford, Pesticide Marketplace):

1. Identification and initial screening of potential leads.
2. Assessment of biological activity. High Throughput Screening identifies biological activity on a cellular or organismal level.
3. Lead Optimisation and Analogue creation. Promising molecules are edited through synthetic chemical processes to create analogues that achieve greater target-activity or reduce off-target activity and environmental impact.
4. Advanced testing, registration and commercialisation.

This thesis has contributed to improving the above pipe-line in a number of ways as described in sections below.

7.2.3 Advancements in understanding of the diamide binding pocket

Investigations of the diamide binding site in this thesis have pinpointed its location, supporting the creation of a 3D homology-model that may aid in Step 1 of the insecticide development pipeline. On average 140,000 initial leads feed into a successful end product (CropLife 2012) and computational screening of identified leads against a 3D model of the target protein can save time and effort.

Binding site investigations have also identified amino acid residues associated with insecticide resistance and also those associated with insecticide selectivity, both of which are crucial aspects of modern insecticidal design (Sparks 2013). The position of these amino acids upon the 3D model can inform the lead optimisation process, to reduce a lead's susceptibility to existing resistance (Step 3).

Residues associated with diamide resistance in this thesis include G4946E, G4946V and I4790M. All three changes are known to exist, individually, in field populations

and were each shown here to elicit a resistance profile of between 10-fold and 144-fold to Chlorantraniliprole and >20-fold vs Flubendiamide.

In terms of improved VSR, a set of five residues were altered upon the *P.xylostella* channel to reflect the *H.sapiens* channel, resulting in a x000-fold reduction in Chlorantraniliprole efficacy in cell lines expressing the altered receptor.

7.2.4 Development of a pestified fly model to facilitate lead development

The creation of ‘pestified fly’ strains in this thesis provides an insect model for use in biological screening (step 2). Biological screening requires an ‘indicator’ organism against which to test compounds which have been shown to exceed a cut-off of in-vitro activityⁱ. The ‘pestified’ *Drosophila* lines created in this thesis express variations of the *P.xylostella* RyR in place of the endogenous *Drosophila* RyR. *Drosophila* are cheap to rear in comparison to ‘non-model’ insect species, such their use as an in-vivo screen could reduce associated overhead costs, whilst providing the benefits associated with working with a model species, including a wider array of applicable tools and background knowledge.

This is the first report of an entire RyR sequence being cloned and inserted into a different species. *D.melanogaster* and *P.xylostella* have a coding nucleotide sequence identity of 71% and have been on separate evolutionary paths for >250million years (Grimaldi and Engel 2005). A ‘pestified’ fly line created here with the I4790M-PxRyR genotype was found to exhibit 198-fold CLR resistance and 97-fold fold FLB resistance with respect to its WT-PxRyR comparator. In particular, the use of pestified *Drosophila* in insecticide screening will facilitate the search for new compounds with high activity against resistant genotypes.

This thesis has thus strengthened the toolset against diamide resistance. It has done so in part by providing tools to speed up the design process for novel diamides, by providing a virtual receptor homology model and by providing an in-vivo experimental *Drosophila* model. Finally, it has done so by providing a rapid TSR-validation method which, if included into existing resistance-monitoring approaches, could improve the shelf-life of existing diamide insecticides.

Appendix

S1 Recipes

S1.1 Molecular Biology recipes

S1.1.1 DNA extraction buffers

1. Buffer A:
 - a. 50µl 10% SDS
 - b. 530µl water
 - c. 200µl TRIS HCL
 - d. 200µl EDTA
 - e. 20µl NaCl
2. Buffer B:
 - a. 2ml CH₃CO₂K (K Ac)
 - b. 1ml LiCl

S1.1.2 LB and cloning reagent recipes

Lysogeny Broth (LB) was prepared from 5 g tryptone, 2.5 g yeast extract and 2.5 g NaCl made up to 500ml in the equivalent volume Duran bottle and autoclaved. For plates, agar was added (7.5 g Bacto-agar per 500ml) and the solution was re-autoclaved before pouring into the plates. For Ampicillin and Kanamycin plates, 250µl of 50 mg/mL stock antibiotic was added to the LB agar when it was at a temperature of 60°C.µl

S1.1.3 TAE x 50 agarose gel electrophoresis buffer (per 500ml)

Tris base	121g
Acetic acid	28.5ml
EDTA 0.5M	50ml

Adjust pH to 7.4 with acetic acid. Make up to 500ml with ddH₂O.

S1.1.4 Standard Ringer's solution (per 1l)

150mM NaCl	8.76g
4mM KCl	0.29g
2mM MgCl ₂	0.19g

2mM CaCl ₂	0.22g
10mM HEPES	2.38g
ddH ₂ O	900ml

pH to .3 with NaOH) and adjust volume to 1 litre with double distilled H₂O. Pass through 0.22µm filter to sterilize.

S1.2 Fly Transformation recipes

S1.2.1 Molasses agar plates for flies

400ml boiling water

160ml molasses

10g agar

10ml ethanol (absolute)

5ml acetic acid (glacial)

1.2.2 Fly food rearing vials

1L boiling water

188g Nutrifly Food (FlyStuff)

5ml Propionic acid

5ml Nipagin (15% in ethanol)

1.2.3 Agar Bioassay vials

1L boiling water

20g Agar

12g sugar

3.9ml Acetic acid

1.2.4 Injection plates

1L boiling water

2 sachets grape juice agar premix (Genesee Scientific)

10g agar

4ml Acetic acid

1.2.5 Drosophila transgenic injection solution

Total injection solution:

0.5ul fluorescent injection buffer

200-800ng/ul donor plasmid

100-250ng/ul (fv) accessory plasmid (UAS insertion)

50-100ng/ul pCFD4-U6:1_U6:3 tandem gRNAs plasmid (CRISPR/Cas9 insertion)

Up to 10ul volume with micropore filtered ddH₂O

1.2.6 Fluorescent Injection Buffer:

0.05 mM sodium phosphate

2.5 mM KCl

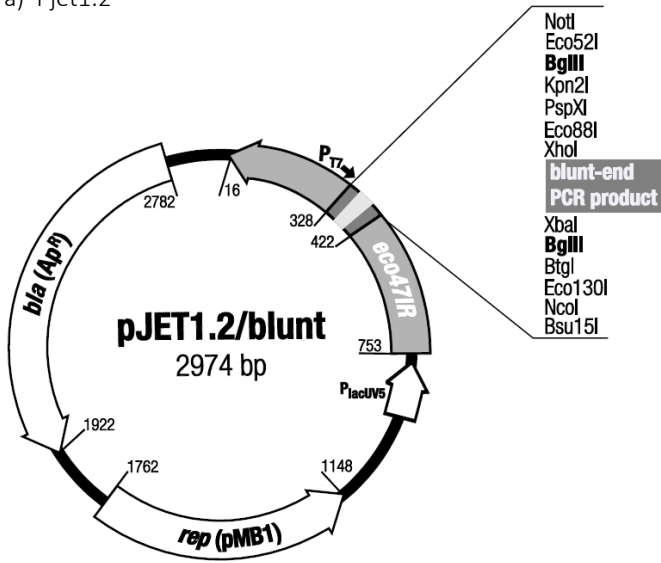
200mg/l Fluorescein sodium salt (Sigma Aldrich)

pH 6.8

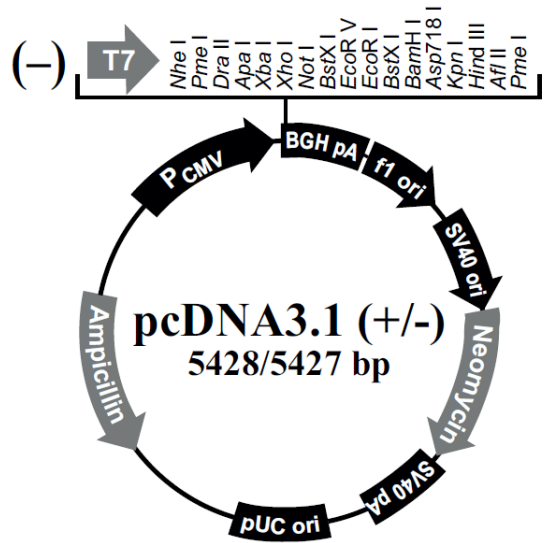
(Store in 1.5ml microcentrifuge tubes, -20C, dark)

S2 Supplementary Materials

a) Pjet1.2



b) pcDNA3.1(-)



b) pcDNA3.1(-)

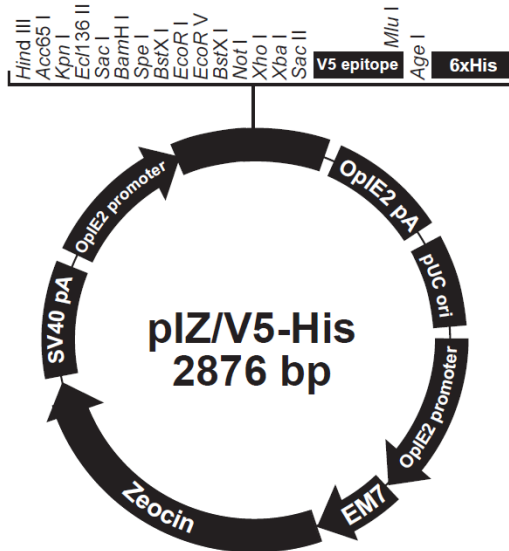


Fig. S1 Vector Maps

Table S1 PxRyR sequencing primers

PxRyR F1	TACAGGACAAGAACATACCGCCC
PxRyR R1	TGTGGTTGCCCTTATGATTGCC
PxRyR F2	ATCTGATCCTGGAGGCGATTGAC
PxRyR R2	GTGTGATCGTAAGCGTGCAACC
PxRyR F3	GCTAGTCGAGTGTCTACTGCCTC
PxRyR R3	ATATGGGCTGGTCCTTCGTGTAC
PxRyR F4	ACGAGCCATTCTGTGTCAACATG
PxRyR R4	TGGAAACTGCATCTTCACACAGC
PxRyR F5	TGCCAAACCAATCTCTGCAAGTC
PxRyR R5	CGATGGTCTGGATCAGCACTTTG
PxRyR F6	AGAAGAGCCAGTGAAGAAGACCC
PxRyR R6	CTACTAGGAAGTCTGACACCGCC
PxRyR F7	GAGACTCAGGAGCTGTTCTACCG
PxRyR R7	TCCTTTAAACTAGCCGCCCTAC
PxRyR F8	ACAAAGCGAAACAGAACAGACCG
PxRyR R8	TGGTTGTATAGCTCTTCCGCCTC
PxRyR F9	TCTACCCGCTGCTCATCAAGTAC
PxRyR R9	GTAGGTAGTCCACGGTGCAGATC
PxRyR F10	CCGGTTCATACAGCTCACTTGTG
PxRyR R10	TGTTTCGCTGGAGATAAGGACGAG
PxRyR F11	GA CTCACGCTTCCGGTTTAATGG
PxRyR R11	CTGCGCCTCTATCCTCTCTTGAG
PxRyR F12	TGGTGAACAAGCCAAGAAGCAAG
PxRyR R12	AAGAACCCTCTGCCCTCATCTTC
PxRyR F13	TCAAGCGTGAGAAGGAGATAGCC
PxRyR R13	CCTAAGTCTACTCTCCCATGGCG

Table S2 HRyR2 sequencing primers

HRyR seq 1F	CCTGCGAACTGATGATGAAGTGG
HRyR seq 1R	GAGGGAGCCAGAAAATTGAGCAC
HRyR seq 2F	GTGCTCAATTTTCTGGCTCCCTC
HRyR seq 2R	GTGCTTCCAAGTTGTAGCCGTAC
HRyR seq 3F	GTACGGCTACAACCTGGAAGCAC
HRyR seq 3R	TTGAATAATCCCGCCGAGAGAGG
HRyR seq 4F	ATTCCTGCGGTTTTTGCACAAG
HRyR seq 4R	TTTCTACCAGGGATAGCAGACGC
HRyR seq 5F	AGCTGGATGAAGATGGGTCTCTG
HRyR seq 5R	GCTGTGCAAAGGTACCGATTGAG
HRyR seq 6F	GATACGGCAGCTTTGAGTGCTAC
HRyR seq 6R	TGCCTGACAAGAAGTCCAAGTTTG
HRyR seq 7F	CTCTGCTCTGGAGGACATGCTTC
HRyR seq 7R	AGAGAGGTCTGCATGGAATACCG
HRyR seq 8F	AAATGAAGCGCAAAGGAGATCGG
HRyR seq 8R	ACCATCTGTTTGCCAATCGTTCC
HRyR seq 9F	GCCCATATGCAGATGAAGCTGTC
HRyR seq 9R	TGACTCTGGCACTTCTGGTTCTC
HRyR seq 10F	AAAGTTGAGGCAGCTTCACACAC
HRyR seq 10R	ACTCCGGGAGTCTCAGAAGAAAATC

Reference List

- All, JN. 1999. Cultural approaches to managing arthropod pests. pp. 395–415 In J. R. Ruberson (ed.), *Handbook of Pest Management*. Marcel Dekker Inc., New York. 842 pp
- Genstat for Windows 20th Edition (2019). Hemel Hempstead, UK
- NATEC (2019) Recent reports of fall armyworm in China. Plant pathogen and pest information 2019-4-26
- Abe T, Ishida H, Matsuno A (1997) Foot Structure and Foot Protein in the Cross Striated Muscle of a Pecten. *Cell structure and function* 22:21-26
- International Energy Agency (2016) *World Energy Outlook*. Organization for Economic Cooperation and Development
- AGI2527 (2017) *Insecticides Market by Type (Pyrethroids, Organophosphorus, Carbamates, Organochlorine, Botanicals), Crop Type, Mode of Application, Formulation (WP, EC, SC, EW, ME, GR), and Region - Global Forecast to 2022*. Markets and Markets
- Johnson I, Dudley N, and Alexander S (2017) *Global Land Outlook UNCCD*
- Alexandratos N, Bruinsma J (2012) *WORLD AGRICULTURE TOWARDS 2030/2050*. FAO Agricultural Development Economics Division ESA Working Paper No. 12-03
- Anderson C, Oakeshott J, Taya W, Gordona K, Zwicka A, Walsh T (2019) Hybridization and gene flow in the mega-pest lineage of moth, *Helicoverpa*. *PNAS* 115:5034. doi:10.1073/pnas.1718831115
- Antaramian A, Butanda-Ochoa A, Vazquez-Martinez O, Diaz-Munoz M, Vaca L (2001) Functional expression of recombinant type 1 ryanodine receptor in insect Sf21 cells. *Cell Calcium* 30 (1):9-17. doi:DOI 10.1054/ceca.2001.0208
- Babu YS SJ, Greenhough TJ, Bugg CE, Means AR, Cook WJ. (1985) Three-Dimensional Structure of Calmodulin. *Nature* 2-8:37-40
- Bajzelj B, Allwood JM, Cullen JM (2013) Designing climate change mitigation plans that add up. *Environ Sci Technol* 47 (14):8062-8069. doi:10.1021/es400399h
- Bale JS, van Lenteren JC, Bigler F (2008) Biological control and sustainable food production. *Philosophical transactions of the Royal Society of London Series B, Biological sciences* 363 (1492):761-776. doi:10.1098/rstb.2007.2182
- Balshaw D, Gao L, Meissner G (1999) Luminal loop of the ryanodine receptor: A pore-forming segment? *Proceedings of the National Academy of Sciences of the United States of America* 96 (7):3345-3347. doi:DOI 10.1073/pnas.96.7.3345
- Bammes B et al (2012) Direct electron detection yields cryo-EM reconstructions at resolutions beyond $\frac{3}{4}$ Nyquist frequency. *J Struct Biol* 177:589
- Bass C, Denholm I, Williamson MS, Nauen, R (2015) The global status of resistance to neonicotinoid insecticides
- Bass C, Field LM (2011) Gene amplification and insecticide resistance. *Pest Management Science* 67 (8):886-890. doi:10.1002/ps.2189
- Battisti DS, Naylor RL (2009) Historical Warnings of Future Food Insecurity with Unprecedented Seasonal Heat. *Science* 323 (5911):240-244. doi:10.1126/science.1164363
- Baumann O (2000) Distribution of ryanodine receptor Ca²⁺ channels in insect photoreceptor cells. *Journal of Comparative Neurology* 421 (3):347-361

- BAYER (2019) Crop Compendium. <https://www.cropsciencebayer.com/en/crop-compendium/pests-diseases-weeds/pests/chilo-suppressalis>
- Benkusky NA, Weber CS, Scherman JA, Farrell EF, Hacker TA, John MC, Powers PA, Valdivia HH (2007) Intact α -Adrenergic Response and Unmodified Progression Toward Heart Failure in Mice With Genetic Ablation of a Major Protein Kinase A Phosphorylation Site in the Cardiac Ryanodine Receptor. *101* (8):819-829. doi:10.1161/circresaha.107.153007
- Berridge MJ, Bootman MD, Roderick HL (2003) Calcium signalling: Dynamics, homeostasis and remodelling. *Nature Reviews Molecular Cell Biology* 4 (7):517-529. doi:10.1038/Nrm1155
- Bers DM (2002) Cardiac excitation-contraction coupling. *Nature* 415 (6868):198-205
- Bers DM (2004) Macromolecular complexes regulating cardiac ryanodine receptor function. *Journal of Molecular and Cellular Cardiology* 37 (2):417-429
- Bezprozvanny IB, Ondrias K, Kaftan E, Stoyanovsky DA, Ehrlich BE (1993) Activation of the calcium release channel (ryanodine receptor) by heparin and other polyanions is calcium-dependent. *Molecular Biology of the Cell* 4 (3):347-352
- Bhat MB, Zhao J, Takeshima H, Ma J (1997) Functional calcium release channel formed by the carboxyl-terminal portion of ryanodine receptor. *Biophysical Journal* 73 (3):1329-1336. doi:10.1016/s0006-3495(97)78166-9
- Biondi A, Guedes RNC, Wan F-H, Desneux N (2018) Ecology, Worldwide Spread, and Management of the Invasive South American Tomato Pinworm, *Tuta absoluta*: Past, Present, and Future. *Annual Review of Entomology* 63 (1):239-258. doi:10.1146/annurev-ento-031616-034933
- Bird LJ (2016) Susceptibility of *Helicoverpa armigera* (Lepidoptera: Noctuidae) to Cyantraniliprole Determined From Topical and Ingestion Bioassays. *109* (3):1350-1356. doi:10.1093/jee/tow027
- Birkett R (2012) DuPont debuts Cyazypyr in Argentina. *Agrow Agribusiness* 29 Oct
- Bischof J, Maeda RK, Hediger M, Karch F, Basler K (2007) An optimized transgenesis system for *Drosophila* using germ-line-specific C31 integrases. *Proceedings of the National Academy of Sciences* 104 (9):3312-3317. doi:10.1073/pnas.0611511104
- Black W, Alphey L, James AA (2011) Why RIDL is not SIT. *Trends Parasitol* 27 (8):362-370. doi:10.1016/j.pt.2011.04.004
- Blayney LM, Lai FA (2009) Ryanodine receptor-mediated arrhythmias and sudden cardiac death. *Pharmacology & Therapeutics* 123 (2):151-177. doi:10.1016/j.pharmthera.2009.03.006
- Boaventura D, Bolzan A, Padovez FEO, Okuma DM, Omoto C, Nauen R (2019) Detection of a ryanodine receptor target-site mutation in diamide insecticide resistant fall armyworm, *Spodoptera frugiperda*. *Pest Manag Sci* [Pre-Print]. doi:10.1002/ps.5505
- Bogart K, Andrews J (2006-2010) Extraction of Total RNA from *Drosophila*. CGB Technical Report. Center for Genomics and Bioinformatics, Indiana University, Bloomington, Indiana. doi:10.2506/cgbtr-200610
- Bolzan A, Padovez FE, Nascimento AR, Kaiser IS, Lira EC, Amaral FS, Kanno RH, Malaquias JB, Omoto C (2019) Selection and characterization of the inheritance of resistance of *Spodoptera frugiperda* (Lepidoptera: Noctuidae) to chlorantraniliprole and cross-resistance to other diamide insecticides. *Pest Manag Sci*. doi:10.1002/ps.5376
- Brand AH, Perrimon N (1993) Targeted gene expression as a means of altering cell fates and generating dominant phenotypes. *Development* 118:401

- Brinkman, Cullen (2011) Food Insecurity and Violent Conflict: Causes, Consequences, and Addressing the Challenges. World Food Programme
- Buchman A, Gamez S, Li M, Antoshechkin I, Li HH, Wang HW, Chen CH, Klein MJ, Duchemin JB, Paradkar PN, Akbari OS (2019) Engineered resistance to Zika virus in transgenic *Aedes aegypti* expressing a polycistronic cluster of synthetic small RNAs. *Proceedings of the National Academy of Sciences of the United States of America* 116 (9):3656-3661. doi:10.1073/pnas.1810771116
- Camors E, Valdivia H (2014) CaMKII regulation of cardiac ryanodine receptors and inositol triphosphate receptors. *Front Pharmacol*
- Campos MR, Silva TBM, Silva WM, Silva JE, Siqueira HAA (2015) Susceptibility of *Tuta absoluta* (Lepidoptera: Gelechiidae) Brazilian populations to ryanodine receptor modulators. *Pest Management Science* 71 (4):537-544. doi:10.1002/ps.3835
- Capinera JL (1999) Beet Armyworm, *Spodoptera exigua* (Hübner) (Insecta: Lepidoptera: Noctuidae). IFAS
- Casida JE (2018) Radioligand recognition of insecticide targets. *Journal of Agricultural and Food Chemistry* 66:3277-3290
- Casper T, Cordova D, Gutteridge S, Rauh JJ, Smith RM, Wu L, Tao Y (2010) Isolation and use of ryanodine receptors. US 07655395,
- Chapman D, Purse BV, Roy HE, Bullock JM (2017) Global trade networks determine the distribution of invasive non-native species. *Global Ecology and Biogeography* 26 (8):907-917. doi:10.1111/geb.12599
- Che W, Shi T, Wu Y, Yang Y (2013) Insecticide Resistance Status of Field Populations of *Spodoptera exigua* (Lepidoptera: Noctuidae) From China. *Journal of Economic Entomology* 106 (4):1855-1862. doi:10.1603/ec13128
- Chen J (2018) Chlorantraniliprole weak activator of mammalian skeletal RyR.
- Chen SRW, Ebisawa K, Li X, Zhang L (1998) Molecular Identification of the Ryanodine Receptor Ca²⁺ Sensor. 273 (24):14675-14678. doi:10.1074/jbc.273.24.14675
- Chen W, Wang R, Chen B, Zhong X, Kong H, Bai Y, Zhou Q, Xie C, Zhang J, Guo A, Tian X, Jones PP, O'Mara ML, Liu Y, Mi T, Zhang L, Bolstad J, Semeniuk L, Cheng H, Zhang J, Chen J, Tieleman DP, Gillis AM, Duff HJ, Fill M, Song L-S, Chen SRW (2014) The ryanodine receptor store-sensing gate controls Ca²⁺ waves and Ca²⁺-triggered arrhythmias. 20 (2):184-192. doi:10.1038/nm.3440
- Cho S-R, et al (2018) Susceptibility of field populations of *Plutella xylostella* and *Spodoptera exigua* to four diamide insecticides. *Korean J Appl Entomol* 57 (1):43-50
- Chorna T, Hasan G (2012) The genetics of calcium signaling in *Drosophila melanogaster*. *Biochimica Et Biophysica Acta-General Subjects* 1820 (8):1269-1282. doi:10.1016/j.bbagen.2011.11.002
- Collet C (2009) Excitation-contraction coupling in skeletal muscle fibers from adult domestic honeybee. *Pflugers Archiv-European Journal of Physiology* 458 (3):601-612. doi:10.1007/s00424-009-0642-6
- Collet C, Belzunces L (2007) Excitable properties of adult skeletal muscle fibres from the honeybee *Apis mellifera*. *J Exp Biol* 210 (Pt 3):454-464. doi:10.1242/jeb.02667
- Insecticide Resistance Action Committee (2019) IRAC Online. <https://www.iraconline.org/about/resistance/mechanisms/>
- Insecticide Resistance Action Committee (2014) eConnection. IRAC Newsletter (Issue 33)

- Cordova D, Benner EA, Sacher MD, Rauh JJ, Sopa JS, Lahm GP, Selby TP, Stevenson TM, Flexner L, Gutteridge S, Rhoades DF, Wu L, Smith RM, Tao Y (2006) Anthranilic diamides: A new class of insecticides with a novel mode of action, ryanodine receptor activation. *Pesticide Biochemistry and Physiology* 84 (3):196-214. doi:10.1016/j.pestbp.2005.07.005
- Coustau C, Chevillon C, Ffrench-Constant R (2000) Resistance to xenobiotics and parasites: can we count the cost? *Evolution* 54 (9):378-383. doi:10.1016/s0169-5347(00)01929-7
- Cunningham JP, Zalucki MP (2014) Understanding Heliiothine (Lepidoptera: Heliiothinae) Pests: What is a Host Plant? *Journal of Economic Entomology* 107 (3):881-896. doi:10.1603/ec14036
- CropLife 2012. www.croplifeamerica.org/
- D'Cruz AA, Babon JJ, Norton RS, Nicola NA, Nicholson SE (2013) Structure and function of the SPRY/B30.2 domain proteins involved in innate immunity. *Protein Science* 22 (1):1-10. doi:10.1002/pro.2185
- Day R, Abrahams P, Bateman M, Beale T, Clottey V, Cock M, Colmenarez Y, Corniani N, Early R, Godwin J, Gomez J, Moreno PG, Murphy ST, Oppong-Mensah B, Phiri N, Pratt C, Silvestri S, Witt A (2017) Fall Armyworm: Impacts and Implications for Africa. *Outlooks on Pest Management* 28 (5):196-201. doi:10.1564/v28_oct_02
- Des Georges A, Clarke OB, Zalk R, Yuan Q, Condon KJ, Grassucci RA, Hendrickson WA, Marks AR, Frank J (2016) Structural Basis for Gating and Activation of RyR1. *Cell* 167 (1):145-157.e117. doi:10.1016/j.cell.2016.08.075
- des Georges AC, O. Zalk, R. Frank, J et al. (2016) Structural basis for gating and activation of RyR1.
- Desneux N, Wajnberg E, Wyckhuys KAG, Burgio G, Arpaia S, Narváez-Vasquez CA, González-Cabrera J, Catalán Ruescas D, Tabone E, Frandon J, Pizzol J, Poncet C, Cabello T, Urbaneja A (2010) Biological invasion of European tomato crops by *Tuta absoluta*: ecology, geographic expansion and prospects for biological control. *Journal of Pest Science* 83 (3):197-215. doi:10.1007/s10340-010-0321-6
- Deutsch CA, Tewksbury JJ, Tigchelaar M, Battisti DS, Merrill SC, Huey RB, Naylor RL (2018) Increase in crop losses to insect pests in a warming climate. *Science* 361 (6405):916-919. doi:10.1126/science.aat3466
- Domingo A, et al (1998) Troponin-T is a calcium-binding protein in insect muscle: in vivo phosphorylation, muscle-specific isoforms and developmental role in *Drosophila melanogaster*. *Journal of Muscle Research and Cell Motility* 19:393-403
- Douris V, Papapostolou K-M, Ilias A, Roditakis E, Kounadi S, Riga M, Nauen R, Vontas J (2017) Investigation of the contribution of RyR target-site mutations in diamide resistance by CRISPR/Cas9 genome modification in *Drosophila*. *Insect Biochemistry and Molecular Biology* 87:127-135. doi:10.1016/j.ibmb.2017.06.013
- Early R, González-Moreno P, Murphy ST, Day R (2018) Forecasting the global extent of invasion of the cereal pest *Spodoptera frugiperda*, the fall armyworm. *NeoBiota* 40:25-50. doi:10.3897/neobiota.40.28165
- Ebbinghaus-Kintscher U, Luemmen P, Lobitz N, Schulte T, Funke C, Fischer R, Masaki T, Yasokawa N, Tohnishi M (2006) Phthalic acid diamides activate ryanodine-sensitive Ca²⁺ release channels in insects. *Cell Calcium* 39 (1):21-33. doi:DOI 10.1016/j.ceca.2005.09.002

- Ebbinghaus-Kintscher U, Lummen P, Raming K, Masaki T, Yasokawa N (2007) Flubendiamide, the first insecticide with a novel mode of action on insect ryanodine receptors. *Pflanzenschutz-Nachrichten Bayer* 60 (2):117-140
- Efremov RG, Leitner A, Aebersold R, Raunser S (2015) Architecture and conformational switch mechanism of the ryanodine receptor. *Nature* 517 (7532):39-43. doi:10.1038/nature13916
- EPA (2019) <https://ecotox.ipmcenters.org/>. Southern IPM Centre
- Ewald JA, Wheatley CJ, Aebischer NJ, Moreby SJ, Duffield SJ, Crick HQP, Morecroft MB (2015) Influences of extreme weather, climate and pesticide use on invertebrates in cereal fields over 42 years. *21* (11):3931-3950. doi:10.1111/gcb.13026
- Fabiato A FF (1977) Calcium release from the sarcoplasmic reticulum. *Circ Res* 40:119-129
- Fader M, Rulli MC, Carr J, Dell'Angelo J, D'Odorico P, Gephart JA, Kummu M, Magliocca N, Porkka M, Prell C, Puma MJ, Ratajczak Z, Seekell DA, Suweis S, Tavoni A (2016) Past and present biophysical redundancy of countries as a buffer to changes in food supply. *Environmental Research Letters* 11 (5). doi:10.1088/1748-9326/11/5/055008
- FAO (2009) Feeding the world in 2050. World agricultural summit on food security, Rome 12-13 October 2009 1-4
- FAO (2017) The Future of Food and Agriculture: Trends and Challenges. Rome
- Ffrench-Constant RH, Bass C (2017) Does resistance really carry a fitness cost? *Current Opinion in Insect Science* 21:39-46. doi:10.1016/j.cois.2017.04.011
- Fill M, Copello JA (2002) Ryanodine receptor calcium release channels. *Physiological Reviews* 82 (4):893-922. doi:DOI 10.1152/physrev.00013.2002
- Foster SP, Denholm I, Rison JL, Portillo HE, Margaritopoulos J, Slatere R (2012) Susceptibility of standard clones and European field populations of the green peach aphid, *Myzus persicae*, and the cotton aphid, *Aphis gossypii* (Hemiptera: Aphididae), to the novel anthranilic diamide insecticide cyantraniliprole. *Pest Management Science* 68 (4):629-633. doi:10.1002/ps.2306
- Ellen MacArthur Foundation(2019) Cities and Circular Economy for Food.
- Fox, Bell J, Shortall C (2018) Insect Population trends and the IUCN
- France-Presse A (2016) Nobel winners slam greenpeace for anti-GMO campaign. *Guardian* 16 June
- Furuichi T, Yoshikawa S, Miyawaki A, Wada K, Maeda N, Mikoshiba K (1989) Primary structure and functional expression of the inositol 1,4,5-trisphosphate-binding protein P400. *Nature* 342 (6245):32-38. doi:10.1038/342032a0
- Gao C, Yao R, Zhang Z, Wu M, Zhang S, Su J (2013) Susceptibility Baseline and Chlorantraniliprole Resistance Monitoring in *Chilo suppressalis* (Lepidoptera: Pyralidae). *106* (5):2190-2194. doi:10.1603/ec13058
- Gao L, Tripathy A, Lu XY, Meissner G (1997) Evidence for a role of C-terminal amino acid residues in skeletal muscle Ca²⁺ release channel (ryanodine receptor) function. *FEBS Letters* 412 (1):223-226. doi:Doi 10.1016/S0014-5793(97)00781-3
- George, CH, Jundi, H, Thomas NL, Fry DL, Lai FA (2007) Ryanodine receptors and ventricular arrhythmias: Emerging trends in mutations, mechanisms and therapies
- George CH, Higgs GV, Lai FA (2003a) Ryanodine receptor mutations associated with stress-induced ventricular tachycardia mediate increased calcium release in stimulated cardiomyocytes. *Circ Res* 93 (6):531-540. doi:10.1161/01.RES.0000091335.07574.86

- George CH, Higgs GV, Mackrill JJ, Lai FA (2003b) Dysregulated ryanodine receptors mediate cellular toxicity - Restoration of normal phenotype by FKBP12.6. *Journal of Biological Chemistry* 278 (31):28856-28864. doi:10.1074/jbc.M212440200
- George CH, Jundi H, Thomas NL, Scoote M, Walters N, Williams AJ, Lai FA (2004) Ryanodine receptor regulation by intramolecular interaction between cytoplasmic and transmembrane domains. *Molecular Biology of the Cell* 15 (6):2627-2638. doi:DOI 10.1091/mbc.E03-09-0688
- George CH, Lai A (2002) In situ regulation of the human cardiac ryanodine receptor (hRyR2) by intramolecular interaction. *Biophysical Journal* 82 (1):624a-624a
- Gillespie (2014) Selecting ions by size in a calcium channel.
- Gilligan T, Goldstein P, Timm A, Farris R, Ledezma L, Cunningham A (2015) Identification of Heliethine (Lepidoptera: Noctuidae) Larvae Intercepted at U.S. Ports of Entry From the New World. *Journal of Economic Entomology* 112:603. doi:10.1093/jee/toy402
- Gnam C, Jeanguenat A, Dutton AC, Grimm C, Kloer DP, Crossthwaite AJ (2012) Novel diamide insecticides: Sulfoximines, sulfonimidamides and other new sulfonimidoyl derivatives. *Bioorganic & Medicinal Chemistry Letters* 22 (11):3800-3806. doi:10.1016/j.bmcl.2012.03.106
- Gordon KHJ, Waterhouse PM (2007) RNAi for insect-proof plants. 25 (11):1231-1232. doi:10.1038/nbt1107-1231
- Grimaldi D, Engel MS (2005) *Evolution of the Insects*. Cambridge University Press,
- Grynkiwicz G, Poenie M, Tsien R (1985) A New Generation of Ca²⁺ Indicators with Greatly Improved Fluorescence Properties. *Journal of Biological Chemistry* 260:3440
- Guedes R, Roditakis E, Campos M, Haddi K, Bielza P, Siqueira H, Tsagkarakou A, Vontas J, Nauen R (2019) Insecticide resistance in the tomato pinworm *Tuta absoluta*: patterns, spread, mechanisms, management and outlook. *Journal of Pest Science*. doi:<https://doi.org/10.1007/s10340-019-01086-9>
- Guedes RNC (2016) Insecticide Resistance, Control Failure Likelihood, & the First Law of Geography. doi:10.1002/ps.4452
- Guillén F (2017) Mechanisms of Ryanodine Receptor 2 Regulation in Cardiac Pathophysiology.
- Guo L, Liang P, Zhou X, Gao X (2014a) Novel mutations and mutation combinations of ryanodine receptor in a chlorantraniliprole resistant population of *Plutella xylostella* (L.). *Scientific Reports* 4. doi:10.1038/srep06924
- Guo L, Wang Y, Zhou X, Li Z, Liu S, Pei L, Gao X (2014b) Functional analysis of a point mutation in the ryanodine receptor of *Plutella xylostella* (L.) associated with resistance to chlorantraniliprole. *Pest management science* 70 (7). doi:10.1002/ps.3651
- Guo T, Cornea R, Fruen B, D. B (2008) FRET between FKBP and CaM located on the Ryanodine Receptor in the Cardiac Myocyte Environment. *Biophys J* 94:2127
- Guo W, Sun B, Xiao Z, Liu Y, Wang Y, Zhang L, Wang R, Chen SRW (2015) The EF-hand Ca²⁺ Binding Domain Is Not Required for Cytosolic Ca²⁺ Activation of the Cardiac Ryanodine Receptor. doi:10.1074/jbc.M115.693325. doi:10.1074/jbc.M115.693325
- Gutierrez-Moreno R, Mota-Sanchez D, Blanco CA, Whalon ME, Teran-Santofimio H, Rodriguez-Maciel JC, DiFonzo C (2019) Field-Evolved Resistance of the Fall Armyworm (Lepidoptera: Noctuidae) to Synthetic Insecticides in Puerto Rico and Mexico. *J Econ Entomol* 112 (2):792-802. doi:10.1093/jee/toy372

- Haghighat-Khah RE, Scaife S, Martins S, St John O, Matzen KJ, Morrison N, Alphey L (2015) Site-Specific Cassette Exchange Systems in the *Aedes aegypti* Mosquito and the *Plutella xylostella* Moth. 10 (4):e0121097. doi:10.1371/journal.pone.0121097
- Hall T (2007) Ecological effects assessment of flubendiamide. *Pflanzenschutz-Nachrichten Bayer* 16:7-182
- Hallman C, al e (2017) More than 75 percent decline over 27 years in total flying insect biomass in protected areas.
- Hamaguchi H, Hirooka T, Masaki T, Lahm GP, Cordova D, Barry JD, Andaloro JT, Annan IB, Marcon PC, Portillo HE, Stevenson TM, Selby TP (2012) Insecticides Affecting Calcium Homeostasis. In: *Modern Crop Protection Compounds*. Wiley-VCH Verlag GmbH & Co. KGaA, pp 1389-1425. doi:10.1002/9783527644179.ch34
- Han P, Bayram Y, Shaltiel-Harpaz L, Sohrabi F, Saji A, Esenali UT, Jalilov A, Ali A, Shashank PR, Ismoilov K, Lu Z-z, Wang S, Zhang G-f, Wan F-h, Biondi A, Desneux N (2018) *Tuta absoluta* continues to disperse in Asia: damage, ongoing management and future challenges. *Journal of Pest Science*. doi:10.1007/s10340-018-1062-1
- He Y, Zhang J, Chen J (2014) Effect of synergists on susceptibility to chlorantraniliprole in field populations of *Chilo suppressalis* (Lepidoptera: Pyralidae). *J Econ Entomol* 107 (2):791-796. doi:10.1603/ec13414
- Herrero M, Henderson B, Havlík P, Thornton PK, Conant RT, Smith P, Wirsenius S, Hristov AN, Gerber P, Gill M, Butterbach-Bahl K, Valin H, Garnett T, Stehfest E (2016) Greenhouse gas mitigation potentials in the livestock sector. *Nature Climate Change* 6 (5):452-461. doi:10.1038/nclimate2925
- Hirooka T, Nishimatsu T, Kodama H, Reckmann U, Nauen R (2007) The biological profile of flubendiamide, a new benzenedicarboxamide insecticide. *Pflanzenschutz-Nachrichten Bayer* 60 (2):183
- Hirooka, T. ***Plant Protection*** 72, 58–63 (2018) (Translated)
- Homem RA, Davies TGE (2018) An overview of functional genomic tools in deciphering insecticide resistance. *Curr Opin Insect Sci* 27:103-110. doi:10.1016/j.cois.2018.04.004
- Hwang JH, Zorzato F, Clarke NF, Treves S (2012) Mapping domains and mutations on the skeletal muscle ryanodine receptor channel. *Trends in Molecular Medicine* 18 (11):644-657. doi:10.1016/j.molmed.2012.09.006
- CABI International (2019) *Invasive Species Compendium*. <https://www.cabi.org/isc/search/index>
- Inui M, Saito A, Fleischer S (1987) Isolation of the ryanodine receptor from cardiac sarcoplasmic-reticulum and identity with the feet structures. *Journal of Biological Chemistry* 262 (32):15637-15642
- IRAC (2019) *Arthropod Pesticide Resistance Database*. <https://www.pesticideresistance.org/displayphp?page=species&arId=571>
Accessed 21/6/2019
- Isaacs AK, Qi S, Sarpong R, Casida JE (2012) Insect ryanodine receptor: distinct but coupled insecticide binding sites for N-C(3)H(3) chlorantraniliprole, flubendiamide, and (3)H ryanodine. *Chemical research in toxicology* 25 (8):1571-1573
- ISKBC (2017) <http://www.iskbc.com/>. 11 Feb
- Janzen D, Hallwachs W (2019) Perspective: Where might be many tropical insects? *Biological Conservation* 233 (102-108). doi:10.1016/j.biocon.2019.02.030
- Jeanguenat A (2013) The story of a new insecticidal chemistry class: the diamides. *Pest Management Science* 69 (1):7-14. doi:10.1002/ps.3406

- Jeschke P (2010) The unique role of halogen substituents in the design of modern agrochemicals. *Pest Management Science* 66 (1):10-27. doi:10.1002/ps.1829
- Kang WJ, Koo H-N, Jeong D-H, Kim HK, Kim J, Kim G-H (2017) Functional and genetic characteristics of Chlorantraniliprole resistance in the diamondback moth, *Plutella xylostella* (Lepidoptera: Plutellidae). *Entomological Research* 47 (6):394-403. doi:10.1111/1748-5967.12258
- Kato K, Kiyonaka S, Sawaguchi Y, Tohnishi M, Masaki T, Yasokawa N, Mizuno Y, Mori E, Inoue K, Hamachi I, Takeshima H, Mori Y (2009) Molecular characterization of flubendiamide sensitivity in the Lepidopterous ryanodine receptor Ca²⁺ release channel. *Biochemistry* 48 (43):10342-10352. doi:10.1021/Bi900866s
- Kfir R (1998) Origin of the Diamondback Moth (Lepidoptera: Plutellidae). *91* (2):164-167. doi:10.1093/aesa/91.2.164
- Kriticos DJ, Ota N, Hutchison WD, Beddow J, Walsh T, Tay WT, Borchert DM, Paula-Moreas SV, Czepak C, Zalucki MP (2015) The Potential Distribution of Invading *Helicoverpa armigera* in North America: Is It Just a Matter of Time? *10* (3):e0119618. doi:10.1371/journal.pone.0119618
- Kuboniwa H, Tjandra N, Grzesiek S, Ren H, Klee CB, Bax A (1995) Solution structure of calcium-free calmodulin. *Nature Structural Biology* 2 (9):768-776. doi:10.1038/nsb0995-768
- Lahm GP, Cordova D, Barry JD (2009) New and selective ryanodine receptor activators for insect control. *Bioorganic & Medicinal Chemistry* 17 (12):4127-4133. doi:10.1016/j.bmc.2009.01.018
- Lahm GP, Stevenson TM, Selby TP, Freudenberger JH, Cordova D, Flexner L, Bellin CA, Dubas CM, Smith BK, Hughes KA, Hollingshaus JG, Clark CE, Benner EA (2007) Rynaxypyr (TM): A new insecticidal anthranilic diamide that acts as a potent and selective ryanodine receptor activator. *Bioorganic & Medicinal Chemistry Letters* 17 (22):6274-6279. doi:10.1016/j.bmc.2007.09.012
- Lai T, Li J, Su J (2011) Monitoring of beet armyworm *Spodoptera exigua* (Lepidoptera: Noctuidae) resistance to chlorantraniliprole in China. *Pesticide Biochemistry and Physiology* 101:198-205
- Larach MG, Gronert GA, Allen GC, Bandom BW, Lehman EB (2010) Clinical presentation, treatment, and complications of malignant hyperthermia in North America from 1987 to 2006. *Anesth Analg* 110 (2):498-507. doi:10.1213/ANE.0b013e3181c6b9b2
- Lee PT, et al (2018) A gene-specific T2A-GAL4 library for *Drosophila*.
- Li N, Wang Q, Sibrian-Vazquez M, Klipp RC, Reynolds JO, Word TA, Scott L, Salama G, Strongin RM, Abramson JJ, Wehrens XHT (2017) Treatment of catecholaminergic polymorphic ventricular tachycardia in mice using novel RyR2-modifying drugs. *International Journal of Cardiology* 227:668-673. doi:10.1016/j.ijcard.2016.10.078
- Li P (2001) Molecular Basis of Ca²⁺ Activation of the Mouse Cardiac Ca²⁺ Release Channel (Ryanodine Receptor). *118* (1):33-44. doi:10.1085/jgp.118.1.33
- Li X-J, et al. (2019) Prediction of migratory routes of the invasive fall armyworm in eastern China using a trajectory analytical approach. [PRE-PRINT]. doi:10.1101/625632
- Lichtenberg EM, Kennedy CM, Kremen C, Batáry P, Berendse F, Bommarco R, Bosque-Pérez NA, Carvalheiro LG, Snyder WE, Williams NM, Winfree R, Klatt BK, Åström S, Benjamin F, Brittain C, Chaplin-Kramer R, Clough Y, Danforth B, Diekötter T, Eigenbrode SD, Ekroos J, Elle E, Freitas BM, Fukuda

- Y, Gaines-Day HR, Grab H, Gratton C, Holzschuh A, Isaacs R, Isaia M, Jha S, Jonason D, Jones VP, Klein A-M, Krauss J, Letourneau DK, Macfadyen S, Mallinger RE, Martin EA, Martinez E, Memmott J, Morandin L, Neame L, Otieno M, Park MG, Pfiffner L, Pocock MJO, Ponce C, Potts SG, Poveda K, Ramos M, Rosenheim JA, Rundlöf M, Sardiñas H, Saunders ME, Schon NL, Sciligo AR, Sidhu CS, Steffan-Dewenter I, Tscharrntke T, Veselý M, Weisser WW, Wilson JK, Crowder DW (2017) A global synthesis of the effects of diversified farming systems on arthropod diversity within fields and across agricultural landscapes. *Global Change Biology* 23 (11):4946-4957. doi:10.1111/gcb.13714
- Lin L, Hao Z, Cao P, Yuchia Z (2019) Homology modeling and docking study of diamondback moth ryanodine receptor reveals the mechanisms for channel activation, insecticide binding and resistance. [PRE-PRINT]. doi:10.1002/ps.5640
- Lin L, Liu C, Qin J, Wang J, Dong S, Chen W, He W, Gao Q, You M, Yuchi Z (2018) Crystal structure of ryanodine receptor N-terminal domain from *Plutella xylostella* reveals two potential species-specific insecticide-targeting sites. *Insect Biochemistry and Molecular Biology* 92:73-83. doi:10.1016/j.ibmb.2017.11.009
- Lister B, Garcia A (2018) Climate Driven declines in insect populations.
- Liu JB, Li FY, Dong JY, Li YX, Zhang XL, Wang YH, Xiong LX, Li ZM (2018) Anthranilic diamides derivatives as potential ryanodine receptor modulators: Synthesis, biological evaluation and structure activity relationship. *Bioorg Med Chem* 26 (12):3541-3550. doi:10.1016/j.bmc.2018.05.028
- Liu Y, Gao Y, Liang G, Lu Y (2017) Chlorantraniliprole as a candidate pesticide used in combination with the attracticides for lepidopteran moths. *PLOS ONE* 12 (6):e0180255. doi:10.1371/journal.pone.0180255
- Lobell DB, Burke MB, Tebaldi C, Mastrandrea MD, Falcon WP, Naylor RL (2008) Prioritizing Climate Change Adaptation Needs for Food Security in 2030. *Science* 319 (5863):607-610. doi:10.1126/science.1152339
- Loboda S, Savage j, Buddle C, Schmidt N, Høye T (2017) Declining diversity and abundance of High Arctic fly assemblages over two decades of rapid climate warming. *Ecography* 41 (2)
- Loy RE, Orynbayev M, Xu L, Andronache Z, Apostol S, Zvaritch E, MacLennan DH, Meissner G, Melzer W, Dirksen RT (2010) Muscle weakness in Ryr1I4895T/WT knock-in mice as a result of reduced ryanodine receptor Ca²⁺ ion permeation and release from the sarcoplasmic reticulum. 137 (1):43-57. doi:10.1085/jgp.201010523
- Lu Y, Wang G, Zhong L, Zhang F, Bai Q, Zheng X, Lu Z (2017) Resistance monitoring of *Chilo suppressalis* (Walker) (Lepidoptera: Crambidae) to chlorantraniliprole in eight field populations from east and central China. *Crop Protection* 100:196-202. doi:10.1016/j.cropro.2017.07.006
- Ma J, Wang Y-P, Wu M-F, Gao B-Y, Liu J, Lee G-S, Otuka A, Hu G (2019) High risk of the Fall Armyworm invading into Japan and the Korean Peninsula via overseas migration. *BioRxiv* <http://dx.doi.org/10.1101/662387>. doi:10.1101/662387
- MacLennan DH, Wong PT (1971) Isolation of a calcium-sequestering protein from sarcoplasmic reticulum. *Proceedings of the National Academy of Sciences of the United States of America* 68 (6):1231-1235
- Macrill J (1999) Protein-protein interactions in intracellular Ca²⁺-release channel function. *Biochem J* 337:345

- McCaffery A (1998) Resistance to insecticides in Heliothine Lepidoptera: a global view. *Phil Trans R Soc Lond B* 353
- McPherson P, Campbell K (1993) Characterization of the major brain form of the ryanodine receptor/Ca²⁺ release channel. *J Biol Chem* 268:19785-19790
- Mei Y, Xu L, Mowrey DD, Mendez Giraldez R, Wang Y, Pasek DA, Dokholyan NV, Meissner G (2015) Channel Gating Dependence on Pore Lining Helix Glycine Residues in Skeletal Muscle Ryanodine Receptor. *J Biol Chem* 290 (28):17535-17545. doi:10.1074/jbc.m115.659672
- Meng X, Dong F, Qian K, Miao L, Yang X, Ge H, Wu Z, J W (2019) Transcriptome analysis reveals global gene expression changes of *Chilo suppressalis* in response to sublethal dose of chlorantraniliprole. *Chemosphere* 234 648-657. doi:10.1016/j.chemosphere.2019.06.129
- Mikoshiba K (2011) Role of IP₃ receptor in development. *Cell Calcium* 49 (5):331-340. doi:10.1016/j.ceca.2010.12.006
- Mohamadi P, Razmjou J, Naseri B, Hassanpour M (2017) Population Growth Parameters of *Tuta absoluta* (Lepidoptera: Gelechiidae) on Tomato Plant Using Organic Substrate and Biofertilizers. *Journal of Insect Science* 17:1–7. doi:10.1093/jisesa/iex011
- Montezano D, Specht A, Sosa-Gómez D, Roque-Specht V, Sousa-Silva J, Paula-Moraes S, Peterson J, Hunt T (2018) Host plants of *Spodoptera frugiperda* (Lepidoptera: Noctuidae) in the Americas. *African Entomology* 26 (2)
- Mukherjee S, Thomas NL, Williams AJ (2012) A mechanistic description of gating of the human cardiac ryanodine receptor in a regulated minimal environment. *J Gen Physiol* 140 (2):139-158. doi:10.1085/jgp.201110706
- Murayama T, Kurebayashi N (2011) 2 RyR isoforms in nonmammals.
- Murayama T (2018) Tryptophan in RyR Caffeine binding site mediates Ca²⁺ sensitivity.
- Nagoshi RN, Koffi D, Agboka K, Tounou KA, Banerjee R, Jurat-Fuentes JL, Meagher RL (2017) Comparative molecular analyses of invasive fall armyworm in Togo reveal strong similarities to populations from the eastern United States and the Greater Antilles. *PLoS One* 12 (7):e0181982. doi:10.1371/journal.pone.0181982
- FAO (2019) FAOSTAT. <http://www.fao.org/faostat/en/#home>
- Nauen R, Steinbach D (2016) Resistance to Diamides in Lepidopteran Pests. In: Horowitz A, Ishaaya I (eds) *Advances in Insect Control and Resistance Management*. Springer International, Switzerland,
- Niu T-K, Ashley RH (2000) Expression of Full-Length and Truncated Recombinant Human Brain Type I Inositol 1,4,5-Trisphosphate Receptors in Mammalian and Insect Cells. *J Biol Chem* 273 (1):123-128. doi:10.1006/bbrc.2000.2884
- Nishimoto, R. 2019. Global Trends in the Crop Protection Industry. *J Pestic Sci.* 20; 44(3): 141–147.
- Oerke EC (2006) Crop losses to pests. *Journal of Agricultural Science* 144:31-43. doi:10.1017/s0021859605005708
- EU Official (2019) Current status of the neonicotinoids in the EU.
- Ottini L, Marziali G, Conti A, Charlesworth A, Sorrentino V (1996) Alpha and beta isoforms of ryanodine receptor from chicken skeletal muscle are the homologues of mammalian RyR1 and RyR3. *Biochem J* 315 (Pt 1):207-216
- Owen LN, Catchot AL, Musser FR, Gore J, Cook DC, Jackson R (2013) Susceptibility of *Chrysodeixis includens* (Lepidoptera: Noctuidae) to Reduced-Risk Insecticides. *J Econ Entomol* 96 (2):554-559. doi:10.1653/024.096.0221
- Peng W, et al (2016) Structural basis for the gating mechanism of the type 2 ryanodine receptor RyR2. *Structure* 354 (6310):301

- Pingali PL (2012) Green Revolution: Impacts, limits, and the path ahead. *Proceedings of the National Academy of Sciences of the United States of America* 109 (31):12302-12308. doi:10.1073/pnas.0912953109
- Popp J, Peto K, Nagy J (2013) Pesticide productivity and food security. A review. *Agronomy for Sustainable Development* 33 (1):243-255. doi:10.1007/s13593-012-0105-x
- Porta M D-SP, Neumann JT, Escobar AL, Fleischer S, Copello JA (2012) Coupled gating of skeletal muscle ryanodine receptors is modulated by Ca²⁺, Mg²⁺, and ATP. *Am J Physiol Cell Physiol* 303:682–697
- Pratissoli D, Lima V, Pirovani V, Lima W (2015) Occurrence of *Helicoverpa armigera* (Lepidoptera: Noctuidae) on tomato in the Espírito Santo state. *Horticultura Brasileira* 33:101. doi:10.1590/S0102-053620150000100016
- Pretty J, Benton TG, Bharucha ZP, Dicks LV, Flora CB, Godfray HCJ, Goulson D, Hartley S, Lampkin N, Morris C, Pierzynski G, Prasad PVV, Reganold J, Rockström J, Smith P, Thorne P, Wratten S (2018) Global assessment of agricultural system redesign for sustainable intensification. *Nature Sustainability* 1 (8):441-446. doi:10.1038/s41893-018-0114-0
- Qi S, Casida J (2013) Species differences in chlorantraniliprole and flubendiamide insecticide binding sites in the ryanodine receptor. *Pesticide Biochemistry and Physiology* 107:321. doi:<http://dx.doi.org/10.1016/j.pestbp.2013.09.004>
- Qin C, Wang C-H, Wang Y-Y, Sun S-Q, Wang H-H, Xue C-B (2018) Resistance to Diamide Insecticides in *Plutella xylostella* (Lepidoptera: Plutellidae): Comparison Between Lab-Selected Strains and Field-Collected Populations. *Journal of Economic Entomology* 111 (2):853-859. doi:10.1093/jee/toy043
- R. H. Phipps JRP (2002) Environmental Benefits of Genetically Modified Crops: Global and European Perspectives on Their Ability to Reduce Pesticide Use. *Journal of Animal and Feed Sciences* 11
- Radermacher M, Wagenknecht T, Grassucci R, Frank J, Inui M, Chadwick C, Fleischer S (1992) Cryo-EM of the native structure of the calcium release channel/ryanodine receptor from sarcoplasmic reticulum. *61 (4):936-940*. doi:10.1016/s0006-3495(92)81900-8
- Ramachandran S, Chakraborty A, Xu L, Mei YW, Samsó M, Dokholyan NV, Meissner G (2013) Structural Determinants of Skeletal Muscle Ryanodine Receptor Gating. *Journal of Biological Chemistry* 288 (9):6154-6165. doi:10.1074/jbc.M112.433789
- Ribeiro LMS, Wanderley-Teixeira V, Ferreira HN, Teixeira AAC, Siqueira HAA (2014) Fitness costs associated with field-evolved resistance to chlorantraniliprole in *Plutella xylostella* (Lepidoptera: Plutellidae). *104 (01):88-96*. doi:10.1017/s0007485313000576
- Rivero A, Magaud A, Nicot A, Vézilier J (2011) Energetic Cost of Insecticide Resistance in *Culex pipiens* Mosquitoes. *48 (3):694-700*. doi:10.1603/me10121
- Roditakis E, et al (2018) A four-year survey on insecticide resistance and likelihood of chemical control failure for tomato leaf miner *Tuta absoluta* in the European/Asian region. *Journal of Pest Science* 91:421
- Roditakis E, Steinbach D, Moritz G, Vasakis E, Stavrakaki M, Ilias A, García-Vidal L, Martínez-Aguirre MDR, Bielza P, Morou E, Silva JE, Silva WM, Siqueira HAA, Iqbal S, Troczka BJ, Williamson MS, Bass C, Tsagkarakou A, Vontas J, Nauen R (2017) Ryanodine receptor point mutations confer diamide insecticide resistance in tomato leafminer, *Tuta absoluta* (Lepidoptera: Gelechiidae).

- Insect Biochemistry and Molecular Biology 80:11-20.
doi:10.1016/j.ibmb.2016.11.003
- Roditakis E, Vasakis E, Grispou M, Stavrakaki M, Nauen R, Gravouil M, Bassi A (2015) First report of *Tuta absoluta* resistance to diamide insecticides. *Journal of Pest Science* 88 (1):9-16. doi:10.1007/s10340-015-0643-5
- Roditakis E, Steinbach D, Moritz G, Vasakis E, Stavrakaki M, Ilias A, García-Vidal L (2016) Ryanodine receptor point mutations confer diamide insecticide resistance in tomato leafminer, *Tuta absoluta* (Lepidoptera: Gelechiidae)
- Royuela M, Fraile B, Arenas MI, Paniagua R (2000) Characterization of several invertebrate muscle cell types: a comparison with vertebrate muscles. *Microscopy Research and Technique* 48 (2):107-115. doi:10.1002/(sici)1097-0029(2000115)48:2<107::Aid-jemt6>3.0.Co;2-u
- Rueda A, Song M, Toro L, Stefani E, Valdivia HH (2006) Sorcin modulation of Ca²⁺ sparks in rat vascular smooth muscle cells. *576 (3):887-901*. doi:10.1113/jphysiol.2006.113951
- Samsó M, Wagenknecht T, Allen PD (2005) Internal structure and visualization of transmembrane domains of the RyR1 calcium release channel by cryo-EM. *Nature Structural & Molecular Biology* 12 (6):539-544. doi:10.1038/Nsmb938
- Sanchez-Bayo, Wyckhuys (2019) Worldwide Decline of the Entomofauna.
- Sang S, Shu B, Yi X, Liu J, Hu M, Zhong G (2016) Cross-resistance and baseline susceptibility of *Spodoptera litura* (Fabricius) (Lepidoptera: Noctuidae) to cyantraniliprole in the south of China. *Pest Manag Sci* 72 (5):922-928. doi:10.1002/ps.4068
- Santulli G, Lewis DR, Marks AR (2017) Physiology and pathophysiology of excitation–contraction coupling: the functional role of ryanodine receptor. *Journal of Muscle Research and Cell Motility* 38 (1):37-45. doi:10.1007/s10974-017-9470-z
- Santulli G, Pagano G, Sardu C, Xie W, Reiken S, D’Ascia SL, Cannone M, Marziliano N, Trimarco B, Guise TA, Lacampagne A, Marks AR (2015) Calcium release channel RyR2 regulates insulin release and glucose homeostasis. *Journal of Clinical Investigation* 125 (5):1968-1978. doi:10.1172/jci79273
- Sattelle DB, Cordova D, Cheek TR (2008) Insect ryanodine receptors: molecular targets for novel pest control chemicals. *Invertebrate Neuroscience* 8 (3):107-119. doi:10.1007/s10158-008-0076-4
- Schnepf E, Crickmore N, Van Rie J, Lereclus D, Baum J, Feitelson J, Zeigler DR, Dean DH (1998) *Bacillus thuringiensis* and its pesticidal crystal proteins. *Microbiology and molecular biology reviews: MMBR* 62 (3):775-806
- Searchinger T, Waite R, Hanson C, Ranganathan J, Dumas P, Matthews E (2018) CREATING A SUSTAINABLE FOOD FUTURE: A Menu of Solutions to Feed Nearly 10 Billion People by 2050. World Resources Institute
- Selby TP, Lahm GP, Stevenson TM (2017) A retrospective look at anthranilic diamide insecticides: discovery and lead optimization to chlorantraniliprole and cyantraniliprole. *Pest Manag Sci* 73 (4):658-665. doi:10.1002/ps.4308
- Selby TP, Lahm GP, Stevenson TM, Hughes KA, Cordova D, Annan IB, Barry JD, Benner EA, Currie MJ, Pahutski TF (2013) Discovery of cyantraniliprole, a potent and selective anthranilic diamide ryanodine receptor activator with cross-spectrum insecticidal activity. *Bioorganic & Medicinal Chemistry Letters* 23 (23):6341-6345. doi:<http://dx.doi.org/10.1016/j.bmcl.2013.09.076>

- Sharanabasappa C, et al (2018) First report of the Fall Armyworm, an alien invasive pest on maize in India. *Pest Management in Horticultural Ecosystems* 24:23-29
- Shortall C, Harrington R (2009) Long term changes in the abundance of flying insects.
- Sial AA, Brunner JF (2012) Selection for resistance, reversion towards susceptibility and synergism of chlorantraniliprole and spinetoram in obliquebanded leafroller, *Choristoneura rosaceana* (Lepidoptera: Tortricidae). 68 (3):462-468. doi:10.1002/ps.2294
- Silva GA, Picanço MC, Bacci L, Crespo ALB, Rosado JF, Guedes RNC (2011) Control failure likelihood and spatial dependence of insecticide resistance in the tomato pinworm, *Tuta absoluta*. 67 (8):913-920. doi:10.1002/ps.2131
- Silva JE, al: e (2018) Field-evolved resistance to chlorantraniliprole in the tomato pinworm *Tuta absoluta*: inheritance, cross-resistance profile, and metabolism. *Journal of Pest Science*. doi:<https://doi.org/10.1007/s10340-018-1064-z>
- Silva JE, Assis CP, Ribeiro LM, Siqueira HA (2016) Field-Evolved Resistance and Cross-Resistance of Brazilian *Tuta absoluta* (Lepidoptera: Gelechiidae) Populations to Diamide Insecticides. *J Econ Entomol*. doi:10.1093/jee/tow161
- Sisay B, Tefera T, Wakgari M, Ayalew G, Mendesil E (2019) The Efficacy of Selected Synthetic Insecticides and Botanicals against Fall Armyworm, *Spodoptera frugiperda*, in Maize. *Insects* 10 (2):45. doi:10.3390/insects10020045
- Sitsapesan R, Williams AJ (1994) Gating of the native and purified cardiac SR Ca(2+)-release channel with monovalent cations as permeant species. *Biophys J* 67 (4):1484-1494. doi:10.1016/S0006-3495(94)80622-8
- Smith DT, DDT resistance, epistasis and male fitness in flies (2011). *J Evol Biol*. Jun;24(6):1351-62. doi: 10.1111/j.1420-9101.2011.02271.x.
- Song DW, Lee JG, Youn HS, Eom SH, Kim DH (2011) Ryanodine receptor assembly: A novel systems biology approach to 3D mapping. *Progress in Biophysics & Molecular Biology* 105 (3):145-161. doi:10.1016/j.pbiomolbio.2010.09.021
- Sparks TC (2013) Insecticide discovery: An evaluation and analysis. *Pesticide Biochemistry and Physiology* 107 (1):8-17. doi:DOI 10.1016/j.pestbp.2013.05.012
- Sparks TC, Lorsbach BA (2016) Perspectives on the Agrochemical Industry and Agrochemical Discovery. doi:10.1002/ps.4457
- Sparks TC, Nauen R (2015) IRAC: Mode of action classification and insecticide resistance management. *Pestic Biochem Physiol* 121:122-128. doi:10.1016/j.pestbp.2014.11.014
- Steinbach D, Gutbrod O, Luemmen P, Matthiesen S, Schorn C, Nauen R (2015) Geographic spread, genetics and functional characteristics of ryanodine receptor based target-site resistance to diamide insecticides in diamondback moth, *Plutella xylostella*. *Insect Biochemistry and Molecular Biology* 63:14-22. doi:10.1016/j.ibmb.2015.05.001
- Steinbach D, Nauen R, Moritz G (2017) Fitness costs of highly insecticide-resistant strains of *Plutella xylostella* at different temperatures.
- Stokstad E (2017) New crop pest takes Africa at lightning speed. *Science* 356 (6337):473-474. doi:10.1126/science.356.6337.473
- Su JY, Lai TC, Li J (2012) Susceptibility of field populations of *Spodoptera litura* (Fabricius) (Lepidoptera: Noctuidae) in China to chlorantraniliprole and the activities of detoxification enzymes. *Crop Protection* 42:217-222. doi:10.1016/j.cropro.2012.06.012

- Sullivan KMC, Scott K, Zuker CS, Rubin GM (2000) The ryanodine receptor is essential for larval development in *Drosophila melanogaster*. *Proceedings of the National Academy of Sciences of the United States of America* 97 (11):5942-5947. doi:10.1073/pnas.110145997
- Y, Xu L, Chen Q, Qin W, Huang S, Jiang Y, Qin H (2018) Chlorantraniliprole resistance and its biochemical and new molecular target mechanisms in laboratory and field strains of *Chilo suppressalis* (Walker). *Pest Management Science* 74 (6):1416-1423. doi:10.1002/ps.4824
- Sylla S, Brévault T, Bal AB, Chailleux A, Diatte M, Desneux N, Diarra K (2017) Rapid spread of the tomato leafminer, *Tuta absoluta* (Lepidoptera: Gelechiidae), an invasive pest in Sub-Saharan Africa. *Entomologia Generalis* 36 (3):269-283. doi:10.1127/entomologia/2017/0453
- Tae H, Casarotto MG, Dulhunty AF (2009) Ubiquitous SPRY domains and their role in the skeletal type ryanodine receptor. *PLoS ONE* 4 (1):51-59. doi:10.1007/s00249-009-0455-8
- Takasago T, Imagawa T, Furukawa K, Ogurusu T, Shigekawa M (1991) Regulation of the cardiac ryanodine receptor by protein kinase-dependent phosphorylation. *Journal of Biochemistry* 109 (1):163-170
- Takekura H, Franzini-Armstrong C (2002) The Structure of Ca²⁺ Release Units in Arthropod Body Muscle Indicates an Indirect Mechanism for Excitation-Contraction Coupling. *Biophysical Journal* 83 (5):2742-2753
- Tao Y, Gutteridge S, Benner EA, Wu L, Rhoades DF, Sacher MD, Rivera MA, Desaegeer J, Cordova D, (Dupont) (2013) Identification of a critical region in the *Drosophila* ryanodine receptor that confers sensitivity to diamide insecticides. *Insect biochemistry and molecular biology* 43 (9):820-828. doi:10.1016/j.ibmb.2013.06.006
- Tay WT, Soria MF, Walsh T, Thomazoni D, Silvie P, Behere GT, Anderson C, Downes S (2013) A Brave New World for an Old World Pest: *Helicoverpa armigera* (Lepidoptera: Noctuidae) in Brazil. *PLoS ONE* 8 (11):e80134. doi:10.1371/journal.pone.0080134
- Taylor CW, Prole DL, Rahman T (2009) Ca²⁺ Channels on the Move. *Biochemistry* 48 (51):12062-12080. doi:10.1021/bi901739t
- Tembrock LR, Timm AE, Zink FA, Gilligan TM (2019) Phylogeography of the Recent Expansion of *Helicoverpa armigera* (Lepidoptera: Noctuidae) in South America and the Caribbean Basin. *Annals of the Entomological Society of America* 112:388. doi:10.1093/aesa/saz019
- Thomas CD, all e (2000) A comparison of fluorescent Ca²⁺ indicator properties and their use in measuring elementary and global Ca²⁺ signals. *Cell Calcium* 28:213-223
- Thomas CD, Jones TH, Hartley SE (2019) "Insectageddon": A call for more robust data and rigorous analyses. *Global Change Biology* 25 (6):1891-1892. doi:10.1111/gcb.14608
- Thomas NL, George CH, Lai FA (2004) Functional heterogeneity of ryanodine receptor mutations associated with sudden cardiac death. *Cardiovasc Res* 64 (1):52-60. doi:10.1016/j.cardiores.2004.06.009
- Toshinishi M (2005) Flubendiamide, a novel insecticide highly active against lepidopterous insect pests. *Journal of Pesticide Science* 30 (4):354-360
- Troccka B (2013) Ryanodine receptors: next generation of insecticide targets – Thesis. Cardiff University, Accessed from <http://orca.cf.ac.uk/60069/>
- Troccka B, Richardson E, Homem R, Davies T (2018) An analysis of variability in genome organisation of intracellular calcium release channels across insect orders. *Gene* 670:70-86

- Trocza B, Williamson M, Field L, Davies E (2016) Rapid selection for resistance to diamide insecticides. *Neurotoxicology*
- Trocza B, Zimmer CT, Elias J, Schorn C, Bass C, Davies TGE, Field LM, Williamson MS, Slater R, Nauen R (2012) Resistance to diamide insecticides in diamondback moth, *Plutella xylostella* (Lepidoptera: Plutellidae) is associated with a mutation in the membrane-spanning domain of the ryanodine receptor. *Insect Biochemistry and Molecular Biology* 42 (11):873-880. doi:<http://dx.doi.org/10.1016/j.ibmb.2012.09.001>
- Trocza BJ, Williams AJ, Williamson MS, Field LM, Luemmen P, Davies TG (2015) Stable expression and functional characterisation of the diamondback moth ryanodine receptor G4946E variant conferring resistance to diamide insecticides. *Sci Rep*, vol 5. doi:10.1038/srep14680
- Truong, Pessah (2019) Comparison of Chlorantraniliprole and Flubendiamide Activity Toward Wild-Type and Malignant Hyperthermia-Susceptible Ryanodine Receptors and Heat Stress Intolerance. *TOXICOLOGICAL SCIENCES* 167 ((2)):509–523
- Tsakok I (2011) Macro and Political Stability Essential Condition for Successful Agricultural Transformation. OCP Policy Centre
- Tung CC, Lobo PA, Kimlicka L, Van Petegem F (2010) The amino-terminal disease hotspot of ryanodine receptors forms a cytoplasmic vestibule. *Nature* 468 (7323):585-U267. doi:10.1038/nature09471
- Uchiyama T, Ozawa A (2014) Rapid development of resistance to diamide insecticides in the smaller tea tortrix, *Adoxophyes honmai* (Lepidoptera: Tortricidae), in the tea fields of Shizuoka Prefecture, Japan. 49 (4):529-534. doi:10.1007/s13355-014-0283-x
- Valdivia H, Kaplan J, Ellis-Davies G, Lederer W (1995) Rapid adaptation of cardiac ryanodine receptors: modulation by Mg²⁺ and phosphorylation. 267 (5206):1997-2000. doi:10.1126/science.7701323
- Van Damme V, Berkvens N, Moerkens R, Berckmoes E, Wittemans L, De Vis R, Casteels H, Tirry L, De Clercq P (2015) Overwintering potential of the invasive leafminer *Tuta absoluta* (Meyrick) (Lepidoptera: Gelechiidae) as a pest in greenhouse tomato production in Western Europe. 88 (3):533-541. doi:10.1007/s10340-014-0636-9
- Van Petegem F (2014) RyR: Allosteric Ion Channel Giants. *J Mol Biol* 427:31–53
- van Strien AJ, van Swaay CAM, van Strien-van Liempt WTFH, Poot MJM, WallisDeVries MF (2019) Over a century of data reveal more than 80% decline in butterflies in the Netherlands. *Biological Conservation* 234:116-122. doi:10.1016/j.biocon.2019.03.023
- Wang BL, Zhu HW, Ma Y, Xiong LX, Li YQ, Zhao Y, Zhang JF, Chen YW, Zhou S, Li ZM (2013a) Synthesis, insecticidal activities, and SAR studies of novel pyridylpyrazole acid derivatives based on amide bridge modification of anthranilic diamide insecticides. *J Agric Food Chem* 61 (23):5483-5493. doi:10.1021/jf4012467
- Wang J, Liu Y, Gao J, Xie Z, Huang L, Wang W, Wang J (2013b) Molecular cloning and mRNA expression of a ryanodine receptor gene in the cotton bollworm, *Helicoverpa armigera*. *Pesticide Biochemistry and Physiology* (0). doi:<http://dx.doi.org/10.1016/j.pestbp.2013.09.006>
- Wehrens XHT, Lehnart SE, Reiken S, Vest JA, Wronska A, Marks AR (2006) Ryanodine receptor/calcium release channel PKA phosphorylation: A critical mediator of heart failure progression. *Proceedings of the National Academy of Sciences of the United States of America* 103 (3):511-518. doi:DOI 10.1073/pnas.0510113103

- Westbrook JK, Nagoshi RN, Meagher RL, Fleischer SJ, Jairam S (2016) Modeling seasonal migration of fall armyworm moths. *Int J Biometeorol* 60 (2):255-267. doi:10.1007/s00484-015-1022-x
- Whalon M, Mota-Sanchez D, Hollingworth R (2016) Arthropod pesticide resistance database. <http://www.pesticideresistance.org/index.php>
- Whitford F et al. The Pesticide Marketplace: Discovering and Developing new products. Purdue Extension. PPP-71.
- WHO (2007) Pests and Pesticides report: Chlorantraniliprole. Joint Meeting on Pesticide Residues
- Williams AJ, Tanna B (2004) The interaction of ryanoids with individual ryanodine receptor channels. *Biological Research* 37 (4):527-538
- Wilson GA, Rannala B (2003) Bayesian Inference of Recent Migration Rates Using Multilocus Genotypes. *Genetics* 163:1177-1191
- Wu L, Wang D, Evans JA (2019) Large teams develop and small teams disrupt science and technology. *Nature*. doi:10.1038/s41586-019-0941-9
- Wu M, Zhang S, Yao R, Wu S, Su J, Gao C (2014) Susceptibility of the Rice Stem Borer, *Chilo suppressalis* (Lepidoptera: Crambidae), to Flubendiamide in China. *Journal of Economic Entomology* 107 (3):1250-1255. doi:10.1603/ec14053
- Wyckhuys K, O'Neil R (2006) Population dynamics of *Spodoptera frugiperda* Smith (Lepidoptera: Noctuidae) and associated arthropod natural enemies in Honduran subsistence maize. *Crop Protection* 25:1180
- Xian X, Han P, Wang S, Zhang G, Liu W, Desneux N, Wan F (2017) The potential invasion risk and preventive measures against the tomato leafminer *Tuta absoluta* in China. *Entomologia Generalis* 36 (4):319-333. doi:10.1127/entomologia/2017/0504
- Xu L, Meissner G (2004) Mechanism of Calmodulin Inhibition of Cardiac Sarcoplasmic Reticulum Ca²⁺ Release Channel (Ryanodine Receptor). 86 (2):797-804. doi:10.1016/s0006-3495(04)74155-7
- Xu T, Yuchi Z (2019) Crystal structure of diamondback moth ryanodine receptor Repeat34 domain reveals insect-specific phosphorylation sites. *BMC Biology* 17:77. doi:<https://doi.org/10.1186/s12915-019-0698-5>
- Xu XH, Bhat MB, Nishi M, Takeshima H, Ma JJ (2000) Molecular cloning of cDNA encoding a *Drosophila* ryanodine receptor and functional studies of the carboxyl-terminal calcium release channel. *Biophysical Journal* 78 (3):1270-1281
- Yamaguchi N, Takahashi N, Xu L, Smithies O, Meissner G (2007) Early cardiac hypertrophy in mice with impaired calmodulin regulation of cardiac muscle Ca²⁺ release channel. *Journal of Clinical Investigation* 117 (5):1344-1353. doi:10.1172/jci29515
- Yan Z, Bai XC, Yan CY, Wu JP, Li ZQ, Xie T, Peng W, Yin CC, Li XM, Scheres SHW, Shi YG, Yan N (2015) Structure of the rabbit ryanodine receptor RyR1 at near-atomic resolution. *Nature* 517 (7532):50-+. doi:Doi 10.1038/Nature14063
- Yao R, et al; (2017) Monitoring and mechanisms of insecticide resistance in *Chilo suppressalis* (Lepidoptera: Crambidae), with special reference to diamides. *Pest Manag Sci* 73:1169
- Magyar Z, Csernoch L, Diszházi G, Péli-Szabó J, Nánási P, Almássy J (2019) The diamide insecticide chlorantraniliprole increases the single-channel current activity of the mammalian skeletal muscle ryanodine receptor. *Gen Physiol Biophys* 38:183–186
- Zalk R, Clarke OB, des Georges A, Grassucci RA, Reiken S, Mancina F, Hendrickson WA, Frank J, Marks AR (2015) Structure of a mammalian ryanodine receptor. *Nature* 517 (7532):44-49. doi:10.1038/nature13950

- Zalk R, Lehnart SE, Marks AR (2007) Modulation of the ryanodine receptor and intracellular calcium. *Annual Review of Biochemistry* 76:367-385. doi:DOI 10.1146/annurev.biochem.76.053105.094237
- Zalucki MP, Shabbir A, Silva R, Adamson D, Liu SS, Furlong MJ (2012) Estimating the Economic Cost of One of the World's Major Insect Pests, *Plutella xylostella* (Lepidoptera: Plutellidae): Just How Long Is a Piece of String? *Journal of Economic Entomology* 105 (4):1115-1129. doi:Doi 10.1603/Ec12107
- Zamparelli C, Macquaide N, Colotti G, Verzili D, Seidler T, Smith GL, Chiancone E (2010) Activation of the cardiac Na⁺-Ca²⁺ exchanger by sorcin via the interaction of the respective Ca²⁺-binding domains. *J Biol Chem* 285 (1):132-141. doi:10.1074/jbc.M109.020003
- Zimmer CT et al. 2018. Neofunctionalization of Duplicated P450 Genes Drives the Evolution of Insecticide Resistance in the Brown Planthopper. *Curr Biol*; 28(2): 268–274.e5. doi: 10.1016/j.cub.2017.11.060
- Zhang J, Khan SA, Heckel DG, Bock R (2017) Next-Generation Insect-Resistant Plants: RNAi-Mediated Crop Protection. *Trends in biotechnology* 35 (9):871-882. doi:10.1016/j.tibtech.2017.04.009
- Zhang L, Kelley J, Schmeisser G, Kobayashi YM, Jones LR (1997) Complex formation between junction, triadin, calsequestrin, and the ryanodine receptor - Proteins of the cardiac junctional sarcoplasmic reticulum membrane. *Journal of Biological Chemistry* 272 (37):23389-23397
- Zhang S-K, Ren X-B, Wang Y-C, Su J (2014) Resistance in *Cnaphalocrocis medinalis* (Lepidoptera: Pyralidae) to New Chemistry Insecticides. *J Econ Entomol* 107 (2):815-820. doi:10.1603/ec13506
- Zhao C, Liu B, Piao S, Wang X, Lobell DB, Huang Y, Huang M, Yao Y, Bassu S, Ciais P, Durand JL, Elliott J, Ewert F, Janssens IA, Li T, Lin E, Liu Q, Martre P, Muller C, Peng S, Penuelas J, Ruane AC, Wallach D, Wang T, Wu D, Liu Z, Zhu Y, Zhu Z, Asseng S (2017) Temperature increase reduces global yields of major crops in four independent estimates. *Proceedings of the National Academy of Sciences of the United States of America* 114 (35):9326-9331. doi:10.1073/pnas.1701762114
- Zhao Y, Xu LP, Tong J, Li YQ, Xiong LX, Li F, Peng LN, Li ZM (2012) Synthesis, crystal structure and biological activity of novel anthranilic diamide insecticide containing alkyl ether group. *Molecular Diversity* 16 (4):711-725. doi:10.1007/s11030-012-9406-x
- Zima AV, Picht E, Bers DM, Blatter LA (2008) Termination of cardiac Ca²⁺ sparks role of intra-SR Ca²⁺, release flux, and intra-SR Ca²⁺ diffusion. *Circulation Research* 103 (8):E105-E115. doi:10.1161/circresaha.107.183236
- Zuo Y, et al. (2019) Identification of the ryanodine receptor mutation I4743M and its contribution to diamide insecticide resistance in *Spodoptera exigua* (Lepidoptera: Noctuidae). *Insect Science* [Pre-Print]
- Zuo Y, Wang H, Xu Y, Huang J, Wu S, Wu Y, Yang Y (2017) CRISPR/Cas9 mediated G4946E substitution in the ryanodine receptor of *Spodoptera exigua* confers high levels of resistance to diamide insecticides. *Insect Biochemistry and Molecular Biology* [Pre-Print]. doi:doi: 10.1016/j.ibmb.2017.09.005
- Zvaritch E, Kraeva N, Bombardier E, McCloy RA, Depreux F, Holmyard D, Kraev A, Seidman CE, Seidman JG, Tupling AR, MacLennan DH (2009) Ca²⁺ dysregulation in Ryr1(I4895T/wt) mice causes congenital myopathy with progressive formation of minicores, cores, and nemaline rods. *Proceedings of the National Academy of Sciences of the United States of America* 106 (51):21813-21818. doi:10.1073/pnas.0912126106
